



HAL
open science

Kinetic modeling of catalytic lignin hydroconversion for aromatic production

Junjie Pu

► **To cite this version:**

Junjie Pu. Kinetic modeling of catalytic lignin hydroconversion for aromatic production. Catalysis. Université de Lyon, 2018. English. NNT : 2018LYSE1216 . tel-02426001

HAL Id: tel-02426001

<https://theses.hal.science/tel-02426001>

Submitted on 1 Jan 2020

HAL is a multi-disciplinary open access archive for the deposit and dissemination of scientific research documents, whether they are published or not. The documents may come from teaching and research institutions in France or abroad, or from public or private research centers.

L'archive ouverte pluridisciplinaire **HAL**, est destinée au dépôt et à la diffusion de documents scientifiques de niveau recherche, publiés ou non, émanant des établissements d'enseignement et de recherche français ou étrangers, des laboratoires publics ou privés.



N°d'ordre NNT :

2018LYSE1216

THESE de DOCTORAT DE L'UNIVERSITE DE LYON

opérée au sein de
l'Université Claude Bernard Lyon 1

Ecole Doctorale N° 206
(Ecole Doctorale de Chimie de Lyon)

Spécialité de doctorat : Procédés
Discipline : Catalyse et Génie des Procédés

Soutenue publiquement le 06/11/2018, par :
Junjie PU

Modélisation cinétique de l'hydroconversion catalytique de la lignine pour la production d'aromatiques

Devant le jury composé de :

M. Fongarland, Pascal	Professeur UCBL1/LGPC	Président du jury
M. Haarlemmer, Geert	Ingénieur de Recherche CEA/LITEN	Rapporteur
M. Pinard, Ludovic	Maître de Conférences ENSIP/IC2MP	Rapporteur
M. Ducrot, Paul-Henri	Directeur de Recherche INRA/IJPB	Examineur
M. Puel, François	Professeur CentraleSupélec/LGPM	Examineur
Mme. Tayakout-Fayolle, Méla	Professeure UCBL1/LAGEPP	Examineur
Mme. Laurenti, Dorothée	Chargée de Recherche/IRCELYON	Directrice de thèse
Mme. Pitault, Isabelle	Chargée de Recherche/LAGEPP	Co-directrice de thèse

N°d'ordre NNT :



2018LYSE1216

THESE de DOCTORAT DE L'UNIVERSITE DE LYON
opérée au sein de
l'Université Claude Bernard Lyon 1

Ecole Doctorale N° 206
(Ecole Doctorale de Chimie de Lyon)

Spécialité de doctorat : Procédés
Discipline : Catalyse et Génie des Procédés

Soutenue publiquement le 06/11/2018, par :
Junjie PU

**Kinetic modeling of catalytic lignin
hydroconversion for aromatic production**

Devant le jury composé de :

M. Fongarland, Pascal	Professeur UCBL1/LGPC	Président du jury
M. Haarlemmer, Geert	Ingénieur de Recherche CEA/LITEN	Rapporteur
M. Pinard, Ludovic	Maître de Conférences ENSIP/IC2MP	Rapporteur
M. Ducrot, Paul-Henri	Directeur de Recherche INRA/IJPB	Examineur
M. Puel, François	Professeur CentraleSupélec/LGPM	Examineur
Mme. Tayakout-Fayolle, Mélaz	Professeure UCBL1/LAGEPP	Examineur
Mme. Laurenti, Dorothée	Chargée de Recherche/IRCELYON	Directrice de thèse
Mme. Pitault, Isabelle	Chargée de Recherche/LAGEPP	Co-directrice de thèse

Remerciment

Ce travail a été réalisé dans le cadre du projet ANR (LIGNAROCAT), en partenariat avec Institut de Recherche sur la Catalyse et l'Environnement de LYON (IRCELYON) et Laboratoire d'Automatique, de Génie des Procédés et de génie Pharmaceutique (LAGEPP).

Tout d'abord, je tiens à exprimer ma gratitude envers M. Michel Lacroix (Ancien directeur de l'IRCELYON), Mme Catherine Pinel (Directrice de l'IRCELYON) et Mme Stéphanie Briançon (Directrice de LAGEPP) pour m'avoir accueilli pendant ces trois ans.

Au cours de ces trois années, j'ai eu la chance d'être encadré par Dorothée Laurenti, Isabelle Pitault et Mélaz Tayakout-Fayolle. Elles ont mis leur énergie, leur savoir, leur patience et leur passion à ma disposition. Je souhaite exprimer ma gratitude à Dorothée Laurenti pour son investissement tout au long de ce travail. J'ai largement profité de sa rigueur scientifique en catalyse et chimie analytique. J'adresse aussi mon remerciement à Isabelle Pitault et Mélaz Tayakout-Fayolle pour la qualité de leur encadrement scientifique en génie des procédés. J'ai particulièrement apprécié leur enthousiasme et leur soutien. Je remercie aussi Christophe Geantet, qui m'a toujours donné des conseils précieux tout au long de cette thèse.

Ce travail n'aurait pas pu être mené à bien sans l'aide du personnel du ECI2D (IRCELYON) et du DYCOP (LAGEPP). Je tiens particulièrement à remercier Chantal Lorentz, Ruben Checa et Emmanuel Leclerc pour leur soutien à l'expérimentation.

Je tiens à exprimer toute ma sympathie à mes camarades de thèse et à mes amis à Lyon: Aurélie, Barbara, Camila, Clément, Eddy, Florina, Junchao, Lei, Maëlen, Minh-tuan, Pedro, Quanyi, Xiaolu, Xinke, Yongxian, Yuanshuang, Yue.

Enfin, je terminerai par une pensée particulière pour mes parents qui m'ont soutenu tout au long de ma vie.

Résumé

De nos jours, en raison de l'épuisement des combustibles fossiles et des préoccupations environnementales, la transformation de la biomasse lignocellulosique devient un gros challenge pour fournir des biocarburants et des bioproduits dans un futur proche. La lignine, qui représente près de 30 %pds de la biomasse lignocellulosique, est la bioressource la plus pertinente et la plus abondante pour produire des composés aromatiques grâce à sa structure polymérique composée d'unités phénylpropane avec des liaisons éthers. Dans ce contexte, l'utilisation de la lignine en tant que précurseur de composés aromatiques suscite beaucoup d'attention de par son faible coût et sa haute disponibilité puisque co-produit dans l'industrie papetière ou les bio-raffineries. Dans la littérature, il apparaît que l'hydroconversion catalytique de la lignine constitue une méthode thermochimique intéressante pour obtenir des rendements élevés en produits liquides. Le but de ce travail était d'étudier les processus réactionnels lors de ce procédé et de développer un modèle cinétique pour l'hydroconversion catalytique de la lignine sur un catalyseur sulfure (CoMoS/Al₂O₃).

Dans la première partie de ce travail, des mesures cinétiques ont été effectuées dans un solvant donneur d'hydrogène (tétraline) à 350 °C et 80 bar en utilisant un réacteur semi-continu, ouvert en phase gazeuse avec l'alimentation continue en H₂ et équipé d'un condenseur à reflux et de pièges refroidis. Les produits récupérés ont été isolés en quatre fractions : gaz (méthane, dioxyde de carbone, hydrocarbures légers, *etc.*), liquide organique (phénols, aromatiques, naphènes, *etc.*), résidus solubles dans le THF et insolubles dans le THF. Grâce à plusieurs outils analytiques appropriés (GPC, RMN, GC×GC, *etc.*), l'évolution et la composition de ces différentes fractions en fonction du temps de réaction ont été étudiés afin de comprendre les transformations lors de la conversion. Un schéma réactionnel (approche regroupée) a été établi sur la base de ces observations.

La deuxième partie de ce travail a été consacrée au développement d'un modèle cinétique paramétré permettant de décrire mathématiquement chaque étape de réaction au cours de l'hydroconversion de la lignine. Premièrement, les phénomènes physiques impliqués (comportement hydrodynamique des gaz dans notre installation, équilibre vapeur-liquide des mélanges et transfert de masse liquide-gaz) ont été caractérisés. Par la suite, un modèle complet de réacteur a été construit en couplant la cinétique chimique appropriée et les caractérisations physiques. En prenant les données expérimentales recueillies comme base, des paramètres cinétiques fiables (constantes de vitesse et coefficients stœchiométriques) pour chaque étape de réaction ont été obtenus au moyen d'une technique de régression non linéaire. Le modèle résultant nous permet d'avoir une compréhension approfondie du processus de conversion de la lignine.

Mot clés :

- ✓ Lignine
- ✓ Hydroconversion catalytique
- ✓ Catalyseur sulfure
- ✓ Schéma réactionnel
- ✓ Modèle cinétique

Abstract

Nowadays, due to the fossil fuels depletion and environmental concerns, transformation of lignocellulosic biomass is becoming a great challenge in order to provide biofuels and biochemicals in a near future. Lignin, which accounts for nearly 30 wt% of lignocellulosic biomass, is the most relevant and abundant bio-resource to produce aromatic compounds because of its original polymeric structure composed by phenylpropane units with ether linkages. In this context, the use of lignin as a precursor of aromatic compounds attracts lots of attention thanks to its low cost and high availability in pulp industry or bio-refinery. In the literature, it appears that an interesting thermochemical method for obtaining high yields of liquid products was the catalytic hydroconversion of lignin. The aim of this work was to investigate the reaction scheme of the catalytic process and develop a kinetic model for catalytic lignin hydroconversion over a sulfided CoMoS/Al₂O₃.

In the first part of this work, kinetic measurements were carried out in a H-donor solvent (tetralin) at 350 °C and 80 bar using a semi-continuous batch reactor, which is opened for gas phase with continuous supply of H₂ and equipped with a condensing reflux followed by cooled traps. The recovered products were isolated in four fractions: gases (methane, carbon dioxide, light hydrocarbons, *etc.*), organic liquid (phenols, aromatics, naphthenes, *etc.*), THF-soluble and THF-insoluble residues. Thanks to several appropriate analytical tools (GPC, NMR, GC×GC, *etc.*), the evolution of these different fractions as a function of reaction time was followed in order to understand the transformations occurring during the conversion. Accordingly, a lumped reaction network was established based on the observed reaction schemes.

The second part of this work was dedicated to the development of a parameterized kinetic model allowing to have a mathematical description for each reaction step involved in the lignin hydroconversion. Firstly, physical phenomena involved (the gas hydrodynamic behavior of our set-up, the vapor-liquid equilibrium of mixtures and the liquid-gas mass transfer) were characterized. Subsequently, a complete reactor model was constructed by coupling the suitable chemical kinetics and these physical characterizations. Taking the gathered experimental data as a basis, reliable kinetic parameters (rate constants and stoichiometric coefficients) for each reaction step were obtained by means of non-linear regression technique. The resulting model allows us to have an in-depth understanding of the lignin conversion process.

Keywords:

- ✓ Lignin
- ✓ Catalytic hydroconversion
- ✓ Sulfided catalyst
- ✓ Reaction scheme
- ✓ Kinetic modeling

Nomenclature

Abbreviations

AK1	Alkanes (<C ₁₃)
AK2	Alkanes (≥C ₁₃)
AP	Alkylphenols
AQ	Anthraquinone
BDE	Bond dissociation enthalpies
BET	Brunauer-Emmett-Teller
BTX	Benzene, Toluene, Xylene
C	Carbon
CHONS	Element analysis of carbon, hydrogen, oxygen, nitrogen and sulfur
CSTR	Continuous stirred-tank reactor
DMSO	Dimethyl sulfoxide
DRI	Differential refractive index
ECN	Effective carbon number
EOS	Equation of state
FID	Flame ionization detector
G	Coniferyl unit in lignin
GC×GC	Two-dimensional gas chromatography
G/L	Gas-liquid
GPC	Gel permeation chromatography
H	<i>p</i> -Coumaryl unit in lignin
HDN	Hydrodenitrogenation
HDO	Hydrodeoxygenation
HDS	Hydrodesulfurization
HRI	Hydrocarbon Research Institute
KF	Karl-Fischer titration
L/S	Liquid-solid
MHV	Modified Huron-Vidal mixing rule
MS	Mass spectrometry
NMR	Nuclear magnetic resonance
NRTL	Non-Random Two Liquid model
HDO	Hydrodeoxygenation
O	Oxygen
P1000	Lignin Protobind 1000
PAN	Polyacrylonitrile
PDI	Polydispersity
PFR	Plug-flow reactor
PLA	Polylactic acid
PMO	Porous metal oxide
PPR78	Predictive Peng-Robinson 1978
PS	Polystyrene
PSRK	Predictive Soave-Redlich-Kwong
RTD	Residence time distribution
S	Sinapyl unit in lignin

SO	Solubilized oligomers
SRK	Soave-Redlich-Kwong
TBD	Triazabicyclodecene
TCD	Thermal conductivity detector
TGA	Thermogravimetric analysis
THF	Tetrahydrofuran
TMDP	2-chloro-4,4,5,5-tetramethyl-1,3,2-dioxapholane
TSB	THF-solubles _B
UNIFAC	Universal Functional Activity Coefficient
UNIQUAC	Universal QuasiChemical
VLE	Vapor-liquid equilibrium
VTPR	Volume-Translated Peng-Robinson

Latin letters

a	Gas-liquid interfacial area (m^{-1})
a_s	Specific area of solid (m^{-1})
A_p	External surface of catalyst particle (m^2)
C	Effective carbon number (-)
	Concentration (mol m^3)
d_p	Equivalent particle size (m)
D	Diffusion coefficient ($\text{m}^2 \text{s}^{-1}$)
D_m	Molecular diffusion coefficient ($\text{m}^2 \text{s}^{-1}$)
$E(t)$	Residence Time Distribution Function (-)
f	Relative response factor (-)
	Fugacity (-)
f_{ex}	External resistance fraction (-)
F	Mass flux (mol s^{-1})
H	Dimensionless Henry's coefficient (-)
J	Objective function of the minimization of the square difference (-)
k	Number of estimated parameters (-)
	Rate constant for first-order reaction (s^{-1})
	Rate constant for second-order reaction ($\text{mol m}^{-3} \text{s}^{-1}$)
k_D	Liquid-solid mass transfer coefficient (m s^{-1})
$k_D a_s$	Volumetric liquid-solid mass transfer coefficient (s^{-1})
k_G	Gas-Liquid mass transfer coefficient for the gas phase (m s^{-1})
k_L	Gas-liquid mass transfer coefficient for the liquid phase (m s^{-1})
$k_L a$	Volumetric gas-liquid mass transfer coefficient (s^{-1})
K	Equilibrium constant (-)
L	Characteristic length of catalyst particle (m)
m	Mass (g)
M	Molar mass (g mol^{-1})
M_w	Weight average molar mass (g mol^{-1})
M_n	Number average molar mass (g mol^{-1})
n	Number of moles (mol)
n_{CSTR}	Number of CSTRs
N	Agitation speed (rpm)

	Interphase mass flux transferred per unit area ($\text{mol m}^2 \text{s}^{-1}$)
	Number of experimental data (-)
N_0	Amount of concentrated tracer (mol)
p	Parameter
P	Pressure (bar)
Q	Volumetric flowrate (NL h^{-1})
	Mass flowrate (g h^{-1})
	Molar flowrate (mol h^{-1})
r	Reaction rate ($\text{mol m}^{-3} \text{s}^{-1}$)
\bar{r}	Apparent reaction rate ($\text{mol m}^{-3} \text{s}^{-1}$)
R	Gas constant ($\text{J mol}^{-1} \text{K}^{-1}$)
	Overall reaction rate ($\text{mol m}^{-3} \text{s}^{-1}$)
Sh	Sherwood number (-)
t	Time (s, h)
t_m	First moment of RTD (min)
T	Temperature ($^{\circ}\text{C}$)
V	Peak volume (-)
	Volume (m^3 , mL)
	Variance (-)
V_{mol}	Molar volume ($\text{m}^3 \text{mol}^{-1}$)
V_P	External volume of catalyst particle (m^3)
w	Mass fraction (wt%)
	Weight factor (-)
x	Liquid molar fraction (-)
X	Remaining percentage (-)
y	Gas molar fraction (-)

Greek letters

α	Condensation ratio in the hot reflux condenser (-)
χ	Conversion (wt%)
τ	Space time (min)
	Characteristic time of reaction (h)
ζ	Dimensionless axial coordinate (-)
σ	Standard deviation
ϕ	Fugacity coefficient (-)
ϕ'_S	Weisz Criterion (-)
γ	Activity coefficient (-)
	Yield (wt%)
ν	Stoichiometric coefficient (-)

Sub/subscripts

e	Effective
G	Gas
H_2	Hydrogen
i	Compound

j
lignin
L
m
mol
*N*₂
r
R
S
st
v
*

Fraction
Family
Lump
Reaction
Lignin
Liquid
Mass
Molar
Nitrogen
Reflux condenser
Reactor
Solid
Standard
Volumetric
Equilibrium

Table of Contents

Remerciment	i
Résumé	iii
Abstract	v
Nomenclature	vi
List of Tables	xiv
List of Figures	xvii
List of Schemes	xxi
General Introduction	1
Chapter I. State of the Art	3
I.1 Lignin overview	3
I.1.1 Lignin structure.....	5
I.1.2 Interunit linkages and functional groups.....	6
I.2 Lignin isolation processes	7
I.2.1 Kraft process.....	7
I.2.2 Sulfite process	8
I.2.3 Soda process.....	9
I.2.4 Organosolv process	10
I.2.5 Comparison of technical lignins.....	11
I.3 Properties of lignin	13
I.3.1 Molecular weight distribution	13
I.3.2 Solubility	13
I.3.3 Thermal behavior	14
I.3.4 Conclusion of lignin overview.....	16
I.4 Lignin valorization	16
I.4.1 Materials.....	17
I.4.1.1 Carbon fiber	17
I.4.1.2 Lignin-based plastics	18
I.4.2 Biorefinery.....	18
I.4.2.1 Pyrolysis	19
I.4.2.2 Gasification	19
I.4.2.3 Hydrolysis.....	20
I.4.2.4 Hydroconversion	20
I.4.2.5 Comparison of different valorization pathways.....	21
I.5 Lignin catalytic hydroconversion	21
I.5.1 Reactions and products	22
I.5.2 Solvents	23
I.5.2.1 In the absence of an external solvent	23
I.5.2.2 In the presence of an external solvent.....	26
I.5.3 Catalysts	33
I.5.4 Reaction set-up.....	34
I.5.5 Conclusion of lignin hydroconversion	34

I.6 Kinetic modeling development of lignin conversion	35
I.7 Conclusion and thesis objectives	39
I.7.1 Conclusion	39
I.7.2 Thesis objectives.....	39
Reference-I.....	41
<i>Chapter II. Materials and Methods.....</i>	<i>48</i>
II.1 Introduction.....	48
II.2 Materials	48
II.2.1 Lignin	48
II.2.2 Chemicals	48
II.2.3 Catalyst.....	49
II.3 Analytical methods	49
II.3.1 Elemental analysis (CHONS)	49
II.3.2 Thermogravimetric analysis (TGA)	49
II.3.3 Gel permeation chromatography (GPC).....	49
II.3.4 Nuclear magnetic resonance (NMR)	50
II.3.5 Karl-Fischer titration.....	51
II.3.6 μ GC-TCD	52
II.3.7 GC \times GC technique	52
II.4 Catalyst activation and characterization	54
II.4.1 Catalyst sulfidation	54
II.4.2 Elemental and textural properties of sulfide catalyst	54
II.5 Hydroconversion experiments.....	55
II.5.1 Experimental set-up	55
II.5.2 Experimentation of catalytic tests.....	56
II.5.3 Product recovery protocol.....	58
II.6 Analytical strategy	59
Reference-II.....	60
<i>Chapter III. Characterization of Lignin Protobind 1000.....</i>	<i>61</i>
III.1 Introduction.....	61
III.2 Solubility	61
III.3 Elemental analysis	62
III.4 Molecular weight distribution	63
III.5 Structural analysis.....	64
III.5.1 ^1H NMR	64
III.5.2 ^{13}C NMR	65
III.5.3 ^{31}P NMR	66
III.6 Conclusion	67
Reference-III.....	67
<i>Chapter IV. Hydroconversion Experiments and Reaction Scheme</i>	<i>69</i>
IV.1 Introduction	69

IV.2 Results of hydroconversion experiments	69
IV.2.1 Characterization of gas phase	71
IV.2.2 Characterization of THF-insoluble residues	74
IV.2.3 Characterization of THF-solubles	75
IV.2.3.1 Molecular weight distribution by GPC	75
IV.2.3.2 ¹ H NMR	77
IV.2.3.3 ¹³ C NMR	79
IV.2.3.4 ³¹ P NMR	81
IV.2.3.5 Elemental analysis	82
IV.2.3.6 Conclusion of the transformations of THF-solubles	84
IV.2.4 Characterization of liquid phase	85
IV.2.4.1 Liquid phase in the reactor	85
IV.2.4.2 Liquid phase in the separator	94
IV.2.4.3 Tetralin conversion in the liquid phase	100
IV.2.4.4 Conclusion of the transformations in the liquid phase	101
IV.3 Construction of reaction scheme	101
IV.4 Evaluation of the role of catalyst	104
IV.5 Comparison of performance with conventional batch system	105
IV.6 Characterization of the used catalysts	106
IV.7 Conclusion	108
Reference-IV	109
Chapter V. Hydrodynamics, Mass transfer and Thermodynamics	110
V.1 Introduction	110
V.2 Hydrodynamics and mass transfer	110
V.2.1 Theory of hydrodynamics	110
V.2.1.1 Pulse input	111
V.2.1.2 RTD of reactors	112
V.2.1.3 Mean residence time	113
V.2.2 Theory of interphase mass transfer	114
V.2.2.1 G/L mass transfer	114
V.2.2.2 L/S mass transfer	115
V.2.3 Experimentation and methods to determine the hydrodynamic behavior and G/L mass transfer coefficient	116
V.2.4 Model and estimation method	117
V.2.4.1 Model description	117
V.2.4.2 Resolution of equation and parameter estimation	120
V.2.5 Results and discussions	121
V.2.5.1 Hydrodynamic behavior	121
V.2.5.2 <i>k</i> _L <i>a</i> estimation	123
V.2.6 Conclusion of hydrodynamics and mass transfer	126
V.3 Thermodynamics	127
V.3.1 VLE models	127
V.3.2 Modeling the condensation effect of hot reflux condenser	129
V.3.2.1 Experimentation and results	129
V.3.2.2 Model description	131
V.3.2.3 Properties of compounds and model parameters	136
V.3.2.4 Model structure and parameter estimation	137

V.3.3 Results and discussions	138
V.3.4 Conclusion of thermodynamics.....	142
V.4 Conclusion	142
Reference-V.....	143
Chapter VI. Kinetic Modeling of Catalytic Lignin Hydroconversion.....	145
VI.1 Introduction	145
VI.2 Model description.....	145
VI.2.1 Interphase mass transfer in the reactor.....	145
VI.2.2 Chemical kinetics.....	146
VI.2.3 Fixed parameters in the model	151
VI.2.4 Material balances.....	154
VI.2.5 Model structure and parameter estimation	156
VI.3 Results and discussions	156
VI.3.1 Model results	156
VI.3.2 Kinetic parameters	161
VI.3.3 Validation of the absence of mass transfer limitation	165
VI.4 Conclusion.....	166
Reference-VI.....	166
Conclusion and Perspectives.....	168
Conclusion.....	168
Perspectives	170
Annex	171
Annex 1 ¹ H spectra of THF-solubles at different reaction times	171
Annex 2 ¹³ C spectra of THF-solubles at different reaction times.....	172
Annex 3 ³¹ P spectra of THF-solubles at different reaction times.....	173
Annex 4 Comparisons between THF-solubles and precipitated lignin-type residue	174
Annex 5 Quantitative data of different alkyl substituents in each family of products (Reactor)	176
Annex 6 Quantitative data of different alkyl substituents in each family of products (Separator)	179
Annex 7 Characterization of the used catalysts	181
Annex 8 Detailed description of PSRK model	183
Annex 9 Comparison of different thermodynamic models for multi-component mixtures.....	185
Scientific Productions.....	190
Publications.....	190
Communications.....	190

List of Tables

Table I.1: Mass composition of lignocellulosic compounds among different sources	4
Table I.2: Percent composition of phenylpropane units among different sources ⁴	5
Table I.3: Common linkage structures and approximate abundance connecting the phenylpropane units in softwood and hardwood lignin	6
Table I.4: Functional groups per 100 phenylpropane units in lignin	7
Table I.5: Monomer molecular formulas and weights of lignin from various sources ³	11
Table I.6: Advantages and disadvantages of various technical lignins ²¹	12
Table I.7: M_n , M_w , and PDI in comparison with technical lignin isolated from different processes ²²	13
Table I.8: Bond dissociation enthalpies (BDE) for lignin linkages ²⁷	15
Table I.9: Advantages and disadvantages of various thermochemical conversions of lignin	21
Table I.10: Principal reactions occurred during the lignin hydroconversion	22
Table I.11: State of the art for lignin hydroconversion in the absence of an external solvent	24
Table I.12: State of the art for lignin hydroconversion in the presence of inert solvents	28
Table I.13: State of the art for lignin hydroconversion in the presence of protic solvents	29
Table I.14: State of the art for lignin hydroconversion in the presence of tetralin	31
Table I.15: Product comparison between tetralin experiments and naphthalene experiment by Connors <i>et al.</i> (400 °C, solvent/lignin = 4:1, reaction time = 15 min)	32
Table I.16: Product comparison between tetralin experiments and tetralin/m-cresol experiments by Vuori <i>et al.</i> (345 °C, solvent/lignin = 7:1, reaction time = 5 h)	32
Table I.17: Products comparison between the experiment using red mud and the experiment using CoMo (400 °C, reaction time = 4 h, initial pressure = 150 bar)	33
Table I.18: State of the art for the kinetic model of lignin conversion	36
Table I.19: Advantages and disadvantages of two modeling approaches	38
Table II.1: Metal composition of the oxidized catalyst	49
Table II.2: NMR chemical shift for ¹ H	51
Table II.3: NMR chemical shift for ¹³ C	51
Table II.4: NMR chemical shift for ³¹ P	51
Table II.5: Contributions to the ECN	54
Table II.6: Textural properties of fresh sulfide catalyst	54
Table II.7: Characterization strategy in our work	60
Table III.1: Elemental analysis and atomic ratios of lignin P1000 and its different fractions	62
Table III.2: Average molar weight and PDI measured by GPC	63
Table III.3: Relative quantification by ¹ H NMR	64

Table III.4: Relative quantification by ^{13}C NMR	66
Table III.5: Relative quantification by ^{31}P NMR	67
Table IV.1: Elemental composition of THF-insoluble residues as a function of residence time.....	74
Table IV.2: Evolution of THF-solubles M_w , M_n and PDI at different reaction times.....	77
Table IV.3: Evolution of elemental analyses and H/C, O/C atomic ratios for THF-solubles.....	83
Table IV.4: Water content of the liquid phase in the reactor by Karl-Fischer titration.....	86
Table IV.5: Evolution of elemental analyses and H/C, O/C atomic ratios for the liquid phase in the reactor	94
Table IV.6: Evolution of elemental analyses for the aqueous phase in the separator	98
Table IV.7: C, S elemental analysis, BET surface area, pore diameter and pore volume for used catalyst and fresh catalyst.....	107
Table IV.8: XPS elemental analysis of the fresh and used CoMoS/ Al_2O_3 catalysts	107
Table IV.9: XPS decomposition of Mo3d and S2P species for fresh and used CoMoS/ Al_2O_3 catalysts.	108
Table V.1: Shape and sizing of each element in the experimental set-up	116
Table V.2: Operating conditions of our experiments	117
Table V.3: Mass balances of N_2 in our experimental set-up	119
Table V.4: Simulation results under Prosim Plus.....	120
Table V.5: Comparison between t_m and τ and optimal n_{CSTR} at different flowrates for Test 1 at ambient temperature	121
Table V.6: Comparison between t_m and τ and optimal n_{CSTR} at different flowrates for Test 2 (Reactor at 350 °C, reflux at 170 °C).....	121
Table V.7: Comparison between t_m and τ at different flowrates for Test 6 (Reactor at 350 °C, reflux at 170 °C)	123
Table V.8: Comparison between t_m and τ at different flowrates in function of the temperature of reflux condenser	124
Table V.9: Estimated value of $k_L a$ at different temperatures.....	125
Table V.10: The mixture of model compounds used in our experiments	130
Table V.11: Material balances for the semi-batch pilot	133
Table V.12: Gas molar volume of H_2 at different temperatures under the pressure of 80 bar	136
Table V.13: Liquid molar volume and equilibrium constant of model compounds at 350 °C.....	136
Table V.14: Estimated diffusivity ratios in tetralin by Reddy-Doraiswamy Equation	137
Table V.15: Parameter estimation results.....	139
Table V.16: Kinetic studies of thermal decomposition of methoxyphenols in the literature.....	142
Table VI.1: Stoichiometric coefficients determined by mass conservation	151
Table VI.2: Average molar mass of liquid lumps after 13 h of reaction	152
Table VI.3: Liquid molar volume and equilibrium constant at 350 °C.....	153

Table VI.4: Condensation ratios for each lump in the model.....	155
Table VI.5: Parameter estimation results of our kinetic model	161
Table VI.6: Rate constants of the depolymerization of different oligomeric entities	162
Table VI.7: Calculated distribution of CH ₄ formation according to its source from the model.....	163
Table VI.8: Calculated distribution of H ₂ O formation according to its source calculated from the model	164
Table VI.9: Calculated distribution of H ₂ consumption according to its source calculated from the model	165

List of Figures

Figure I.1: Schematic representation of structure in lignocellulosic biomass ²	3
Figure I.2: Structure model of lignin from softwood ³	4
Figure I.3: Structure model of lignin from hardwood ³	5
Figure I.4: Broken bonds during kraft process ⁸	7
Figure I.5: Structure model of kraft lignin ⁹	8
Figure I.6: Structure model of liginosulfonate ⁹	9
Figure I.7: Structure of alkali lignin ¹⁶	10
Figure I.8: Structure model of organosolv lignin ¹⁸	11
Figure I.9: Thermal degradation curves of cellulose, hemicellulose, and lignin ²⁶	14
Figure I.10: Generalized catalytic and thermal decomposition of lignin to low-molecular-weight compounds ³²	16
Figure I.11: Schematic representation of carbon fiber production from lignin ⁴¹	17
Figure I.12: Major thermochemical conversion processes of lignin and their potential products and uses	19
Figure I.13: Proposed hydrolysis pathways of lignin ⁵⁷	20
Figure I.14: Examples of lumped kinetic model by some authors: (a) Adam et al. ⁹⁸ ; (b) Faraf et al. ⁹⁹ ; (c) Forchheim et al. ¹¹⁰	37
Figure I.15: Reference units in lignin feed ¹⁰¹	38
Figure II.1: Configuration of columns and modulator ⁴	52
Figure II.2: 2D image reconstruction method ⁵	53
Figure II.3: N ₂ -adsorption isotherm curve of fresh sulfide catalyst.....	55
Figure II.4: BJH desorption curves of fresh sulfide catalyst.....	55
Figure II.5: Photo of the experimental set-up.....	55
Figure II.6: Schematic diagram of the experimental set-up.....	56
Figure II.7: Example of monitored parameter profiles of the experimental set-up (3 h).....	57
Figure II.8: Product recovery protocol for the reacted mixture.....	58
Figure II.9: Example of dynamic gas flow out of set-up (9 h).....	59
Figure II.10: Example of the evolution of gas composition out of set-up (9 h)	59
Figure III.1: Photo of lignin Protobind 1000.....	61
Figure III.2: Molecular weight distributions of the acetylated lignin P1000 and the initial THF-soluble fraction	63
Figure III.3: ¹ H NMR spectra of lignin P1000.....	64
Figure III.4: ¹³ C NMR spectra of lignin P1000.....	65

Figure III.5: ³¹ P NMR spectra of lignin P1000	66
Figure IV.1: Evolution of the fraction yields and H ₂ consumption as a function of reaction time over CoMoS/Al ₂ O ₃ at 350 °C	70
Figure IV.2: Dynamic gas composition at the outlet of set-up (a) CH ₄ , CO ₂ , CO and C ₂ -C ₆ ; (b) H ₂	71
Figure IV.3: Dynamic gas mass flow at the outlet of set-up (a) CH ₄ ; (b) CO ₂	72
Figure IV.4: Cumulative gas mass yields as a function of reaction time.....	73
Figure IV.5: GPC curves of THF-solubles at t ₀ and the initial THF-soluble fraction.....	75
Figure IV.6: GPC curves of the THF-solubles at different reaction times	76
Figure IV.7: Variation in the number of moles for each H group in THF-solubles versus reaction time	77
Figure IV.8: Remaining percentage of H groups (mol%) in THF-solubles versus reaction time	78
Figure IV.9: Variation in the number of moles for each C group in THF-solubles versus reaction time.	80
Figure IV.10: Remaining percentage of C groups (mol%) in THF-solubles versus reaction time.....	80
Figure IV.11: Evolution of OH groups of lignin by ³¹ P NMR as a function of residence time.....	82
Figure IV.12: Van Krevelen diagram of THF-solubles in function of reaction time	83
Figure IV.13: Mass distribution of liquids phases in function of reaction time	85
Figure IV.14: GPC curves of the liquid phase at different reaction times compared to the THF-solubles at 13 h.....	86
Figure IV.15: GC×GC-FID chromatogram of the liquid phase in the reactor after t ₀ point.....	88
Figure IV.16: GC×GC-FID chromatogram of the liquid phase in the reactor after 5 h	89
Figure IV.17: GC×GC-MS chromatogram of the liquid phase in the reactor after 13 h	90
Figure IV.18: Evolution of main families of products in the reactor as a function of reaction time; (a) Oxygenated compounds (b) Non-oxygenated compounds	92
Figure IV.19: GC×GC-FID chromatogram of the organic phase (a) 1 h; (b) 5 h; (c) 13h	96
Figure IV.20: GC×GC-FID chromatogram of the aqueous phase (a) 1 h; (b) 5 h; (c) 13h	97
Figure IV.21: Evolution of main product families in the organic phase as a function of reaction time..	98
Figure IV.22: Evolution of aromatics, naphthenes and alkylphenols as a function of reaction time	99
Figure IV.23: Tetralin/naphthalene mass ratio as a function of reaction time	100
Figure IV.24: Progressive transformation scheme of lignin to oligomers and monomers under catalytic hydroconversion with CoMoS/Al ₂ O ₃	102
Figure IV.25: Distribution of lignin hydroconversion products with and without catalyst.....	104
Figure IV.26: Gaseous production distributions with and without catalyst	104
Figure IV.27: Performance comparison of lignin conversion between the semi-batch system and the conventional batch system	105
Figure IV.28: Comparison of H ₂ consumption between the semi-batch system and the conventional batch system.....	106
Figure V.1: Principle of RTD measurements	111

Figure V.2: Concentration-time curve at the inlet and outlet of the reactor for a pulse injection	111
Figure V.3: E(t) curves of ideal reactors: (a) CSTR; (b) PFR.....	112
Figure V.4: Schematic representation of Tanks-in-series model.....	113
Figure V.5: E(t) of Tank-in-series model in function of the number of CSTRs.....	113
Figure V.6: Concentration profile for a typical pseudo-component in the model	114
Figure V.7: Schematic diagram of the experimental set-up for RTD tests and k_La measurements.....	116
Figure V.8: Physical representation of the experimental set-up.....	118
Figure V.9: Model structure and parameter estimation procedure for this study.....	120
Figure V.10: Comparison between experimental (marker) and simulated (line) data after the optimization of n_{CSTR} at ambient temperature.....	122
Figure V.11: Comparison between experimental (marker) and simulated (line) data after the optimization of n_{CSTR} in the case where the temperature of reactor is 350 °C and the temperature of reflux condenser is 170 °C	122
Figure V.12: Experimental RTD curves in function of the temperature of reflux condenser	124
Figure V.13: Comparison between experimental (marker) and simulated (line) data of Test 6 (100 g of tetralin, $T_{Reactor} = 350$ °C, $T_{Reflux} = 170$ °C).....	125
Figure V.14: Comparison between experimental (marker) and simulated (line) data at different temperatures of reactor under the flowrate of 40 NL/h	126
Figure V.15: Product distributions in the reactor and the separator versus time.....	131
Figure V.16: Schematic representation of our general model (black: liquid, white: gas)	133
Figure V.17: Process flow diagram used for the flash calculation under Prosim Plus.....	137
Figure V.18: Model structure and parameter estimation procedure	138
Figure V.19: Comparison between experimental data and model outputs at different residence times	141
Figure V.20: Comparison between the calculated outlet gas flow and experimental data	141
Figure VI.1: Reaction network for catalytic lignin hydroconversion	147
Figure VI.2: Simplified reaction network used for the kinetic model.....	148
Figure VI.3: Evolution of THF-solubles _A and THF-solubles _B in the model.....	149
Figure VI.4: Estimation of the liquid molar volume of lump “aromatics” by interpolation method	152
Figure VI.5: Estimation of the equilibrium constant of lump “alkylphenols” by interpolation method	153
Figure VI.6: Estimation of α_i for lump “alkylphenols” by interpolation method.....	155
Figure VI.7: Comparison between experimental data and model results for the yield of THF-insolubles, THF-solubles and solubilized oligomers versus reaction time	157
Figure VI.8: Comparison between experimental data and model results for outlet flowrate of CO ₂ and CH ₄ versus reaction time.....	157
Figure VI.9: Comparison between experimental data and model results for outlet flowrate of CO and C ₂ -C ₆ versus reaction time	158

Figure VI.10: Comparison between experimental data and model results for outlet H ₂ flowrate versus reaction time	158
Figure VI.11: Comparison between experimental data and model results for outlet H ₂ flowrate versus reaction time	159
Figure VI.12: Comparison between experimental data and model results for the liquid composition in the reactor versus reaction time	160
Figure VI.13: Comparison between experimental data and model results for the liquid composition in the separator versus reaction time.....	160

List of Schemes

Scheme I.1: Schematic representation of the lignin sulfonation	9
Scheme I.2: Schematic representation of lignin copolymerization with lactide ⁴⁸	18
Scheme I.3: Mechanism of stabilizing radicals by tetralin	30
Scheme II.1: Acetylation of hydroxyl groups in lignin	50
Scheme II.2: Reaction of tag hydroxyls presented in lignin with 2-chloro-4,4,5,5-tetramethyl-1,3,2-dioxaphospholane ³	50
Scheme IV.1: Reaction scheme A of lignin hydroconversion	71
Scheme IV.2: Reaction scheme of decarboxylation	73
Scheme IV.3: Reaction scheme of demethylation and demethoxylation of -OCH ₃	73
Scheme IV.4: Reaction scheme B of lignin hydroconversion	76
Scheme IV.5: Breakup of ether bonds and creating of free phenolics OH.....	79
Scheme IV.6: Methyl-substitution reaction due to a heterolytic cleavage of -OCH ₃ bond	79
Scheme IV.7: Reaction scheme C of lignin hydroconversion	84
Scheme IV.8: Reaction scheme D of lignin hydroconversion	87
Scheme IV.9: Conversion of cutin-like moieties to long-chain alkanes.....	91
Scheme IV.10: Transformation of methoxy-substituted phenols to alkylphenols	93
Scheme IV.11: Conversion of the ferulic acid ester into 4-ethylphenol.....	93
Scheme IV.12: Conversion of benzofurane entities into 2-ethylphenol	94
Scheme IV.13: Reaction scheme for hydrodeoxygenation of alkylphenols	99
Scheme IV.14: General depolymerization of lignin.....	103
Scheme IV.15: Transformation of monomers in the liquid phase	103

General Introduction

Thesis background

Lignin, along with cellulose and hemicellulose, is one of the principal organic substrates in lignocellulosic biomass. Being the second most abundant biomass component, it is an aromatic-based macromolecule which can be the perfect precursor of aromatic compounds for the chemical industry. It is originally constructed by three phenylpropane units and interconnected by C-O-C bonds and C-C bonds. Nowadays, as a byproduct from the paper industry, it has a production of 50 million tons/year and mainly valorized as a low-value fuel to generate heat and electricity. Considering the announced development of biorefinery for cellulosic ethanol, more and more lignin can be co-produced in a near future. In this context, finding a practical way of lignin valorization instead of simple combustion is highly desirable. However, after fractionation process, lignin could be more condensed (C-C bonds), mixed with inorganics (Ca, Na, Si, *etc.*) and also could contain water and rest of hemicellulose, and cellulose. Different thermochemical approaches have been investigated, including the utilization for producing materials (carbon fiber, polymers, *etc.*) and the conversion to platform chemicals (phenols, aromatics, cycloalkanes, *etc.*).

In order to obtain platform chemicals, lignin must be depolymerized into monomers by thermochemical methods through C-O or C-C bond cleavage. Among the different methods (pyrolysis, gasification, hydrolysis and hydroconversion) proposed in the literature, it appears that lignin hydroconversion under H₂ pressure using a hydrotreating catalyst in the presence of a H-donor solvent was the most promising way to get high yields of liquid products. Effectively, the use of solvent such as tetralin, alcohols and formic acid strongly reduced the condensation reactions between formed radicals and thus increased the depolymerization. Concerning the catalysts, various types of solids were employed for the lignin conversion, including zeolites (e.g., HZSM-5), supported noble metals (e.g., Pd/C, Pd/Al₂O₃, Ru/HZSM-5, Ru/TiO₂, Ru/C), metal chlorides (e.g., ZnCl₂, CuCl₂, AlCl₃) and conventional bimetallic oxides or sulfides (e.g., NiMo/Al₂O₃, CoMo/Al₂O₃). With the participation of some of these catalysts, it has been reported that the depolymerization of lignin and the hydrogenolysis/hydrogenation reactions are promoted, leading to a high yield of deoxygenated liquid products.

Kinetic modeling can play an important role in understanding, describing and scaling-up the lignin conversion. According to our knowledge, kinetic modeling studies of lignin conversion are quite scarce due to the lack of complete characterization of lignin feedstock, the limitation of characterization tools for numerous products and the relatively complex reaction network. Moreover, under the conditions of high temperature and pressure, the study of vapor-liquid equilibrium (VLE) appears necessary to correctly illustrate the phase distribution. By neglecting the liquid vaporizations and gas dissolutions for a heterogeneous reaction, the modeled reaction kinetics are always impacted.

Thesis objectives

In the framework of French National Research Project "LIGNAROCAT", the aim of this thesis was to investigate the reaction mechanisms and develop a kinetic model for catalytic lignin hydroconversion over a sulfided CoMoS/Al₂O₃ catalyst. The work consisted of two main parts:

- The first part focused on the experimental kinetic study of catalytic hydroconversion of a wheat straw soda lignin using sulfided CoMoS/Al₂O₃. The kinetic measurements were carried out in a H-donor solvent (tetralin) at 350 °C and 80 bar using a semi-continuous batch reactor, which is opened on the gas phase with continuous supply of H₂ and equipped with a condensing reflux followed by cooled traps. The recovered products were isolated in four fractions: gases (methane, carbon dioxide, light alkanes, *etc.*), organic liquid (phenols, aromatics, naphthenes, *etc.*), THF-soluble and THF-insoluble residues. Thanks to several appropriate analytical tools (GPC, NMR, GC×GC, *etc.*), the evolution of these different fractions as a function of reaction time was followed in order to understand the transformations occurring during the conversion. Accordingly, a lumped reaction network was established based on the observed reaction mechanisms.
- The second part was dedicated to the development of a kinetic model, which allows to better understand and to describe mathematically each reaction step involved in the catalytic hydroconversion of lignin. In order to achieve the accurate kinetic parameters, many chemical engineering aspects (the gas hydrodynamic behavior of our set-up, the VLE of mixtures and the liquid-gas mass transfer) were emphasized and characterized. Taking the gathered experimental data as a basis, reliable kinetic parameters (rate constants and stoichiometric coefficients) for each reaction step were obtained by means of non-linear regression technique.

Thesis outline

The thesis is divided in six chapters:

- ❖ Chapter I: It gives a literature review on lignin itself (composition, structure and properties), different processes for lignin isolation and different approaches of lignin valorization (particularly hydroconversion). With regard to lignin hydroconversion, the reaction mechanisms and products, the solvents and the catalysts employed are presented. The development of kinetic modeling for lignin conversion is also discussed.
- ❖ Chapter II: It presents the materials and methods used in our experiments, as well as the description of the experimental set-up and protocols.
- ❖ Chapter III: It shows the characterization of the wheat straw soda lignin used in this work.
- ❖ Chapter IV: The experimental results of lignin catalytic hydroconversion using CoMoS/Al₂O₃ are presented and discussed. The relevant products properties and compositions were determined and rationalized according to the residence time so as to elucidate the chemical transformations occurring during the conversion. Based on the experimental observations, a suitable reaction network was proposed.
- ❖ Chapter V: The following issues of gas hydrodynamics, gas/liquid (G/L) mass transfer and thermodynamic model for VLE are addressed. Gas hydrodynamics was realized by Residence Time Distribution (RTD) measurements and a volumetric mass transfer coefficient ($k_L a$) was estimated on the basis of the N₂ absorption/desorption phenomena in solvent. The choice of thermodynamic VLE model and a physical representation of the reflux condenser were finally described.
- ❖ Chapter VI: A complete reactor model is built by coupling the chemical kinetic model and the physical characterizations of our reaction system. The kinetic parameters (rate constants and stoichiometric coefficients) for each reaction step were estimated by minimization of the sum squared differences between the gathered experimental data and the model outputs. A discussion of estimated parameters was also undertaken at the end of this chapter.

Chapter I. State of the Art

I.1 Lignin overview

Lignin, along with cellulose and hemicellulose, is one of the principal organic compounds in lignocellulosic biomass¹. A schematic representation of the structure in lignocellulosic biomass is given in Figure I.1. Cellulose, the main structural component of cell walls, is a long linear chain of several hundred to thousand glucose units, linked to one another primarily by glycosidic bonds. Hemicellulose is rather a family of polysaccharides, composed of different five and six carbon monosaccharide units, linking cellulose and lignin to create a complex network of bonds to provide structural strength. Finally, lignin, a three-dimensional polymer of phenylpropanoid units, plays a vital role in providing mechanical support and forming an effective barrier against attack by insects and fungi.

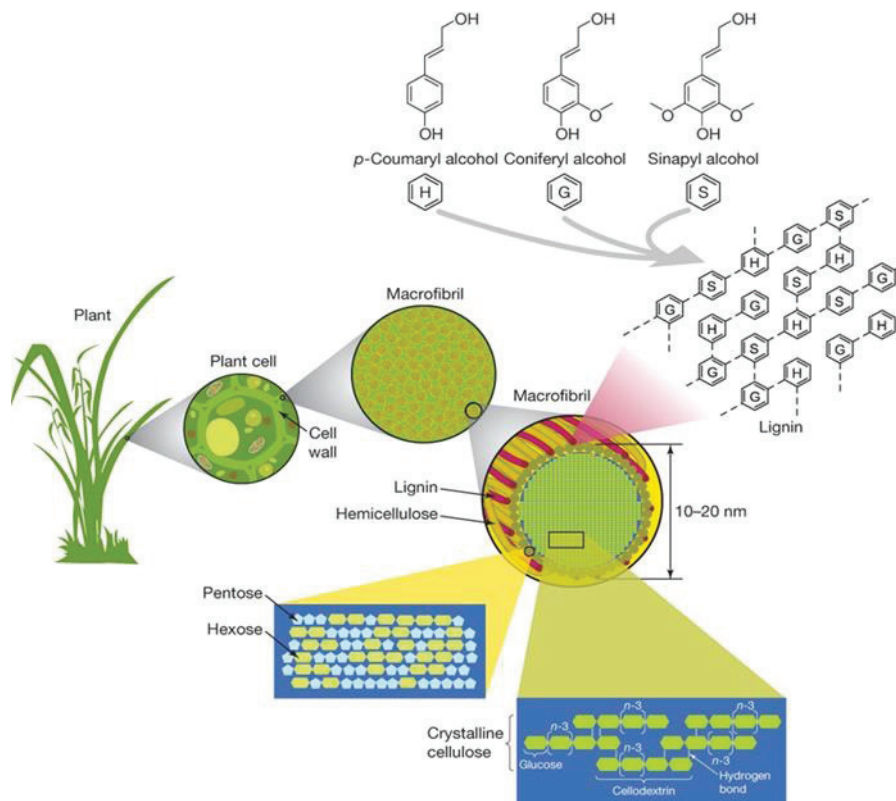


Figure I.1: Schematic representation of structure in lignocellulosic biomass²

In nature, the mass composition of lignocellulosic biomass highly depends on its source whether it is derived from hardwood, softwood, corn cob or grass. Table I.1 presents the typical mass composition of three components among different sources¹.

Table I.1: Mass composition of lignocellulosic compounds among different sources

Source	Cellulose (wt%)	Hemicellulose (wt%)	Lignin (wt%)
Sugarcane bagasse	42	25	20
Sweet sorghum	45	27	21
Hardwood	40-55	24-40	18-25
Softwood	45-50	25-35	25-35
Corn cobs	45	35	15
Corn stover	38	26	19
Rice straw	32.1	24	18
Nut shells	25-30	25-30	30-40
Newspaper	40-55	25-40	18-30
Grasses	25-40	25-50	10-30
Wheat straw	29-35	26-32	16-21
Banana waste	13.2	14.8	14
Bagasse	54.87	16.52	23.33
Sponge gourd fiber	66.59	17.44	15.46

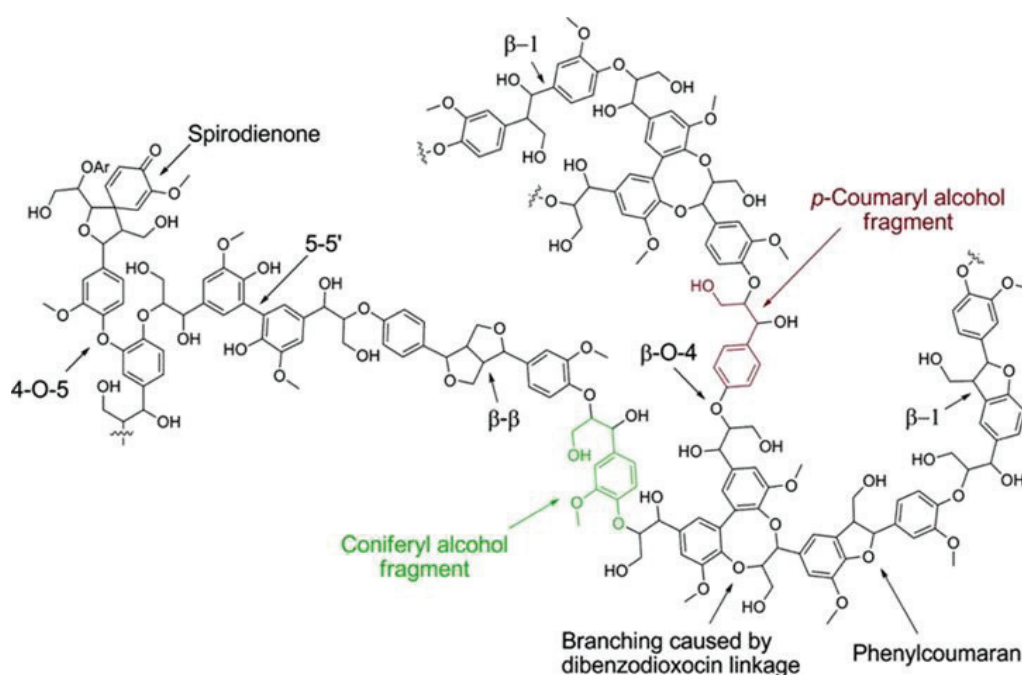


Figure I.2: Structure model of lignin from softwood³

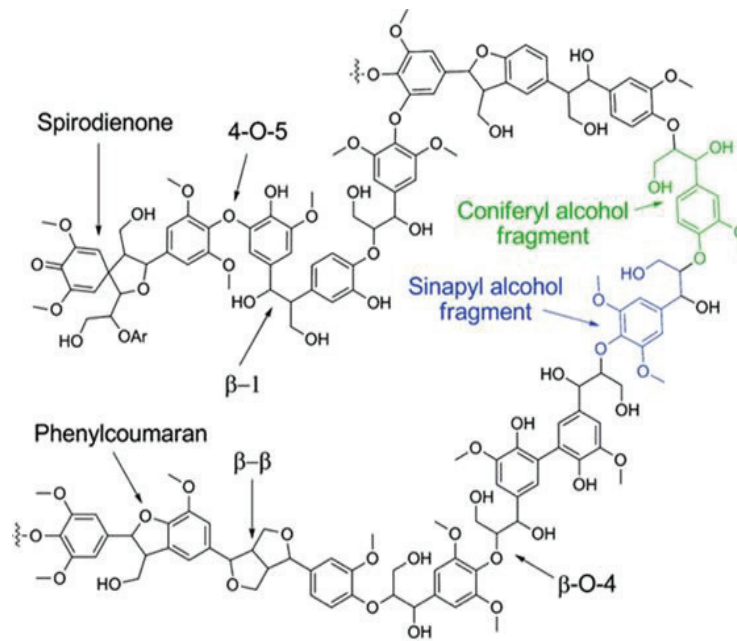


Figure 1.3: Structure model of lignin from hardwood²

Table 1.2: Percent composition of phenylpropane units among different sources⁴

Name	<i>p</i> -Coumaryl [H]	Coniferyl [G]	Sinapyl [S]
Monomer structure			
Softwood (%)	-	90-95	5-10
Hardwood (%)	-	50	50
Grass (%)	5	75	25

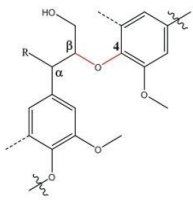
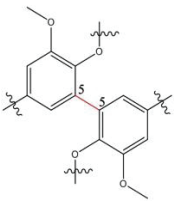
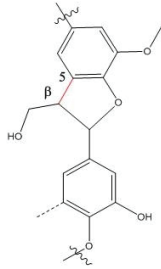
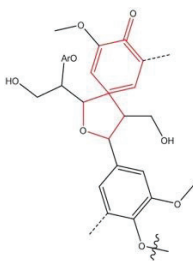
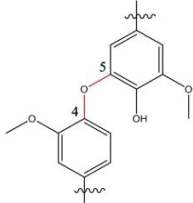
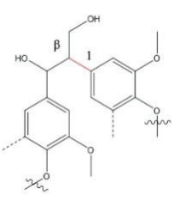
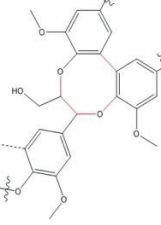
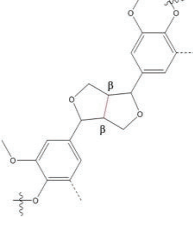
1.1.1 Lignin structure

Lignin is a complex biopolymer consisting of methoxylated phenylpropane units. Figure 1.2 and 1.3 show the proposed structural models of lignin extracted from softwood and hardwood, respectively. As seen, lignin makes up of three basic units (*p*-coumaryl [H], coniferyl [G] and sinapyl [S]). These three units are derived from three phenylpropane alcohols that contain zero until two methoxy groups (-OCH₃), forming the structure of lignin by enzymatic dehydrogenated polymerization². The composition of phenylpropane units varies largely among different sources, as listed in Table 1.2. Compared to hardwood, softwood contains a higher proportion of coniferyl units whereas no *p*-coumaryl units present in both of them. However, a small quantity of *p*-coumaryl units (5 %) existed in the grass.

I.1.2 Interunit linkages and functional groups

Regarding the lignin framework, it is constructed by interunit linkages between monomers and monomers, monomers and oligomers and oligomers and oligomers. The phenylpropane units are mainly connected by ether (C-O-C) and carbon-carbon (C-C) bonds. Among different types of linkages shown in Table I.3, β -O-4 (β carbon in branched-chain connecting with 4 aryl-carbon by an oxygen atom) and 5-5 (5 aryl-carbon connecting with 5 aryl-carbon) linkages are found to be the most abundant ones, constituting approximately 45-62 % and 3-27 % in lignin, respectively⁵. The remaining, less abundant (< 10 %) linkages existing in lignin include β -5, 4-O-5, β -1, and so on. As shown in Table I.3, the proportions of these linkages vary significantly among various resources.

Table I.3: Common linkage structures and approximate abundance connecting the phenylpropane units in softwood and hardwood lignin

Linkage	β -O-4	5-5	β -5	Spirodienone
Structure				
Hardwood (%)	45-50	19-27	9-12	n.d.
Softwood (%)	60-62	3-9	3-11	3-5
Linkage	4-O-5	β -1	Dibenzodioxocin	β - β
Structure				
Hardwood (%)	4-5	7-9	n.d.	2-6
Softwood (%)	6.5-9	1-7	1-2	3-12

* n.d. = not determined

Apart from these interunit linkages, lignin macromolecules also contain a variety of functional groups which result in the reactivity of lignin. Lignin contains methoxy groups, phenolic hydroxyl groups, benzyl alcohols, carbonyl groups and aliphatic hydroxyl groups. Only a small proportion of phenolic OH groups are free since most of them are occupied to form ether linkages with other phenylpropane units. Benzyl alcohols and carbonyl groups are incorporated into the lignin structure during the enzymatic dehydrogenation. Table I.4 illustrates the percentage of some common functional groups found in hardwood and softwood lignin⁶. As seen, there are more methoxy groups in hardwood than in softwood, since there are more sinapyl units in it.

Table I.4: Functional groups per 100 phenylpropane units in lignin

Group	Softwood	Hardwood
Methoxy	92-97	139-158
Phenolic hydroxyl	15-30	10-15
Benzyl alcohol	30-40	40-50
Carbonyl	10-15	n.d.

1.2 Lignin isolation processes

In lignocellulosic biomass, lignin is co-existing with cellulose and hemicellulose. Regardless of whether compound we desired to obtain, the isolation process is mandatory to get relative pure one. In pulping manufacture, massive lignocellulosic biomass is used as raw material to produce papers. The principle is removing lignin and hemicellulose as much as possible without disturbing the cellulose fibers. In general, isolation processes can be classified into two main categories: solvent fractionation (kraft, sulfite, soda and organosolv pulping), and biological treatment (using fungi). Thus, lignin is isolated from lignocellulosic biomass, as a waste product after pulping.

1.2.1 Kraft process

Kraft pulping is the most dominant technique employed in chemical pulping industry, with about 90 % of total lignin production. In this process, it uses a considerable amount of aqueous NaOH and Na₂S (white liquor) at a temperature range of 155-175 °C for several hours to dissolve about 90-95 % of lignin and hemicellulose presenting in the starting biomass⁷. Then, cellulose is separated as a solid from the solution. After pulping, the mixture of lignin and hemicellulose that is dissolved in the pulping stage is known as “black liquor”.

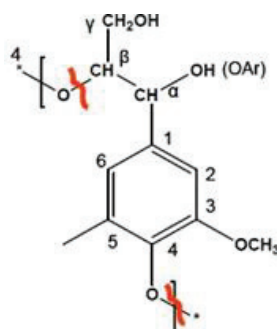


Figure I.4: Broken bonds during kraft process⁸

According to Tejado *et al.*⁸, kraft process partially cleaves β -O-4 and α -O-4 linkages (Figure I.4), resulting in massive amounts of non-etherified phenolic groups in the lignin structure (Figure I.5). Since kraft lignin has no sulfonate groups, it is only soluble in alkaline solution (pH > 10). Therefore, kraft lignin can be precipitated from black liquor by lowering the pH to 10 with a suitable acid.

Although kraft process is the most used isolation process worldwide, the recovery of kraft lignin for commercial uses is not very extended because isolated kraft lignin is mainly sent to a recovery system where it is burned for process heating. Until nowadays, kraft lignin with high purity is currently produced by MeadWestvaco, the world's largest producer of kraft lignin at a scale of about 60 kt/year¹⁰, and by the LignoBoost technology, a demonstration pilot owned by Mesto Corporation with an annual production of 4 kt, in which lignin is extracted from pulping mill black liquor¹¹.

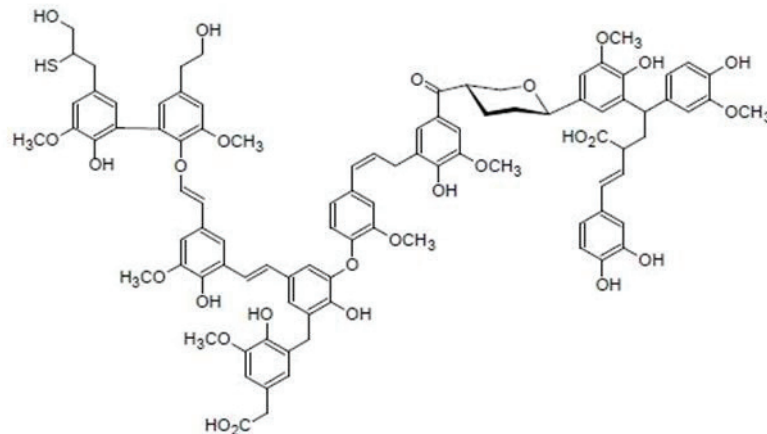
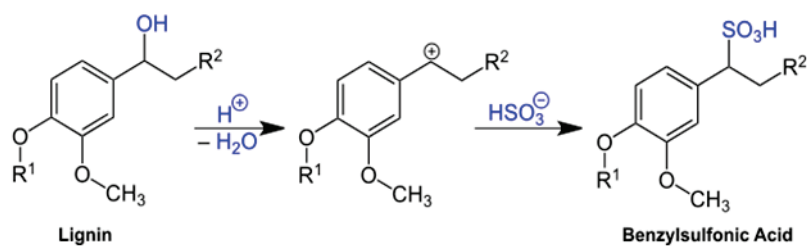


Figure 1.5: Structure model of kraft lignin⁹

1.2.2 Sulfite process

As kraft process has become the most widely used pulping method in the world, the early sulfite process has dramatically decreased to less than 10 % of the total pulping industry¹². In principle, the sulfite pulping is more flexible compared to kraft pulping since it can be implemented in the entire pH range by changing the dosage and the composition of cooking chemicals¹³. Typical chemicals used in the process are based on an aqueous sulfur dioxide and a base such as calcium (Ca⁺²), sodium (Na⁺) or magnesium (Mg⁺²) as the counterion. The pulp is in contact with the cooking chemicals for 4-14 hours at temperatures ranging from 125 to 180 °C.

During the pulping process, the principal reaction occurring is the sulfonation of lignin through the introduction of sulfonic acid to the α -carbon atoms (Scheme 1.1). The sulfur content of obtained lignin namely liginosulfonate (Figure 1.6), is rather higher than kraft lignin, making liginosulfonate soluble over almost the entire pH range⁹. Sulfite pulping does not selectively remove lignin and cellulose fibers, so cellulose appears to be chemically attached to the liginosulfonate fragments. Thus, purified lignin is obtained by the removal of cellulose impurities by additional treatment, such as fermentation, ultrafiltration or chemical separation¹⁴. Nowadays, liginosulfonate has developed an excellent destination market to cement industry as the additive and to make concrete and plasticizers¹⁵. Main commercial producers worldwide are LignoTech, Rayonier, La Rochette Nippon Paper and Domsjo Farbriker with total production around 1000 kt/year¹⁰.



Scheme I.1: Schematic representation of the lignin sulfonation

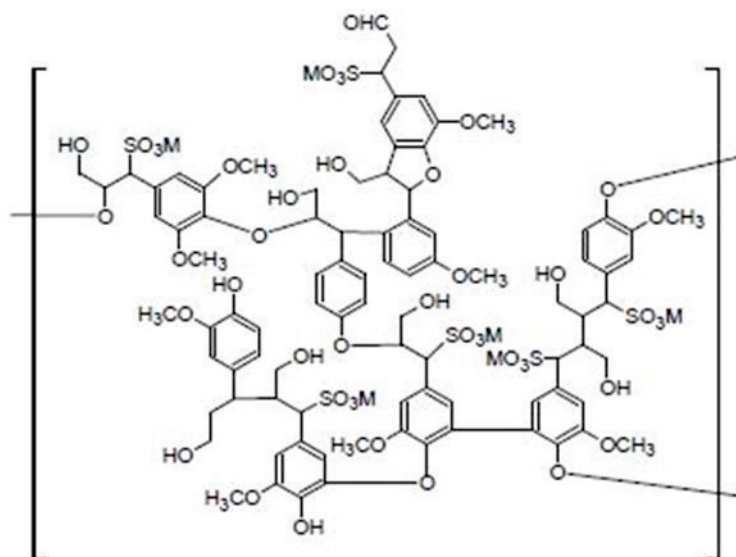


Figure I.6: Structure model of liginosulfonate⁹

I.2.3 Soda process

Soda pulping is a chemical process using NaOH instead of sulfide sodium as the cook chemical, accounting for nearly 5 % of the total pulp production¹². The typical feedstock used in soda pulping includes agricultural wastes such as straw and bagasse, which have lower lignin contents. Soda process involves the partial cleavage of the ether bonds via the formation of small quantities of phenolic hydroxy groups and the loss of the primary aliphatic hydroxyls (Figure I.7).

The disadvantage of the soda process is that cellulose is also degraded together with lignin. In order to decrease the cellulose degradation, anthraquinone (AQ) has been proposed to use as a catalytic additive. Currently, it is only commercially operated by GreenValue Company with a production of 5-10 kt/year¹⁷. Although the rate of lignin removal is still lower compared to conventional processes, it is expected that alkali lignin from soda pulping may become more and more important in the context of biorefinery as alkali lignin is essentially sulfur-free.

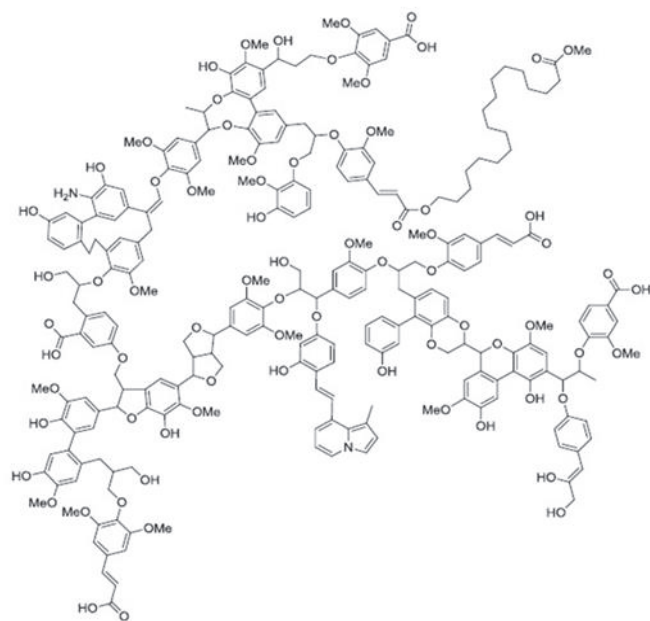


Figure 1.7: Structure of alkali lignin¹⁶

1.2.4 Organosolv process

The organosolv process refers to a group of the pulping process based on organic solvents. This process causes lignin to break down by partial hydrolytic cleavage of ether bonds. Majority of organic solvents involved are alcohols such as methanol and ethanol (or mixed with water), or organic acids such as formic and acetic acids. The principal advantage of this process is that it can isolate cellulose, hemicellulose, and lignin essentially, allowing each fraction to implement a more specific downstream process. Furthermore, the process is generally considered environmentally friendly compared to conventional processes owing to its sulfur-free and less-condensed structure (Figure 1.8). The major organosolv processes are the following:

- Alcell process of Lignol Innovation: the process uses aqueous ethanol solutions (40-60 vol%) to remove lignin from wood at the temperature from 180-210 °C and 2-3.5 MPa. Ethanol is recovered by flash evaporation, vapor condensation, and vacuum stripping¹⁹.
- CIMV process: wheat straw is treated with acetic acid/formic acid/water (30/55/15 vol%) for 3.5 h at 105 °C under atmospheric pressure²⁰.

However, considering the high cost of solvent recovery, these processes are not commercial yet but have been demonstrated at pilot and demonstration scale with a total production of less than 4 kt/year¹⁰.

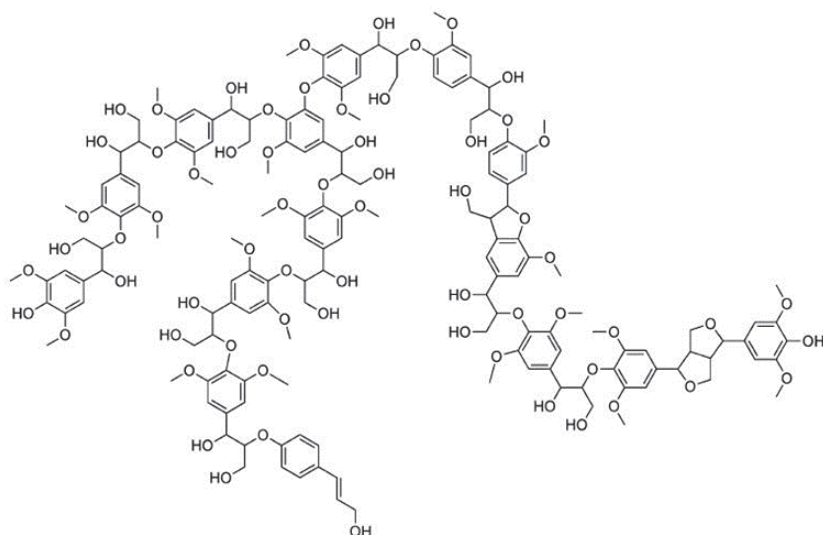


Figure 1.8: Structure model of organosolv lignin¹⁸

1.2.5 Comparison of technical lignins

A standard procedure for lignin isolation does not exist, lignin from different isolation processes, so-called technical lignin, vary largely in chemical structure and composition. However, all the technical lignins undergo significant structural and functional changes regardless of the methods and the feedstock of plant employed, making them different from raw lignin. A comparison of monomeric molecular formula and weight of lignin obtained from different isolation processes is included in Table 1.5. From monomer molecular formula, sulfur is incorporated in the structure of lignin obtained from kraft and sulfite processes. Moreover, lignosulfonate displays a higher monomer molecular weight, due to a more significant content of sulfur.

Table 1.5: Monomer molecular formulas and weights of lignin from various sources³

Type	Monomer molecular formula	Monomer molecular weight (g/mol)
Kraft lignin	$C_9H_{8.5}O_{2.1}S_{0.1}(OCH_3)_{0.8}(CO_2H)_{0.2}$	180
Lignosulfonate (Softwood)	$C_9H_{8.5}O_{2.5}(OCH_3)_{0.85}(SO_3H)_{0.4}$	215-254
Lignosulfonate (Hardwood)	$C_9H_{7.5}O_{2.5}(OCH_3)_{0.39}(SO_3H)_{0.6}$	188
Organosolv lignin	$C_9H_{8.53}O_{2.45}(OCH_3)_{1.04}$	n.d.
Alkali lignin	$C_9H_{8.53}O_{2.45}(OCH_3)_{1.04}$	188

In reality, the variety of technical lignin is not yet represented in the industrial scale because isolation, purification, and drying add up to the cost of producing lignin. Lignin sale prices vary from 50-500 euros/ton depending on the isolation processes as well as the quality of lignin¹¹. The low-grade lignin with the lowest purity and the most massive production, representing the lowest price between 50-100 euros/ton, is co-produced by the pulping industry and biorefinery. However, the low quality hampers its valorization and is currently used mainly as an energy source. Following by the low grade lignin, lignosulfonate with a price of 250-350 euros/ton is produced by 1 Mt/year. Kraft, soda and

organosolv lignin with a much lower production, which could be produced with higher purity, represent a higher price between 350-500 euros/ton.

A comparison of the advantages and disadvantages of different isolation processes is shown in Table I.6, with taking all the factors (availability, property and price) into consideration.

Table I.6: Advantages and disadvantages of various technical lignins²¹

Isolation process	Advantages	Disadvantages
Kraft process	<ul style="list-style-type: none"> (1) High availability (2) Low price (3) High phenolic content 	<ul style="list-style-type: none"> (1) Contains sulfurs (2) Contains repolymerization products (3) Partially contains hemicelluloses (4) Low side-chain functionality (5) Mostly insoluble in organics (6) Variation in quality
Sulfite process	<ul style="list-style-type: none"> (1) High availability (2) Low price (3) Soluble in water 	<ul style="list-style-type: none"> (1) Contains sulfurs (2) Contains repolymerization products (3) Partially contains hemicellulose (4) Mostly insoluble in organics (5) Low side-chain functionality (6) Low phenolic content (7) Aliphatic functionalities blocked by sulfonic acid groups
Soda process	<ul style="list-style-type: none"> (1) High availability (2) Low price (3) Sulfur free (4) High aliphatic and aromatic functionality (5) Partially soluble in organics 	<ul style="list-style-type: none"> (1) Partially contains hemicellulose (2) Variation in quality (3) High silicate content in annual plants
Organosolv process	<ul style="list-style-type: none"> (1) Sulfur free (2) Hemicellulose free (3) Constant quality (4) High solubility in organics 	<ul style="list-style-type: none"> (1) Low availability (2) High cost (3) Aliphatic hydroxyl and phenol groups etherified

I.3 Properties of lignin

I.3.1 Molecular weight distribution

In polymers, the individual polymer chains rarely have the same degree of polymerization and molecular weight, so there is always a distribution of molecular weight. As lignin is a non-uniform biopolymer, the determination of its molecular weight distribution is one of the principal approaches to study to understand the reactivity and physicochemical properties of lignin. The two common averages to characterize its molecular weight are the number average molecular weight (M_n) and the weight average molecular weight (M_w). The polydispersity index (PDI) indicates the uniform degree of the polymers. The value of PDI is close to 1, indicating that the unit chains of the polymer are more uniform. Tolbert *et al.* tested several technical lignins from different isolation processes and sources, seen in Table I.7. All the three parameters significantly vary in magnitude depending on its sources and isolation methods.

Table I.7: M_n , M_w , and PDI in comparison with technical lignin isolated from different processes²²

Isolation process	Source	M_w (g/mol)	M_n (g/mol)	PDI
Kraft process	Birch	19650	7523	2.7
	Hardwood	3300	1000	3.3
	Softwood	6500	1600	4.1
	Spruce + Pine	4500	1000	4.5
Sulfite process	Pine	1440	810	1.8
	Softwood	14000	4800	2.9
Soda process	Bamboo	2840	1860	1.5
	Poplar	2330	1510	1.5
	Rye Straw	8000	1670	4.8
Organosolv process	Bamboo	3260	1680	1.9
	Birch	10860	5860	1.9
	Poplar	8550	3170	2.7
	Rye Straw	8680	1701	5.1

I.3.2 Solubility

Native lignin, showing a three-dimensional network and a polar aromatic polymer, behaves as insoluble in most of the common solvents at ambient temperature. However, a partial dissolution can be obtained in aqueous NaOH solution at a temperature higher than 100 °C, which is already employed by soda pulping¹². Compared to native lignin, technical lignins are more soluble in a wide range of solvents and temperatures since isolation processes modify the structure and the functional groups, and decrease the molecular weight of native lignin, which may improve its solubility. Depending on the isolation process, isolated lignins with different solubility can be obtained. For example, kraft lignin is only soluble in alkaline solutions whereas lignosulfonate is water-soluble over an entire pH range.

The ability of solvents to dissolve a variety of technical lignin is reported to be associated to their hydrogen-bonding capacities²³. Typical solvents are dioxane^{24,25}, acetone²⁵, tetrahydrofuran (THF)¹⁶, and dimethyl sulfoxide (DMSO). Therefore, acetone and THF are widely used as extraction solvents for residual lignin in literature.

1.3.3 Thermal behavior

For the depolymerization of lignin, it is usually thought that the first reaction step is the thermal rupture of lignin linkages to small molecular units (oligomers, monomers, and gases). An example of thermal analysis of lignocellulosic components is shown in Figure 1.9, indicating the thermal stability of cellulose, hemicellulose, and lignin. A sharp peak of mass loss rate before 400 °C was observed for both cellulose and hemicellulose, corresponding to a fast formation of volatile products. However, only a small peak of mass loss rate was noticed between 80 and 200 °C for lignin, probably corresponding to a fast elimination of water. Overall, lignin decomposes much lower, over a broader temperature range (200-800 °C) than cellulose and hemicellulose.

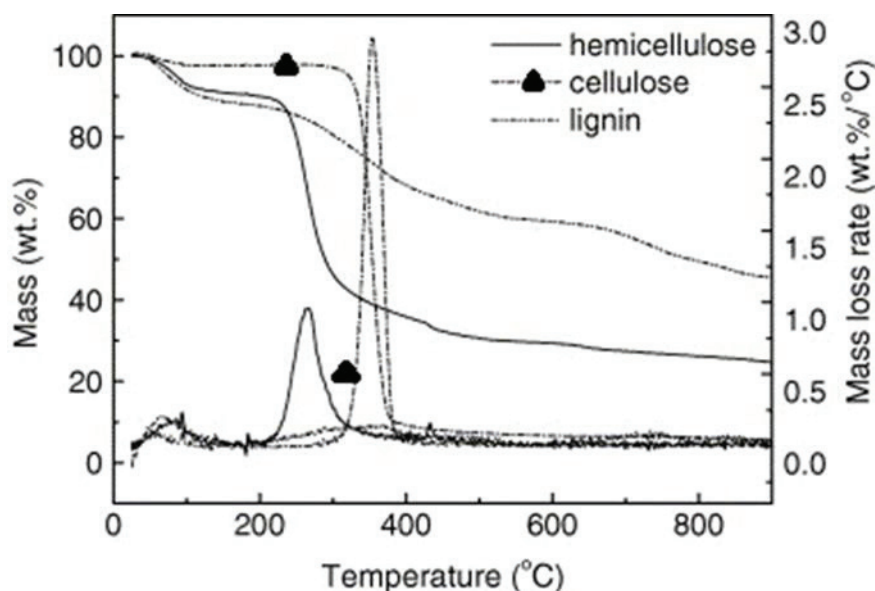


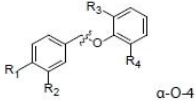
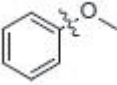
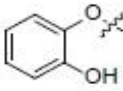
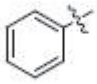
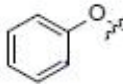
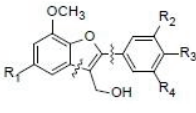
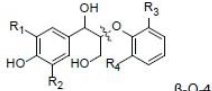
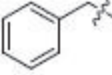
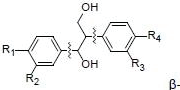
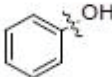
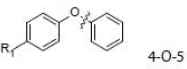
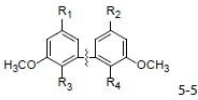
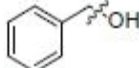
Figure 1.9: Thermal degradation curves of cellulose, hemicellulose, and lignin²⁶

Apparently, slow thermal decomposition of lignin can be explained by its complex composition and structure. Different linkages in lignin have different thermal stability, thus their ruptures occur at different temperatures. Table 1.8 presents the calculated bond dissociation enthalpies (BDE) of typical linkages in lignin model compounds reported in literature. BDE represents the energy needed to break the bond. As the temperature increases, it was also proved by experimental results that the most likely bond ruptures in order are:

- 1) Ether bonds (α -O-4, methoxy groups, and β -O-4)^{28,29};
- 2) The homolytic cleavage between C_{ar} and C_{β} (β -5, β -1), C_{ar} and C_{α} ³⁰.
- 3) C_{ar} -OH and C_{ar} - C_{ar} (5-5)³¹.

As such, at the relatively low temperature, ether bonds are easy to be broken thermally. The main challenge of lignin thermal decomposition is to cleave C_{ar} -OH and C_{ar} - C_{ar} , which have higher BDEs.

Table I.8: Bond dissociation enthalpies (BDE) for lignin linkages²⁷

Model compounds	BDE (kJ/mol)	Model compounds	BDE (kJ/mol)
 α -O-4	220±16		419±4
	235±4		427±4
	263±4	 β -5	430±8
 β -O-4	281±1		435±4
 β -1	289±2		463±4
 4-O-5	332±7	 5-5	482±12
	334±4		

During thermal decomposition, many valuable monomeric compounds are decomposed directly from lignin or further reactions of lignin fragments, as shown in Figure I.10, including aromatic hydrocarbons and lots of oxygenated products having phenolic OH groups that match exactly with calculated BDEs. Meanwhile, some highly reactive and unstable free radicals may further react through rearrangement or radical-radical interaction, to form irreversible products known as char or coke with high thermal stability³³. Some acetic acids and non-condensable gases, the main of which are CO, CO₂, and CH₄, are also released during thermal decomposition.

Catalytic thermal cracking is a process extensively employed in petroleum refineries to convert high-boiling hydrocarbons into more valuable products by C-C bond cleavage³⁴. In this context, lignin is thought to be cracked catalytically as well, to cleave ether bonds, some weak C-C bonds, and hydroxyl groups. Catalysts, consisting of zeolites or amorphous silica-alumina with various compositions, were reported to be active for the cracking of lignin³⁵⁻³⁷. The performance of these catalysts is found to be strongly dependent on the structural characteristics of the catalysts, including the pore size and the presence and strength of acid sites³⁶. The effectiveness of the catalysts in reducing coke formation decreased with increasing the pore size³⁵. The acidity of the catalyst is favorable in cracking the lignin.

Additionally, water is found to have an opposite effect on catalyst performance by decreasing the number of acid sites in the catalyst³⁵.

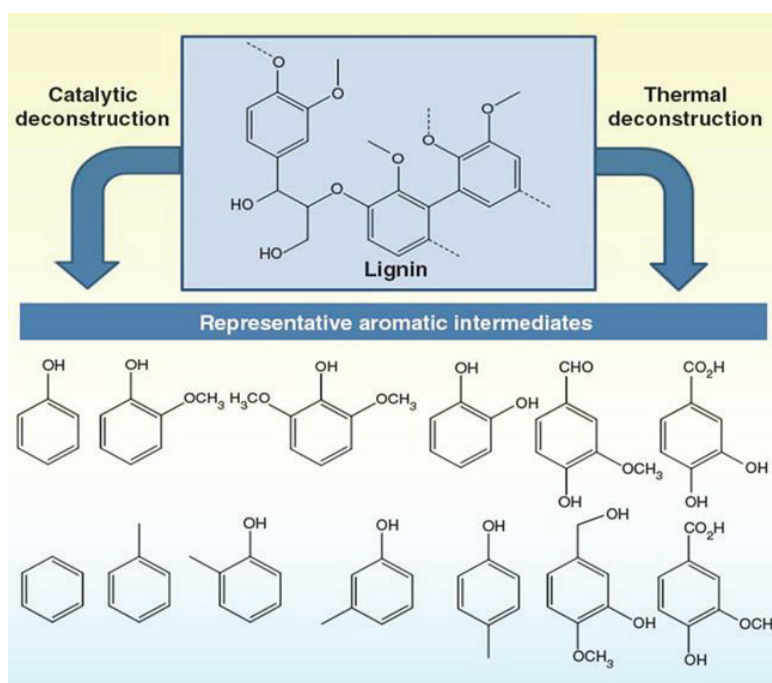


Figure I.10: Generalized catalytic and thermal decomposition of lignin to low-molecular-weight compounds³²

I.3.4 Conclusion of lignin overview

In nature, a huge amount of lignin exists as an organic substance, constituting wood and plants. It is an aromatic macromolecule, constructed by three types of phenylpropane units. These units are interconnected by several types of linkages, mainly are ether bonds and C-C bonds. In addition, the composition of lignin and the proportion of linkages vary among various resources.

Different isolation processes are employed to get isolated lignin from lignocellulosic biomass, especially solvent fractionation. Owing to the variety of biomass resources and solvents used, technical lignin varies in their chemical composition, as well as their properties. Thus, good knowledge of targeted lignin is indispensable before the investigation. In view of the natural aromatic structure and the functional groups existing in lignin, the interesting pathways to lignin valorization must be based on these intrinsic properties.

I.4 Lignin valorization

Nowadays, only about 2 % of the lignin produced in the pulp and paper industry is commercially used for high-value usages, comprising of about one million tons/year of lignosulphonate originating from sulfite process and less than one hundred thousand tons/year of kraft lignin produced in the kraft process³⁸. The rest of large quantity of lignin is mainly valorized as a low-value fuel to generate electricity and heat. Thanks to the increasing production of cellulosic ethanol, it is predictable that the

development of biorefinery will provide a more considerable amount of lignin in the near future. Therefore, finding a practical way of lignin valorization instead of simple combustion is highly desirable. In literature and practice, different approaches and strategies have been reported for lignin valorization, mainly on two pathways: materials and biorefinery.

I.4.1 Materials

I.4.1.1 Carbon fiber

A promising material derived from lignin is carbon fiber. Nowadays, the main precursor for the manufacturing of carbon fiber is polyacrylonitrile (PAN), which constitutes approximately 90 % of all commercially produced carbon fiber³⁹. Petroleum pitch, a highly aromatic mixture, is also considered to be another suitable precursor to produce carbon fiber⁴⁰. Regarding that the property of lignin is very similar to petroleum pitch and a large amount of lignin exists in nature, thus lignin could be an ideal precursor for carbon fibers.

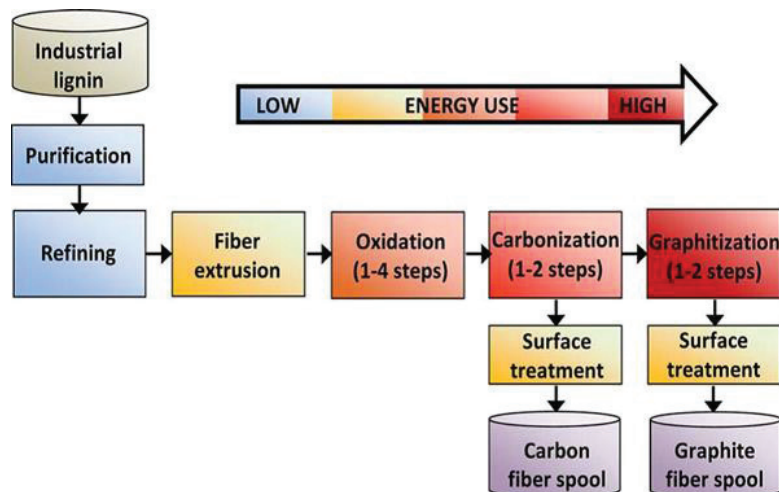


Figure I.11: Schematic representation of carbon fiber production from lignin⁴¹

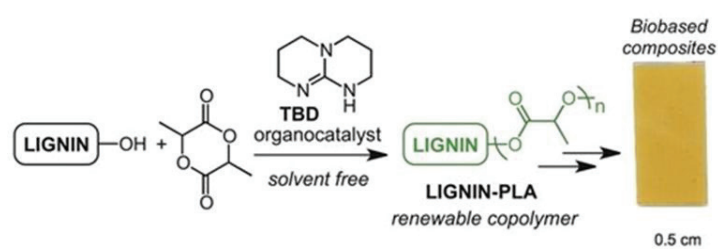
Schematic representation of a current method for the manufacture of carbon fiber from lignin is presented in Figure I.11. Firstly, it involves the presentation of industrial lignin that melt-spun into the fiber under an inert atmosphere. Then the lignin fiber is oxidatively thermostabilized and carbonized. In practice, careful control of the lignin, spinning conditions, treatment temperatures, and ramping profiles are required to obtain carbon fiber of superior strength.

Compared to the high cost for carbon fiber derived from PAN, cost estimations for lignin as a precursor show remarkable reduction⁴². Nevertheless, the understanding of the fundamental chemistry involved in the process where carbon fiber is made from lignin is extremely limited. Thus until now, only one carbon fiber with lignin has been commercialized: the kayo carbon fiber produced by Nippon Kayaku Co. during 1967-1973⁴³. The precursor lignin used was liginosulphonate, which is an industrial lignin originating from sulfite process.

1.4.1.2 Lignin-based plastics

Another high-volume lignin application to materials is lignin-based plastics. Numerous studies have been reported to integrate lignin with currently available petroleum-based synthetic polymers via copolymerization. Since lignin contains various functional groups, particularly hydroxyl groups, which can be used to form many lignin-based polymers such as polyurethane, phenol formaldehyde, epoxy resins and polyesters via polycondensation reaction⁴⁴⁻⁴⁷. Generally, the first step is to modify the chemical properties of lignin, and then modified lignin is copolymerized with other polymers. Finally, the synthesized lignin-based polymer needs to be tested under various conditions to assess its potential utility in a given application⁴⁴. An example of lignin copolymerization was reported by researchers at Stanford University: a catalytic and solvent-free method for synthesis of a lignin-based plastic, as shown in Scheme 1.2. As seen, the hydroxyl groups (-OH) in lignin are replaced with lactide grafts by using triazabicyclodecene (TBD) during the ring opening polymerization of lactide to polylactic acid (PLA).

In general, process impurities, variable molecular weights, and poor reactivity hinder the value of most current technical lignin to lignin-based plastics³².



Scheme 1.2: Schematic representation of lignin copolymerization with lactide⁴⁸

1.4.2 Biorefinery

In biorefinery, the depolymerization and conversion of lignin can be achieved by thermochemical pathways through breaking down the linkages in the polymer. Low-molecular-weight species are generated, including a lot of platform chemicals (BTX, phenolics and syngas). Figure 1.12 summarizes four major conversion processes of lignin (pyrolysis, gasification, hydroconversion and hydrolysis) and their potential products⁴⁹.

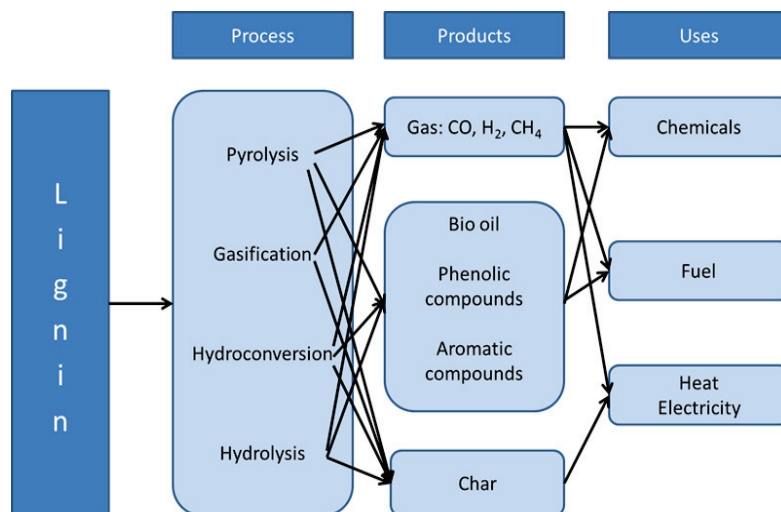


Figure I.12: Major thermochemical conversion processes of lignin and their potential products and uses

I.4.2.1 Pyrolysis

Pyrolysis is a typical thermochemical process that converts lignin to a liquid product known as bio-oil, as well as solid product char and gases in the absence of oxygen and at a relatively low pressure⁵⁰⁻⁵³. Pyrolysis can be divided into two categories: slow pyrolysis and fast pyrolysis. Slow pyrolysis is performed at about 500 °C with a long residence time of 5-30 minutes, in order to enhance solid char production. However, slow pyrolysis has some disadvantages such as long decomposition time, very low heat transfer and subsequently requiring high energy consumption⁵³. Hence, these disadvantages make it less suitable for getting high liquid yield and high quality of bio-oil. Compared to slow pyrolysis, fast pyrolysis is carried out at a higher temperature (600-1000 °C) with a shorter residence time of 0.5-10 seconds to reach a higher yield of liquid products^{50,51}.

Normally, cracking catalysts are utilized for both slow pyrolysis and fast pyrolysis. The liquid yield of pyrolysis is generally around 40-60 wt%, comprising of water, unsaturated compounds and aromatic oxygenated compounds⁵². The instability of bio-oil makes their uses for chemicals and fuel problematic, thus pyrolysis is better to be integrated into a two-step process with further treatment like gasification and hydrotreating.

I.4.2.2 Gasification

Unlike pyrolysis, gasification is aimed at forming a mixture of small gas molecules such as H₂, CO, CO₂ and CH₄ instead of liquid bio-oil, with varying ratios depending on the sources, the presence of air or not, reaction temperature and pressure⁵⁴⁻⁵⁶. In order to break most of the bonds in lignin, gasification is usually achieved at a very high temperature (> 700 °C). Currently, the gasification of lignin is achieved from three distinct processes:

- 1) Conventional gasification in the presence of oxygen at a high temperature and a low pressure⁵⁴;
- 2) Pyrolytic gas release in the absence of air or steam⁵⁵;
- 3) Catalytic supercritical water gasification at moderate temperatures and high pressures⁵⁶;

The resulting gas mixture, known as syngas, has already applied for the generation of electricity and synthetic liquid fuels through Fischer-Tropsch process.

1.4.2.3 Hydrolysis

Hydrolysis is a thermochemical process in which subcritical or supercritical water is used to produce small fragments through breaking down the linkages of lignin⁵⁷. Hydrolysis and alkylation occur when processing lignin in a hydrothermal condition, resulting in mixed products of methoxylated benzene, alkylated benzenes, and phenols, shown in Figure I.13. Additionally to depolymerization, it was also noticed that a high yield of char is obtained⁵⁸. Thus, the prevention of repolymerization and the suppression of char formation attract more and more attention. The presence of alkaline solution is proved to have a positive effect on the liquid yield, enhancing lignin solubilization and avoiding char formation⁵⁹. The use of a mixture of water with other solvents has also been proposed in the literature, such as water-phenol, water-ethanol, and water-formic acid, which has been proved to increase the bio-oil productivity greatly^{58,60,61}.

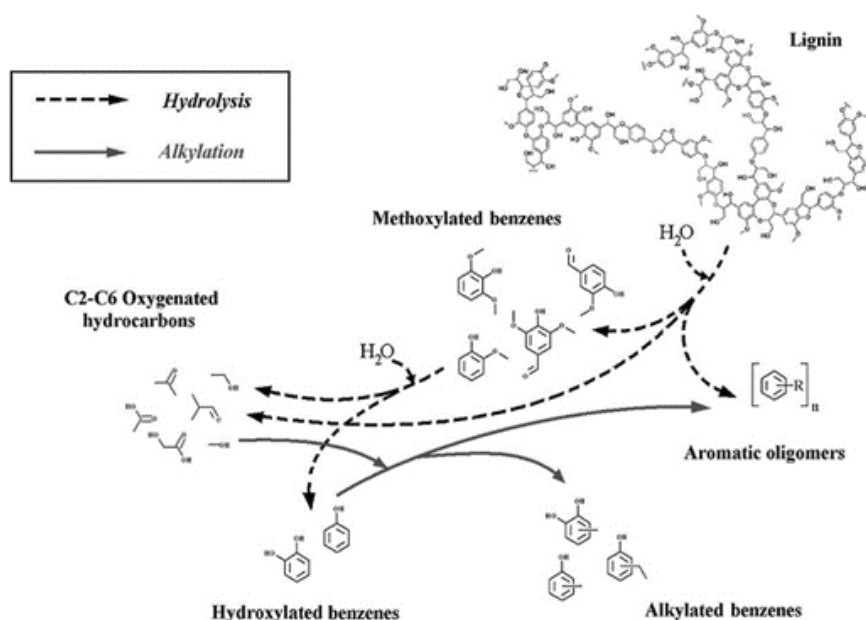


Figure I.13: Proposed hydrolysis pathways of lignin⁵⁷

1.4.2.4 Hydroconversion

Compared to three thermochemical processes mentioned above, hydroconversion seems to be the most promising way to obtain a high yield of liquid products under the literature results^{30,62,63}. The process is carried out using a hydrotreating catalyst in a H-donor solvent or not with the addition of molecular hydrogen or not. The combination of thermal depolymerization and stabilization of free radicals by hydrotreating catalysts, H-donor solvents and molecular hydrogen can avoid severe condensation reaction and char formation⁵². H-donor solvent and molecular hydrogen are used as capping agent to form stable lignin fragments. Under these conditions, a high yield of stable liquid products and a low quantity of char can be obtained. The liquid products are a mixture of phenols, aromatics, naphthenes and alkanes.

1.4.2.5 Comparison of different valorization pathways

In the present section, different lignin valorization pathways are briefly reviewed, mainly towards materials and biorefinery. In biorefinery, thermochemical pathways cover a range of processes from pyrolysis to hydroconversion, for the purpose of converting lignin into valuable products. These pathways are either catalytic or non-catalytic, holding their own advantages and disadvantages, listed in Table I.9.

With the aim to obtain high-value products, pyrolysis, hydrolysis and hydroconversion with a higher liquid yield seem to conform it. Compared to pyrolysis and hydrolysis, hydroconversion shows a higher liquid yield, at a relatively modest reaction condition. Thus, our objective is fixed at studying lignin hydroconversion and in the next section, the detailed about lignin hydroconversion will be presented.

Table I.9: Advantages and disadvantages of various thermochemical conversions of lignin

Process	Advantages	Disadvantages
Pyrolysis	(1) Operation at atmospheric pressure and modest temperature (2) High yield of bio-oil	(1) High oxygen and water content of bio-oil (2) Condensation of unstable liquid products and corrosion of containers
Gasification	(1) Feedstock flexibility (2) High product selectivity (3) Integration easy	(1) Low-value products (2) High capital cost
Hydrolysis	(1) No drying process (2) Cheap solvent (3) High yield of platform chemicals	(1) Severe operational conditions (2) High corrosion to the installation due to alkali condition
Hydroconversion	(1) Highest yield of liquid products (2) Partial deoxygenated of products (3) Modest operational condition	(1) Addition of expensive H ₂

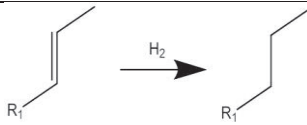
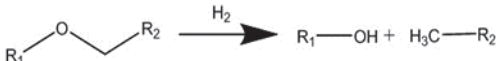
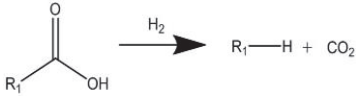
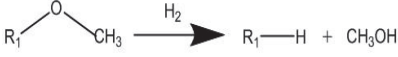
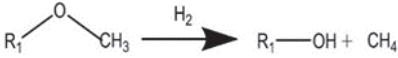

1.5 Lignin catalytic hydroconversion

Hydroconversion is a thermochemical process where the reactant is reacted in the form of hydrocracking in which hydrogenation and cracking co-occur. In early studies, the combination of thermal cracking reactions and the stabilization of formed radicals by molecular hydrogen, H-donor solvent as well as hydrotreating catalyst were widely used in the liquefaction of solid coal⁶⁴. Due to the high similarity between coal and lignin in term of their structure, this methodology can readily adopt to lignin^{30,34}. Either metallic, oxide or sulfide heterogeneous catalysts may activate hydrogen and promote hydrogenation and hydrogenolysis reactions. Typical reaction temperatures are between 300 and 500 °C and hydrogen pressure between 10 and 150 bar. Compared to lignin pyrolysis, lignin hydroconversion can always reach a higher liquid yield and get more stable liquid products due to radical stabilization.

I.5.1 Reactions and products

During lignin thermochemical conversion, by increasing the reaction temperature, a part of bonds in lignin were broken down, leading to lower-molecular-weight oligomer fragments or low-molecular-weight monomers. While performing lignin hydroconversion, various types of reactions may take place with the participation of H₂, as listed in Table I.10. Examples are hydrogenation, hydrogenolysis, decarboxylation, demethoxylation, demethylation and hydrodeoxygenation (HDO). These reactions can occur directly on the lignin, in addition to the lignin fragments. Besides these reactions, recondensation of highly reactive intermediates, ultimately leading to solid char of high carbon content, may take place to a certain extent and should be taken into consideration.

Table I.10: Principal reactions occurred during the lignin hydroconversion

Reaction	Scheme
Hydrogenation	
Hydrogenolysis	
Decarboxylation	
Demethoxylation	
Demethylation	
Hydrodeoxygenation	

Since lignin is complex in chemical composition, various types of primary and secondary reactions can generate numerous products from lignin. In general, a complex mixture after the lignin hydroconversion can be divided into three categories according to their states^{16,65}:

- **Gases** For lignin hydroconversion, non-condensable gaseous products are mainly composed of CH₄, CO₂, light alkanes with C₂-C₆ carbons and traces of CO⁶⁵. The formation of CO₂ and CO can be explained by decarboxylation/decarbonylation reactions and water gas shift reactions, the formation of CH₄ by methylation and methanation, the latter being thermodynamically favored in those conditions⁶⁶. The light alkanes come from the C-C cleavage of alkyl chains of the lignin.
- **Liquid** Primary reaction to depolymerize lignin is started by cleavage of β-O-4 ether bonds between the aromatic units, generated free radicals being stabilized by hydrogen to form

stable phenolic compounds. The formed phenolic compounds could be methoxylated or not, depending on the type of phenylpropane units. Afterward, formed phenolic compounds undergo further secondary reactions to other monomeric products, such as aromatics by direct HDO and naphthenes by aromatic-ring hydrogenation followed by HDO. It has to be pointed out that, besides these identified monomeric products, a significant part of relative high-molecular-weight liquid fraction (oligomers depolymerized from lignin) cannot be identified, owing to the complexity of liquid mixture and the limit of analytical methods, mentioned by lots of authors^{65,67,68}. Generally, the identified percentage is always lower than 40 wt% regardless of analytical methods and reaction time.

- **Solid** According to their origin, solid parts are divided into two parts:
 - 1) Char, a high carbon content compound originating from the recondensation of unstable intermediate products, is not soluble in any solvents.
 - 2) Residual lignin, partially converted lignin, has a lower molecular weight than initial lignin. It can be solid or probably soluble in liquid depending on the remaining organic functions and the molecular structure⁶⁵.

Normally, when it comes to calculating the lignin conversion, the solid part is often not included although actually it is also a type of lignin product. With the aim to obtain monomeric phenols and aromatics, the liquid yield and monomeric product selectivity are more meaningful to compare.

1.5.2 Solvents

In literature, the majority of studies have been performed in the presence of an external solvent whereas a very limited number of solvent-free studies have been reported. For the cases of employing solvent-free conditions, molten lignin (melting point of lignin is reported around 200-300 °C depending on the type of lignin) can act as the initial solvent, later diluted with low-molecular lignin products when the reactions are carried out. For other cases employing external solvents, the external solvent can solubilize molten lignin and lignin fragments. However, under operating conditions, the external solvent is usually not inert and can directly react with lignin fragments. This severely complicates product separations and further analysis. In the following part, the role of different solvents in lignin hydroconversion are discussed.

1.5.2.1 In the absence of an external solvent

A very limited number of solvent-free approaches have been reported in the literature^{62,67-71}, as listed in Table I.11. Various solvent-free experiments have been explored using a large number of catalysts (e.g., Pd/C^{67,69}, Ru/C⁶⁷, NiMo^{62,68,69}, CoMo⁶⁸, etc.), at a wide range of temperature (350-420 °C) and a wide range of initial pressure (30-125 bar at room temperature).

Table I.11: State of the art for lignin hydroconversion in the absence of an external solvent

#	Lignin	Process	Catalyst	Catalyst/Lignin (g/g)	T (°C)	t (h)	P (bar)	Main products (wt%)	Liquefaction (wt%)	Ref
1	KL	Batch	NiMo (S) on AS with Cr ₂ O ₃	7/70	395	0.58-0.67	100 (*)	Phenolics (5.3-9.3) Aromatics (6.1-10.4)	63-65	[62]
2	OL	Batch	NiMo (S) on AS with Cr ₂ O ₃	7/70	395	0.5-0.67	100 (*)	Phenolics (7.6-8.9) Aromatics (8.8-10.5)	52-71	[62]
3	AL	Batch	Ru/C	0.75/15	400	4	100 (*)	Phenolics (9.0) Aromatics (3.2)	63.9	[67]
4	AL	Batch	Ru/TiO ₂	0.75/15	400	4	100 (*)	Phenolics (9.1) Aromatics (2.5)	78.3	[67]
5	AL	Batch	Pd/C	0.75/15	400	4	100 (*)	Phenolics (8.1) Aromatics (4.3)	67.5	[67]
6	AL	Batch	Cu/ZrO ₂	0.75/15	400	4	125 (*)	Phenolics (4.7) Aromatics (1.3)	71.8	[67]
7	AL	Batch	Pd/Al ₂ O ₃	0.75/15	400	4	100 (*)	Phenolics (7.3) Aromatics (2.0)	75.1	[67]

AL: Alcell Lignin; OL: Organocell Lignin; KL: Kraft Lignin; AS: Aluminosilica; PL: Pyrolytic Lignin
 *: initial pressure at room temperature

Table I.11: State of the art for lignin hydroconversion in the absence of an external solvent

#	Lignin	Process	Catalyst	Catalyst/Lignin (g/g)	T (°C)	t (h)	P (bar)	Main products	Liquefaction (wt%)	Ref
8	KL	Batch	NiMo (S)	0.75/15	350	4	100 (*)	Phenolic (10.5-15.7) Aromatics (3.0-5.9)	40.8-57.8	[68]
9	KL	Batch	CoMo (S)	0.75/15	350	4	100 (*)	Phenolics (7.1-12.6) Aromatics (3.0-5.3)	29.8-52.8	[68]
10	OL	Batch	Pd/C	15/40	380	0.25	100 (*)	Cyclohexanones	80.6	[69]
11	OL	Batch	Fe ₂ O ₃	15/40	380	0.25	100 (*)	Phenolics	17	[69]
12	OL	Batch	Raney Ni	15/40	380	0.25	100 (*)	Phenolics	53.6	[69]
13	OL	Batch	NiMo on AS	15/40	350-450	0-2	30-120 (*)	Demethoxylated phenolics	17.3-53.6	[69]
14	KL	Batch	NiMo on AS	15/40	420	0.25	100 (*)	Demethoxylated phenolics	61.6	[69]
15	PL	Batch	Ru/C	0.75/15	400	4	100 (*)	Phenolics (18.9-20.5) Aromatics (7.3-14.1)	75.4-75.8	[70]

Apart from the nature of catalysts and origin of lignin, the operating conditions (reaction temperature and pressure) also play an important role in liquid products, as well as the distribution of desired monomeric products. According to the test carried out by Meier *et al.*⁶⁹, the liquid yield increased from 18.4 wt% to 63.2 wt% by increasing initial pressure from 20 bar to 120 bar. Similar results were observed by Horaček *et al.*⁷¹ using sulfide NiMo catalyst. Hence, H₂ pressure seems to be significant to obtain a high liquid yield in the absence of an external solvent. It can be explained that, under high H₂ pressure, sufficient available hydrogen atoms can quickly stabilize unstable free radicals to avoid the recondensation reactions between them, thereby the liquid yield increases and the solid yield decreases with increasing pressure.

Furthermore, the influence of reaction temperature was investigated by Meier *et al.*⁶⁹. They performed a series of experiments between 350 °C and 420 °C at the initial pressure of 100 bar. At 350 °C, the liquid yield was only 40 wt% of lignin intake while residual lignin fragment yield was 22 wt%. By increasing the reaction temperature, the liquid yield increased and the residual lignin yield decreased, indicating that the cleavage of lignin bonds was governed by temperature. Meanwhile, the char formation increased with increasing temperature since free radicals were rapidly formed due to a temperature increase and molecular hydrogen cannot stabilize them in time.

To be concluded, solvent-free conditions facilitate the product work-up and mass balance closure. However, an obvious drawback is that a high yield of non-convertible char formation seems to be severer than that in solvent-assisted conditions. In order to avoid this disadvantage for achieving a high yield of liquid products, reaction pressure must be sufficiently high (> 200 bar at operating temperature). Moreover, high reaction temperature favors the depolymerization of lignin, but rapid char formation should be avoided as well. Variation of original lignin and extraction methods make hard to draw general conclusions regarding the best catalyst and operating conditions. Overall, at the solvent-free conditions, the operating conditions are really harsh. Concerning the monomeric product yield, phenolic yields lower than 16 wt% and aromatic yields lower than 11 wt% were found in all cases (pyrolytic lignin studies not included).

1.5.2.2 In the presence of an external solvent

Thermal degradation, combined with various solvents or solvent mixtures, were already proposed for coal liquefaction studies. Considering that the solid state and the polymer property of coal are very similar to that of lignin, solvents available for coal liquefaction have been transplanted to lignin liquefaction studies. Various solvents have been explored with a range of polarity (from dodecane to water). Both noble metal-based catalysts, as well as non-noble metal-based catalysts, have been explored. Since solvent-assisted conditions complicate the product separation and analysis, as well as mass balance determination. Therefore in most cases, the liquid yield is not mentioned or meaningless. In literature, employed solvents can be classified into four types:

- A. Inert solvent
- B. Protic solvent
- C. Lignin-derived oil
- D. H-donor solvent

Inert solvent

Here, inert solvents represent the solvents with poor hydrogen donating ability, and not interacting with lignin-derivatives. Examples are dioxane, dodecane, naphthalene and 1-methylnaphthalene⁷²⁻⁷⁶, listed in Table I.12. Dioxane as a solvent was firstly reported to be able to dissolve a small amount of

lignin⁷⁷. Considering its low boiling point, the reaction temperature for the hydrotreatment of lignin were relatively mild (below 260 °C)⁷²⁻⁷⁴. At a relatively low temperature, it was possible to obtain a large amount of oxygenated and methoxylated phenolics since the bonds of C_{ar}-OH and C_{ar}-OCH₃ remain.

Dodecane and 1-methylnaphthalene were chosen as external solvents due to their supposed stability at high temperature and high pressure^{75,76}. However, the results show that these solvents may not be suitable for lignin conversion in the view of low aromatic yield. Moreover, it was observed that 1-methylnaphthalene was quite reactive to lignin fragments since 6 wt% of naphthalene and 8 wt% of dimethylnaphthalene were found.

Overall, for an inert solvent assisted reaction, the addition of solvents like dioxane, dodecane, and 1-methylnaphthalene may favor catalytic performance by improving gas-liquid-solid contact better than solvent-free conditions. Consequently, the mass ratio between catalyst and lignin is mostly lower than that of solvent-free conditions. However, the participation of solvent in reaction does not seem significant on account of low hydrogen donating ability. In all cases using inert solvents, the yields of phenolics and aromatic products were relatively low, showing no distinct improvement than the solvent-free condition. That is to say, it seems to be that inert solvent is not effective for lignin hydroconversion.

Protic solvent

In chemistry, protic solvent is a solvent containing a labile H⁺; in general, it that has a hydrogen atom bound to an oxygen (as in a hydroxyl group) or a nitrogen (as in an amine group). Typical examples include water, most alcohols and formic acid⁷⁸⁻⁸³, listed in Table I.13. In most cases, hydrothermal degradation of lignin with water leads to the formation of monomeric catechols.

Strüven *et al.* reported that catechols were further converted to phenols with the use of Raney Ni⁷⁸. When Barta *et al.* depolymerized lignin using Cu porous metal oxide (PMO) in methanol, the results showed that lignin could be selectively cleaved into C₉-catechols with a yield of 54.8 wt%. It was proved that Cu catalyst can catalyze the decomposition of methanol to produce CO and H₂. In this way, methanol would serve as the in-situ hydrogen source to have the hydrogenolysis/hydrogenation reactions. Oregui-Bengoechea *et al.* replaced methanol with formic acid⁸³, the decomposition of formic acid to H₂ was also observed. Other studies^{80-82,84} using ethanol as solvent show that, ethanol is a better solvent than other alcohols because ethanol can stabilize the phenolic intermediate by O-alkylation of hydroxyl groups and by C-alkylation of the aromatic rings⁸⁴ resulting in a high yield of liquid. Furthermore, in general, while using these protic solvents are used, high temperature and high pressure are often associated, inducing to subcritical/supercritical state where the fluid has a strong solvating power which can have a positive impact on the lignin depolymerization.

To be concluded, the protic solvents are used to stabilize the highly reactive lignin fragments. However, their participation to reaction is unavoidable. Furthermore, the influence of protic solvents is largely seen in an improving solubility of both the lignin and its reaction products.

Table I.12: State of the art for lignin hydroconversion in the presence of inert solvents

#	Lignin	Process	Solvent	Catalyst	Catalyst/Lignin (g/g)	T (°C)	t (h)	P (bar)	Main products (wt%)	Liquefaction (wt%)	Ref
1	EL	Batch	Dioxane	CuCrO	7/1.5	260	18-22	220 (*)	Cyclohexanols	70	[72]
2	ML	Batch	Dioxane/water (3 % NaOH)	Raney Ni	n.d.	173	5-6	34-200 (*)	4-ethylsyringols (16.4)	66	[73]
3	WBL	Batch	Dioxane/water (1 % H ₃ PO ₄)	Rh/C Pt/C	0.3/4.0	200	4	40 (*)	Syringylpropane (21.1-34.8)	< 60	[74]
4	OL	Batch	1-methylnaphalene	CoMoS/ Al ₂ O ₃	0.2/1.9	404	1	70 (*)	Phenolics (2.2)	< 70	[75]
5	PL	Batch	Dodecane	Ru/C	0.1/2	350	1	100	Cyclohexanol, alkanes	n.d.	[76]

EL: Ethanol extracted Lignin; ML: Maple Lignin; WBL: White Birch Lignin; OL: Organosolv Lignin; PL: Pyrolytic Lignin
 (*): Initial pressure at room temperature

Table 1.13: State of the art for lignin hydroconversion in the presence of protic solvents

#	Lignin	Process	Solvent	Catalyst	Catalyst/Lignin (g/g)	T (°C)	t (h)	P (bar)	Main products (wt%)	Liquefaction (wt%)	Ref
1	OL	Batch	Water	Raney Ni	3/25	360	3	70 (*)	Phenols and catechols (10.1)	n.d.	[78]
2	ML	Batch	Methanol	Cu-PMO	0.8/1	180	14	40 (*)	C ₉ -catechols (54.8)	n.d.	[79]
3	PL	Batch	Ethanol	Ru/ZrO ₂ on SBA-15	1.5/3.0	260	8	20 (*)	Phenolics and alkanes	n.d.	[80]
4	OL	Batch	Ethanol/water	Ru/C, Pd/C, Pt/C	0.2/1.0	200-275	1.5-3	10-60 (*)	4-ethylphenol (0.13-3.10)	n.d.	[81]
5	AL	Batch	Ethanol	ZnCl ₂	0.5/1.0	300	2	70 (*)	Phenolics (15.79) Guaiacols (15.09)	75.8	[82]
6	EL	Batch	Formic acid	NiMo/sulfated Al ₂ O ₃	0.82/8.16	320	6	17.5 (*)	n.d.	26.6	[83]

OL: Organosolv Lignin; ML: Methanol-extracted Lignin; PL: Pyrolytic Lignin; AL: Alkali Lignin; EL: Eucalyptus Lignin

(*): Initial pressure at room temperature

Lignin-derived oil

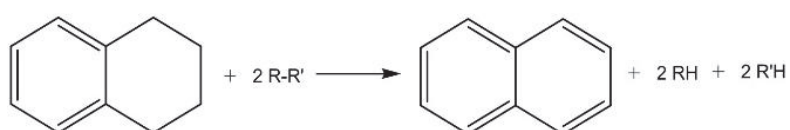
Apart from the solvents mentioned above, several authors proposed to employ lignin-derived oil as external solvents. Examples are cyclohexanol, phenols and lignin-derived mixture⁸⁵⁻⁸⁸. They are considered to have an excellent solubility with lignin and lignin-derived products.

Two famous early studies on the hydroconversion of lignin using lignin-derived oil solvent were reported by two Japanese institutes: Noguchi Institute and Hydrocarbon Research Institute (HRI). The Noguchi process carried out the conversion of lignin in a mixture of phenols and lignin-derived oil. The reaction was performed under harsh conditions: temperatures between 350 and 400 °C, H₂ pressure between 150 and 300 bar. Using a Fe-promoter-sulfur as a catalyst, the liquid yield reached 95 wt% while the yield of phenol was 21 wt% after 2 h. Lignol process, proposed by HRI, was targeted to produce phenols and benzene from lignin. The lignin was mixed with process oil into an ebullated hydrocracking reactor, then followed by a post-thermal dealkylation step. The final products were phenols and aromatics with short alkyl chains. It is claimed to produce about 37.5 wt% alkylated phenols on lignin intake. The advantages of the Lignol process compared to the Noguchi process are a higher amount of phenol fraction (37.5 wt% vs. 21 wt% on lignin intake) and a lower amount of heavy oils. However, several authors claimed that their works were not reproducible.

Although a fairly high liquefaction and a high yield of monophenols have been reported, it must be pointed out that these solvents are very active in the catalytic condition, producing the similar products as lignin. That really makes the analysis and evaluation of the process very complicated. Moreover, the solvent recovery was always low that makes the process economically unattractive.

H-donor solvent

An attractive alternative is the use of hydrogen donating solvents, usually are polycyclic naphthenic-aromatic hydrocarbons that can be reversibly hydrogenated-dehydrogenated in the reacting mixture. These solvents are thought to have more powerful hydrogen donating ability than other solvents. The degraded unstable fragments can be stabilized by in-situ hydrogen, which is donated by them. Tetralin has been demonstrated to be an effective alternative solvent for coal liquefaction. The process of coal liquefaction by tetralin can be summarized simply, as shown in Scheme I.3. Upon dehydrogenation, tetralin is primarily to naphthalene, a relatively stable compound.



Scheme I.3: Mechanism of stabilizing radicals by tetralin

A lot of early studies focused on the use of tetralin as a sole hydrogen donor to replace pressurized H₂ for lignin hydrotreatment, so-called solvolysis^{28,30,90} (see Table I.14). Kleinert *et al.* studied the conversion of lignin in tetralin up to 300 °C without catalyst⁹⁰. The liquid yield was very low, since it is not enough to break bonds between phenolic units under the low temperature in the absence of the catalyst.

Table I.14: State of the art for lignin hydroconversion in the presence of tetralin

#	Lignin	Process	Solvent	Catalyst	Catalyst/Lignin (g/g)	T (°C)	t (h)	P (bar)	Main products (wt%)	Liquefaction (wt%)	Ref
1	KL	Batch	Tetralin	-	-	375-400	0.25-1.7	55-108	Phenolics (0.50-3.15) Catechols (0-3.26)	n.d.	[30]
2	KL	Batch	Tetralin/m-cresol	CoMo/Al ₂ O ₃	2.7/27	345	5	20 (*)	n.d.	7.0-20.3	[28]
3	RL	Batch	Tetralin	Red mud (S), CoMo (S)	3/60	400	4	150 (*)	Phenolics (18.0-21.3)	75-78	[89]
4	AL	Batch	Tetralin	NiW, Ni	1/20	370-410	0.25-1	10 (*)	Phenolics Catechols	< 50	[34]
5	PL	Batch	Tetralin	NiMoS/Al ₂ O ₃	3/30	350	5	80	Phenolics Aromatics	65	[16]

KL: Kraft Lignin; RL: Rye straw Lignin; AL: Alcell Lignin; PL: Protobind 1000 Lignin
 (*): Initial pressure at room temperature

Later, Connors *et al.* established the hydrogen donating effect of tetralin on the hydrocracking of kraft lignin and model compounds such as *p*-ethylguaiacol and dehydrodihydrodiisoeugenol³⁰. To illustrate the importance of hydrogen donor effect, they firstly compared experiments using tetralin with experiments using naphthalene, a non-hydrogen-donating solvent, shown in Table I.15. As seen, the liquid yield of tetralin experiments was almost four times higher than that of naphthalene experiments. Moreover, extensive conversion to char took place in the experiment using naphthalene. It appears, therefore, that in the absence of a H-donor solvent, the intermediate free radicals recombine quickly to produce char. With the help of hydrogen atoms donated by tetralin, free radicals can be stabilized and formed stable liquid products.

Table I.15: Product comparison between tetralin experiments and naphthalene experiment by Connors *et al.* (400 °C, solvent/lignin = 4:1, reaction time = 15 min)

Product yield (wt%)	Tetralin	Naphthalene
Char	9.7	38.5
Liquid	39.7	8.8
Residual lignin	40.4	18.3
Gases	n.d.	n.d.

Secondly, they performed a series of experiments in tetralin with varying reaction time between 0.25 and 1.7 h. NMR spectra test for residual lignin suggests the following sequence of reactivity for functional groups in hydrocracking: aliphatic OH > aromatic -OCH₃ > aromatic OH. Besides, from the analysis for the liquid fraction, the relatively large quantities of C₁-side-chains as well as phenolic products with no side-chains suggest strongly that homolytic cleavage between α and β carbon atoms as well as between the ring and the α carbons are frequent in hydrocracking.

Later, Vuori *et al.* studied lignin conversion using CoMo/Al₂O₃ in a mixture of tetralin and *m*-cresol²⁷. The product between tetralin experiments and tetralin/*m*-cresol are compared in Table I.16. The yield of liquid products was much higher when a tetralin/*m*-cresol mixture was used as a solvent than when tetralin was used alone. This is related to the accelerating effect of phenols which can cleave ether linkages. Meanwhile, experiments with a heterogeneous catalyst demonstrated that the presence of the CoMo/Al₂O₃ catalyst had only a slight effect on the liquid yield, surprisingly leading to a higher char formation and gas formation. This indicated that the catalyst enhanced the reaction of depolymerization of lignin, but recondensation reactions prevailed.

Table I.16: Product comparison between tetralin experiments and tetralin/*m*-cresol experiments by Vuori *et al.* (345 °C, solvent/lignin = 7:1, reaction time = 5 h)

Product yield (wt%)	Tetralin	Naphthalene	Tetralin + catalyst
Gases	3.8	4.3	7.1
Liquid	7.0	20.3	11.5
Solid	56.2	59.1	72.4

Therefore, using the hydrogen-donating solvent as a sole hydrogen resource, the hydrogen is evidently not sufficient to react with rapidly formed free radicals. For achieving more valuable liquid products,

either supplying more available hydrogen or slowing down lignin depolymerization should be taken into consideration. Therefore, in several studies^{89,91}, the addition of molecular hydrogen was involved in order to get a higher yield. Oshima *et al.* studied the catalytic hydrocracking of lignin under hydrogen pressure with tetralin as solvent⁹¹. At the temperature of 430 °C, the reaction time of 4 h, and the ratio of tetralin/lignin equal to 3:1 resulted in a complete conversion of lignin. It indicates that molecular hydrogen can indeed help the stabilization of free radicals to prevent recondensation reaction. However, the conditions used by them are so severe that the phenolic units were totally destroyed.

Following those investigations, Klopries *et al.* realized the conversion of rye straw lignin with sulfided red mud and sulfided CoMo with tetralin under hydrogen pressure⁸⁹. The distribution of products using two different catalysts is shown in Table I.17. 95 wt% of lignin intake is converted to gas and liquid products. By comparing the liquid products, CoMo indicated a higher hydrogenation activity than red mud, with less heavy oil content. However, it is impossible to get further catalytic effects since detailed liquid distribution was not mentioned in this work. Compared to previous investigations, the addition of molecular hydrogen indeed promoted the liquefaction of lignin by preventing char formation.

Table I.17: Products comparison between the experiment using red mud and the experiment using CoMo (400 °C, reaction time = 4 h, initial pressure = 150 bar)

Product yield (wt%)	Sulfided red mud		Sulfided CoMo	
	Liquid	Gasoline	16.2	Gasoline
Phenolics		21.3	Phenolics	18.0
Heavy oil		37.9	Heavy oil	27.8
Gas	19.1		17.8	
Char	5.5		4.0	

Later, Thring *et al.* also underlined the extra need of molecular hydrogen to achieve higher liquid yield and lower char formation³⁴. It was also pointed out that the high yields of either solid char or residual lignin was governed by reaction temperature. At high severity, significant cracking of lignin occurs, the high yield of solid char is due to an inadequate amount of hydrogen atoms presenting in the reactor.

Overall, the advantage of tetralin as a hydrogen-donor solvent include its high boiling point as well as its ready release atoms under hydrocracking conditions, leading to the formation of naphthalene, a relatively stable compounds. Moreover, tetralin and its derived compounds are not parts of lignin products, avoiding the difficulty of mass balance calculation, that is different from others in-situ hydrogen sources like alcohols and formic acid.

1.5.3 Catalysts

While performing lignin hydroconversion with the aim of obtaining a high yield of liquid, heterogeneous catalysts are often used to activate H₂ and promote hydrogenation/hydrogenolysis reactions. Various types of catalysts were investigated in literature, including monometallic, bimetallic and bifunctional catalysts.

The monometallic catalysts are normally the expensive noble metal-based ones (e.g., Ru^{67,70,76,80,81}, Rh⁷⁴, Pd^{67,69,81} and Pt^{74,81}) with various support (e.g., C, TiO₂, Al₂O₃, SiO₂ and ZrO₂) and a few of Fe or Cu based ones^{67,69,72,79}. Many studies using noble-based metals illustrates that noble-based catalysts have a high

activity of hydrogenation, converting phenolic compounds into naphthenes and cyclohexanols^{69,76}. On the contrary, the Fe and Cu based catalysts show insufficient catalytic activity.

In the case of bimetallic catalysts, a combination of conventional metals such as Co, Ni, Mo and W are widely studied^{16,28,34,62,68,69,75,83}, either in the state of oxide or sulfide. By comparing the liquid yield, the sulfided catalyst exhibited better performance than the oxidized one. These well-known hydrotreating sulfided catalysts are originally developed for the removal of sulfur (HDS) and nitrogen (HDN) for oil purification and upgrading processes. Therefore, it may provide a useful lead for the removal of oxygen (HDO) for biomass-derived components. Early studies have been done by carrying out the HDO studies on model molecules, such as phenol⁹², guaiacol⁹³ and anisole⁹⁴. It was shown that with the aid of these catalysts, HDO can be accomplished by two paths: either direct deoxygenation of phenols to non-oxygenated aromatics or aromatic-ring saturation followed by a deoxygenation step. The latter one is much favored at high pressures. More recently, a lot of works studied the lignin conversion by sulfided catalysts. It appeared that when using sulfided catalysts, the liquid yield was quite higher than other catalysts^{16,89}. Furthermore, the aromatic-ring saturation to cycloalkanes did not occur severely.

In turn, a bifunctional catalyst means the catalyst having both hydrogenation and cracking functions. It contains both metal and acid or base active sites. Several combinations of hydrogenation catalyst (e.g. Ni, Ru) catalysts and solid acid catalysts (e.g., SBA-15, Al-SBA-15, HZSM-5) were investigated⁹⁵⁻⁹⁶. The final products were usually alkanes and naphthenes, illustrating a highly active cracking activity. It is also claimed that the dehydration step is highly dependent on the acidity of the support.

1.5.4 Reaction set-up

Since the lignin is only soluble in few organic solvents and it is solid at room temperature, these properties make it problematic to feed lignin continuously. For this reason, most studies on the lignin hydroconversion are carried out in batch set-up. Typically, the lignin feed, solvent and H₂ are fed into a closed reactor before each test. The unavoidable drawbacks of using batch set-ups for lignin conversion are as follows:

- As reaction time increased and H₂ was consumed continuously, the conversion rate may slow down due to the shortage of molecular hydrogen.
- The formed aromatic compounds stayed in batch for long reaction time, being risk to have over-hydrogenation reactions.
- For HDO studies, released water from reaction was thought to be responsible for the deactivation of several catalysts.

Investigations using continuous set-up are really scarce in literature as well as in practice. While performing lignin conversion in continuous set-up, it is better that lignin feeding was in the state of liquid. For achieving that, either the lignin feed should be dissolved in an organic solvent or the lignin should be molten in harsh conditions.

1.5.5 Conclusion of lignin hydroconversion

In general, for a lignin hydroconversion process, two separate steps are existing for the production of valuable platform chemicals. In the first step, various oxygenated aromatics can be generated by the depolymerization of lignin itself. These products still have a fairly high oxygen content and keep the original building blocks of lignin, that is, consist of substituted syringyl, guaiacyl and phenolic moieties.

In the second step, catalysts can play an important role on the upgrading of the primary products from the first step. Therefore, the final products highly depend on the catalysts used.

1.6 Kinetic modeling development of lignin conversion

Kinetic modeling is useful for chemical engineering since it can provide the quantitative information which can serve for reactor design, reaction optimization and process control. With a reliable kinetic model, the yield of desired and undesired at different operating conditions using a given reactor and catalyst can be well predicted. Therefore, the goal of kinetic model is as follows:

- 1) Determining the reaction mechanisms involving the feedstock, various intermediates and the final products.
- 2) Deriving the rate parameters which can predict the rate of reaction in function of other parameters such as temperature, pressure, composition, catalysts and so on.

The construction of the reaction mechanism used for the kinetic modeling is always based on the experimental measurements combined with the knowledges from other fields, such as the fluid composition by analytical chemistry, the fluid state by physical chemistry, the phase equilibrium by thermodynamics and the parameter estimations by mathematics. To proceed a development of a kinetic model, the following steps should be predefined:

- 1) Feedstock description, especially for the cases of the complex mixtures.
- 2) Reaction network, describing the reactions occurring.
- 3) Reaction rate equations, describing the rate of production and consumption for each component.
- 4) The characteristics of reactor in which the reactions take place.

The same methodology of modeling is applicable for the conversion of lignin. However, kinetic modeling studies of lignin conversion are quite scarce⁹⁷⁻¹¹⁰. The difficulties can be attributed to three main aspects:

- 1) The detailed and comprehensive characterization of lignin feedstock is still absent, making the description of feedstock problematic.
- 2) The conversion processes involve numerous extremely reactions and end up with a large number of intermediate and final products.
- 3) The limitation of analytical tools makes the qualitative and quantitative characterizations of products problematic.

As listed in Table 1.18, two approaches are proposed on the kinetic modeling of different lignin conversion processes⁹⁷⁻¹¹⁰: lumped kinetic model and molecule-based kinetic model.

Table I.18: State of the art for the kinetic model of lignin conversion

Authors	Lignin conversion process	Modeling approach	Analytical method	Number of Reaction pathways	Number of involved species	Reference
Jegers <i>et al.</i>	Pyrolysis	Lumped kinetic modeling	GC/MS-FID	7	7	[97]
Adam <i>et al.</i>	Pyrolysis	Lumped kinetic modeling	GC/MS	4	4	[98]
Farag <i>et al.</i>	Pyrolysis	Lumped kinetic modeling	GC/MS	7	8	[99]
Klein <i>et al.</i>	Pyrolysis	Molecule-based kinetic modeling	TGC, GC/MS-FID	n.d.	53	[100]
Faravelli <i>et al.</i>	Pyrolysis	Molecule-based kinetic modeling	TGA	500	100	[101]
Hou <i>et al.</i>	Pyrolysis	Molecule-based kinetic modeling	n.d.	n.d.	624	[102]
Hough <i>et al.</i>	Pyrolysis	Molecule-based kinetic modeling	TGA	406	93	[103]
Yanez <i>et al.</i>	Pyrolysis	Molecule-based kinetic modeling	GC/MS-FID	4313	1615	[104]
Zhang <i>et al.</i>	Hydrolysis	Lumped kinetic modeling	n.d.	2	4	[105]
Gasson <i>et al.</i>	Solvolysis	Lumped kinetic modeling	GC/MS-FID	13	11	[106,107]
Yong <i>et al.</i>	Hydrolysis	Lumped kinetic modeling	HPLC	20	10	[108,109]
Forchheim <i>et al.</i>	Hydrolysis	Lumped kinetic modeling	GC/MS-FID	13	10	[110]

The lumped kinetic model consists of regrouping chemical compounds by the similar properties (e.g., boiling point, functional group and carbon number). Each ensemble of compounds is called “lump”, which is considered homogeneous and shares the same reactions. The lumped kinetic model is aimed to evaluate the temporal variations of the yield of bulk products such as gases, liquids and residual solids, especially in pyrolysis and hydrolysis. First attempts were done using extremely simplified reaction network^{98,105}, which followed by more complex reaction models^{99,106-110}, involving several competing reactions, as illustrated in Figure I.14.

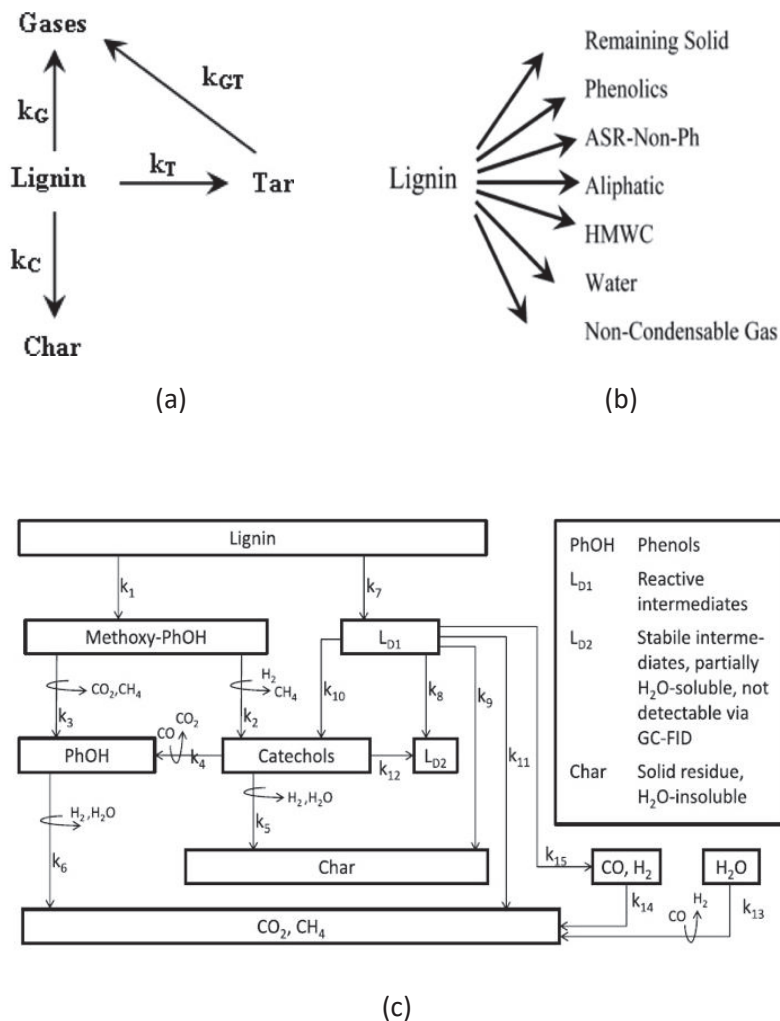


Figure I.14: Examples of lumped kinetic model by some authors: (a) Adam et al.⁹⁸; (b) Faraf et al.⁹⁹; (c) Forchheim et al.¹¹⁰

Molecule-based kinetic model describes the reactions at a semi-detailed molecular level¹⁰⁰⁻¹⁰⁴. This approach is aimed to elucidate a detailed mechanistic route from the reactant to the final products. Therefore, the models usually involve a complex reaction network and a hug amount of intermediate and final products up to thousands. The first step in the implementation of molecule-based kinetic modeling is always to determine the molecular-level composition of the feedstock, since it has all the important information such as the composition, the interunit linkages, the side chains and the chain

length. Typically, accurate description can be obtained by advanced characterization tools. However in the case of lignin, a complete construction of lignin structure and composition are really difficult. Proposed by several authors, molecular reconstruction methods are used to create numerically a molecular representation of lignin. For example, Faravelli *et al.* chose three reference monomers as the basic units in the lignin feed¹⁰¹, illustrate in Figure I.15. The equivalent molecular composition of the lignin feed was then obtained by using the conservation of elemental composition. On the basis of these three hypothetical units, the resulting reaction network involved about 100 species which undergo the ether-bond breaking reaction, decomposition reaction, condensation and radical combinations.

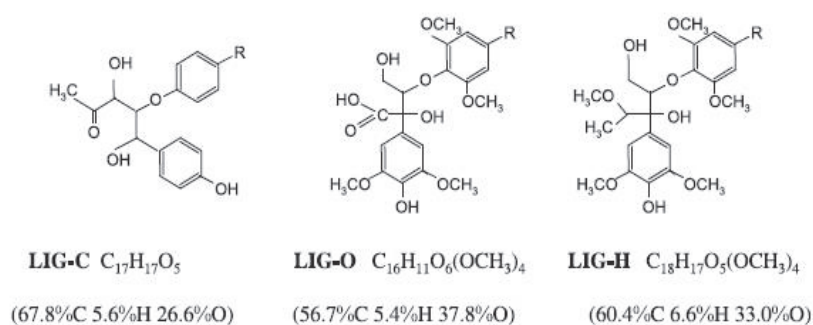


Figure I.15: Reference units in lignin feed¹⁰¹

By comparing the simplicity, the focusing points and the analog results, the advantages and disadvantages of two modeling approaches are clearly seen, as listed in Table I.19. Compared to molecule-based approach, lumped approach is relatively quick and easy to be implemented. However, the resulting kinetic model of lumped approach shows a lower performance on the mechanistic representation and product prediction.

Table I.19: Advantages and disadvantages of two modeling approaches

Approach	Advantages	Disadvantages
Lumped kinetic model	<ul style="list-style-type: none"> The number of lumps and reactions is limited. Limited computing power is required. The simple analytical tools are usually used. 	<ul style="list-style-type: none"> The resulting model is feed dependent. The product distribution inside each lump is not represented.
Molecule-based kinetic model	<ul style="list-style-type: none"> A detail explicit description of the reaction pathway is well elucidated. The resulting model is feed independent by changing its molecular description. 	<ul style="list-style-type: none"> Numerous number of species and reactions Requirement of really strong computing power Requirement of advanced and detailed analysis

In general, most of modeling studies putted emphasis on the reaction aspects of lignin conversion. However, at the operating conditions of high temperature and high pressure, sufficient vaporization of light or heavy products are unavoidable. Neglecting this factor, the observed reaction kinetics are always impacted, especially for a heterogeneous system. Moreover, according to our knowledge, most of kinetic modeling studies were performing using simple model compounds. The kinetic modeling on the catalytic hydroconversion of lignin feed still lacks until now.

1.7 Conclusion and thesis objectives

1.7.1 Conclusion

Lignin is one of the major components of lignocellulosic biomass. It accounts for nearly 30 wt% of lignocellulosic biomass, and it is the most relevant and abundant bio-resource to produce aromatic compounds because of its original polymer structure composed by phenylpropane units with ether linkages. It is currently obtained as a by-product from paper industry and biorefinery. In this context, the use of lignin as a precursor of aromatic compounds attracts lots of attention thanks to its low cost and high availability. In the literature, different thermochemical processes (pyrolysis, gasification, hydrolysis and hydroconversion) can be proposed applied for the direct conversion of lignin. It appears that lignin hydroconversion under H₂ pressure using a hydrotreating catalyst in the presence of a H-donor solvent was the most promising way to get high yields of liquid products. Effectively, the use of solvent such as tetralin, alcohols and formic acid strongly reduced the condensation reactions between formed radicals and thus increased the depolymerization. With the participation of some catalysts, it has been reported that the depolymerization of lignin and the hydrogenolysis/hydrogenation reactions are promoted, leading to a high yield of deoxygenated liquid products. According to the literature results, sulfided catalysts seem to be interesting to be employed in the lignin conversion, since about 80 wt% of liquid yield was obtained. In addition, kinetic modeling studies of lignin conversion are quite scarce because of the lack of complete characterization of lignin feedstock, the limitation of characterization tools for numerous products and the relatively complex reaction network. Therefore, we are interested in studying the reaction mechanisms and developing a kinetic model for the catalytic hydroconversion of lignin.

1.7.2 Thesis objectives

Project description

The thesis was undertaken in the framework of French National Research Project “LiGNAROCAT”, Project ID: ANR-14-CE05-0039. The project was aimed at improving the lignin conversion into liquids, optimizing the selectivity of aromatic compounds as well as developing the catalytic hydroconversion of lignin toward a continuous process. It is collaborated between four partners (IRCELYON, LAGEPP, LGPM and Total) and divided into several tasks. The main tasks are as follows:

- 1) Investigating the solubility of several lignins in different solvents for a range of temperature, and developing a dissolution kinetic rate by numerical simulation based on a population balance model (leader: LAGEP & LGPM).
- 2) Screening various catalysts for lignin hydroconversion and identifying the best candidate by comparing the conversion and the selectivity toward aromatic compounds (leader: IRCELYON).
- 3) Catalytic testing in a semi-batch pilot and modeling the physical and chemical phenomena involved during the lignin hydroconversion in order to better understand the reaction

mechanisms and achieve the valuable chemical kinetic parameters (leader: IRCELYON & LAGEPP).

- 4) Optimizing the lignin dissolution with a solvent at a moderate temperature and developing a continuous process for lignin conversion potentially usable in a biorefinery (leader: IRCELYON & LAGEPP).
- 5) Studying the process flexibility and evaluating the economic viability of lignin conversion (leader: TOTAL).

The thesis involved in the project was Task 3, which is aimed to develop a kinetic model to simulate the temporal evolution of chemical compounds using the best catalyst. The developed kinetic model will play a crucial role in understanding, describing and scaling up the catalytic hydroconversion of lignin.

Batch reactor → Semi-batch reactor

Before the start-up of this project, previous works dedicated to lignin hydroconversion have already been performed by IRCELYON, using a wheat straw soda lignin (Protobind 1000), in tetralin with a sulfided NiMo catalyst under H₂ pressure in a conventional batch reactor^{16,65}. The separation protocol and analytical tools were well chosen, leading an excellent mass balance. As mentioned above, such a batch set-up may cause several drawbacks. Thus in this project, we upgraded the conventional batch reactor into a semi-opened batch system, which is a batch process for the liquid phase and continuous for the gas phase. By this way, the fresh H₂ can be introduced continuously and the gas phase can be removed and monitored in real-time. On one hand, the conversion can be more efficient by improving the H₂ partial pressure. On the other hand, the accurate real-time information about gas phase can help us understand the consumption of H₂ as well as the transformation of gases. Of course, it is also helpful for the kinetic modeling with lots of experimental points.

Thesis outline

According to the working content, the work of this thesis consists of two main parts:

- 1) The first part focuses on the experimental study of the catalytic hydroconversion of a wheat straw soda lignin over CoMoS/Al₂O₃ catalyst. The main objective is to gain insights for the chemical evolutions in function of reaction time. For achieving that, various analytical tools were applied to characterize the initial lignin feed and the effluents after reaction, presented in **Chapter II** accompanied with the description about the experimental set-up and protocol. In **Chapter III**, the characteristics of initial lignin feed are presented according to the analytical tools. The access of these information is mandatory to follow the transformations of lignin. Experimental results at various reaction times are provided in **Chapter IV**. In this chapter, relevant product properties and compositions were determined and rationalized in function of reaction time so as to elucidate the reaction mechanisms. Based on the experimental observations, a global reaction scheme for the catalytic hydroconversion of lignin with CoMoS/Al₂O₃ is proposed.
- 2) The second part is concentrated in the modeling the physical and chemical phenomena during the lignin hydroconversion using a semi-batch pilot. In order to achieve the accurate physico-chemical parameters by modeling, many chemical engineering aspects should be taken into consideration (hydrodynamics, mass transfer, vapor-liquid equilibrium (VLE) and reaction kinetics). In **Chapter V**, the following issues are presented and addressed:

- A. The gas hydrodynamics characterization of the flowing reactor has to be performed by residence time distribution (RTD) measurements in order to develop a gas flow model to describe the gas mixing inside correctly. By this way, the outlet gases can be treated accurately.
- B. For a multiphase reaction, dealing with mass transfer resistances is necessary to know the concentration changes within different phases. Typically, the mass transfer between gas and liquid was characterized using a linear driving force (ΔC) with the volumetric gas-liquid mass transfer coefficient ($k_L a$). Based on the measurements of N_2 absorption/desorption, the parameter of $k_L a$ of N_2 in operating conditions was able to be determined.
- C. At reaction conditions, the H_2 is mostly in the vapor phase with some dissolved in the liquid and considerable vaporization of compounds was not negligible. These two factors really impact the observed reaction kinetics. With the additional knowledge of VLE model, the H_2 concentration in the liquid phase and the vaporization ratio of compounds could be simulated, which improves the accuracy of kinetic modeling.

Finally, in **Chapter VI**, a tentative kinetic model was able to be established according to the proposed reaction scheme. The kinetic model was combined with the system mass balances to get a set of differential and algebraic equations, which can describe the dynamic variations of compounds in our set-batch reactor mathematically. The model simulation was performed with Matlab programming platform. The rate constants and the stoichiometric coefficients for the proposed reaction scheme were estimated by minimization of the sum squared differences between all the experimental points and corresponding simulated points.

Reference-I

- [1] Anwar, Z., Gulfraz, M., Irshad, M., 2014. Agro-industrial lignocellulosic biomass a key to unlock the future bio-energy: A brief review. *Journal of Radiation Research and Applied Sciences* 7, 163–173.
- [2] Rubin, E. M., 2008. Genomics of cellulosic biofuels. *Nature* 454, 841–845.
- [3] Zakzeski, J., Bruijninx, P.C.A., Jongerius, A. L., Weckhuysen, B.M., 2010. The Catalytic Valorization of Lignin for the Production of Renewable Chemicals. *Chemical Reviews* 110, 3552–3599.
- [4] Azadi, P., Inderwildi, O.R., Farnood, R., King, D.A., 2013. Liquid fuels, hydrogen and chemicals from lignin: A critical review. *Renewable and Sustainable Energy Reviews* 21, 506–523.
- [5] Zakzeski, J., Weckhuysen, B.M., 2011. Lignin Solubilization and Aqueous Phase Reforming for the Production of Aromatic Chemicals and Hydrogen. *ChemSusChem* 4, 369–378.
- [6] SJÖSTRÖM, E., Chapter 4 - LIGNIN, In *Wood Chemistry (Second Edition)*, Academic Press, San Diego, 1993, Pages 71-89, ISBN 978008092589.
- [7] Calvo-Flores, F. G., Dobado, J. A., Isac-García, J. and Martín-Martínez, F. J., 2015. Isolation of Lignins. In *Lignin and Lignans as Renewable Raw Materials*, 113-144.
- [8] Tejado, A., Peña, C., Labidi, J., Echeverria, J.M., Mondragon, I., 2007. Physico-chemical characterization of lignins from different sources for use in phenol-formaldehyde resin synthesis. *Bioresource Technology* 98, 1655–1663.

- [9] Holladay, J.E., White, J.F., Bozell, J.J., Johnson, D., 2007. Top Value-Added Chemicals from Biomass - Volume II—Results of Screening for Potential Candidates from Biorefinery Lignin.
- [10] Gosselink, R.J.A., 2011. Lignin as a renewable aromatic resource for the chemical industry. Ph.D. thesis, Wageningen, NL.
- [11] Tomani, P., 2010. The ligninboost process. *Cellulose chemistry & Technology* 44, 53-58.
- [12] Patt, R., Kordsachia, O., Süttinger, R., 2011. Pulp. In *Ulmann's Encyclopedia of industrial chemistry*.
- [13] The sulfite pulping process.
http://ied.ineris.fr/sites/default/interactive/brefpap/bref_pap/english/bref_gb_sulfite.htm. Accessed: 2016-10-20
- [14] Lora, J., 2008. Industrial commercial lignins: Sources, properties and applications. In: *Monomers, polymers and composites from renewable resources*. Belgacem, N.M. Gandini, A., (Eds). Elsevier publications, 225-241
- [15] Lignosulfonate application. <http://www.greenagrochem.com/application/>. Accessed: 2016-10-24.
- [16] Joffres, B., Lorentz, C., Vidalie, M., Laurenti, D., Quoineaud, A.-A., Charon, N., Daudin, A., Quignard, A., Geantet, C., 2014. Catalytic hydroconversion of a wheat straw soda lignin: Characterization of the products and the lignin residue. *Applied Catalysis B: Environmental* 145, 167–176.
- [17] Abächerli, A., Doppenberg, F., 2001, Method for preparing alkaline solutions containing aromatic polymers. US patent 6239198B1.
- [18] Barta, K., Matson, T.D., Fettig, M.L., Scott, S.L., Iretskii, A.V., Ford, P.C., 2010. Catalytic disassembly of an organosolv lignin via hydrogen transfer from supercritical methanol. *Green Chemistry* 12, 1640.
- [19] Arato, C., Pye, E.K., Gjennestad, G., 2005. The lignol approach to biorefining of woody biomass to produce ethanol and chemicals. *Applied biochemistry and biotechnology* 123, 871–882.
- [20] CIMV process. <http://www.cimv.fr/>. Accessed: 2016-10-25.
- [21] Arato, C., Pye, E.K., Gjennestad, G., 2005. The lignol approach to biorefining of woody biomass to produce ethanol and chemicals. *Applied biochemistry and biotechnology* 123, 871–882.
- [22] Tolbert, A., Akinosho, H., Khunsupat, R., Naskar, A.K., Ragauskas, A.J., 2014. Characterization and analysis of the molecular weight of lignin for biorefining studies. *Biofuels, Bioproducts and Biorefining* 8, 836–856.
- [23] Evstigneev, E.I., 2011. Factors affecting lignin solubility. *Russian Journal of Applied Chemistry* 84, 1040–1045.
- [24] Pepper, J.M., Baylis, P.E.T., Adler, E., 1959. The isolation and properties of lignins obtained by the acidolysis of spruce and aspen woods in dioxane-water medium. *Canadian Journal of Chemistry* 37, 1241–1248.
- [25] Onnerud, H., 2002. Polymerization of Monolignols by Redox Shuttle-Mediated Enzymatic Oxidation: A New Model in Lignin Biosynthesis I. *THE PLANT CELL ONLINE* 14, 1953–1962.
- [26] Yang, H., Yan, R., Chen, H., Lee, D.H., Zheng, C., 2007. Characteristics of hemicellulose, cellulose and lignin pyrolysis. *Fuel* 86, 1781–1788.

- [27] Kloekhorst, A., 2015. Biobased chemicals from lignin. PhD thesis, University of Groningen, NL.
- [28] Vuori, A., Bredenberg, J.B., 1988. Liquefaction of Kraft Lignin: 1. Primary Reactions under Mild Thermolysis Conditions. *Holzforschung* 42, 155–161.
- [29] Huibers, D.T., Parkhurst Jr, H.J., 1983. Lignin hydrocracking process to produce phenol and benzene. Google Patents.
- [30] Connors, W.J., Johanson, L.N., Sarkanen, K.V., Winslow, P., 1980. Thermal Degradation of Kraft Lignin in Tetralin. *Holzforschung* 34, 29–37.
- [31] Brebu, M., Vasile, C., 2010. Thermal degradation of lignin—a review. *Cellulose Chemistry & Technology* 44, 353.
- [32] Ragauskas, A.J., Beckham, G.T., Bidddy, M.J., Chandra, R., Chen, F., Davis, M.F., Davison, B.H., Dixon, R.A., Gilna, P., Keller, M., Langan, P., Naskar, A.K., Saddler, J.N., Tschaplinski, T.J., Tuskan, G.A., Wyman, C.E., 2014. Lignin Valorization: Improving Lignin Processing in the Biorefinery. *Science* 344, 1246843–1246843.
- [33] Afifi, A.I., Hindermann, J.P., Chornet, E., Overend, R.P., 1989. The cleavage of the aryl-O-CH₃ bond using anisole as a model compound. *Fuel* 68, 498–504.
- [34] Thring, R.W., Breau, J., 1996. Hydrocracking of solvolysis lignin in a batch reactor. *Fuel* 75, 795–800.
- [35] Sharma, R.K., Bakhshi, N.N., 1991. Catalytic upgrading of biomass-derived oils to transportation fuels and chemicals. *The Canadian Journal of Chemical Engineering* 69, 1071–1081.
- [36] Adjaye, J.D., Bakhshi, N.N., 1995. Production of hydrocarbons by catalytic upgrading of a fast pyrolysis bio-oil. Part II: Comparative catalyst performance and reaction pathways. *Fuel Processing Technology* 45, 185–202.
- [37] Sheu, Y.-H.E., Anthony, R.G., Soltes, E.J., 1988. Kinetic studies of upgrading pine pyrolytic oil by hydrotreatment. *Fuel Processing Technology* 19, 31–50.
- [38] Gosselink, R.J.A., de Jong, E., Guran, B., Abächerli, A., 2004. Co-ordination network for lignin—standardisation, production and applications adapted to market requirements (EUROLIGNIN). *Industrial Crops and Products* 20, 121–129.
- [39] Top 9 things you didn't know about carbon fiber. <http://energy.gov/articles/top-9-things-you-didn-t-know-about-carbon-fiber>. Accessed: 2016-11-22,
- [40] Park, S.-J., Heo, G.-Y., 2015. Precursors and Manufacturing of Carbon Fibers, in: *Carbon Fibers*. Springer Netherlands, Dordrecht, pp. 31–66.
- [41] Baker, D.A., Rials, T.G., 2013. Recent advances in low-cost carbon fiber manufacture from lignin. *Journal of Applied Polymer Science* 130, 713–728.
- [42] Mainka, H., Täger, O., Körner, E., Hilfert, L., Busse, S., Edelmann, F.T., Herrmann, A.S., 2015. Lignin – an alternative precursor for sustainable and cost-effective automotive carbon fiber. *Journal of Materials Research and Technology* 4, 283–296.
- [43] Otani, S., Fukuoka, Y., Igarashi, B., Sasaki, K., 1969. Method for producing carbonized lignin fiber. US patent 3461082A.

- [44] Chemistry of lignin-based materials, 2013. *Green Materials* 1, 137–160.
- [45] Bonini, C., D’Auria, M., Emanuele, L., Ferri, R., Pucciariello, R., Sabia, A.R., 2005. Polyurethanes and polyesters from lignin. *Journal of Applied Polymer Science* 98, 1451–1456.
- [46] Cetin, N.S., Özmen, N., 2002. Use of organosolv lignin in phenol–formaldehyde resins for particleboard production: I. Organosolv lignin modified resins. *International Journal of Adhesion and Adhesives* 22, 477–480.
- [47] Zhao, B., Chen, G., Liu, Y., Hu, K., Wu, R., 2001. Synthesis of lignin base epoxy resin and its characterization. *Journal of Materials Science Letters* 20, 859–862.
- [48] Chung, Y.-L., Olsson, J.V., Li, R.J., Frank, C.W., Waymouth, R.M., Billington, S.L., Sattely, E.S., 2013. A Renewable Lignin–Lactide Copolymer and Application in Biobased Composites. *ACS Sustainable Chemistry & Engineering* 1, 1231–1238.
- [49] Pandey, M.P., Kim, C.S., 2011. Lignin Depolymerization and Conversion: A Review of Thermochemical Methods. *Chemical Engineering & Technology* 34, 29–41.
- [50] Li, X., Su, L., Wang, Y., Yu, Y., Wang, C., Li, X., Wang, Z., 2012. Catalytic fast pyrolysis of Kraft lignin with HZSM-5 zeolite for producing aromatic hydrocarbons. *Frontiers of Environmental Science & Engineering* 6, 295–303.
- [51] Bridgwater, A.V., Peacocke, G.V.C., 2000. Fast pyrolysis processes for biomass. *Renewable and Sustainable Energy Reviews* 4, 1–73.
- [52] Joffres, B., Laurenti, D., Charon, N., Daudin, A., Quignard, A., Geantet, C., 2013. Thermochemical Conversion of Lignin for Fuels and Chemicals: A Review. *Oil Gas Sci. Technol. – Rev. IFP Energies Nouvelles* 68, 753–763.
- [53] Elfadly, A.M., Zeid, I.F., Yehia, F.Z., Rabie, A.M., Aboualala, M.M., Park, S.-E., 2016. Highly selective BTX from catalytic fast pyrolysis of lignin over supported mesoporous silica. *International Journal of Biological Macromolecules* 91, 278–293.
- [54] Wiinikka, H., Carlsson, P., Granberg, F., Löfström, J., Marklund, M., Tegman, R., Lindblom, M., Gebart, R., 2010. Design and methodology of a high temperature gas sampling system for pressurized black liquor gasification. *Fuel* 89, 2583–2591.
- [55] Ferdous, D., Dalai, A.K., Bej, S.K., Thring, R.W., 2002. Pyrolysis of Lignins: Experimental and Kinetics Studies. *Energy & Fuels* 16, 1405–1412.
- [56] Furusawa, T., Sato, T., Sugito, H., Miura, Y., Ishiyama, Y., Sato, M., Itoh, N., Suzuki, N., 2007. Hydrogen production from the gasification of lignin with nickel catalysts in supercritical water. *International Journal of Hydrogen Energy* 32, 699–704.
- [57] Barbier, J., Charon, N., Dupassieux, N., Loppinet-Serani, A., Mahé, L., Ponthus, J., Courtiade, M., Ducrozet, A., Quoineaud, A.-A., Cansell, F., 2012. Hydrothermal conversion of lignin compounds. A detailed study of fragmentation and condensation reaction pathways. *Biomass and Bioenergy* 46, 479–491.
- [58] Saisu, M., Sato, T., Watanabe, M., Adschiri, T., Arai, K., 2003. Conversion of Lignin with Supercritical Water–Phenol Mixtures. *Energy & Fuels* 17, 922–928. <https://doi.org/10.1021/ef0202844>
- [59] Ramsurn, H., Gupta, R.B., 2012. Production of Biocrude from Biomass by Acidic Subcritical Water Followed by Alkaline Supercritical Water Two-Step Liquefaction. *Energy & Fuels* 26, 2365–2375.

- [60] Oregui Bengoechea, M., Hertzberg, A., Miletić, N., Arias, P.L., Barth, T., 2015. Simultaneous catalytic de-polymerization and hydrodeoxygenation of lignin in water/formic acid media with Rh/Al₂O₃, Ru/Al₂O₃ and Pd/Al₂O₃ as bifunctional catalysts. *Journal of Analytical and Applied Pyrolysis* 113, 713–722.
- [61] Yuan, Z., Cheng, S., Leitch, M., Xu, C. (Charles), 2010. Hydrolytic degradation of alkaline lignin in hot-compressed water and ethanol. *Bioresource Technology* 101, 9308–9313.
- [62] Oasmaa, A., Alén, R., Meier, D., 1993. Catalytic hydrotreatment of some technical lignins. *Bioresource Technology* 45, 189–194.
- [63] Meier, D., Berns, J., Faix, O., Balfanz, U., Baldauf, W., 1994. Hydrocracking of organocell lignin for phenol production. *Biomass and Bioenergy* 7, 99-105,
- [64] McMillen, D.F., Malhotra, R., Tse, D.S., 1991. Interactive effects between solvent components: possible chemical origin of synergy in liquefaction and coprocessing. *Energy & Fuels* 5, 179–187.
- [65] Joffres, B., Nguyen, M.T., Laurenti, D., Lorentz, C., Souchon, V., Charon, N., Daudin, A., Quignard, A., Geantet, C., 2016. Lignin hydroconversion on MoS₂-based supported catalyst: Comprehensive analysis of products and reaction scheme. *Applied Catalysis B: Environmental* 184, 153–162.
- [66] Pinheiro, A., Hudebine, D., Dupassieux, N., Geantet, C., 2009. Impact of Oxygenated Compounds from Lignocellulosic Biomass Pyrolysis Oils on Gas Oil Hydrotreatment. *Energy & Fuels* 23, 1007–1014.
- [67] Kloekhorst, A., Heeres, H.J., 2015. Catalytic Hydrotreatment of Alcell Lignin Using Supported Ru, Pd, and Cu Catalysts. *ACS Sustainable Chemistry & Engineering* 3, 1905–1914.
- [68] Kumar, C.R., Anand, N., Kloekhorst, A., Cannilla, C., Bonura, G., Frusteri, F., Barta, K., Heeres, H.J., 2015. Solvent free depolymerization of Kraft lignin to alkyl-phenolics using supported NiMo and CoMo catalysts. *Green Chem.* 17, 4921–4930.
- [69] Meier, D., Ante, R., Faix, O., 1992. Catalytic hydrolysis of lignin: Influence of reaction conditions on the formation and composition of liquid products. *Bioresource Technology* 40, 171–177.
- [70] Kloekhorst, A., Wildschut, J., Heeres, H.J., 2014. Catalytic hydrotreatment of pyrolytic lignins to give alkylphenolics and aromatics using a supported Ru catalyst. *Catal. Sci. Technol.* 4, 2367–2377.
- [71] Horáček, J., Homola, F., Kubičková, I., Kubička, D., 2012. Lignin to liquids over sulfided catalysts. *Catalysis Today* 179, 191–198.
- [72] Harris, E.E., D'Ianni, J., Adkins, H., 1938. Reaction of hardwood lignin with hydrogen. *Journal of the American Chemical Society* 60, 1467–1470.
- [73] Pepper, J.M., Hibbert, H., 1948. Studies on Lignin and Related Compounds. LXXXVII. High Pressure Hydrogenation of Maple Wood¹. *Journal of the American Chemical Society* 70, 67–71.
- [74] Yan, N., Zhao, C., Dyson, P.J., Wang, C., Liu, L., Kou, Y., 2008. Selective Degradation of Wood Lignin over Noble-Metal Catalysts in a Two-Step Process. *ChemSusChem* 1, 626–629.
- [75] Ratcliff, M. A., Johnson, D. K., Posey, F. L., Chum, H. L., 1988. Hydrodeoxygenation of Lignins and Model Compounds. *Applied biochemistry and biotechnology* 17, 151-160.
- [76] De Wild, P., Van der Laan, R., Kloekhorst, A., Heeres, E., 2009. Lignin valorisation for chemicals and (transportation) fuels via (catalytic) pyrolysis and hydrodeoxygenation. *Environmental Progress & Sustainable Energy* 28, 461–469.

- [77] Košíková, B., Polčín, J., 1973. 55_Isolation of lignin from spruce by acidolysis in dioxane. *Wood Science and Technology* 7, 308–316.
- [78] Strüven, J.O., Meier, D., 2016. Hydrocracking of Organosolv Lignin in Subcritical Water to Useful Phenols Employing Various Raney Nickel Catalysts. *ACS Sustainable Chemistry & Engineering* 4, 3712–3721.
- [79] Barta, K., Warner, G.R., Beach, E.S., Anastas, P.T., 2014. Depolymerization of organosolv lignin to aromatic compounds over Cu-doped porous metal oxides. *Green Chem.* 16, 191–196.
- [80] Tang, Z., Zhang, Y., Guo, Q., 2010. Catalytic Hydrocracking of Pyrolytic Lignin to Liquid Fuel in Supercritical Ethanol. *Industrial & Engineering Chemistry Research* 49, 2040–2046.
- [81] Ye, Y., Zhang, Y., Fan, J., Chang, J., 2012. Selective production of 4-ethylphenolics from lignin via mild hydrogenolysis. *Bioresource Technology* 118, 648–651.
- [82] Zhang, X., Zhang, Q., Long, J., Xu, Y., Wang, T., Ma, L., Li, Y., 2014. Phenolics Production through Catalytic Depolymerization of Alkali Lignin with Metal Chlorides. *BioResources* 9, 3347–3360.
- [83] Oregui-Bengoechea, M., Gandarias, I., Arias, P.L., Barth, T., 2017. Unraveling the Role of Formic Acid and the Type of Solvent in the Catalytic Conversion of Lignin: A Holistic Approach. *ChemSusChem* 10, 754–766.
- [84] Huang, X., Korányi, T.I., Boot, M.D., Hensen, E.J.M., 2015. Ethanol as capping agent and formaldehyde scavenger for efficient depolymerization of lignin to aromatics. *Green Chemistry* 17, 4941–4950.
- [85] Huibers, D.T., Parkhurst Jr, H.J., 1983. Lignin hydrocracking process to produce phenol and benzene. US Patent 4420644A.
- [86] Motoyoshi, O., Yoshio, M., Kan, K., 1965. Method for liquefying lignin, US patent 3223698A.
- [87] Oshima, M., Kashima, K., Kubo, T., Tabata, H., Watanabe, H., 1966. Studies of the hydrocracking of lignin. I. The hydrocracking of desulfonated sulfite waste lignin. *Bulletin of the Chemical Society of Japan* 39, 2750–2755.
- [88] Oshima, M., Kashima, K., Tabata, H., Watanabe, H., Kubo, T., 1966. Studies of the Hydrocracking of Lignin. IV. The Evaluation of the Catalysts. *Bulletin of the Chemical Society of Japan* 39, 2763–2767.
- [89] Klopries, B., Hodek, W., Bandermann, F., 1990. Catalytic hydroliquefaction of biomass with red mud and CoO-MoO₃ catalysts. *Fuel* 69, 448–455.
- [90] Kleinert, T., 1952. Hydrogenation of Lignin with Cyclohexanol. *Monatsh* 83, 623–628.
- [91] Oshima, M., Kashima, K., 1960. Solubilization of Lignin, Japanese patent 7058.
- [92] Turpeinen, E.-M., 2011. Hydrodeoxygenation of methyl heptanoate and phenol over sulphided supported NiMo and CoMo catalysts. PhD thesis, Aalto University.
- [93] Bui, V.N., Laurenti, D., Afanasiev, P., Geantet, C., 2011. Hydrodeoxygenation of guaiacol with CoMo catalysts. Part I: Promoting effect of cobalt on HDO selectivity and activity. *Applied Catalysis B: Environmental* 101, 239–245.
- [94] Rahimpour, H.R., Saidi, M., Rostami, P., Gates, B.C., Rahimpour, M.R., 2016. Experimental Investigation on Upgrading of Lignin-Derived Bio-Oils: Kinetic Analysis of Anisole Conversion on

Sulfided CoMo/Al₂O₃ Catalyst: EXPERIMENTAL INVESTIGATION ON UPGRADING OF LIGNIN-DERIVED BIO-OILS. *International Journal of Chemical Kinetics* 48, 702–713.

[95] Wang, X., Rinaldi, R., 2016. Bifunctional Ni catalysts for the one-pot conversion of Organosolv lignin into cycloalkanes. *Catalysis Today* 269, 48–55.

[96] Zhang, W., Chen, J., Liu, R., Wang, S., Chen, L., Li, K., 2014. Hydrodeoxygenation of Lignin-Derived Phenolic Monomers and Dimers to Alkane Fuels over Bifunctional Zeolite-Supported Metal Catalysts. *ACS Sustainable Chemistry & Engineering* 2, 683–691.

[97] Jegers, H.E., Klein, M.T., 1985. Primary and secondary lignin pyrolysis reaction pathways. *Industrial & Engineering Chemistry Process Design and Development* 24, 173–183.

[98] Adam, M., Ocone, R., Mohammad, J., Berruti, F., Briens, C., 2013. Kinetic Investigations of Kraft Lignin Pyrolysis. *Industrial & Engineering Chemistry Research* 52, 8645–8654.

[99] Farag, S., Kouisni, L., Chaouki, J., 2014. Lumped Approach in Kinetic Modeling of Microwave Pyrolysis of Kraft Lignin. *Energy & Fuels* 28, 1406–1417.

[100] Klein, M.T., Virk, P.S., 2008. Modeling of Lignin Thermolysis. *Energy & Fuels* 22, 2175–2182.

[101] Faravelli, T., Frassoldati, A., Migliavacca, G., Ranzi, E., 2010. Detailed kinetic modeling of the thermal degradation of lignins. *Biomass and Bioenergy* 34, 290–301.

[102] Hou, Z., Bennett, C.A., Klein, M.T., Virk, P.S., 2010. Approaches and Software Tools for Modeling Lignin Pyrolysis. *Energy & Fuels* 24, 58–67.

[103] Hough, B.R., Schwartz, D.T., Pfaendtner, J., 2016. Detailed Kinetic Modeling of Lignin Pyrolysis for Process Optimization. *Industrial & Engineering Chemistry Research* 55, 9147–9153.

[104] Yanez, A.J., Natarajan, P., Li, W., Mabon, R., Broadbelt, L.J., 2018. Coupled Structural and Kinetic Model of Lignin Fast Pyrolysis. *Energy & Fuels* 32, 1822–1830.

[105] Zhang, B., Huang, H.J., Ramaswamy, S., 2008. Reaction Kinetics of the Hydrothermal Treatment of Lignin. *Applied Biochemistry and Biotechnology* 147, 119–131.

[106] Gasson, J.R., Forchheim, D., Sutter, T., Hornung, U., Kruse, A., Barth, T., 2012. Modeling the Lignin Degradation Kinetics in an Ethanol/Formic Acid Solvolysis Approach. Part 1. Kinetic Model Development. *Industrial & Engineering Chemistry Research* 51, 10595–10606.

[107] Forchheim, D., Gasson, J.R., Hornung, U., Kruse, A., Barth, T., 2012. Modeling the Lignin Degradation Kinetics in a Ethanol/Formic Acid Solvolysis Approach. Part 2. Validation and Transfer to Variable Conditions. *Industrial & Engineering Chemistry Research* 51, 15053–15063.

[108] Yong, T.L.-K., Matsumura, Y., 2012. Reaction Kinetics of the Lignin Conversion in Supercritical Water. *Industrial & Engineering Chemistry Research* 51, 11975–11988.

[109] Yong, T.L.-K., Matsumura, Y., 2013. Kinetic Analysis of Lignin Hydrothermal Conversion in Sub- and Supercritical Water. *Industrial & Engineering Chemistry Research* 52, 5626–5639.

[110] Forchheim, D., Hornung, U., Kruse, A., Sutter, T., 2014. Kinetic Modelling of Hydrothermal Lignin Depolymerisation. *Waste and Biomass Valorization* 5, 985–994.

Chapter II. Materials and Methods

II.1 Introduction

In our study, a commercial technical lignin named Protobind 1000 (P1000) was chosen to investigate the catalytic hydroconversion over CoMoS/Al₂O₃ catalyst. The catalytic tests were carried out in a semi-continuous set-up, open for gas phase with continuous feeding of H₂, and equipped with a condensing reflux followed by cooled traps. A series of kinetic study was carried out at several residence times (0-13 h). Due to the set-up and an adapted recovery protocol, gaseous, solid and liquid products were well separated and quantified. Comprehensive analyses were performed to each fraction in order to describe and understand the various reactions occurring versus residence time.

In this chapter, the materials used in our experiment are reported firstly. Secondly, different analytical methods used are presented. Thirdly, the preparation and the characterization of the employed catalyst are described. At last, the experimental protocol as well as the separation method are described.

II.2 Materials

II.2.1 Lignin

Protobind 1000 lignin used in these experiments was produced by soda pulping of wheat straw and was supplied by GreenValue (Switzerland). It is a type of lignin with a low content of ashes and carbohydrates. It has a very low water solubility at neutral and acid pH. Under alkaline conditions (pH > 12), complete solubility is achieved.

II.2.2 Chemicals

The reagents used were as follows:

- ❖ 1,2,3,4-tetrahydronaphthalene (tetralin), Sigma-Aldrich, ≥ 99.0 %.
- ❖ Pyridine, Carlo-Erba, ≥ 99.9 %.
- ❖ Acetic anhydride, Prolabo, analytic grade.
- ❖ Tetrahydrofuran (THF), Sigma-Aldrich, ≥ 99.9 %.
- ❖ *N*-heptane, Carlo-Erba, 99.2 % pure.
- ❖ 2-chloro-4,4,5,5-tetramethyl-1,3,2-dioxapholane (TMDP), Sigma-Aldrich, 95 %.
- ❖ CDCl₃, Sigma-Aldrich, 99.8 % atom D.
- ❖ DMSO-d₆, Sigma-Aldrich, 99.9 % atom D.
- ❖ Aniline, Sigma-Aldrich, ≥ 99.5 %.
- ❖ Tetramethylthiourea, Sigma-Aldrich, 98 %.
- ❖ Cyclohexanol, Sigma-Aldrich, 99 %.
- ❖ Chromium (III) acetylacetonate, Sigma-Aldrich, 97 %.

II.2.3 Catalyst

The catalyst used was an industrial CoMo catalyst (HR306) produced by Axens France. Its main properties are reported in Table II.1. It is in oxidized state in the form of extrudates (length: 2-10 mm, diameter: 1.2 mm), composed of CoO (3 wt%), MoO₃ (14 wt%), and γ -Al₂O₃ (83 wt%). Before each test, the catalyst was activated by an ex-situ sulfidation.

Table II.1: Metal composition of the oxidized catalyst

Metal	wt%
Cobalt (Co)	2.6
Molybdenum (Mo)	9.3

II.3 Analytical methods

II.3.1 Elemental analysis (CHONS)

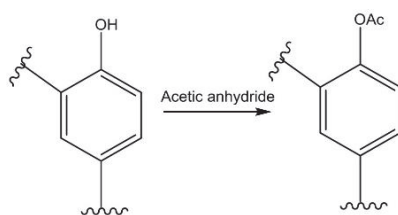
For the measurement of C, H, O, N and S mass fraction, a Thermo Scientific Flash 2000 apparatus was used. C, H, S and N in the liquid or solid samples were combusted (up to 1800 °C) to CO₂, H₂O, SO₂ and NO_x respectively. These gases were first separated, followed by quantification via thermal conductivity detection. To analyze oxygen, the sample was pyrolyzed to CO and the quantification was performed by thermal conductivity detection. It should be pointed out that the obtained oxygen content from the analysis does not include the oxygen from water.

II.3.2 Thermogravimetric analysis (TGA)

The lignin was thermally characterized by TGA with a SETARAM TGA 92 featuring automated temperature and weight control as well as data acquisition. The samples were analyzed as received using a heating rate of 5 °C/min from 25 to 800 °C. Air was used as carrier gas. The weight loss at 100 °C corresponds to the water content, whereas the remaining weight at the end corresponds to the ash content.

II.3.3 Gel permeation chromatography (GPC)

The GPC analyses were based on the previously developed methods for determining the molecular weight distribution of lignin^{1,2}. Analyses were performed by using an Agilent apparatus (1200 series) equipped with two PLgel columns (50 and 500 Å) and a differential refractive index (DRI) detector. Analyses were carried out at 35 °C using a THF as eluent at a flow rate of 1 mL/min. Samples were dissolved at around 1 wt% in THF before injection. The GPC system was calibrated with polystyrene standards in a molecular range from 162 to 55100 g/mol. Depicted chromatograms were normalized to the sample weight. Since the initial lignin is not entirely soluble in the eluent, the acetylation of initial lignin sample is required to dissolve it entirely (Scheme II.1). The residual lignin obtained after each test was completely soluble in THF and did not need to be acetylated.

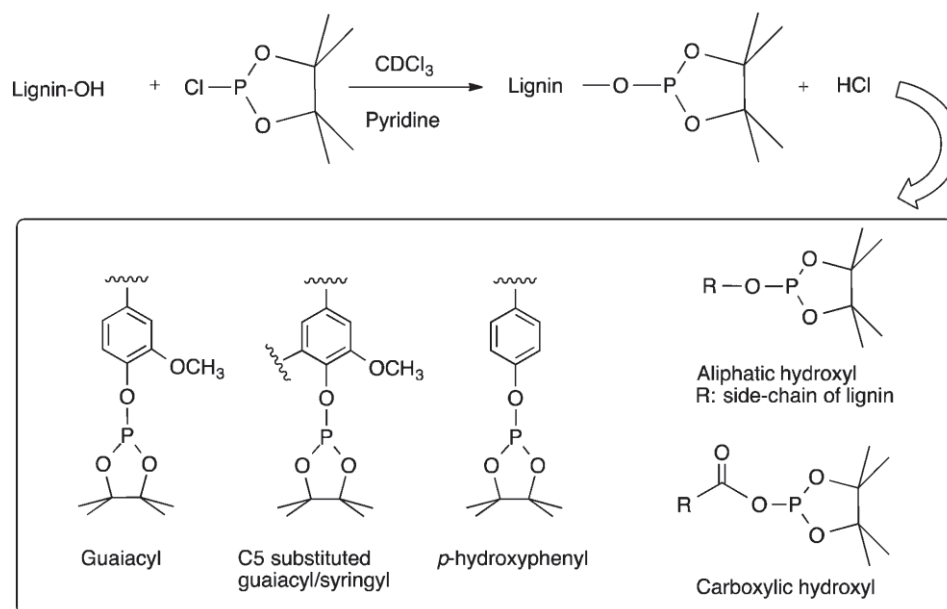


Scheme II.1: Acetylation of hydroxyl groups in lignin

II.3.4 Nuclear magnetic resonance (NMR)

The ^1H and ^{13}C NMR techniques enable basic structural characterizations. Around 50 mg of sample was dissolved in 1000 mg of DMSO-d_6 using a Bruker Avance 1000MHz. ^1H spectra were acquired with single pulse acquisitions, ^{13}C spectra with inverse gated decoupling. All the acquisitions were carried out by heating the sample at 50 °C. Tetramethylthiourea ($\text{C}_5\text{H}_{12}\text{N}_2\text{S}$) with 1 bond of C=S and 12 bonds of C-H was used as an internal standard for quantification (Table II.2 and II.3).

^{31}P NMR data were obtained with a Bruker Avance III 500MHz. ^{31}P NMR technique was used for the characterization and the quantification of OH groups on the basis of previously developed methods involving a prior derivative phosphitylation step (Scheme II.2). The phosphorous atoms bonded to former alcohol or phenols have different chemical shifts that enabled us to quantify each OH groups (Table II.4). Samples were accurately weighted (c.a 30 mg) and dissolved in a solution containing 200 mg of pyridine, 100 mg of an internal standard solution in pyridine (cyclohexanol: 15.7 mg/g), 100 mg of 2-chloro-4,4,5,5-tetramethyl-1,3,2-dioxaphospholane (TMDP), and 200 mg of CDCl_3 .



Scheme II.2: Reaction of tag hydroxyls presented in lignin with 2-chloro-4,4,5,5-tetramethyl-1,3,2-dioxaphospholane³

Table II.2: NMR chemical shift for ^1H

Chemical shift (^1H) ppm	Characteristic groups
0.2-2.4	Aliphatic <u>H</u>
3	<u>H</u> in tetramethylthiourea (standard)
4.1-4.6	<u>H</u> of $-\text{OCH}_3$
4.8-5.6	Unsaturated aliphatic <u>H</u>
6.0-7.8	Aromatic <u>H</u>
7.8-9.4	<u>H</u> of phenolic OH
9.4-10.8	<u>H</u> of $-\text{CHO}$
11.6-13.6	<u>H</u> of $-\text{COOH}$

Table II.3: NMR chemical shift for ^{13}C

Chemical shift (^{13}C) ppm	Characteristic groups
10-36	Aliphatic <u>C</u>
54-58	Methoxy $-\text{O}\underline{\text{C}}\text{H}_3$
58-90	Aliphatic <u>C</u> -O (without $-\text{OCH}_3$)
102-125	<u>C</u> _{aromatic} -H
125-142	<u>C</u> _{aromatic} -C
142-162	<u>C</u> _{aromatic} -O
166-180	R(H)-O- <u>C</u> =O
192-195	<u>C</u> =S in tetramethylthiourea (standard)

Table II.4: NMR chemical shift for ^{31}P

Chemical shift (^{31}P) ppm	Characteristic groups
133-135	Carboxylic $\text{COO}\underline{\text{H}}$
136.4-137.6	<i>p</i> -hydroxyphenolic units
137.6-138.6	Catechol units
138.6-140.2	Guaiacyl phenolic units
140.2-143.8	Syringyl phenolic units + condensed phenolic units
143.8-145	<u>OH</u> in cyclohexanol (standard)
145-150.5	Aliphatic <u>OH</u>

II.3.5 Karl-Fischer titration

Karl-Fischer titration is a classic titration method to determine the water content in a sample. Analyses were performed with a Metrohm Titrando 852 via coulometric titration. Before each analysis, the sample (organic phase and aqueous phase) was diluted with THF in order to make its concentration of water around 300 ppm.

II.3.6 μ GC-TCD

The μ GC-TCD technique was used to identify and quantify non-condensable gases formed during lignin hydroconversion. The μ GC (SRA instruments R) was equipped with three columns and a TCD detector. A 5 Å molecular sieve column (length: 10 m, diameter: 12 μ m) was used to analyze H₂, CH₄ and CO; the carrier gas was helium; the backflush injector temperature was maintained at 80 °C and the column temperature was kept constant at 80 °C. A Poraplot U column (length: 8 m, diameter: 30 μ m) was used to separate CO₂, ethane, and ethylene; the carrier gas was hydrogen; the backflush injector temperature was maintained at 90 °C and the column temperature was kept at 80 °C. An alumina column (length: 10 m, diameter: 3 μ m) was used to analyze C₃-C₆ hydrocarbons; the carrier gas was hydrogen; injection temperature was maintained at 90 °C, while the column temperature was kept at 70 °C. Before carrying out the analyses, the μ GC was calibrated with standard gas mixtures (hydrogen, carbon monoxide, carbon dioxide, methane, ethane, propane, *n*-butane, isobutene, pentane, isopentane, hexane, 2-methylpentane, ethylene, propylene, 1-butene, 1,3-butadiene, 1-pentane, 1-hexene).

II.3.7 GC \times GC technique

GC \times GC is a two-dimensional gas chromatography designed to separate complex organic mixtures. It is equipped with two different chromatographic columns, as shown in Figure II.1. The two columns are connected via a modulator which quickly traps the effluent from the first dimension, then injects into the second column. This process can create two dimensional chromatogram⁴, illustrated in Figure II.2. The set of two columns can be configured with various types. The traditional set is the first dimension column with a non-polar column, followed by a polar column. In our case for the separation of polar compounds in a non-polar matrix, a reverse-phase column set gives more resolutions. In this situation, the first dimension column is more polar than the second column.

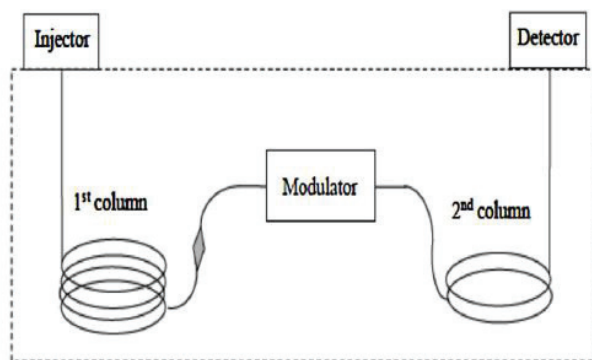


Figure II.1: Configuration of columns and modulator⁴

In our study, samples were injected without any further dilution since the liquid samples were prior diluted by the presence of tetralin. MS chromatograms were recorded using an Agilent 6890 apparatus with a liquid nitrogen cryogenic jet modulation from Zoex Corporation coupled with a 5975B qMS (Scan parameters: from 45 to 300 μ at 22 scan/s) detector. The first column was a moderately polar VF1701

column (30 m × 0.25 mm × 0.25 μm) and the second column was an apolar DB1 column (2 m × 0.1 mm × 0.1 μm). The temperature program of the first oven started at 50 °C for 5 min and then was heated up to 350 °C with a heating rate of 1.8 °C/min until 350 °C. The second oven started at 50 °C for 0 min and then heated up at 1.8 °C/min until 320 °C. The modulation time was 12 s and the modulator hot jet temperature was set to 280 °C. GC×GC-FID analyses were carried out using the same columns set on the same apparatus equipped with an FID detector. Extra addition of aniline was used as external standard for all samples.

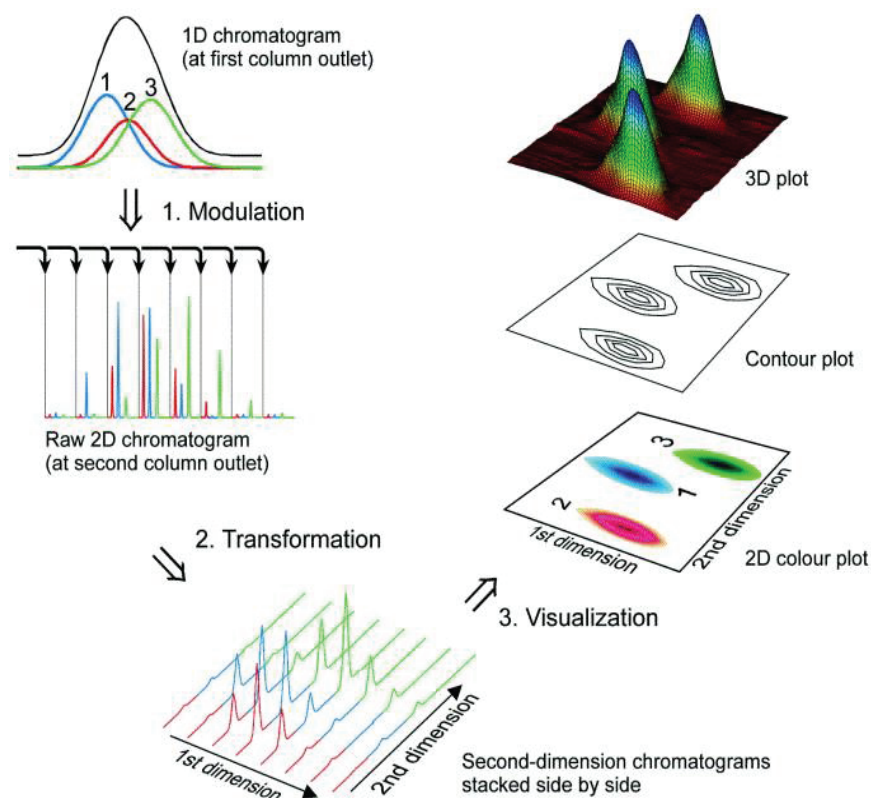


Figure II.2: 2D image reconstruction method⁵

With the aid of the GC Image software, the contour plotting, peak fitting and blob integration were performed. The NIST-MS 2011 was used for peak identification. Quantification was performed using Effective Carbon Number⁶ (ECN) to predict FID response factors for identified compounds (Table II.5). The mass fraction (w_i) of each compound (family) was calculated using the mass fraction (w_{st}) of aniline, peak volumes obtained and the response relative to aniline:

$$w_i = \frac{f_i V_i}{f_{st} V_{st}} \times w_{st} \quad (2.1)$$

where f_i is the response factor for compound (family) i , V_i is the peak volume of compound (family) i , f_{st} is the response factor for aniline and V_{st} is the peak volume of aniline.

Table II.5: Contributions to the ECN

Type of atom	ECN contribution
Aliphatic and aromatic C	1
Olefinic C	0.95
Carbonyl and carboxyl C	0
Ether O	-1
Primary alcoholic O	-0.6 (*)
Secondary alcoholic O	-0.75
Tertiary alcoholic O	-0.25

- * The ECN contribution of primary alcoholic O was modified from -0.5 to -0.6 in order to improve the accuracy

II.4 Catalyst activation and characterization

II.4.1 Catalyst sulfidation

The catalyst sulfidation was undertaken at atmospheric pressure and 400 °C, using a continuous-flow of H₂S/H₂ (15/85 vol%) for 4 h. The volumetric flow rate was 4 L/h. After the sulfidation, the reactor was cooled and swept with nitrogen for 30 min to evacuate sulfur excess.

II.4.2 Elemental and textural properties of sulfide catalyst

The content of sulfur in the fresh sulfide catalyst was analyzed with Thermo Scientific Flash 2000 apparatus. Its sulfur content was 7.5 wt%, which is close to its theoretical maximal value at complete sulfidation. The textural properties were characterized by the N₂ isotherm adsorption at 77 K (reported in Table II.6), measured on Micrometrics ASAP 2010 equipment. Before the N₂ adsorption, the sulfide catalyst was out-gassed at 300 °C for 3 hours under vacuum. The surface area was determined by the BET model (Figure II.3), and the total pore volume and the average pore size were characterized by the BJH method (Figure II.4). The nitrogen isotherm curves show that the catalyst is mesoporous (> 2 nm), and the size distribution of pore is monomodal.

Table II.6: Textural properties of fresh sulfide catalyst

Bet surface area (m ² /g)	193
Total pore volume (cm ³ /g)	0.47
Average porous size (nm)	7.94

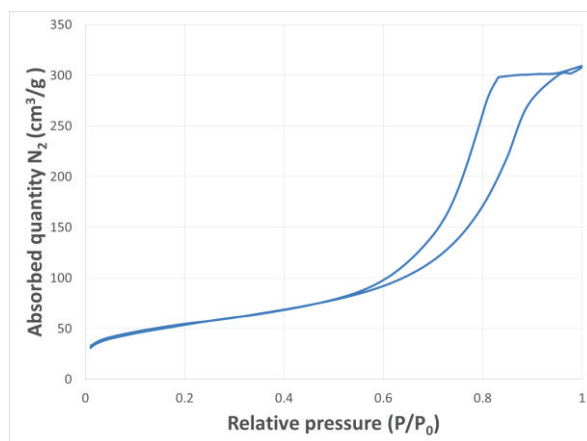


Figure II.3: N_2 -adsorption isotherm curve of fresh sulfide catalyst

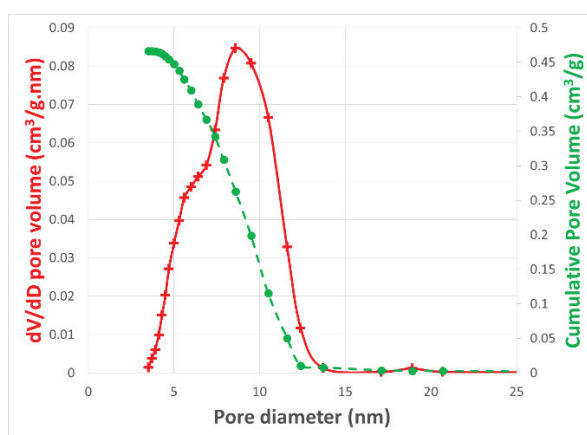


Figure II.4: BJH desorption curves of fresh sulfide catalyst

II.5 Hydroconversion experiments

II.5.1 Experimental set-up

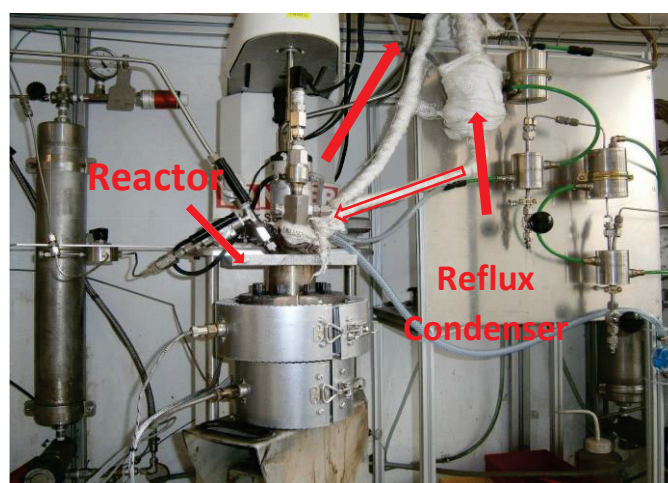


Figure II.5: Photo of the experimental set-up

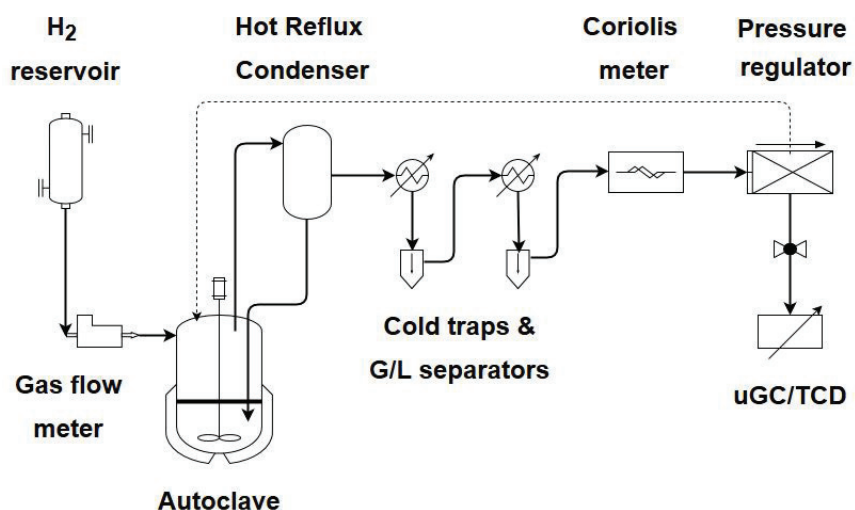


Figure II.6: Schematic diagram of the experimental set-up

A semi-continuous set-up consisting of several sections was designed for the study of lignin hydroconversion, as shown in Figure II.5. A simplified schematic diagram of the experimental set-up is presented in Figure II.6. The reactor is a magnetically stirred autoclave (Parr Instrument) of 300 mL, equipped with a gas-inducing Rushton impeller and the baffles. A H₂ reservoir was located at the left side of the set-up, and the inlet H₂ flow was controlled by a gas flow meter (maximal flow: 200 NL/h). Using a downstream pressure regulator, the pressure inside of the set-up was maintained at a defined value during the experiment, thereby the vapor phase in the reactor was continuously removed to a hot reflux condenser at the upper left side. The hot reflux condenser is an approximative cylindrical vessel of 150 mL that operates at a lower temperature than that of the reactor, allowing to condensate a part of vapors into liquid. The bottom of the condenser was linked to the reactor via a connecting tube (extended into the liquid phase), so the condensed liquid can be recycled continuously into the reactor by the motor of gravity. Here, the function of the hot reflux condenser is not only condensing the solvent as it is essential not only for a recycle/economy purpose, but also removing water (which might be poisonous to the catalyst) and some relatively light products to avoid over-hydrogenation.

Afterward, two series of cold trap (1 m of spiral steel tube) and a gas/liquid (G/L) separator (17.6 mL) are used to split gaseous products and liquid products further, respectively at 15 and 4 °C. The trapped liquids were cumulated in the gas-liquid separator during a run without sampling. At the outlet of set-up, the non-condensable gases were quantified by a Coriolis meter and analyzed online by a μ GC-TCD.

II.5.2 Experimentation of catalytic tests

Before each test, the lignin P1000 was dried at 80 °C under vacuum for 4 h to eliminate the water content. For each test, 30 g of dried lignin and 70 g of tetralin were introduced into the reactor with 3 g of fresh sulfide CoMo/ γ -Al₂O₃ catalyst. The reactor was closed and flushed 3 times with 10 bar of H₂ to remove the air. The experimental procedure of experimentation was as follows (Figure II.7):

1) Pressurisation period

The set-up was pressurized to 80 bar with a maximal flow of H₂.

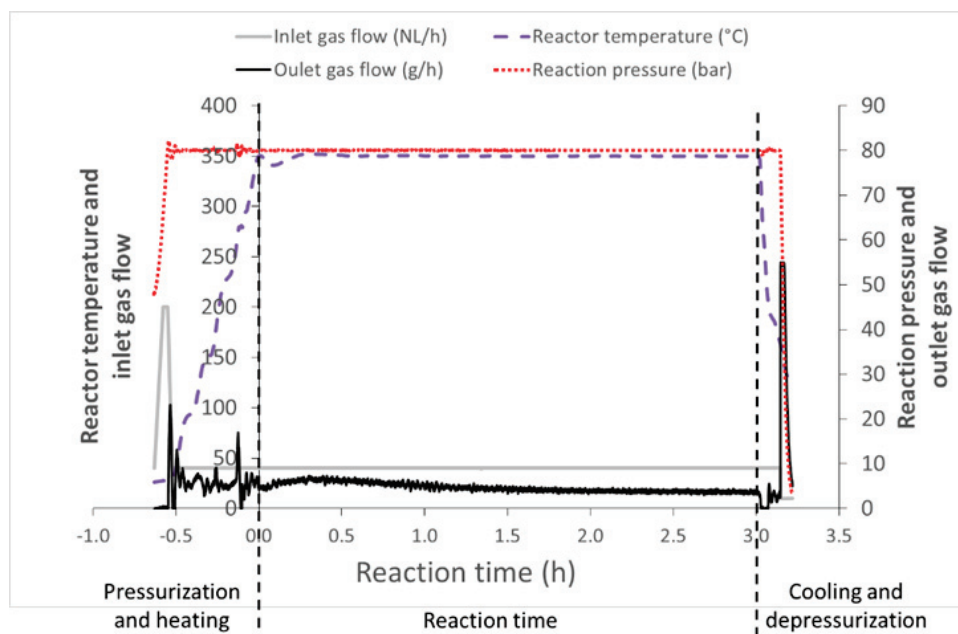


Figure II.7: Example of monitored parameter profiles of the experimental set-up (3 h)

2) Heating period

As soon as the pressure reached 80 bar, the reactor and the hot reflux condenser were heating up and the agitation ($N = 800$ rpm) started. Meanwhile, inlet flow (Q_{H_2}) decreased to 40 NL/h. Heating the reflux condenser to 160 °C needs about 20 min and heating the reactor to the desired temperature of 350 °C takes about 40 min, and the moment is the starting point of residence time, so-called t_0 point. The pressure was kept constant at 80 bar during the whole period.

3) Stationary period

The length of the stationary period is the reaction time of lignin conversion. The operating conditions were maintained during the whole period:

- * $T_{\text{Reactor}} = 350$ °C
- * $T_{\text{Reflux}} = 160$ °C
- * $P = 80$ bar
- * $N = 800$ rpm
- * $Q_{H_2} = 40$ NL/h

4) Cooling and depressurization period

After the residence time, the bottom of the reactor was cooled using an ice bath, while the top of the reactor was still heated to remove moisture deposition at the top of the reactor. When the temperature of the reactor was 160 (± 10) °C, a fast depressurization started and all the gases inside of set-up were evacuated.

During the whole experimentation, the outlet gases were quantified by a Coriolis meter every second and analyzed by $\mu\text{GC-TCD}$ every 3.5 minutes to assess the gas composition evolution.

II.5.3 Product recovery protocol

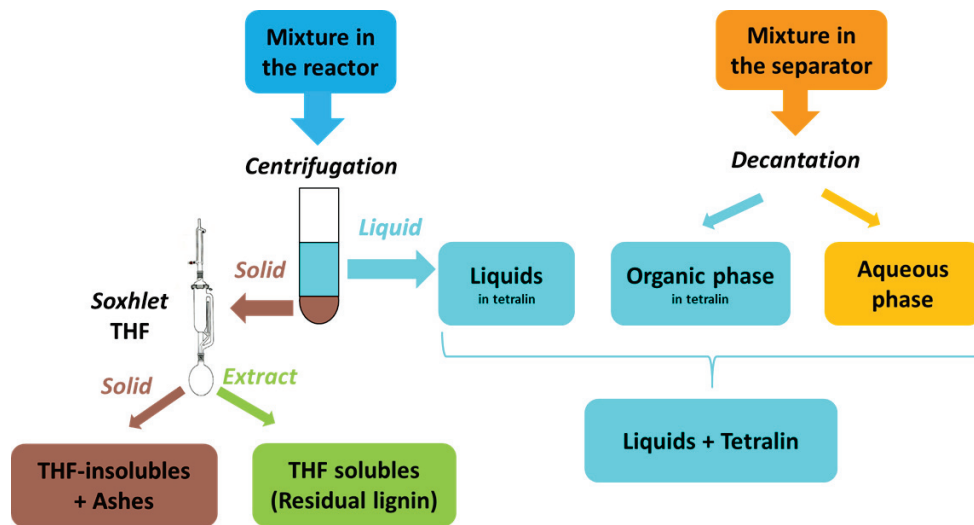


Figure II.8: Product recovery protocol for the reacted mixture

As shown in Figure II.8, two reacted mixtures were obtained for each test. The reacted mixture in the reactor was firstly centrifugated to separate liquids and solids. Afterward, the solids were extracted in a Soxhlet apparatus using THF. After this step, the obtained THF-insoluble solids contained the used catalysts (extrudate cylindrical solid) and a part of THF-insoluble lignin residues (fine black powder). The THF-insoluble residues were separated from the used catalysts by sieving. In this thesis, the part of THF-insoluble lignin residues will be further referred as “THF-insoluble residues”. However, the initial non-convertible ashes were still present in the THF-insoluble residues. By subtracting the ashes content, the remaining convertible THF-insoluble lignin residues as so-called “THF-insolubles”.

$$m_{\text{THF-insolubles}} = m_{\text{THF-insoluble residues}} - m_{\text{initial ashes}} \quad (2.2)$$

The THF-soluble fraction (black granules) was recovered after THF evaporation. In this thesis, the part of solid lignin residue will be further referred as “THF-solubles”. The two parts of liquids in the reactor and the separator were both mixed with tetralin and its derivatives. The cumulated mixture in the separator was decanted to separate the organic phase and the aqueous phase. The total liquid production from lignin was calculated by summing all the liquid fractions and subtracting the initial solvent (assuming the mass of tetralin does not change during the reaction).

$$m_{\text{liquids}} = m_{\text{liquids in the reactor}} + m_{\text{liquids in the separator}} - m_{\text{tetralin}} (70 \text{ g}) \quad (2.3)$$

The gas mixture was composed of H_2 , CH_4 , CO_2 , CO , and light alkanes C_2 - C_6 . Its total mass flow rate (Q_m) was quantified by the Coriolis meter, as shown in Figure II.9. The gas composition (y_i) in function of time was analyzed by the $\mu\text{GC-TCD}$, as shown in Figure II.10. The fraction of H_2 was estimated by summing all the gases equal to 1. By combining the two curves, it allows to calculate the partial mass flux ($Q_{i,m}$) and the cumulated production (m_i^{total}) of each gas compound (except H_2).

$$Q_{i,m} = \frac{Q_m M_i}{\sum y_i M_i} \quad (2.4)$$

$$m_i^{total} = \int Q_{i,m} dt \quad (2.5)$$

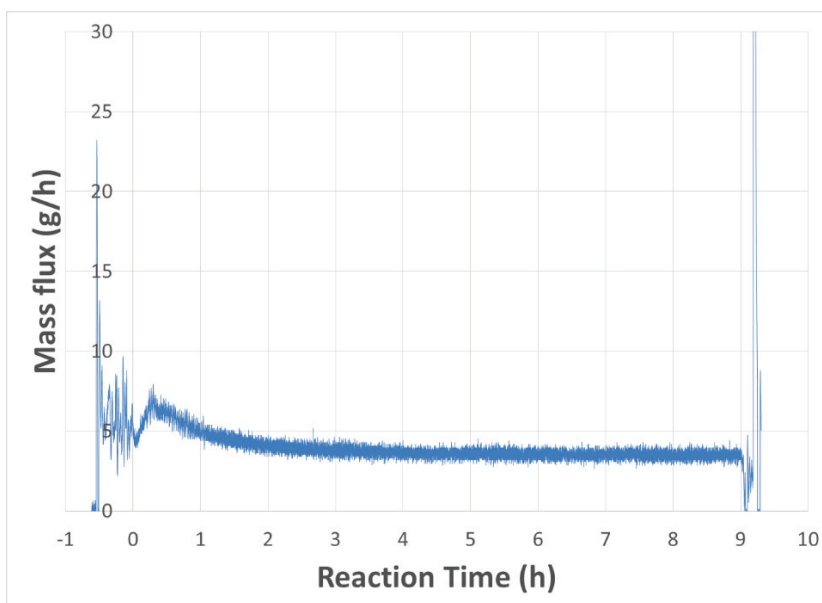


Figure II.9: Example of dynamic gas flow out of set-up (9 h)

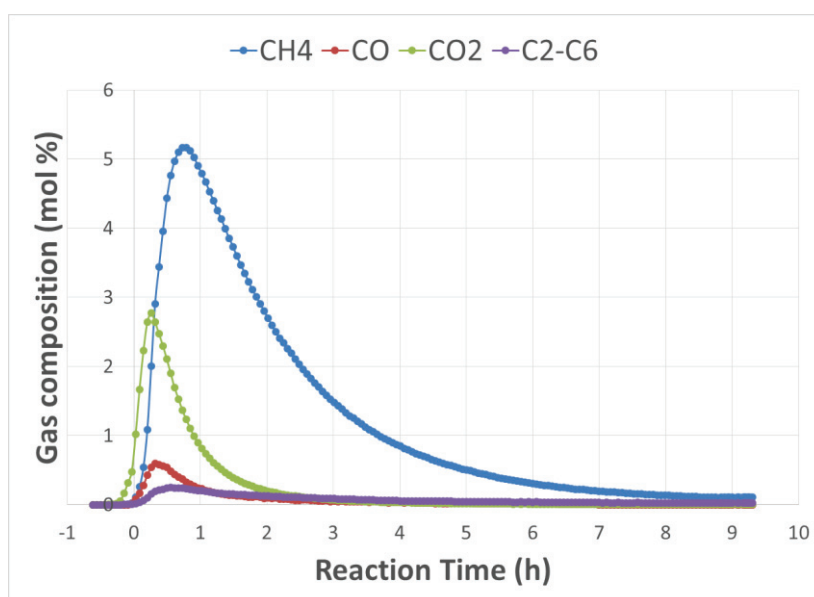


Figure II.10: Example of the evolution of gas composition out of set-up (9 h)

II.6 Analytical strategy

For the conversion study, analytical strategy is very important to follow the transformations. The analytical strategy of our study is listed in Table II.7. Before the conversion, a comprehensive knowledge of starting lignin is necessary in view of its complexity and its associations with the

converted products. As a result, the reference lignin was characterized by various analytical tools (CHONS, TGA, GPC and NMR). These quantitative and qualitative information provide an overall picture of how what the initial lignin looks like. In addition, it can be considered as a reference to investigate the transformations. The detailed characterization of lignin will be discussed in the following chapter.

After the conversion, different fractions of products were recovered: gas, solids and liquids. In order to better understand the transformations, a wide range of characterizations were performed for different fractions. In this way, the lignin conversion was monitored and allowed us to establish the evolution of different fractions versus residence time in order to understand and prove the transformations occurring during the process. The results of the catalytic test will be presented within **Chapter IV**. Furthermore, the used catalysts were characterized to evaluate how the catalysts were affected during the reactions.

Table II.7: Characterization strategy in our work

	Type	Techniques
Feedstock	Lignin P1000	CHONS, TGA, GPC, NMR (¹ H, ¹³ C, ³¹ P)
Product	Gas	μGC-TCD
	THF-insoluble residues	CHONS
	THF-soluble residual lignin	CHONS, GPC, NMR (¹ H, ¹³ C, ³¹ P)
	Liquid fraction in the reactor	CHONS, GPC, NMR (¹³ C), GC×GC-MS/FID, Karl Fischer
	Organic phase in the separator	CHONS, GC×GC-MS/FID
	Aqueous phase in the separator	CHONS, GC×GC-MS, Karl Fischer
Catalyst	CoMoS/Al ₂ O ₃	CHONS, BET

Reference-II

- [1] Milne, T.A., Chum, H.L., Agblevor, F., Johnson, K., 1992. Standardized analytical methods. *Biomass and Bioenergy* 2, 341-366.
- [2] Cathala, B., Saake, B., Faix, O., Monties, B., 2003. Association behaviour of lignins and lignin model compounds studied by multidetector size-exclusion chromatography. *Journal of Chromatography A* 1020, 229–239.
- [3] Yoo, C.G., Li, M., Meng, X., Pu, Y., Ragauskas, A.J., 2017. Effects of organosolv and ammonia pretreatments on lignin properties and its inhibition for enzymatic hydrolysis. *Green Chemistry* 19, 2006–2016.
- [4] Lorentz, C., Laurenti, D., Zotin, J.L., Geantet, C., 2017. Comprehensive GC × GC chromatography for the characterization of sulfur compound in fuels: A review. *Catalysis Today* 292, 26–37.
- [5] Dallüge, J., Beens, J., Udo, A., 2003. Comprehensive two-dimensional gas chromatography: a powerful and versatile analytical tool. *Journal of Chromatography A* 1000, 69–108.
- [6] Scanlon, J.T., Willis, D.E., 1985. Calculation of flame ionization detector relative response factors using the effective carbon number concept. *Journal of Chromatographic Science* 23, 333–34.

Chapter III. Characterization of Lignin Protobind 1000

III.1 Introduction

The lignin we studied is a type of technical lignin isolated from wheat straw by soda process. During the isolation treatment, NaOH was employed as cook chemical and some ether bonds were cleaved to create free phenolic OHs. The supplier did not provide further information about the precipitation process and the intrinsic characteristics of lignin¹. Hence, comprehensive characterizations of lignin P1000 are required to understand more about it.

Before the catalytic conversion, various analytic tools were used to characterize the initial lignin, including TGA, CHONS, GPC and NMR. In parallel, we studied the lignin solubility and analyzed the two fractions found in the initial lignin after dissolving in THF (THF-insoluble fraction and THF-soluble fraction). For the concern of analysis and reaction conversion, this THF-insoluble fraction should be distinguished from the THF-soluble fraction. In the chapter, the characteristics of lignin P1000 are presented according to the analytical tools.

III.2 Solubility

The starting lignin Protobind 1000 is in the form of fine brown powder, as shown in Figure III.1. The lignin shows a limited solubility in water at atmospheric temperature. However, it is more soluble in polar aprotic solvents like acetone, DMSO and THF. Like many studies²⁻⁴, THF is employed as the extraction solvent for residual lignin.



Figure III.1: Photo of lignin Protobind 1000

Lignin P1000 is not 100 wt% soluble in THF. For this reason, soxhlet extracting using THF is employed to determine the corresponding content of the initial THF-soluble fraction as well as the initial THF-insoluble fraction. The result indicates that 91 wt% of the initial lignin was soluble in THF, and 9 wt% of the initial lignin was not soluble in THF.

III.3 Elemental analysis

Element analysis, ash and water contents as well as the H/C and O/C atomic ratios of lignin P1000, are reported in Table III.1. The contents of water (at 100 °C) and ashes (at 600 °C) were determined by TGA and were respectively equal to 2.1 wt% and 3.1 wt% of the lignin. H/C and O/C atomic ratios are respectively 1.12 and 0.37. In the literature, H/C is near 1.1 and O/C is between 0.25 and 0.4^{2,5}, so lignin P1000 we used is one type of lignin moderately oxygenated. In addition, less than 1 wt% of both sulfur and nitrogen contents were found in the lignin. This sulfur content is lower than that of kraft lignin and lignosulfonate.

Table III.1: Elemental analysis and atomic ratios of lignin P1000 and its different fractions

wt%	P1000	THF-soluble fraction (91 wt%)	THF-insoluble fraction (9 wt%)	P1000 reconstruction (*)
C	61.1	63.2	39.0	61.1
H	5.7	6.2	3.6	6.0
O	29.9	28.5	35.9	29.1
N	0.7	0.7	0.9	0.7
S	0.9	0.8	5.1	1.2
Ashes	3.1	n.d.	n.d.	n.d.
Water	2.1	n.d.	n.d.	n.d.
Total	103.4	99.4	84.6	98.1
Atomic ratios				
H/C	1.12	1.18	1.11	1.17
O/C	0.37	0.34	0.69	0.36

* The reconstruction is estimated by the sum of CHONS contributions found for THF-insoluble and THF-soluble fractions in proportion to their weights. These calculated values are close to the measurements of P1000.

The THF-soluble fraction, representing 91 wt% of lignin P1000, has nearly the same elemental composition as lignin P1000. However, the THF-insoluble fraction, representing 9 wt% of P1000, is much more oxygenated than the THF-soluble fraction (O/C ratio: 0.69 > 0.34). The total organic content of THF-insoluble fraction is far less than 100 wt%, probably because the insoluble fraction contains the majority of ashes (3 wt%) in the lignin. Therefore, by deducting the ash content, about 6 wt% of initial lignin is not soluble in THF but still convertible.

The analysis of ashes was not carried out in our work. However, a previous analysis of ICP-AES was performed by *Joffres et al.*⁶ on the same type of lignin, but not on the same lot. The results show the inorganics present in this lignin are Si (0.3-0.4 wt%), Na (0.2 wt%) and other minor metals (Fe, Al, Ca, etc.).

III.4 Molecular weight distribution

An acetylation of the -OH groups was done to ensure the entire dissolution of lignin P1000 in THF before the GPC analysis. GPC analysis was also performed only for the initial THF-soluble fraction. The molecular weight distribution curves are given in Figure III.2 and relative quantifications are reported in Table III.2. Here, it must be pointed out that GPC provides a way to measure the molecular weight distribution easily and rapidly, but the results it gives are not absolute and quantitative. For the lignin study, the GPC is usually sufficient to characterize the molar mass averages and distributions.

The mass average molar weight (M_w) of acetylated lignin P1000 is 2929 g/mol in polystyrene (PS) equivalent with a PDI of 2.8. Thus, lignin P1000 is a type of technical lignin severely degraded after the soda isolation process⁷. By comparing to the initial lignin, the THF-soluble fraction has smaller intensities in the region of high-molecular-weight molecules (right part of GPC curve), showing a smaller M_w of 1644 g/mol. It can be assumed that the THF-insoluble fraction contains a lot of higher size molecules that makes its dissolutions in THF difficult. In this work, GPC analysis was not performed solely for the initial THF-soluble fraction. Given the similarity of structure between the THF-soluble fraction and the THF-insoluble fraction, a value of M_w at about 16000 g/mol can be estimated for the initial THF-soluble by deducting of the THF-soluble fraction from the initial lignin. The value of M_w for the THF-insoluble fraction will be necessary in the kinetic modeling (**Chapter VI**).

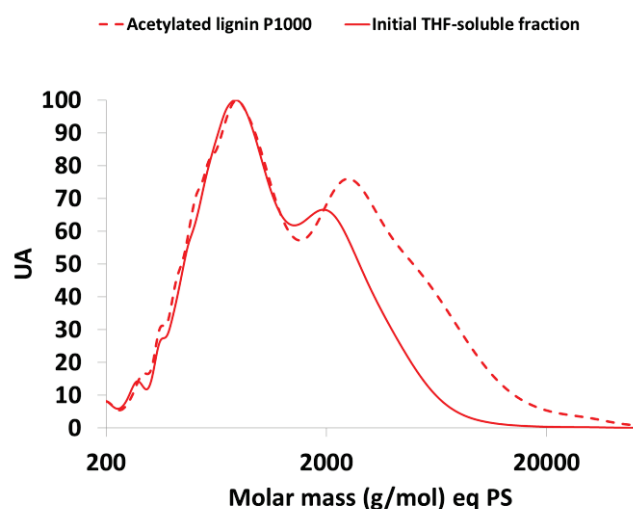


Figure III.2: Molecular weight distributions of the acetylated lignin P1000 and the initial THF-soluble fraction

Table III.2: Average molar weight and PDI measured by GPC

	wt%	M_w (g/mol)	PDI
Acetylated lignin P1000	100	2929	2.8
THF-soluble fraction	91	1644	1.9
THF-insoluble fraction	9	16000 (estimated)	n.d.

III.5 Structural analysis

III.5.1 ^1H NMR

^1H NMR spectra obtained for lignin P1000 is illustrated in Figure III.3. This technique allows to identify and quantify several characteristic groups. After the attribution of different peaks, relative quantifications for different groups are listed in Table III.3.

The total quantified H concentration by this technique is $29.6 \text{ mmol/g}_{\text{lignin}}$, which accounts for 52 wt% of the H mass fraction measured by elemental analysis ($57 \text{ mmol/g}_{\text{lignin}}$). The proportion is relatively low since a portion of unsaturated aliphatic H and aliphatic oxygenated H was not quantified, including the ether bonds, the methoxy units and the aliphatic OH. Effectively those peaks are located in the region of 3-6 ppm and are superposed with the peaks of water and internal standard (tetramethylthiourea), making their quantifications impossible. The phenolic OH quantification is $3.7 \text{ mmol/g}_{\text{lignin}}$, and the carboxylic COOH is $0.6 \text{ mmol/g}_{\text{lignin}}$.

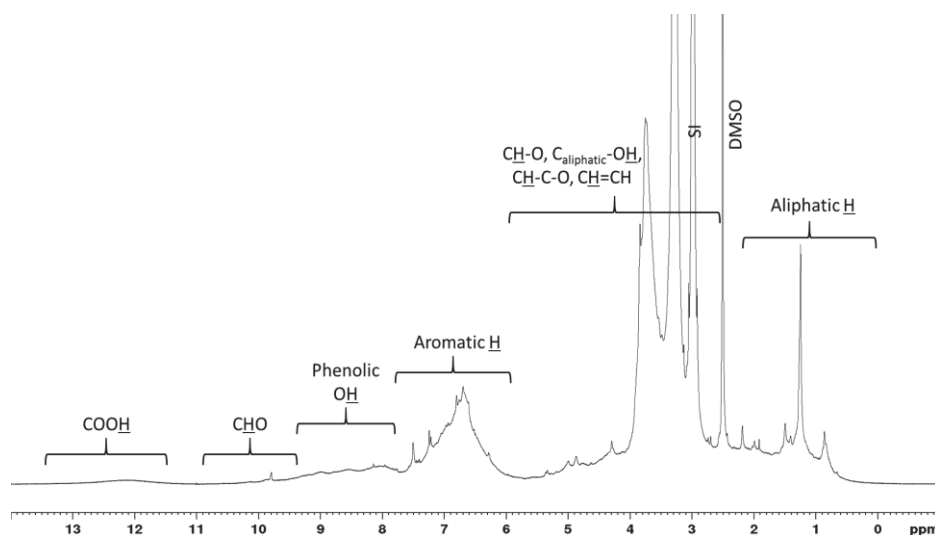


Figure III.3: ^1H NMR spectra of lignin P1000

Table III.3: Relative quantification by ^1H NMR

Chemical shift (^1H) ppm	Characteristic groups	Concentration ($\text{mmol/g}_{\text{lignin}}$)
0.2-2.4	Aliphatic <u>H</u>	11.6
6.0-7.8	Aromatic <u>H</u>	12.0
7.8-9.4	Phenolic <u>OH</u>	3.7
9.4-10.8	Aldehyde <u>CH=O</u>	1.7
11.6-13.6	Carboxylic <u>COOH</u>	0.6
Total quantified <u>H</u>		29.6
3.0-6.0	Aliphatic oxygenated H (<u>CH-O</u> , <u>C_{aliphatic}-OH</u> , <u>CH-C-O</u>) and unsaturated aliphatic H (<u>CH=C-</u>)	n.d.

III.5.2 ^{13}C NMR

^{13}C NMR spectra obtained for lignin P1000 is illustrated in Figure III.4. Unlike ^1H NMR, ^{13}C NMR can access the quantification information of oxygenated aliphatic groups without the problem of superposition. The relative quantifications of different carbon groups are listed in Table III.4.

By the addition of all the groups, the total detected carbon concentration by ^{13}C NMR is 52 mmol/ g_{lignin} , corresponding to 62 wt% of initial lignin. The mass proportion of carbon is in good accordance with the result of 61 wt% carbon obtained by elemental analysis, indicating that the ^{13}C NMR technique can efficiently detect all carbons.

The content of aromatic rings in lignin can be calculated easily from the analysis $(C_{\text{aromatic-H}} + C_{\text{aromatic-C}} + C_{\text{aromatic-O}})/6$: 5.7 mmol/ g_{lignin} . Thereby, the aromatic rings available for the depolymerization represent about 40 wt% of the studied lignin P1000. Furthermore, the average number of methoxy groups per aromatic ring is 0.8. The concentration of aliphatic C-O (without $-\text{OCH}_3$) is 2.5 mmol/ g_{lignin} and aliphatic C-OH (^{31}P NMR in § III.5.3) is 1.5 mmol/ g_{lignin} , so the ether bonds of aliphatic C-O-C can be estimated to be 1 mmol/ g_{lignin} . Therefore, we can postulate that 18 ether bonds are present per 100 aromatic units. This ether linkage abundance is relatively low compared to native lignin (40-50 %) which is not so surprising since the soda isolation process may cleave the ether bonds partially.

CO_2 is formed from the decarboxylation of $-\text{COOR}$ (H). Assuming that carboxylic groups are fully converted to CO_2 , for the conversion of 30 g lignin, the maximal CO_2 obtained is about 2.4 g (8 wt% of initial feed).

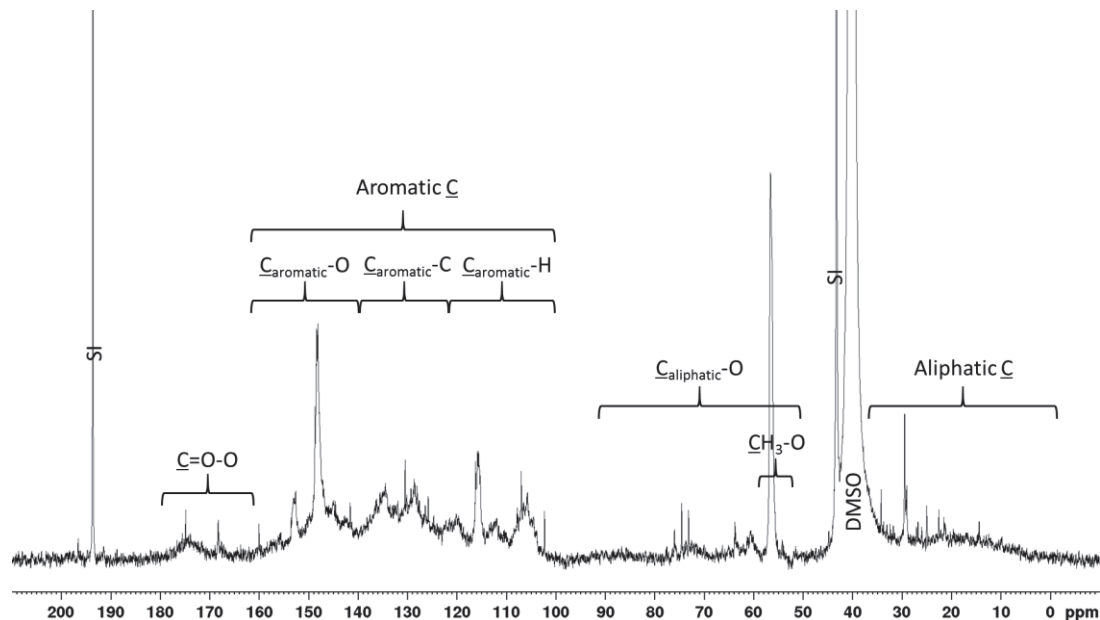


Figure III.4: ^{13}C NMR spectra of lignin P1000

Table III.4: Relative quantification by ^{13}C NMR

Chemical shift (^{13}C) ppm	Characteristic groups	Concentration (mmol/g _{lignin})
10-36	Aliphatic $\underline{\text{C}}$	8.8
54-58	$-\text{O}\underline{\text{C}}\text{H}_3$	4.8
58-90	Aliphatic $\underline{\text{C}}-\text{O}$ (without $-\text{OCH}_3$)	2.5
102-125	$\underline{\text{C}}_{\text{aromatic}}-\text{H}$	11.0
125-142	$\underline{\text{C}}_{\text{aromatic}}-\text{C}$	11.7
142-162	$\underline{\text{C}}_{\text{aromatic}}-\text{O}$	11.5
166-180	$\text{O}-\underline{\text{C}}=\text{O}-\text{R}$ (H)	1.8
Total quantified $\underline{\text{C}}$		52

III.5.3 ^{31}P NMR

^{31}P NMR spectra obtained for lignin P1000 is illustrated in Figure III.5. The identification and quantification of different OH groups after phosphitylation are listed in Table III.5.

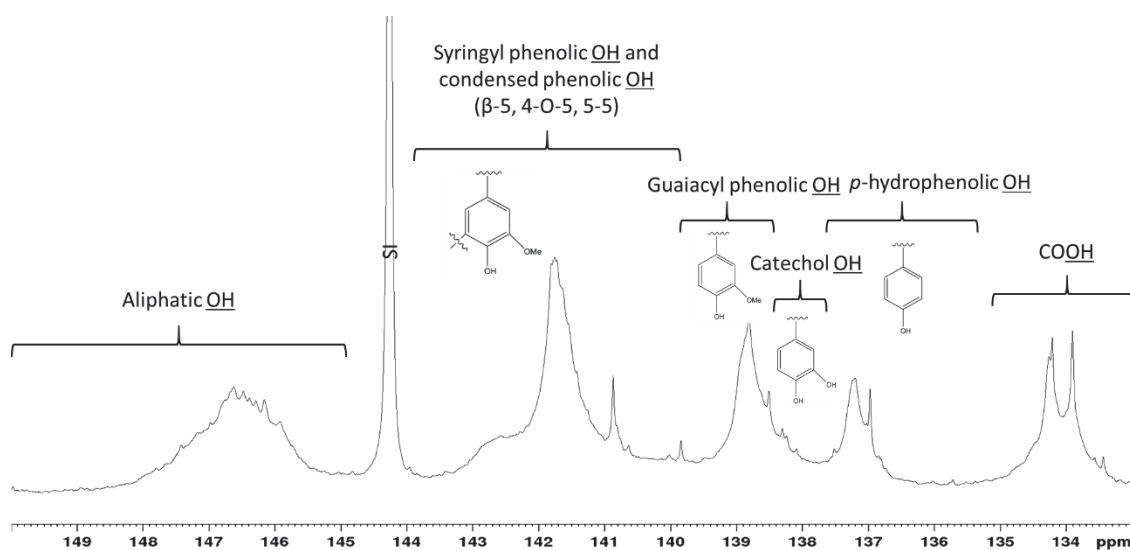


Figure III.5: ^{31}P NMR spectra of lignin P1000

The presence of aliphatic OH is confirmed and quantified (1.5 mmol/g_{lignin}). The concentration of $-\text{COOH}$ is 0.8 mmol/g_{lignin}, which is relatively in accordance with the ^1H NMR analysis (0.6 mmol/g_{lignin}). The quantification of total phenolic OH (p -Hydroxyphenolic units [H] + guaiacyl phenolic units [G] + syringyl phenolic units + condensed phenolic units [S]) is 3.8 mmol/g_{lignin}, which is also relatively in accordance with the analysis ^1H NMR (3.7 mmol/g_{lignin}). The proportions of S/G/H units among the phenolic units of lignin P1000 is about 52/34/13. However, the proportion of syringyl units was overestimated due to the signals of condensed phenolic units in the same region. In addition, no catechol units were detected.

H₂O can be produced from the dehydroxylation of aliphatic or phenolic OH. Assuming that aliphatic OH groups fully dehydroxylated to H₂O, for the conversion of 30 g lignin, the water obtained is about 0.8 g (2.7 wt% of initial feed). Similarly, assuming that phenolic OH groups are fully dehydroxylated to H₂O, the water obtained is about 2.1 g (6.8 wt% of initial feed).

Table III.5: Relative quantification by ³¹P NMR

Chemical shift (³¹ P) ppm	Characteristic groups	Concentration (mmol/g _{lignin})
133-135	Carboxylic COOH	0.8
136.4-137.6	<i>p</i> -Hydroxyphenolic units	0.5
137.6-138.6	Catechol units	0
138.6-140.2	Guaiacyl phenolic units	1.3
140.2-143.8	Syringyl phenolic units + condensed phenolic units	2.0
145-150.5	Aliphatic OH	1.5
Total quantified OH		6.1

III.6 Conclusion

In the chapter, we used various analytical tools to deeply characterize the starting lignin P1000. Qualitative and quantitative information about its elemental composition, molecular weight distribution and characteristic groups were achieved. According to CHONS analysis, we know that lignin has a higher oxygen content compared to the petroleum. Thus, for the production of BTX or fuels, it will be necessary to achieve high yields of deoxygenated products. On the contrary, for the production of phenolic compounds, the depolymerization of lignin without extensive deoxygenation is preferred. In addition, we were able to obtain the information about lignin structure by NMR technique. These oxygen atoms in lignin are involved in different bonds and functional groups, including ether bonds, aliphatic OH, carboxylic groups, methoxy groups and phenolic OH. By ³¹P NMR after phosphorylation, the ratio of fundamental phenolic units (S/G/H) was seen.

Overall, the access of all the lignin characterizations will be essential to follow the transformations occurring of lignin by the thermochemical processes.

Reference-III

- [1] www.bio-based.eu/ibib/pdf/47.pdf. Accessed: 2017-12-23.
- [2] Huang, X., Korányi, T.I., Boot, M.D., Hensen, E.J.M., 2014. Catalytic Depolymerization of Lignin in Supercritical Ethanol. *ChemSusChem* 7, 2276–2288.
- [3] Okuda, K., Umetsu, M., Takami, S., Adschiri, T., 2004. Disassembly of lignin and chemical recovery-rapid depolymerization of lignin without char formation in water–phenol mixtures. *Fuel Processing Technology* 85, 803–813.

- [4] Huang, X., Korányi, T.I., Boot, M.D., Hensen, E.J.M., 2015. Ethanol as capping agent and formaldehyde scavenger for efficient depolymerization of lignin to aromatics. *Green Chemistry* 17, 4941–4950.
- [5] Oasmaa, A., Johansson, A., 1993. Catalytic hydrotreating of lignin with water-soluble molybdenum catalyst. *Energy & Fuels* 7, 426–429.
- [6] Joffres, B., 2013. Synthèse de bio-huile de seconde génération par hydroliquéfaction catalytique de la lignine. PhD thesis, Université Claude Bernard Lyon 1.
- [7] http://biorefinery.utk.edu/pdf/Molecular_Weight_Distribution_of_Lignin.pdf. Accessed: 2016-11-15.

Chapter IV. Hydroconversion Experiments and Reaction Scheme

IV.1 Introduction

As presented in **Chapter II**, the catalytic hydroconversion of lignin P1000 was carried out in a semi-batch reactor, in tetralin solvent, with a CoMoS/Al₂O₃ catalyst under H₂ pressure at 350 °C. The reaction takes place in tetralin, a H-donor solvent, which allows avoiding the condensation reactions between the generated free radicals. The reactor we used is opened for gas phase with a continuous feeding of H₂ and a condensing reflux at 160 °C followed by cooled traps. Fresh H₂ is fed to keep the H₂ partial pressure at a high level, and the formed water as well as light products can be removed from the reactor to avoid long contact of the catalyst with water and over-conversion of lights to gases.

Catalytic tests were performed at various reaction times between 0 h and 13 h in order to understand the lignin conversion process. After each reaction, four different fractions were found and separated with good mass balance: THF-insoluble residues, THF-solubles, gases and liquids. The quantified and detailed analyses for each fraction were performed with adapted analytical tools presented in **Chapter II**.

In this chapter, we investigate the evolution of these different fractions so as to describe the various reactions occurring versus reaction time in addition to the role of solvent. Meanwhile, a lumped reaction scheme representing the lignin hydroconversion process is established step-by-step on the basis of experimental observations.

IV.2 Results of hydroconversion experiments

Lignin hydroconversion was performed at various reaction times (t_0 , 1 h, 3 h, 5 h, 9 h and 13 h). The mass balance of all the catalytic tests reached 95 wt%. The t_0 point (time where the reaction temperature is reached) was taken into account the non-negligible conversion due to the heating slope. After reaction, four product fractions were obtained: THF-insolubles residues (THF-insolubles + ashes), THF-soluble residues, gases and liquids. For the liquids, it can be further divided into organic liquid fraction and aqueous fraction. For each fraction (compound) i , the corresponding yield was calculated as follows:

$$\gamma_i = \frac{m_i}{m_{\text{initial lignin}}} \quad (4.1)$$

where m_i is the mass of the fraction (compound) and $m_{\text{initial lignin}}$ is the mass of initial lignin feed (30 g). In the literature, many authors considered only solid residues as non-converted lignin, so the lignin conversion was always calculated as follows:

$$\chi = 1 - \frac{m_{\text{solid residues}}}{m_{\text{initial lignin}}} \quad (4.2)$$

The level of conversion can be very high even if the chemical changes on the lignin residues are few, thus the conversion value is not very helpful. In many cases, the lignin was highly converted with relatively high yields of liquid monomers. Therefore, we focus more on the yields of each fraction in our work. Figures IV.1 shows the evolution of different fractions as a function of reaction time, as well as additional information of hydrogen consumption.

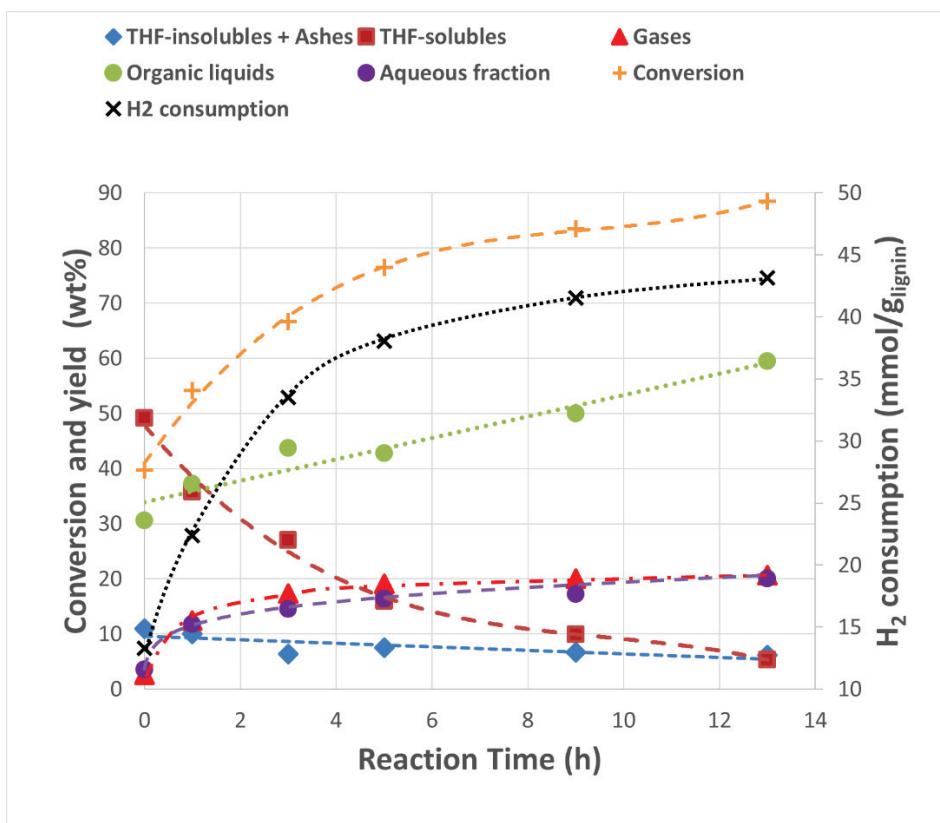
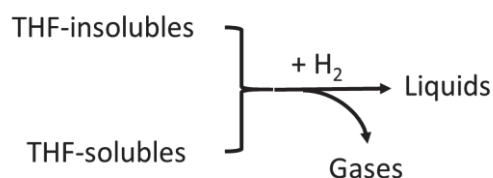


Figure IV.1: Evolution of the fraction yields and H₂ consumption as a function of reaction time over CoMoS/Al₂O₃ at 350 °C

At t_0 , we can see that 34 wt% of lignin was converted to liquids (30.6 wt% of organic liquids and 3.6 wt% of aqueous fraction), and 2.6 wt% of lignin was converted to gaseous products. The conversion of lignin during the heating period was thus not negligible. The consumption of H₂ was also observed, corresponding to 13 mmol/g_{lignin}. We notice that the THF-insoluble residues (including 3 wt% of initial ashes) represented 11.3 wt%, a slightly higher than 9 wt% initially determined by THF extraction. This slight increase could be due to the formation of solid via condensation reaction of free radicals. The liquid yield increased continuously up to 80 wt% (59.4 wt% of organic liquids and 20.1 wt% of aqueous fraction) after 13h while the yield of THF-solubles decreased progressively from 49 wt% at t_0 to 5 wt% at 13 h. We can also observe that the gaseous product yield was almost constant after 5 h (around 20 wt%). The yield of THF-insoluble residues also decreased to a plateau after 3 h which corresponds to about 6 wt% of lignin. As expected, the H₂ consumption increased with the conversion of lignin. However, H₂ consumption seemed to stay at the same level between 5 and 13 h, suggesting that hydrogenation/hydrogenolysis reactions did not occur severely.

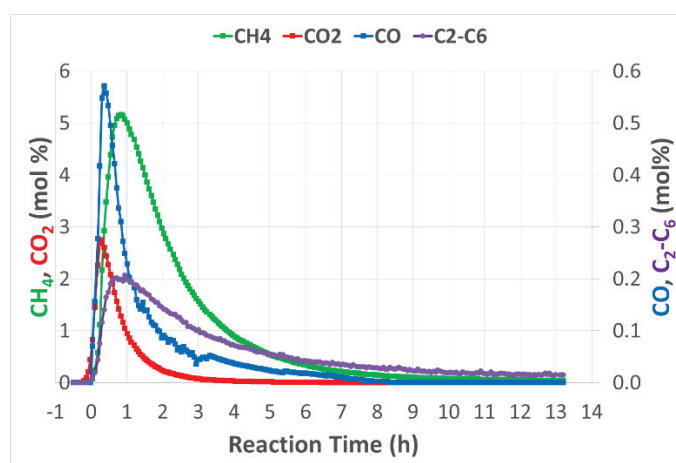
From the overall evolution trend of different fractions, a simplified reaction scheme from experimental observations can be suggested (Scheme IV.1): liquids and gases were produced from THF-solubles and THF-insolubles with the participation of H₂. However, it should be underlined that the conversion of tetralin to naphthalene by dehydrogenation can also provide H₂ in the liquid phase, then released H₂ can directly be involved in hydrogenation and hydrogenolysis reactions. This contribution to reactions will be discussed in the following section ([§ IV.2.4.3](#)).



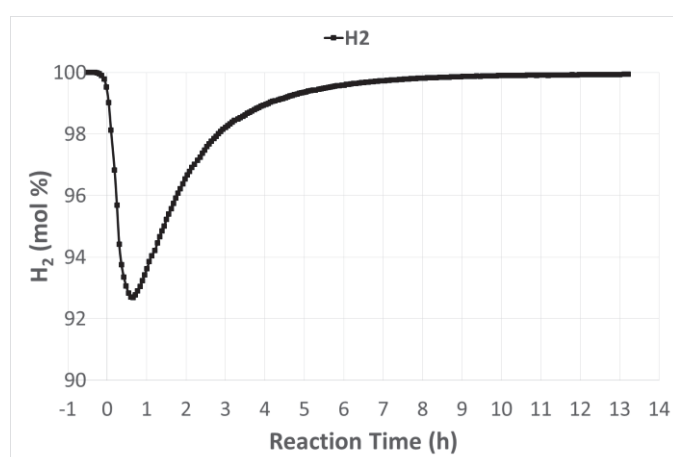
Scheme IV.1: Reaction scheme A of lignin hydroconversion

IV.2.1 Characterization of gas phase

For gas phase, the evolution of the composition (H₂, CH₄, CO₂, CO and C₂-C₆) at the outlet was followed during each test. An example of the longest test of 13 h is illustrated in Figure IV.2. CO₂ and CH₄ were the main gaseous products, and CO and C₂-C₆ were minor ones. A severe consumption of H₂ was observed between t_0 and 5 h in parallel with the formation of the main gases.



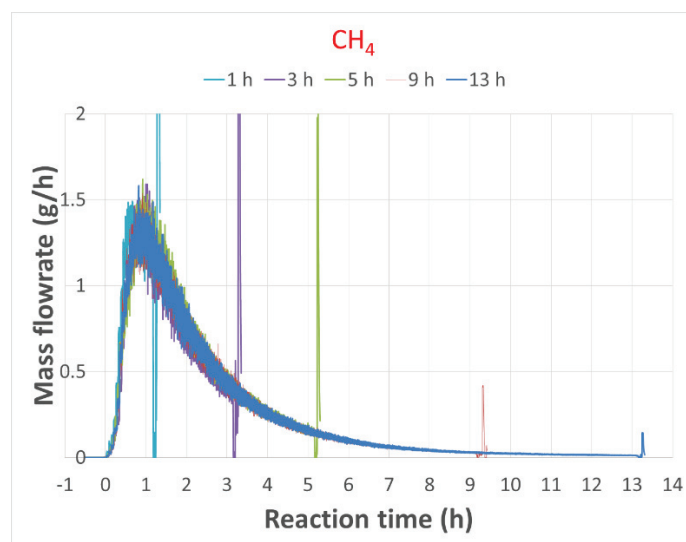
(a)



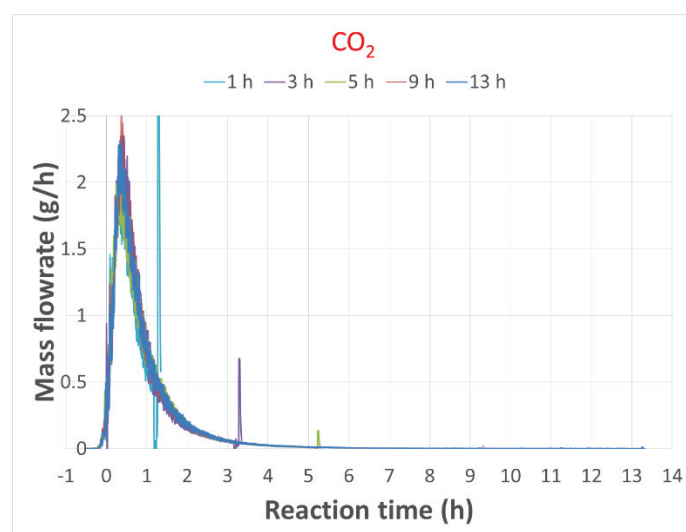
(b)

Figure IV.2: Dynamic gas composition at the outlet of set-up (a) CH₄, CO₂, CO and C₂-C₆; (b) H₂

A series of the dynamic gas composition and mass flowrate profiles at the outlet were measured for the different reaction times. After post-processing, the partial mass flowrate of each gaseous compound in function of reaction time was obtained. The superimposition of partial mass flowrate for major gaseous products (CH_4 and CO_2) at various reaction times is illustrated in Figure IV.3. The excellent overlaps of outlet gas indicate that the runs were quite reproducible. The raised tail part in each curve end corresponds to the increasing gas flow due to the depressurization.



(a)



(b)

Figure IV.3: Dynamic gas mass flow at the outlet of set-up (a) CH_4 ; (b) CO_2

The cumulative gas mass yields in function of reaction time are shown in Figure IV.4. At t_0 , the primary formed gas was CO_2 (2.3 wt% of lignin), with little traces of other components (CH_4 : 0.18 wt%, CO : 0.14 wt%, $\text{C}_2\text{-C}_6$: 0.02 wt%). Thus, the split of $-\text{OCH}_3$ group was barely seen below 350 °C. However, the fast formation of CO_2 suggested that a fast decarboxylation of carboxylic acids occurred at a lower temperature than 350 °C (Scheme IV.2), which was confirmed by the disappearance of carboxylic acids

in the THF-solubles (^1H NMR in § IV.2.3.2 and ^{31}P NMR in § IV.2.3.4) at t_0 point. The presence of CO can be explained by the decarboxylation of $-\text{CHO}$ or reverse water gas shift reaction from CO_2 .

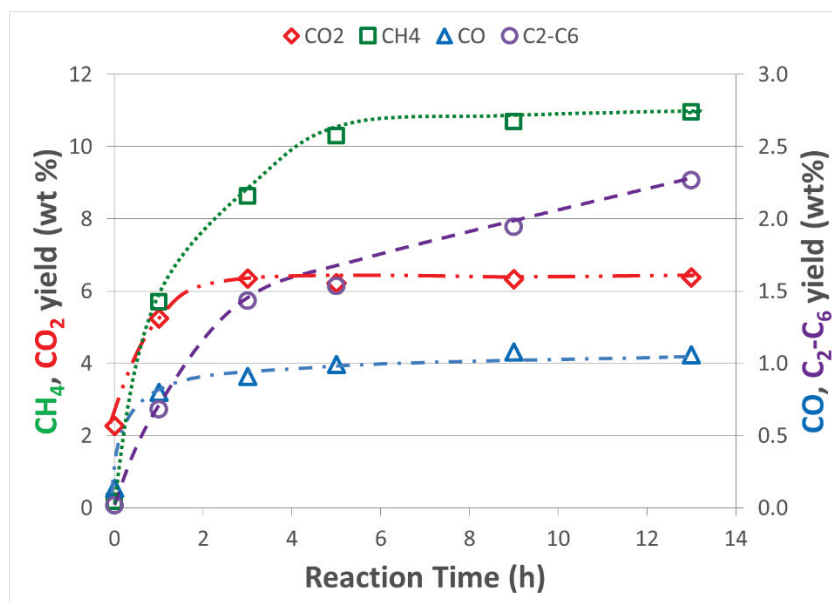
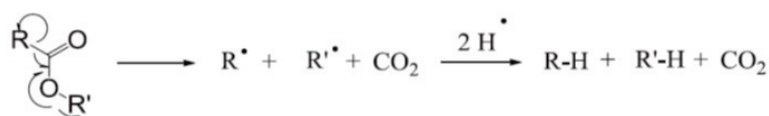
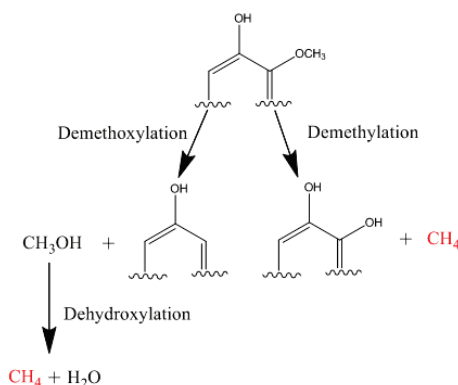


Figure IV.4: Cumulative gas mass yields as a function of reaction time



Scheme IV.2: Reaction scheme of decarboxylation



Scheme IV.3: Reaction scheme of demethylation and demethoxylation of $-\text{OCH}_3$

After 1 h, the production of CO_2 was more than twice higher, CO was formed rapidly to 0.8 wt% of lignin and the yield of $\text{C}_2\text{-C}_6$ reached 0.7 wt% of lignin. The yield of CH_4 increased quickly from 0.18 wt% to 5.7 wt%, accompanied by a severe H_2 consumption between t_0 and 1 h. The severe consumption can be explained by the occurrence of strong hydrogenolysis of $-\text{COOR}$ and $-\text{OCH}_3$ functions. The

formation of CH₄ by demethylation or demethoxylation of -OCH₃ was much favored after reaching 350 °C (Scheme IV.3).

After 3 h, the yields of CO₂ and CO were nearly stable since their resources were almost running out, which was proved by the total disappearance of -COOR (¹³C NMR in § IV.2.3.3) both in the liquid phase and in the THF-solubles. CH₄ was still formed progressively with the decrease of -OCH₃ group in the system (¹³C NMR in § IV.2.3.3). Between 5 and 13 h, the production of CH₄ increased slightly due to the shortage of -OCH₃. The light alkanes (C₂-C₆) that came from the C-C cleavage of the alkyl chains still increased.

IV.2.2 Characterization of THF-insoluble residues

The fraction of THF insoluble residues contains the initial ashes and the THF-insolubles. Due to the low amounts and the insolubility of these solids in classical solvents including THF, only elemental characterization was performed on the solid fraction, listed in Table IV.1.

At *t*₀ point, compared to the THF-insoluble fraction obtained from initial lignin, the O content decreased to 23.2 wt% and the H content decreased from 3.6 wt% to 2.5 wt% while the C content remained around 40 wt%. As time increased, the C content decreased from 40 wt% to 16 wt% and H content decreased from 2.5 wt% to 1.3 wt% respectively while the O content decreased slightly from 23 wt% to 19 wt%. The high ratio of O/C may suggest a formation of condensed phenolic moieties. Unsurprisingly, the ash content, evaluated by subtraction of the organic part, increased in function of reaction time. After 13 h, the organic fraction represented about 47.3 wt% of THF-insoluble residues, which means that the ash content reached 52.7 wt%, corresponding well to the initial ash content (3 wt% of initial lignin). Thus, the yield of THF-insolubles (ashes not included) remained about 3 wt% after 13 h of reaction.

Table IV.1: Elemental composition of THF-insoluble residues as a function of residence time

	Initial THF-insoluble fraction (9 wt%)	0 h (11.3 wt%)	1 h (10.1 wt%)	3 h (6.3 wt%)	5 h (7.6 wt%)	9 h (6.7 wt%)	13 h (6.2 wt%)
C	39.0	40.5	34.9	22.5	27.1	19.0	16.2
H	3.6	2.5	2.3	1.7	2.0	1.6	1.3
O	35.9	23.2	21.2	22.3	23.6	20.4	19.3
N	0.9	1.0	0.8	0.5	0.6	0.4	0.3
S	5.1	6.1	6.5	9.1	8.1	9.4	10.2
Ashes (*)	15.4	26.7	34.3	43.8	38.5	49.2	52.7
Atomic ratios							
H/C	1.11	0.75	0.80	0.90	0.90	0.99	0.98
O/C	0.69	0.43	0.46	0.74	0.65	0.81	0.89

* Values obtained by subtraction of the organic fraction (can be considered as ashes content)

IV.2.3 Characterization of THF-solubles

THF-solubles (THF-soluble residues) is the fraction of partially converted lignin which is completely soluble in THF after reaction, which is in the form of solid at room temperature. It is still an oligomeric/polymeric entity, but it is already different from the initial lignin on the chain size and the structure since some interunits were already split and some functional groups were removed. It might come from the depolymerization of initial THF-insoluble fraction, or the partial depolymerization of initial THF-soluble fraction. In order to understand the transformations, this THF-soluble fraction after reaction was analyzed by the same techniques used for the characterization of the initial lignin.

IV.2.3.1 Molecular weight distribution by GPC

The GPC curves of initial THF-soluble fraction and the THF-solubles at t_0 are shown in Figure IV.5. The initial THF-soluble P1000 had a bimodal distribution, two peaks respectively at 2000 g/mol and 800 g/mol. Compared to the initial THF-soluble fraction, THF-solubles at t_0 showed a decline at the peak of 2000 g/mol but had a slight increase on the right part of the GPC curve which represents the heavy molecules. The new generated heavier molecules of THF-solubles must be degraded from the initial THF-insoluble fraction that contains high-molecular-weight molecules, highlighting that at the heating slope, THF-insolubles was supposed to be depolymerized into the lighter fraction, which may become soluble in THF. As the reaction time increased, THF-insolubles were observed to be converted continuously (See Figure IV.1).

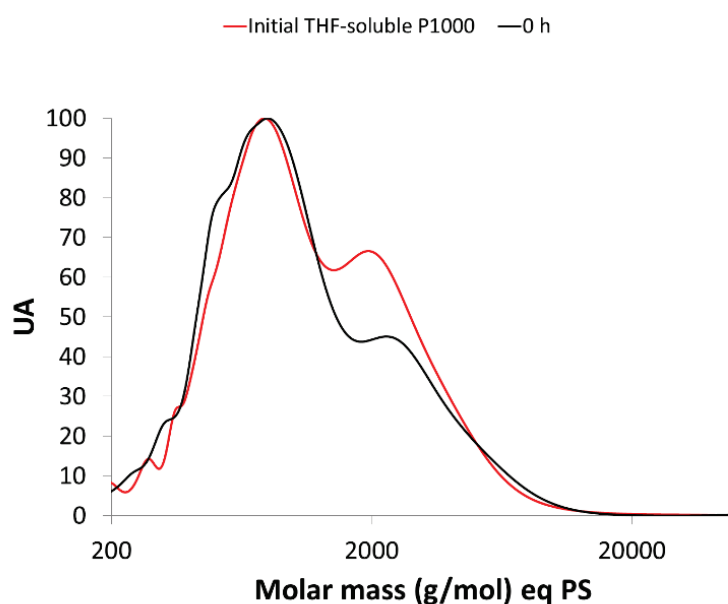
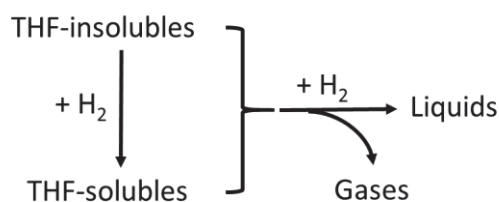


Figure IV.5: GPC curves of THF-solubles at t_0 and the initial THF-soluble fraction

From the above discussion, it becomes evident that the reaction pathway of transforming THF-insolubles into THF-solubles indeed exists during the lignin hydroconversion (Scheme IV.4).



Scheme IV.4: Reaction scheme B of lignin hydroconversion

The GPC curves and the quantitative evolution of THF-solubles at different reaction times are shown in Figure IV.6 and Table IV.2. At the early stage of reaction between t_0 and 1 h, the mass average molar mass (M_w) of THF-solubles decreased from 1522 g/mol to 1205 g/mol. The apparent change was the rapid disappearance of heavy molecules in the region higher than 2000 g/mol whereas the left peak around 800 g/mol was still there.

Between 3 and 13 h, the M_w remained at around 1000 g/mol. The GPC curve was entirely shifted to the left side, indicating that the chains of THF-solubles were becoming shorter and lighter as a function of reaction time due to the depolymerization. At 13 h, the final peak of the GPC curve was centered around 500 g/mol. However, the PDI of THF-solubles kept always around 1.9, indicating that for any chains in lignin, no matter how long the chain is, the weight loss on each chain is proportional to its molecular weight. This is quite expected since the reactive linkages and functional groups on each chain are also proportional to the molecular weight of the chain.

In conclusion to all this, the GPC evolution confirmed that the THF-solubles has a polymer structure as initial lignin, but having shorter and lighter chains due to the depolymerization.

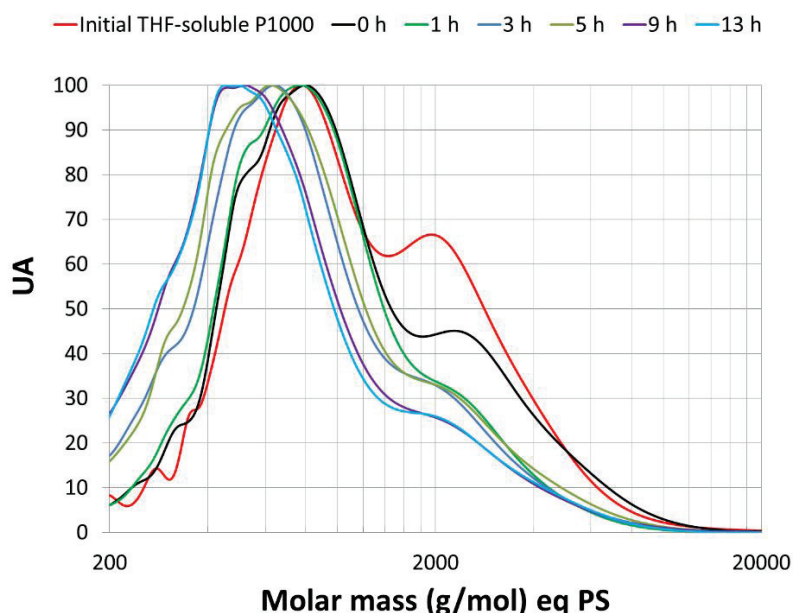


Figure IV.6: GPC curves of the THF-solubles at different reaction times

Table IV.2: Evolution of THF-solubles M_w , M_n and PDI at different reaction times

	Initial THF-soluble fraction	0 h	1 h	3 h	5 h	9 h	13 h
M_n	863	780	687	602	612	525	542
M_w	1644	1522	1205	1082	1187	986	1090
PDI	1.9	2.0	1.8	1.8	1.9	1.9	2.0

IV.2.3.2 1H NMR

In order to determine the evolution of the organic functions on lignin residues, we performed 1H , ^{31}P and ^{13}C NMR analyses. The 1H spectra of THF-solubles at different reaction times are illustrated in [Annex 1](#) with their corresponding quantifications. Here, we present the evolution of H group distribution in THF-solubles (Figure IV.7 and IV.8).

Figure IV.7 shows the variation in the number of moles for each H group remained in THF-solubles. The number of moles for each H group in THF-solubles was calculated as follows:

$$n_{H\ group} = C_{H\ group} \cdot m_{THF-solubles} \quad (4.3)$$

where $C_{H\ group}$ is the concentration of each H group in THF-solubles per unit of mass and $m_{THF-solubles}$ is the mass of THF-solubles.

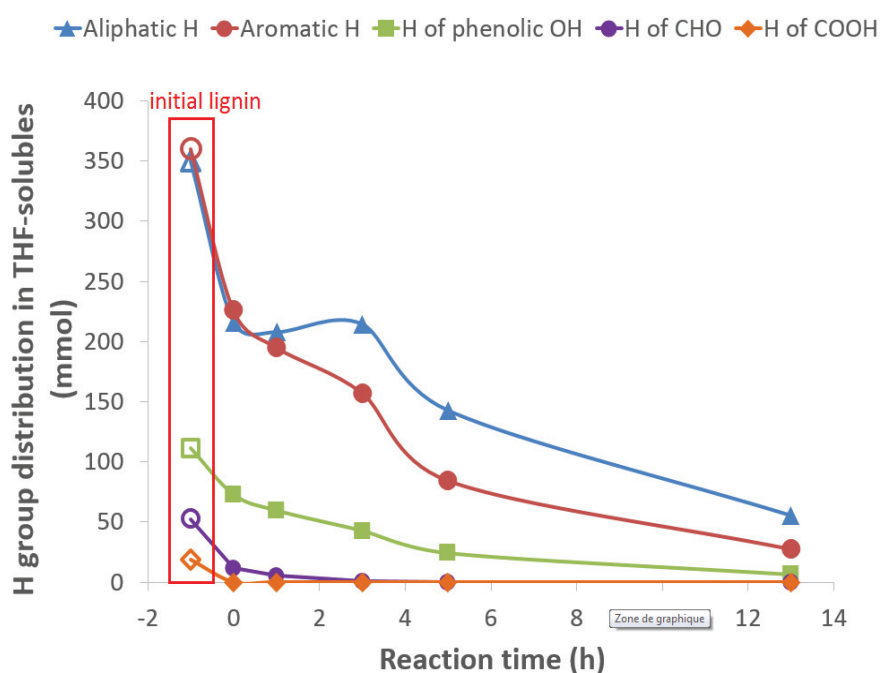


Figure IV.7: Variation in the number of moles for each H group in THF-solubles versus reaction time

Figure IV.8 shows the remaining percentage (mol%) of each H group in THF-solubles at different reaction times compared to that of the initial lignin. It was calculated as follows:

$$X_{\text{H group}} = \frac{n_{\text{H group in the THF-solubles}}}{n_{\text{H group in the initial lignin}}} \quad (4.4)$$

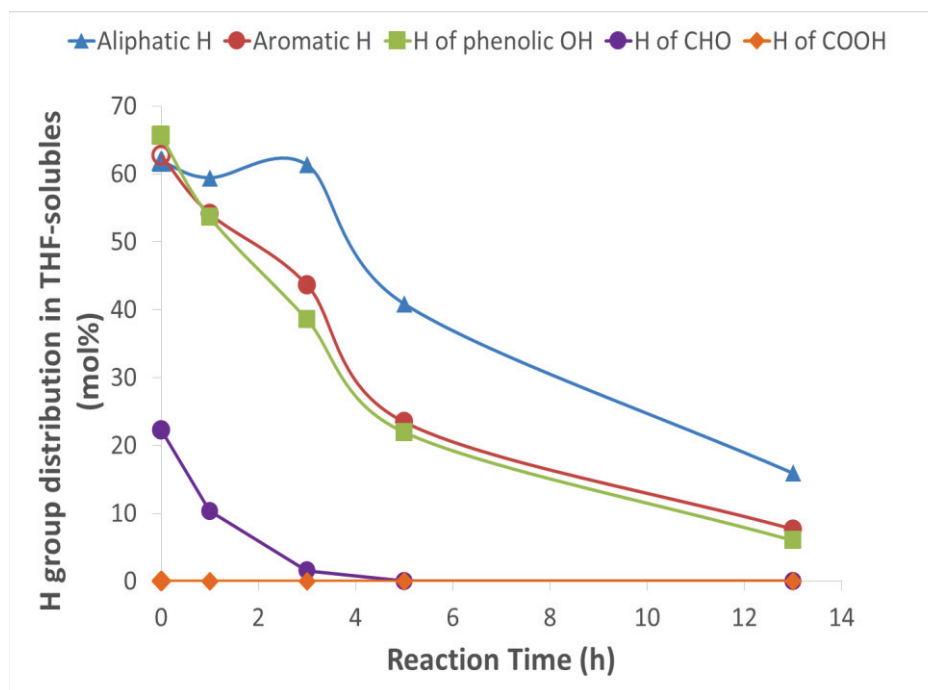
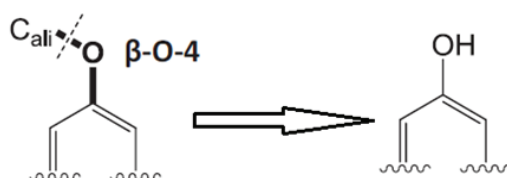


Figure IV.8: Remaining percentage of H groups (mol%) in THF-solubles versus reaction time

At t_0 point, the yield of THF-solubles was 49 wt%. Several reactions at the heating slope were confirmed from the observations by ^1H NMR:

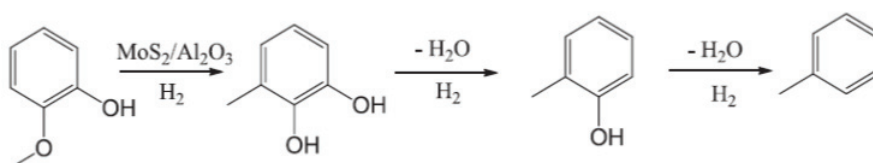
- ✓ The total disappearance of $-\text{COOH}$ by decarboxylation was noticed, which corresponded well to the fast formation of CO_2 at t_0 point (§ IV.2.1).
- ✓ About 80 % of $-\text{CHO}$ was removed, which might be explained by decarbonylation of aldehydes to CO or by hydrogenation of aldehydes to alcohols followed by dehydroxylation. Considering the low formation of CO at t_0 , the hydrogenation followed by dehydroxylation could be considered to be the dominant reaction.
- ✓ The decrease of aliphatic H, aromatic H and phenolic OH was respectively 38 %, 37 % and 34 %. These groups are transferred into the liquid phase during the depolymerization. The decrease of phenolic OH was a slightly lower than those of other H groups. It can be probably explained by the cleavage of $\beta\text{-O-4}$ ether bonds which may create new phenolic OH units in THF-solubles (Scheme IV.5).



Scheme IV.5: Breakup of ether bonds and creating of free phenolics OH

Between t_0 and 3 h, the yield of THF-solubles decreased from 49 wt% to 27 wt%. The -CHO groups were removed entirely due to the hydrogenation while phenolic OH and aromatic H decreased. In contrast, the quantity of aliphatic H was nearly stable (216 to 214 mmol). In order to explain this, we can assume a demethylation followed by a methyl substitution reaction step:

- Demethylation reaction followed by a methyl substitution reaction was proposed in several studies of lignin model compounds¹⁻⁴. With alumina-supported catalysts, after a demethylation step, several positively charged methyl group may substitute in the nearest position of the aromatic ring (Scheme IV.6). The formed catechol structure (observed in the THF-solubles by ³¹P NMR in § IV.2.3.4) was then dehydroxylated, forming methyl-substituted phenolic or aromatic structure. In this case, the transformation of 1 mmol of -OCH₃ groups may create 3 mmol of aliphatic H (-CH₃), and 1 mmol phenolic OH or 1 mmol aromatic H. Therefore, a certain amount of aliphatic H is formed, which could compensate its loss led by the depolymerization.



Scheme IV.6: Methyl-substitution reaction due to a heterolytic cleavage of -OCH₃ bond

Between 3 and 13 h, the yield of THF-solubles passed from 27 wt% to 5 wt%. The -OCH₃ group disappeared entirely in THF-solubles (¹³C NMR in § IV.2.3.3). Therefore, no more aliphatic H was formed from the methyl-substitution reaction. Thanks to the progressive depolymerization, the decrease trend of all the H groups (phenolic OH, aliphatic H and aromatic H) in the THF-solubles seemed quite similar. That indicates, the fragments containing only alkylphenolic units were continuously removed from the THF-solubles.

IV.2.3.3 ¹³C NMR

The ¹³C spectra of THF-solubles at different reaction times are illustrated in Annex 2 with their corresponding quantifications. From the trend of total carbon concentration, we can notice that the C content in the THF-solubles increased in function of reaction time. Here, we present the variation in the number of moles for each H group remained in THF-solubles in Figure IV.9, and Figure IV.10 gives the remaining percentage (mol%) of each H group in THF-solubles at different reaction times compared to that of the initial lignin.

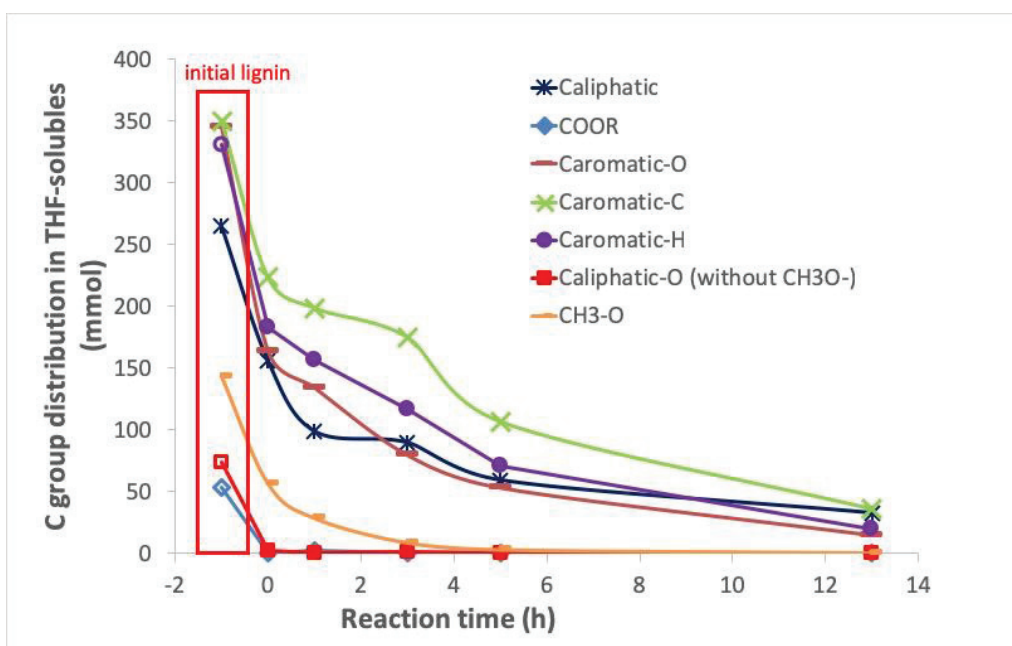


Figure IV.9: Variation in the number of moles for each C group in THF-solubles versus reaction time

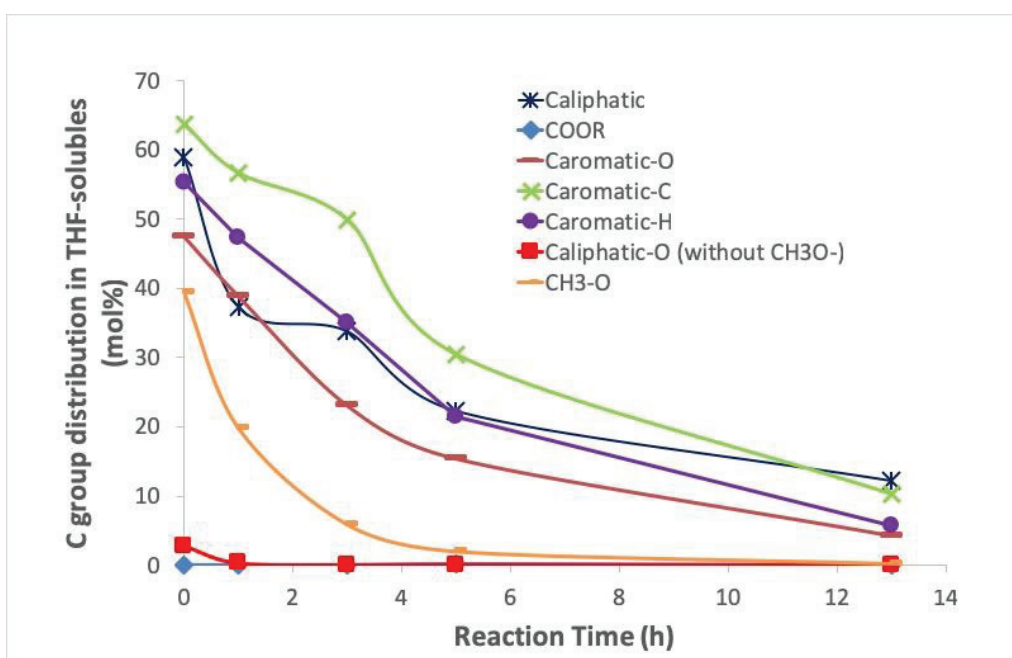


Figure IV.10: Remaining percentage of C groups (mol%) in THF-solubles versus reaction time

At t_0 point, several observations were as follows:

- ✓ The $C_{\text{aliphatic-O}}$ (without $-\text{OCH}_3$) represents the ether bonds as well as the aliphatic OH. The weakness of ether bonds was mentioned before, thereby the ether bonds were quickly broken down even during the heating slope. Aliphatic OH were entirely removed from THF-solubles in accordance with the ^{31}P NMR analysis in [§ IV.2.3.4](#).

- ✓ -COOR consists of carboxylic acids and esters. If -COOR was converted entirely, the yield of CO₂ was supposed to be 8 wt%. Experimentally, we only got 2.3 wt% for CO₂. It must have a portion of -COOR released into the liquid phase. By GC×GC analysis in [§ IV.2.4.1](#), some ester compounds were clearly found in the liquid phase.
- ✓ The decrease of -OCH₃ in the THF-solubles was slightly higher than that of other C groups. This variation can be attributed to the direct removal of methoxy-substituted fragments in the form of monomers or oligomers. This observation was in accordance with the high concentration of methoxy-substituted phenols in the liquid phase at t_0 ([§ IV.2.4.1](#)).
- ✓ The aromatic carbons, except C_{aromatic-O}, seemed to be more resistant at this period since C_{aromatic-C} and C_{aromatic-H} cannot be split at the relatively low temperature.

Between t_0 and 3 h, the yield of THF-solubles decreased from 49 wt% to 27 wt% (22 wt% of decrease). The evolution of C groups was as follows:

- ✓ The -OCH₃ decreased quite faster than other groups. On one hand, the methoxy-substituted lignin fragments were directly released from THF-solubles. On the other hand, the methoxy groups on the THF-solubles were reacted by the direct demethylation or demethoxylation reaction. It was proved by the rapid formation of CH₄ during this period ([§ IV.2.1](#)). Numerically (See Scheme IV.3), 1 mmol of -OCH₃ is reacted by direct demethoxylation, consuming 1 mmol C_{aromatic-O} and creating 1 mmol C_{aromatic-H}. If 1 mmol of -OCH₃ is reacted by demethylation followed by methyl-substitution reaction, no C_{aromatic-O} was consumed, no C_{aromatic-H} was created and 1 mmol C_{aromatic-C} was created.
- ✓ The decrease of C_{aromatic-O} (from 47 to 23 %) and C_{aromatic-H} (from 55 to 35 %) was quite close to the yield decrease of THF-solubles. The variations of C_{aromatic-O} and C_{aromatic-H} seemed not to be affected by the consumption of -OCH₃. The decrease of C_{aromatic-C} is evidently lower (from 64 to 50 %) due to the methyl-substitution reaction. That is to say, the demethylation of -OCH₃ is the priority reaction, which is in accordance with the mechanism mentioned above.
- ✓ For C_{aliphatic}, it is difficult to draw a general conclusion about the variation since various reactions (depolymerization, dealkylation, demethylation and methyl-substitution reaction) involved.

Between 3 and 13 h, the yield of THF-solubles decreased from 27 wt% to 5 wt%. All the C groups decreased as reaction time increased. At 13 h, no -OCH₃ was found and only aromatic and aliphatic carbons presents in the THF-solubles.

IV.2.3.4 ³¹P NMR

The ³¹P spectra of THF-solubles at different reaction times are illustrated in [Annex 3](#) with their corresponding quantifications. Here, we present the variation in the number of moles for each OH group in THF-solubles in Figure IV.11.

At t_0 point, all the aliphatic OH groups were removed by dehydroxylation and all the carboxylic acids were removed by decarboxylation. Catechol (benzenediol) function which was not present on initial lignin was detected, indicating that demethylation reaction from guaiacyl units occurred. A significant decrease of syringyl (S) and condensed phenolic units as well as guaiacyl units (G) was seen, in accordance with the high concentration of dimethoxyphenols and methoxyphenols found in the liquid phase at t_0 ([§ IV.2.4.1](#)).

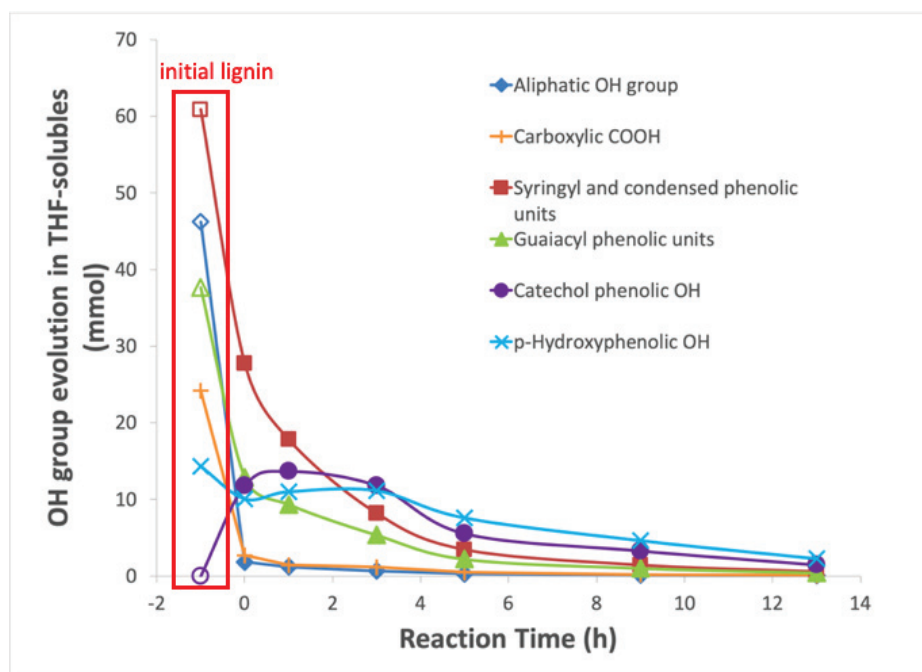


Figure IV.11: Evolution of OH groups of lignin by ^{31}P NMR as a function of residence time

By increasing reaction time, syringyl and condensed phenolic units and guaiacyl units were progressively removed or converted. Guaiacyl units were converted to catechol units by demethylation or to *p*-hydroxyphenolic units (H) by demethoxylation reaction. Catechol units were formed rapidly at short reaction time, and then were successively dehydroxylated to *p*-hydroxyphenolic or benzene units. The successive formation of *p*-hydroxyphenolic units from other syringyl and guaiacyl units compensated its loss due to the depolymerization. Consequently, the decrease of *p*-hydroxyphenolic units was slower. At 13 h, only about 4-5 mmol in total of *p*-hydroxyphenolic and catechol units was still present in THF-solubles.

IV.2.3.5 Elemental analysis

The evolution of elemental composition of THF-solubles is shown in Table IV.3 and the Van krevelen diagram (showing the O/C versus H/C ratios) in function of reaction time is reported in Figure IV.12. Compared to the initial lignin, 60 wt% deoxygenating level was reached at t_0 point for the lignin residue and 98 wt% of oxygen removal was obtained after 13 h by conversion.

From the diagram, we can clearly see that the deoxygenation process was divided into two steps: a rapid step at the heating slope (O/C decreasing from 0.34 to 0.25 in about 40 min) and a slower step (O/C decreasing from 0.25 to 0.09 in 13 h). This decrease was evidently caused by several pathways we identified above:

- 1) Fast decarboxylation of carboxylic acids and dehydroxylation of aliphatic OHs at the heating slope;
- 2) Hydrogenation of -CHO followed by dehydroxylation;
- 3) Demethoxylation of -OCH₃, or demethylation of -OCH₃ followed by the dehydroxylation.

From the evolution of H/C, it can be suggested that the THF-solubles underwent two different stages:

- 1) A rapid decrease in H/C after the heating slope due to the reactions of dehydroxylation of aliphatic OHs and fast carboxylation of carboxylic acids.
- 2) A slow increase in H/C from 0 h to 13 h thanks to the hydrogenation and hydrogenolysis reactions.

Table IV.3: Evolution of elemental analyses and H/C, O/C atomic ratios for THF-solubles

	P1000	Initial THF-soluble fraction (91 wt%)	0 h (49 wt %)	1 h (36 wt%)	3 h (27 wt%)	5 h (16 wt%)	9 h (10 wt%)	13 h (5 wt%)
C	61.1	63.2	71.7	74.2	78.6	80.9	82.5	81.8
H	5.7	6.2	5.9	6.2	6.7	7.0	7.4	7.5
O	29.9	28.5	23.7	20.7	14.4	11.4	10.1	9.5
N	0.7	0.7	0.8	1.0	1.1	1.3	1.3	1.3
S	0.9	0.8	0.3	0.2	0.1	0.1	0.1	0.1
Ashes	3.1	n.d.	n.d.	n.d.	n.d.	n.d.	n.d.	n.d.
Water	2.1	n.d.	n.d.	n.d.	n.d.	n.d.	n.d.	n.d.
Total	103.4	99.4	102.5	102.2	100.9	100.8	101.3	100.2
Atomic ratios								
H/C	1.12	1.18	0.99	1.01	1.02	1.04	1.07	1.10
O/C	0.37	0.34	0.25	0.21	0.14	0.11	0.09	0.09

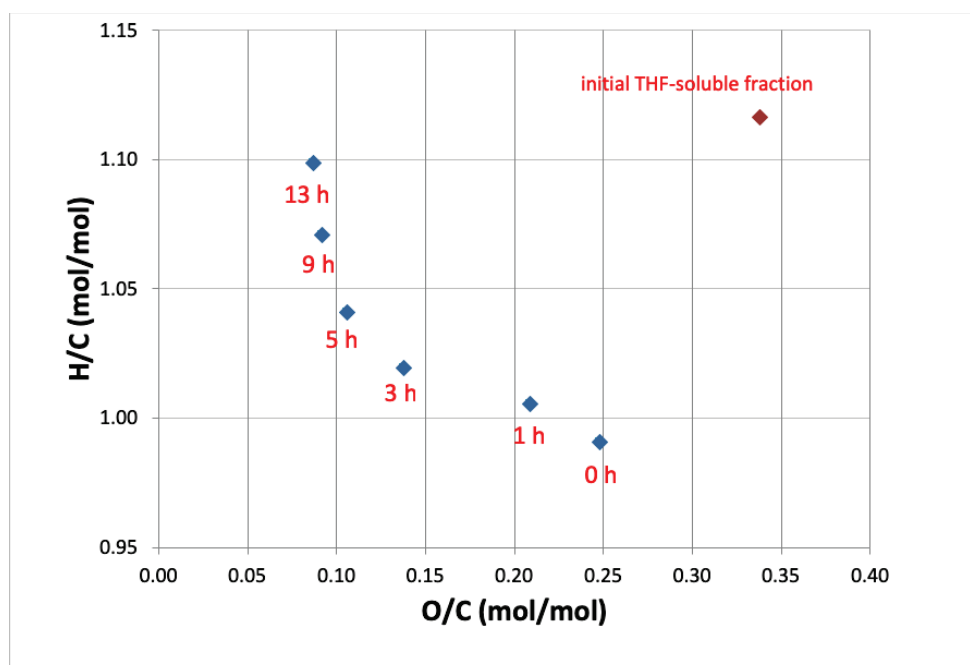


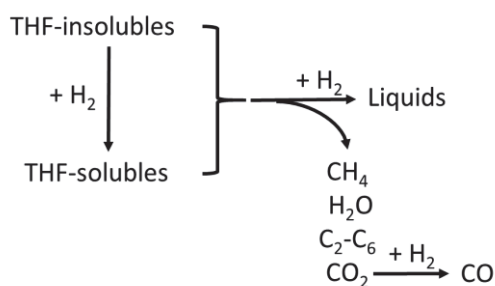
Figure IV.12: Van Krevelen diagram of THF-solubles in function of reaction time

IV.2.3.6 Conclusion of the transformations of THF-solubles

From the above discussions, several conclusions on the transformation of THF-solubles can be done:

- ✓ A part of THF-solubles came from the depolymerization of THF-insolubles.
- ✓ The chains of THF-solubles were becoming shorter and lighter thanks to the progressive depolymerization and the removal of functional groups.
- ✓ At the early stage of conversion, acidic carboxylic functions are removed by decarboxylation, the weakest ether bonds ($C_{\text{aromatic}}\text{-O-}C_{\text{aliphatic}}$ or C_{aromatic}) were cleaved leading to phenol units and dehydroxylation of aliphatic OH groups took place.
- ✓ In the second time, the demethylation, demethoxylation and dehydroxylation of phenolic OH occurred progressively. The demethoxylation should form an intermediate product: CH_3OH . However, it is impossible for us to detect the presence of CH_3OH and to quantify CH_3OH owing to the non-adapted μGC columns and the high volatility during the recovery step.
- ✓ CO was also formed by decarbonylation but mainly by reverse water gas shift reaction.
- ✓ $\text{C}_2\text{-C}_6$ came from the C-C cleavage of the alkyl chains.

Although the analyses were not done for THF-insolubles, the same types of transformations as THF-solubles were supposed to occur on the THF-insolubles since both of them have the same basic units. The assumption has been experimentally validated by the previous work which was carried out in our team⁵. By performing the individual conversion of the soluble and insoluble fractions, the result showed that the products distribution were relatively identical. Hence, the previously proposed simplified reaction scheme B can be modified according to Scheme IV.7.



Scheme IV.7: Reaction scheme C of lignin hydroconversion

Apparently after 13 h of reaction time, the relatively size of THF-solubles was much reduced compared to the initial lignin. The NMR analyses demonstrate the total disappearance of these oxygenated groups: aliphatic OH, -CHO, -COOH, ether bonds and -OCH₃. Only aromatic and aliphatic carbons still present in THF-solubles (5 wt% of lignin feed) with little oxygen content:

- $C_{\text{aromatic-C}}$: 36 mmol, $C_{\text{aromatic-O}}$: 15 mmol, $C_{\text{aromatic-H}}$: 19 mmol
- $C_{\text{aliphatic}}$: 32 mmol, $H_{\text{aliphatic}}$: 56 mmol
- H/C = 1.10, O/C = 0.09
- Phenolic OH: 4-5 mmol

Therefore, at 13 h, the THF-soluble fraction has an oxygen-containing condensed aromatic structure with alkyl side chains.

IV.2.4 Characterization of liquid phase

After each test, two liquid mixtures were recovered, respectively in the reactor and the separator. As mentioned in **Chapter II**, an organic phase and an aqueous phase were obtained in the separator. Their mass distributions in function of reaction time are reported in Figure IV.13. As expected, liquid compounds were flowed away from the reactor continuously and the cumulative mass of liquids in the separator increased as time increased. We can see from Figure IV.13 that aqueous fraction which is mainly composed of water reached 6 g after 13 h in the separator, the organic fraction in the separator is also continuously increased and reached 10.8 g after 13h. In the following part, each fraction will be further characterized.

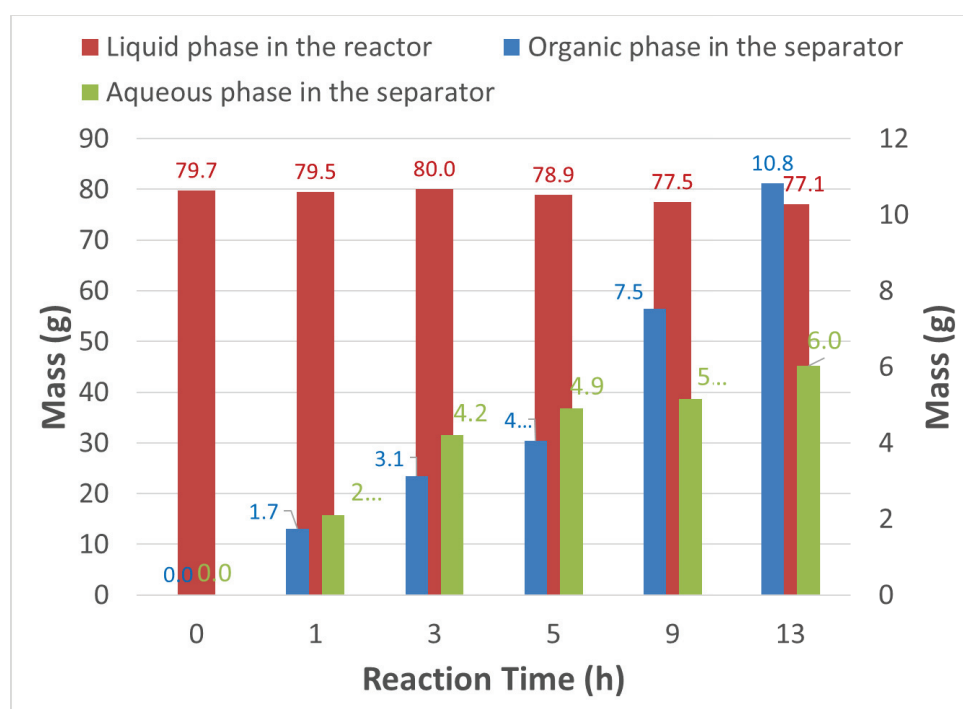


Figure IV.13: Mass distribution of liquids phases in function of reaction time

The best achievement in our study is the extensive use of GC×GC to identify and quantify monomeric products in the complex mixture. The extended information about monomers can help us better understand the depolymerization process of lignin, as well as investigate the catalytic transformation of monomers over CoMoS/Al₂O₃.

IV.2.4.1 Liquid phase in the reactor

Water content

After reaction, the mixture in the reactor is a dark brown liquid containing liquid products and tetralin. No clear aqueous phase was observed, thus Karl-Fischer titration was done to determine its water content (Table IV.4). It was found that at the early stage of reaction between 0 and 1 h, the liquid phase contained more than 1 g of water. As time progressed, water was almost totally recovered in the separator (See Figure IV.13).

Table IV.4: Water content of the liquid phase in the reactor by Karl-Fischer titration

Reaction time (h)	0	1	3	5-13
H ₂ O content (wt%)	1.4	1.8	0.2	0
H ₂ O content (g)	1.1	1.4	0.2	0

Solubilized oligomers

Over the storage time, we observed the presence of a certain amount of solid lignin-type residues which precipitates. It can be guessed that some soluble oligomeric entities must also co-exist in the mixture. For proving that, the GPC analysis was performed to evaluate the molecular weight distribution of the liquid phase, and it is illustrated in Figure IV.14. The indeed existence of high molar mass molecules validates the presence of solubilized oligomers in the liquid fraction. Compared to the THF-solubles at 13 h, the soluble oligomers in the liquid phase had a narrower distribution. That indicates that the soluble oligomers have a lower molar mass, which could probably make them soluble in liquid at room temperature depending on the remaining functional groups. The variation of molecular weight distribution in function of reaction time was not significant, always having a signal peak centered around 450 g/mol.

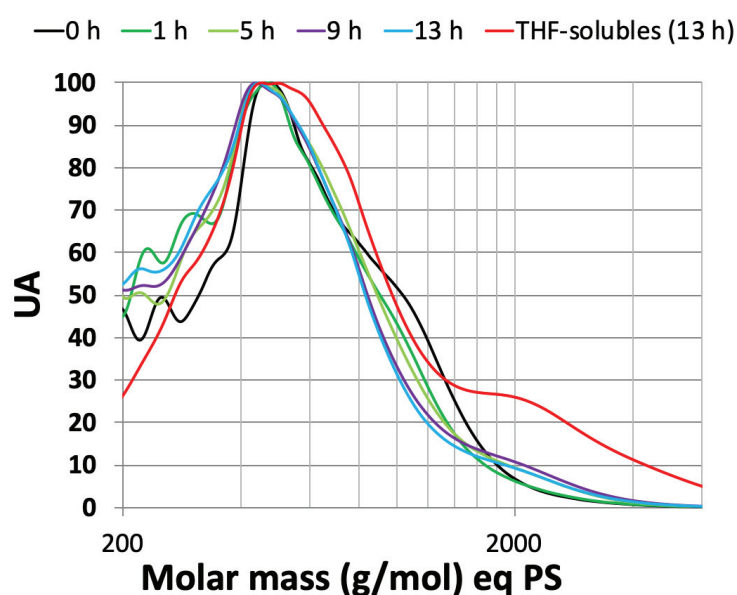
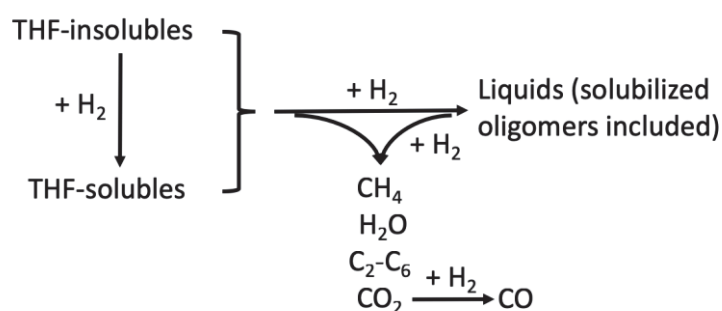


Figure IV.14: GPC curves of the liquid phase at different reaction times compared to the THF-solubles at 13 h

In Joffres's thesis⁵, a procedure to recover this solubilized oligomers was developed: an experimentally-determined heptane-to-liquid mass ratio of 7/10 was added to the liquid fraction to recover it by precipitation. The precipitated lignin-type residues were then analyzed by CHONS, GPC and NMR to compare with the THF-solubles (illustrated in [Annex 4](#)). The comparison of CHONS and

NMR analyses showed that this heptane precipitate was quite similar to the THF-solubles in elemental composition and chemical structure, but the curve of GPC indicates that it had a narrower size distribution and shorter chains. The structural evolution of the heptane precipitate also indicates that it underwent the same types of deoxygenating reactions as the THF-solubles. Here, it should be emphasized that, this method of precipitation by heptane was not reproducible and the heptane precipitate represents only a specific fraction of the solubilized oligomers. However, the analysis of the heptane precipitates indeed can help us understand the reaction that occurs in the liquid phase.

The short-chain solubilized oligomers should be produced from the depolymerization of heavy lignin fragments like THF-insolubles and THF-solubles. Here, we assume that all the solubilized oligomers underwent the same types of deoxygenating reactions (decarboxylation, demethylation, demethoxylation, and dehydroxylation) as the heptane precipitate. Therefore, the reaction scheme C can be modified as shown in Scheme IV.8. Due to the high boiling point, most of these solubilized oligomers, except some dimers (biphenols in Figure IV.15) cannot eluted during the usual GC×GC analysis. So, the quantification of this solubilized oligomers was estimated by subtraction of all the monomers from the produced organic liquids ($m_{\text{solubilized oligomers}} = m_{\text{organic liquids}} - m_{\text{monomers}}$), may leading to a wide margin of experimental error.



Scheme IV.8: Reaction scheme D of lignin hydroconversion

Monomers

For most studies on lignin conversion, the liquid phase is always the most challenging part to analyze. On one hand, the monomers produced from lignin are quite numerous and diverse. On the other hand, the liquid contained a significant amount of solvent and its derivatives. Thanks to a GC×GC system with an adapted system of columns, a good separation of the numerous compounds was obtained. With the aid of the GC Image software, the contour plotting, peak fitting and blob integration were performed. The identification of liquid compounds was done with NIST MS standard library. The quantification of liquid compounds was done with the FID detector. The GC×GC FID images of the liquid phase in the reactor at three representative reaction times (t_0 , 5 h and 13 h) were illustrated in Figure IV.15, IV.16 and IV.17. At the same axial (vertical) coordinate, the boiling point of the monomers increased from left to right and the polarity from the top to the bottom.

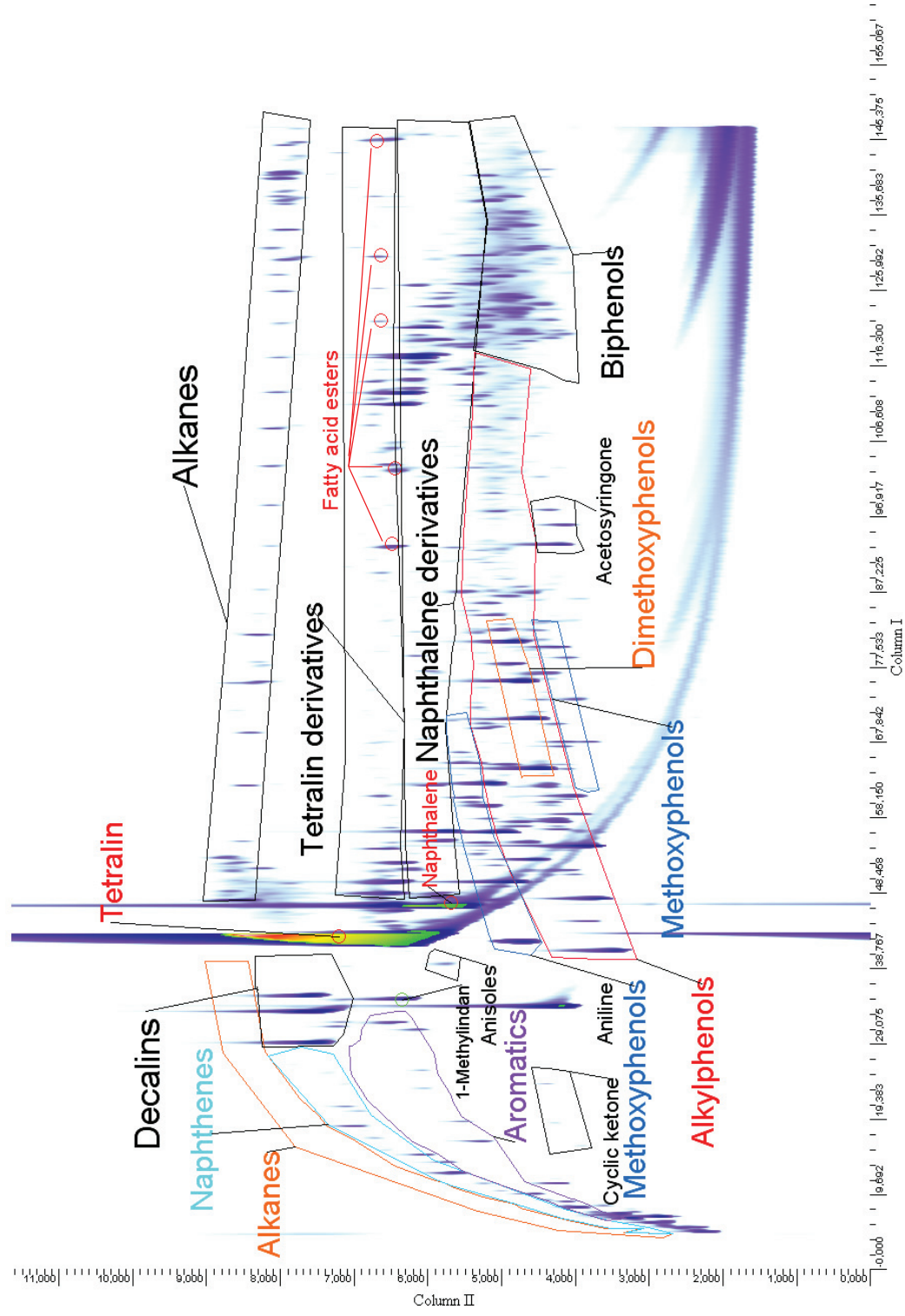


Figure IV.15: GCxGC-FID chromatogram of the liquid phase in the reactor after t_0 point

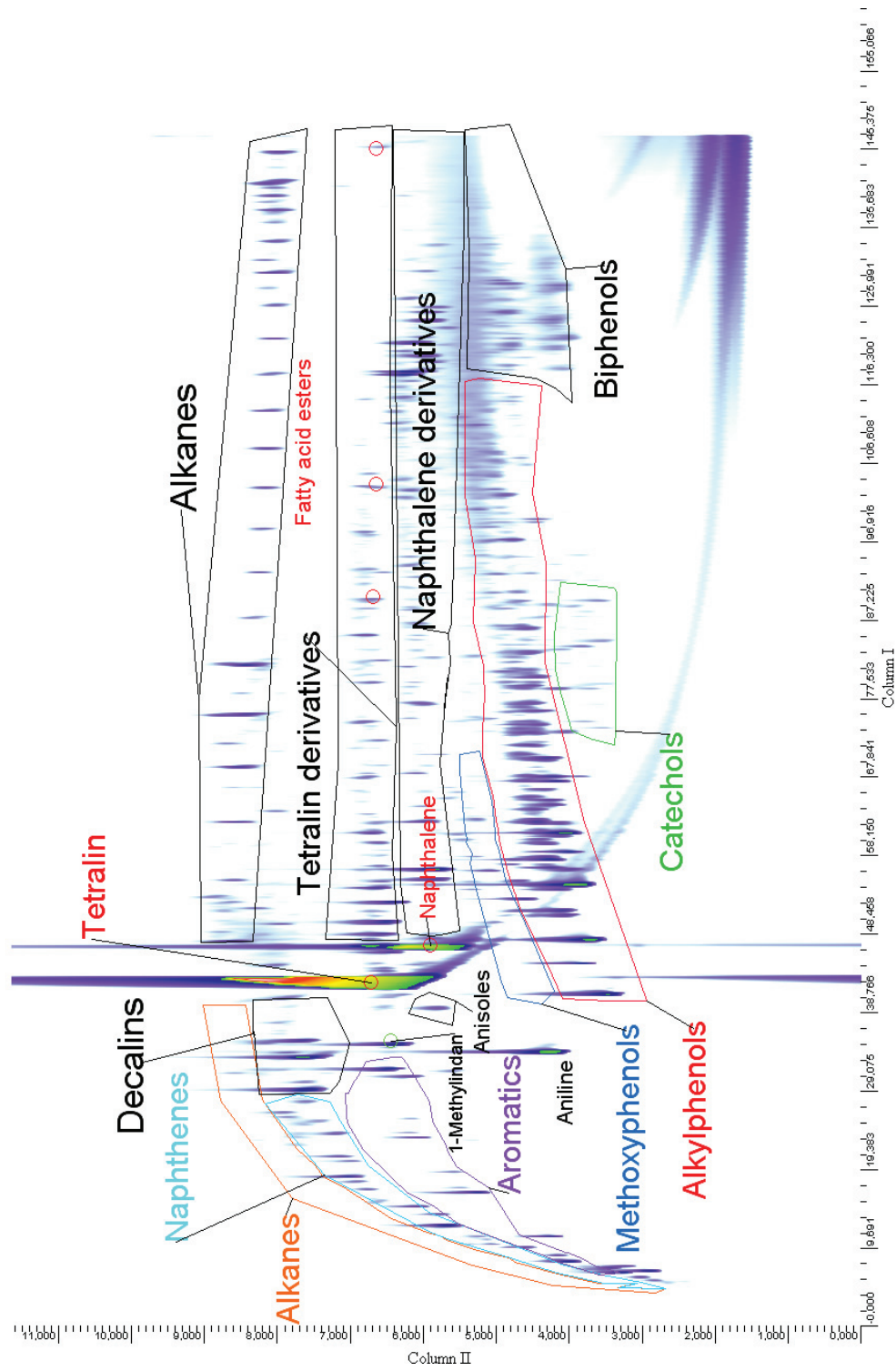


Figure IV.16: GCxGC-FID chromatogram of the liquid phase in the reactor after 5 h

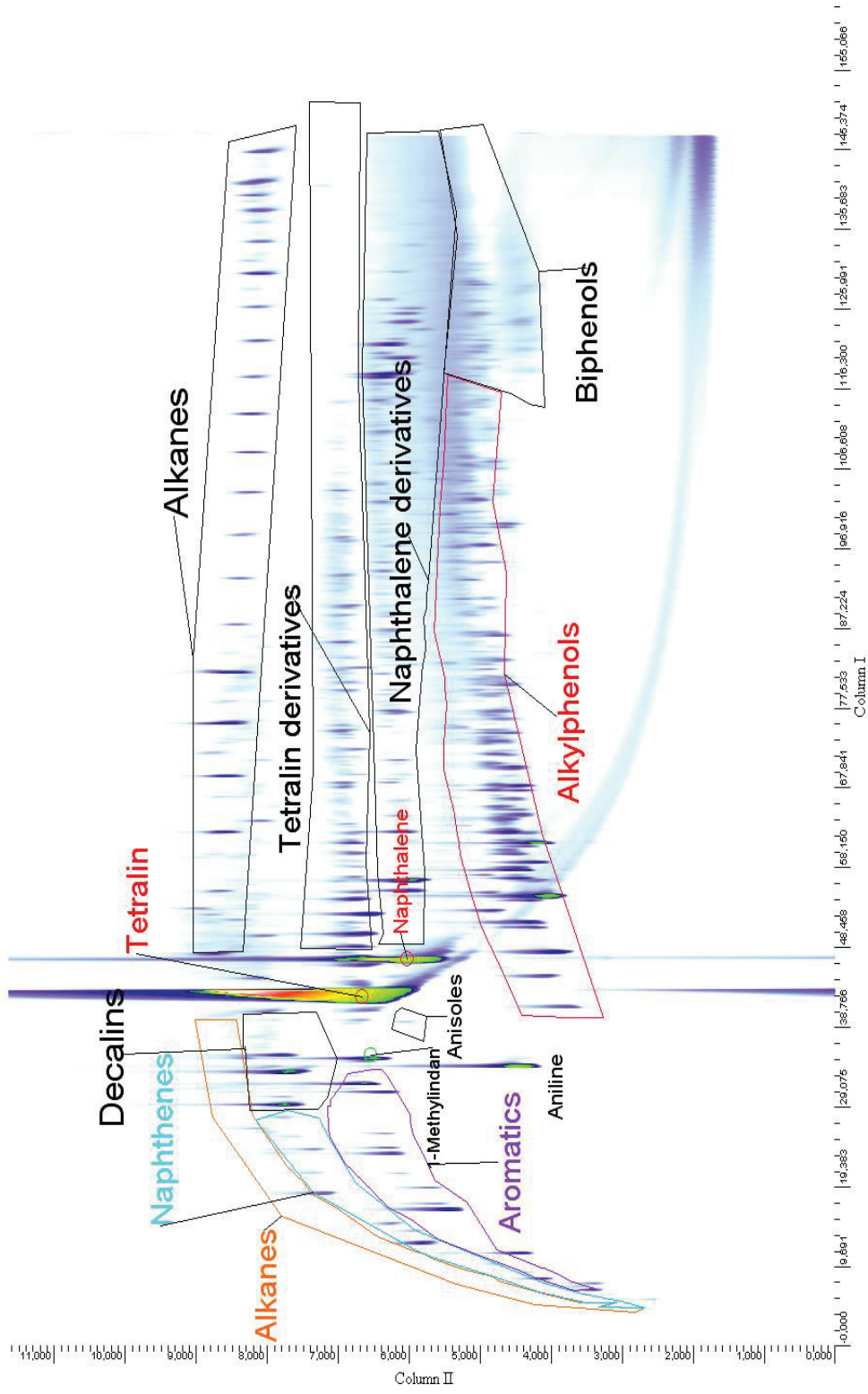
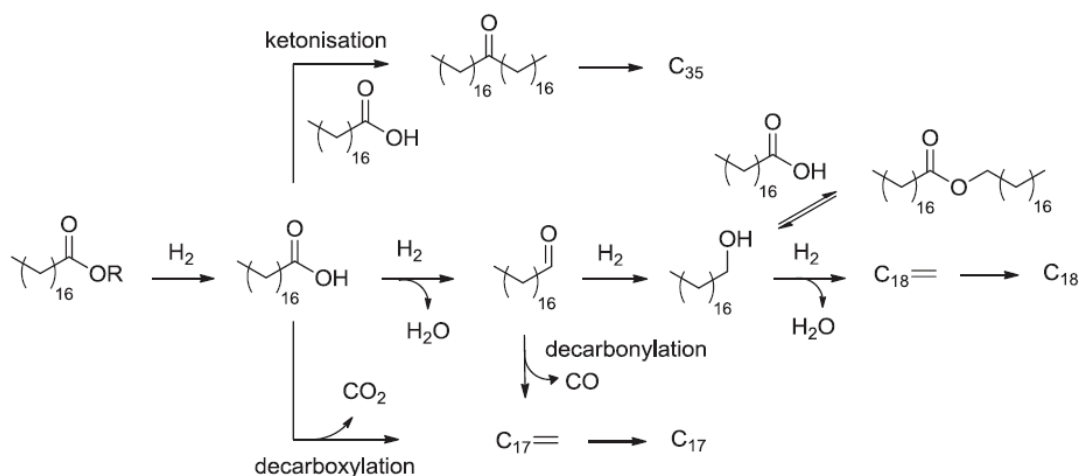


Figure IV.17: GCxGC-MS chromatogram of the liquid phase in the reactor after 13 h

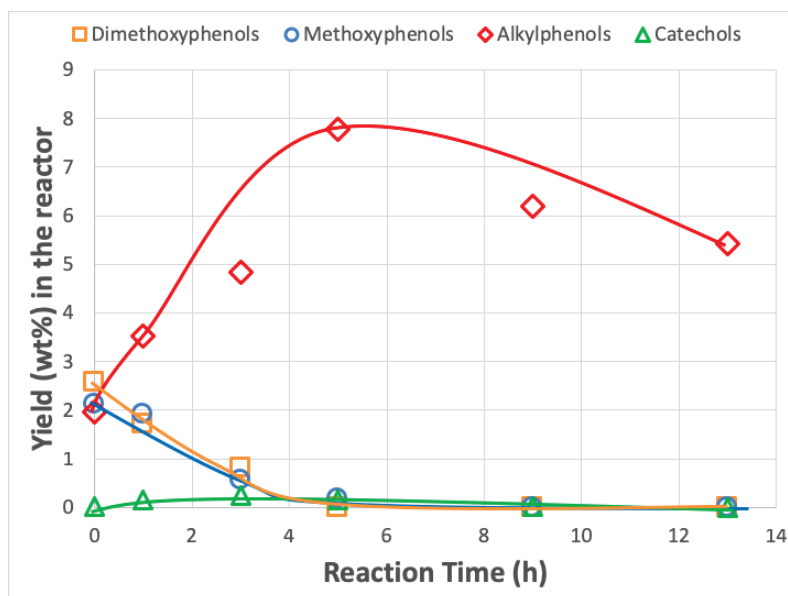
At t_0 point, the following main families of products were clearly distinguished: alkanes, naphthenes (cycloalkanes and cycloalkenes), aromatics, alkylphenols, methoxyphenols, dimethoxyphenols as well as tetralin and its derivatives. Inside each main family, the molecules with a C_1 , C_2 , C_3 , C_4 or C_5 alkyl substituent were successfully identified. The significant presence of phenolic compounds (alkylphenols, methoxyphenols and dimethoxyphenols) proved the pathway of direct removal of phenolic units from lignin. Alkanes higher than C_{13} were detected despite not expected in the liquid phase. The presence of these alkanes was explained by the hydrogenation of acid methyl esters (C_4 - C_{19}) found in the liquid phase (Scheme IV.9). Those acid methyl esters are probably coming from some cutin or suberin moieties, some lipophilic polymers present in the initial wheat straw and which are composed by C_{16} to C_{18} esters⁶. Additionally, some minor isolated products (anisole, cyclohexanone, furans, thiophenes, etc.) were also detected.



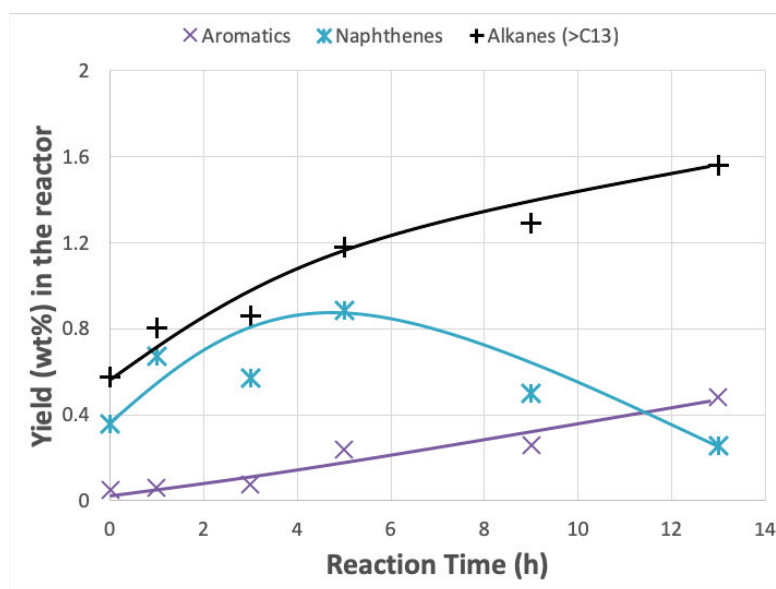
Scheme IV.9: Conversion of cutin-like moieties to long-chain alkanes

At 5 h, all the methoxy-substituted phenols were converted as seen by their total disappearance in the chromatogram. Meanwhile, a novel type of species (catechols) was detected. The formed catechols come from direct demethylation of methoxyphenols. At 13 h, the catechols disappeared via dihydroxylation/hydrogenation steps and only alkylphenols, naphthenes and aromatics were still detected with the alkanes present since the beginning.

In a second step, quantification was achieved by performing additional GC×GC/FID analyses on the same samples. A standard external method using aniline was employed, using the ECN model to predict relative FID response factors of hydrocarbons and oxygenated compounds. The quantifications allow us to calculate the yield of the main families of products in the reactor. The evolution of main oxygenated and non-oxygenated families is shown in Figure IV.18. Inside each family of products, the quantitative data obtained for different alkyl substituents are given in [Annex 5](#). Concerning the monomeric products in the reactor, we will firstly focus on the evolution of relatively heavy boiling products (dimethoxyphenols, methoxyphenols, catechols and alkanes $\geq C_{13}$) which were barely found in the separator. For the lighter products like alkylphenols, aromatics and naphthenes, it makes more sense to combine their mass in the separator to evaluate their yields.



(a)



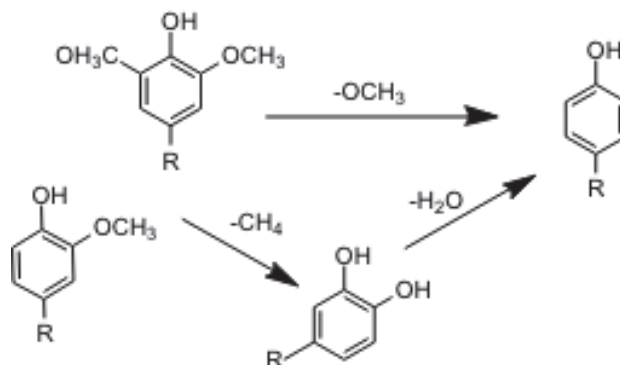
(b)

Figure IV.18: Evolution of main families of products in the reactor as a function of reaction time; (a) Oxygenated compounds (b) Non-oxygenated compounds

At t_0 , the main compounds in the reactor were methoxy-substituted phenols (dimethoxyphenols: 2.6 wt% and methoxyphenols: 2.1 wt%) and alkylphenols (2 wt%). After 5 h of reaction, the methoxy-substituted phenols disappeared entirely whereas the yield of alkylphenols increased from 2 wt% to 8.5 wt%: 7.8 wt% in the reactor and 0.7 wt% in the separator (presented in § [IV.2.4.2](#)). The significant increase of alkylphenols should be attributed to two reaction pathways:

- 1) A portion of alkylphenols was produced in the liquid by the direct removal of *p*-hydroxyphenolic units from oligomeric entities: THF-insolubles, THF-solubles and the solubilized oligomers.

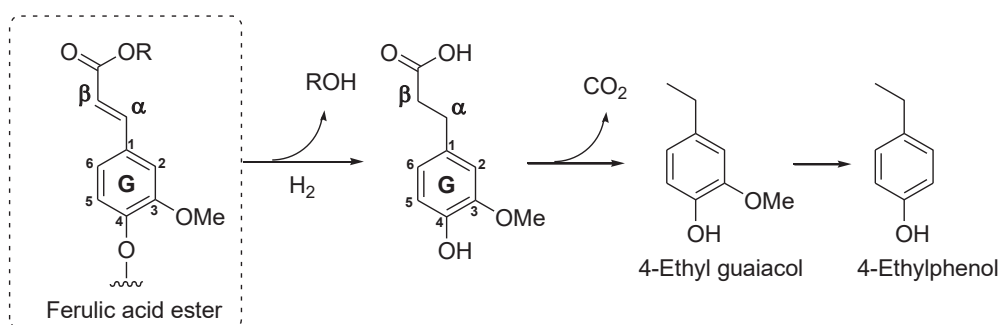
- 2) Similar to the transformation of lignin residues, monomeric methoxy-substituted phenols in the liquid phase can be converted to alkylphenols by direct demethoxylation or demethylation to catechols followed by dehydroxylation (Scheme IV.10). Thus, the maximal yield of catechols as intermediate products was observed at 3 h.



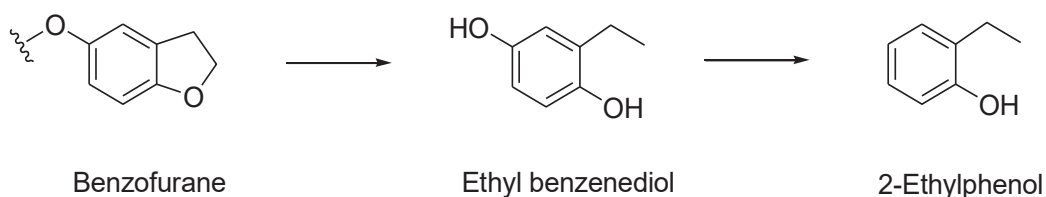
Scheme IV.10: Transformation of methoxy-substituted phenols to alkylphenols

Between 5 and 13 h, the decrease of both alkylphenols and catechols was observed, indicating that the deoxygenation proceeded continuously. At 13 h of reaction, alkylphenols were the only oxygenated compounds found in the reactor.

From the distributions of alkyl substituents shown in [Annex 5](#), the C₂ (mainly 4-ethyl) substituted compounds were observed to be the main components. The occurrence of these C₂ products and the few amounts of light alkanes in the gas phase, suggest the presence of ferulic acid ester or benzofuran unit in the starting lignin. Effectively these two precursors can be converted into 4-ethyl or 2-ethyl phenol by hydrogenation/decarboxylation and hydrodeoxygenation respectively² (Schemes IV.11 and IV.12). According to the quantification, the main phenol was 4-ethylphenol, indicating the predominance of the ferulic units in the starting lignin.



Scheme IV.11: Conversion of the ferulic acid ester into 4-ethylphenol



Scheme IV.12: Conversion of benzofurane entities into 2-ethylphenol

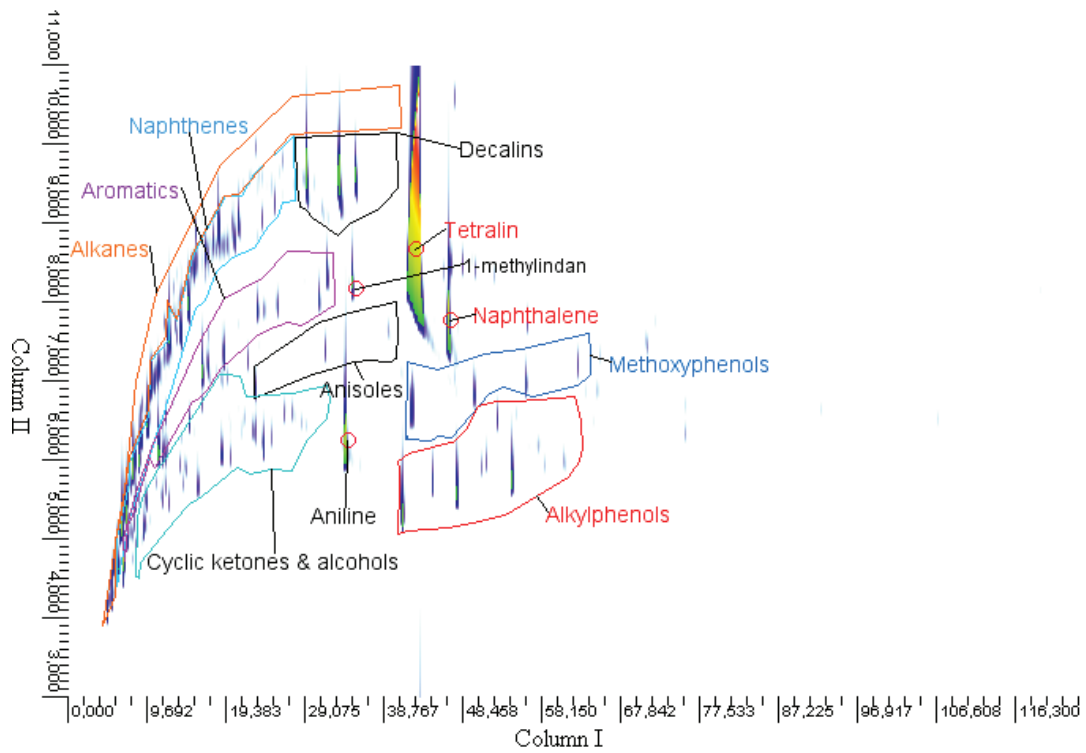
Because the liquid phase in the reactor was mixed and diluted by tetralin and its derivatives, we can not pursue precisely the elemental evolution of liquid products derived from lignin. At least, the elemental analysis for the liquid reported in Table IV.5 can prove that the successive deoxygenation process has been carried out within the liquid, in accordance with the progressive disappearance of oxygenated monomers. At 13 h, only about 18 wt% of initial oxygen was found in the liquid of reactor.

Table IV.5: Evolution of elemental analyses and H/C, O/C atomic ratios for the liquid phase in the reactor

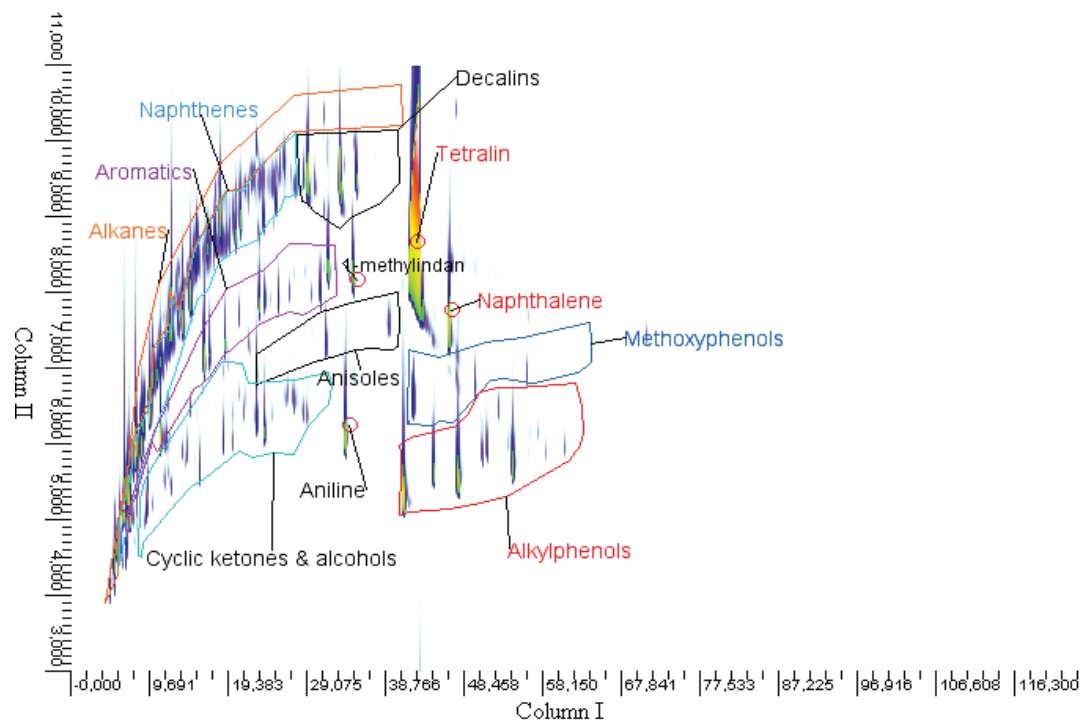
	P1000	0 h	1 h	3 h	5 h	9 h	13 h
C	61.1	88.1	87.8	88.5	88.5	88.3	89.2
H	5.7	9.0	9.0	8.8	9.1	8.8	9.0
O	29.9	3.6	3.8	3.5	3.3	3.0	2.1
N	0.7	0.1	0.1	0.1	0.2	0.2	0.2
S	0.9	0.0	0.0	0.0	0.0	0.0	0.0
Ashes	3.1	n.d.	n.d.	n.d.	n.d.	n.d.	n.d.
Water	2.1	n.d.	n.d.	n.d.	n.d.	n.d.	n.d.
Total	103.4	100.7	100.7	100.9	101.1	100.4	100.6
Atomic ratio							
H/C	1.12	1.23	1.23	1.19	1.23	1.20	1.21
O/C	0.37	0.03	0.03	0.03	0.03	0.03	0.02

IV.2.4.2 Liquid phase in the separator

Due to the separation with hot reflux condenser, some monomeric products, formed water and tetralin and some derivatives were able to pass the reflux condenser and be cumulated in the separator. The mixture in the separator contains clearly two phases: an organic phase and an aqueous phase. The GCxGC FID images of the organic phase and the aqueous phase at 1 h, 5 h and 13 h were illustrated in Figure IV.19 and IV.20. The following families were clearly found in the organic phase: alkanes, naphthenes, aromatics, alkylphenols, methoxyphenols, cyclic ketones and alcohols as well as tetralin and its derivatives. In the aqueous phase, water-soluble compounds (ketones, alcohols and some alkylphenols) were identified. Compared to the liquid phase in the reactor, most of heavy products on the right side of tetralin were not found in the separator, suggesting a relatively good performance of our reflux condenser.



(a) 1 h



(b) 5 h

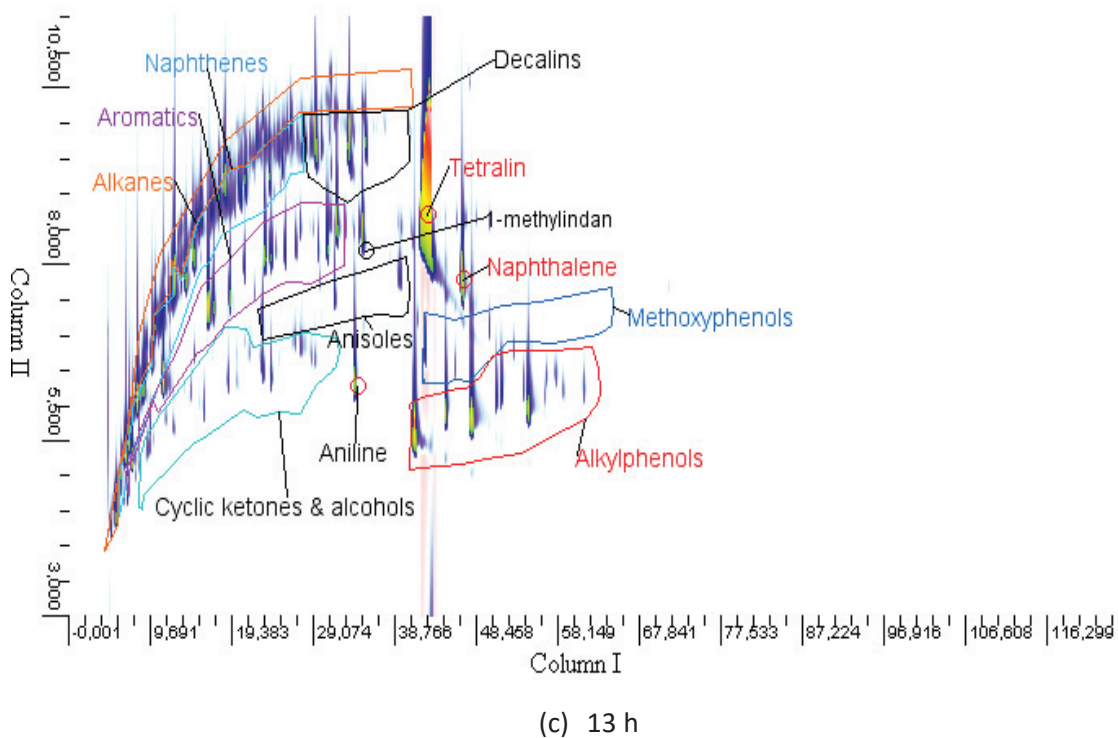
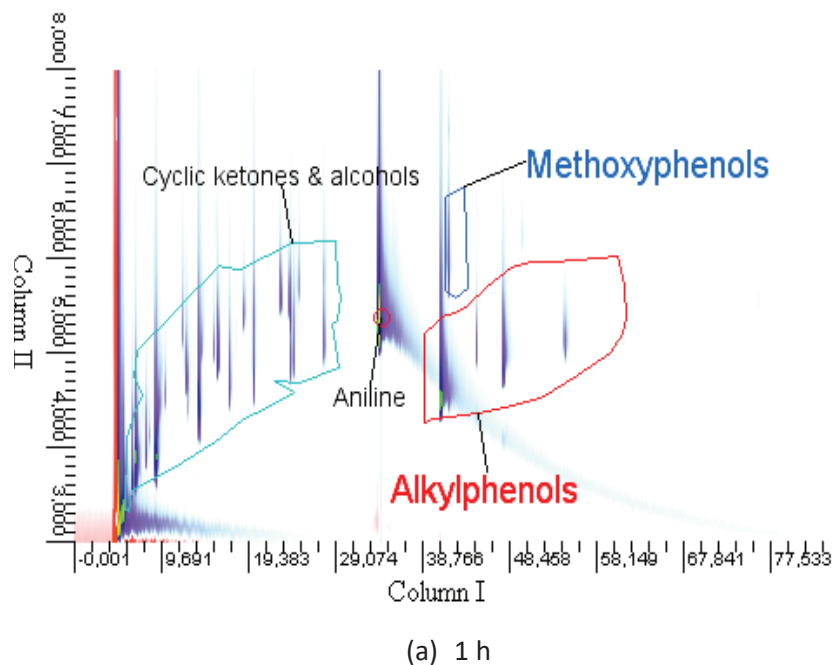
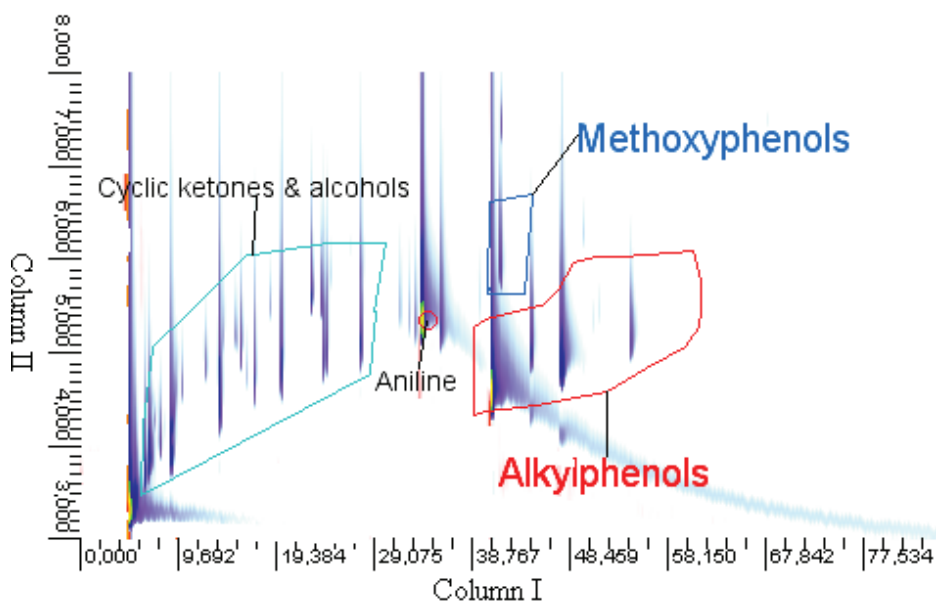
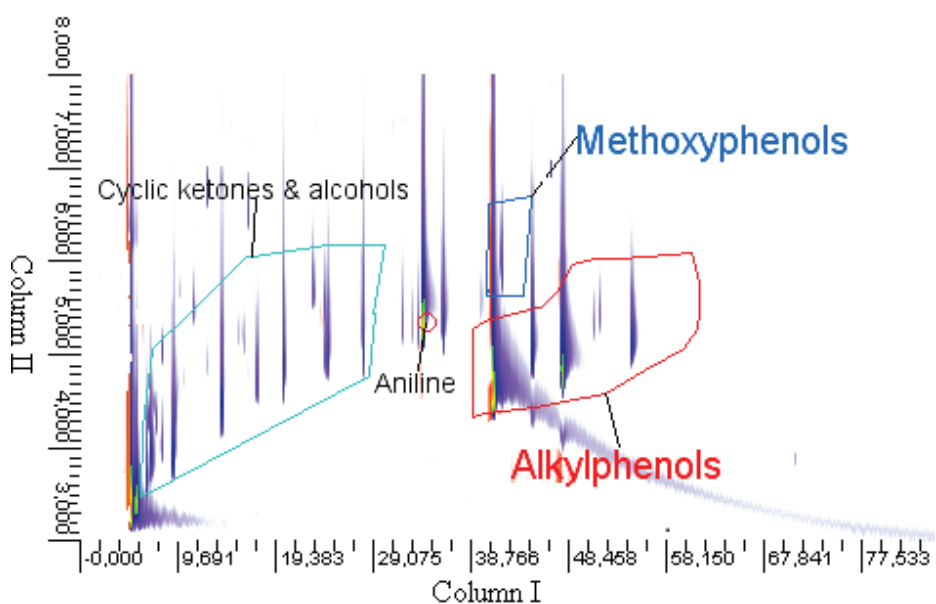


Figure IV.19: GCxGC-FID chromatogram of the organic phase (a) 1 h; (b) 5 h; (c) 13h





(b) 5 h



(c) 13 h

Figure IV.20: GCxGC-FID chromatogram of the aqueous phase (a) 1 h; (b) 5 h; (c) 13h

The quantification of identified products in the aqueous phase was not performed, but the elemental analysis and some Karl Fischer titration were carried out to determine CHONS and water content in the aqueous phases. The Karl Fischer titration shows that the aqueous phases had around 90-92 wt% of water content. The evolution of elemental analyses for the aqueous phase is listed in Table IV.6. We can observe that the soluble organic compounds bring 3-4 wt% of carbon in the aqueous phase, the latter representing maximum 20 wt% starting lignin at 13 h. The two analyses show that around 480-600 mg approximately of organic products were neglected in our study.

Table IV.6: Evolution of elemental analyses for the aqueous phase in the separator

Reaction Time (h)	1	3	5	9	13
C	3.1	3.7	4.3	3.3	3.2
H	12.0	11.7	11.9	11.8	11.8
O (*)	84.7	84.2	83.3	84.2	84.4
N	0.3	0.4	0.5	0.7	0.7
S	0	0	0	0	0

* The oxygen content is calculated by deduction.

The quantifications of each family identified in the organic phase were done by the same standard external method, illustrated in Figure IV.21. Inside each main family of products, the quantitative data obtained for the molecules of different alkyl substituents in the organic phase are given in [Annex 6](#). Unsurprisingly, as the reaction time increased, relatively light compounds (alkylphenols, aromatics and naphthenes) were flowed away from the reactor, being cumulated in the separator. At 13 h, about 3.5 wt% of naphthenes, 3.2 wt% of alkylphenols and 1.7 wt% of aromatics were found in the separator.

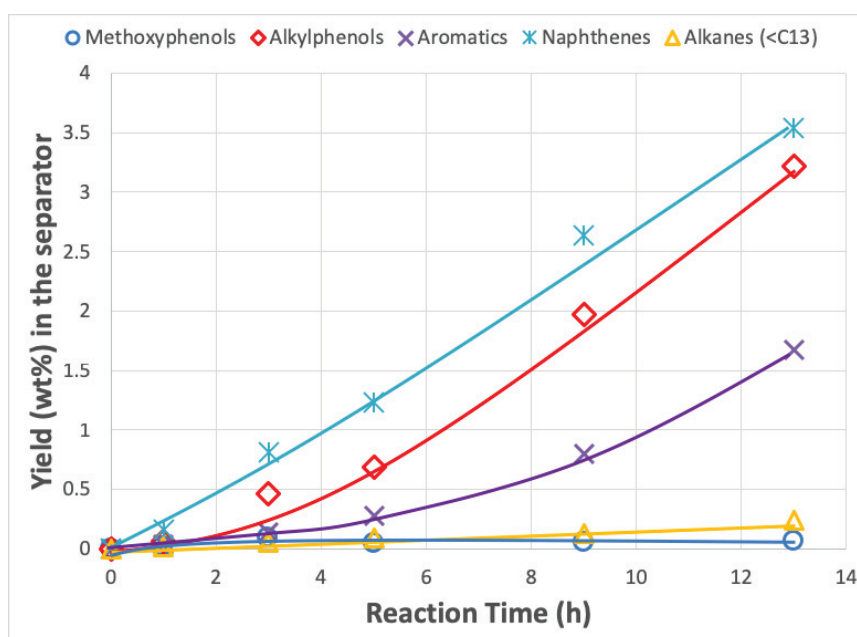
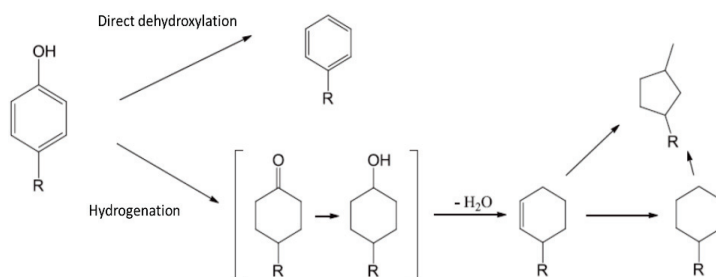


Figure IV.21: Evolution of main product families in the organic phase as a function of reaction time

The nature of these compounds was in accordance with the transformations observed on the hydrodeoxygenation (HDO) of lignin model compound (guaiacol) with metal sulfide catalyst¹. The alkylphenols still present in reactor were converted on the catalyst by HDO to aromatics and naphthenes (Scheme IV.13). The alkylphenols, aromatic and naphthenes existed both in the reactor and the separator. Thus, the addition of each product family at these two locations was done in order to evaluate their total yields in function of reaction time, presented in Figure IV.22.

As expected, the total yields of aromatics and naphthenes increased in function of reaction time thanks to the conversion of alkylphenols. Compared to their yields, it appears that the reaction route of alkylphenols into naphthenes is more favored under the operating conditions.



Scheme IV.13: Reaction scheme for hydrodeoxygenation of alkylphenols

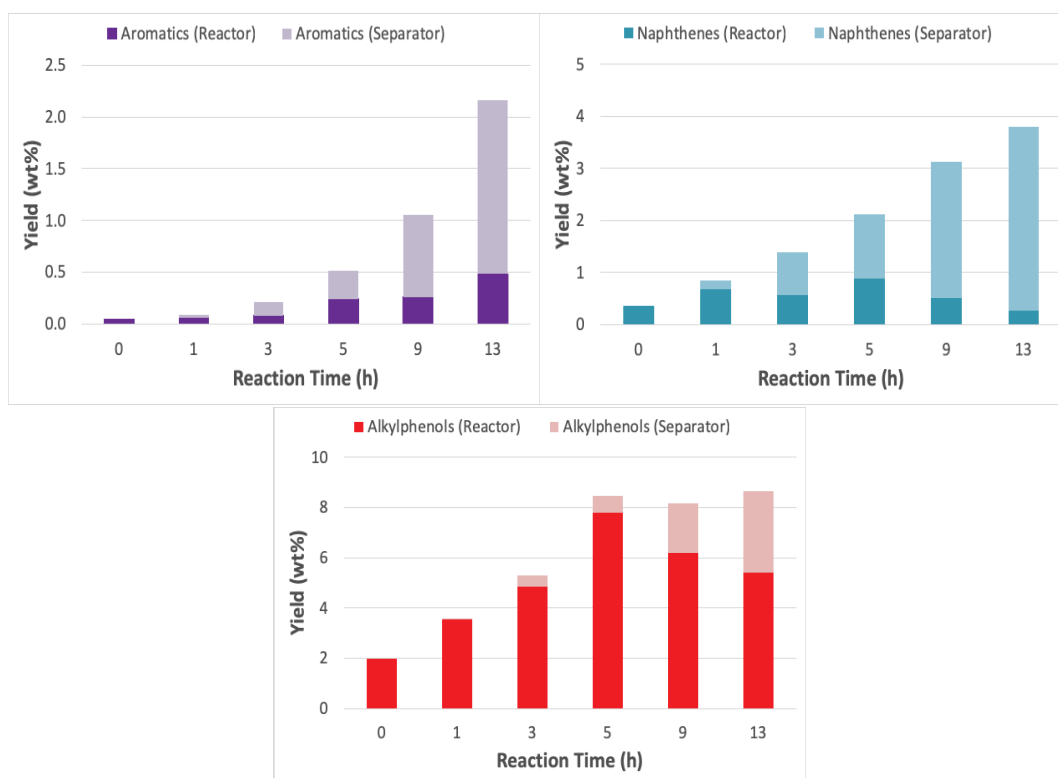


Figure IV.22: Evolution of aromatics, naphthenes and alkylphenols as a function of reaction time

For the yield trend of alkylphenols, it was observed that it increased during the first 5 hours and kept almost stable between 5 and 13 h. During the first 5 hours, the yield of THF-solubles decreased from 49 wt% to 16 wt% (33 wt% of decrease). The alkylphenols were rapidly produced from 2 wt% to 8.5 wt% thanks to the depolymerization of oligomeric entities in addition to the transformations of other phenolic monomers such as dimethoxyphenols, methoxyphenols and catechols (t_0 : 4.7 wt%; 5 h: 0.4 wt%). Between 5 and 13 h, we noticed that the variation of THF-solubles represented only 11 wt% (from 16 wt% to 5 wt%) and all the methoxy-phenols were consumed. We can assume that, from 5 h, the production rate of alkylphenols slowed down due to the shortage of reactants. At the meantime,

aromatics and naphthenes were supposed to be formed more quickly owing to the abundance of alkylphenols in the reactor, which probably makes the yield of alkylphenols kept nearly constant between 5 and 13 h. This assumption will be validated by the developed kinetic model in **Chapter VI**.

IV.2.4.3 Tetralin conversion in the liquid phase

As tetralin is not inert under this operating conditions, many types of derivatives transformed from tetralin were found in the liquid: naphthalene by dehydrogenation, decalin by hydrogenation, methylindan by isomerization, butyl-benzene by ring-opening and their alkyl-substituted derivatives from alkylation as well as some condensed tetralin compounds (some hydroxylated derivatives naphthenols. Considering the complexity and the great number of these derivatives, it makes difficult to calculate the mass balance of tetralin after the conversion. In our case, the major derivative was naphthalene by dehydrogenation, which confirms the efficient hydrogen-donating character of the solvent. The conversion of tetralin to naphthalene can indeed provide H_2 directly in the liquid phase (2 moles of H_2 per moles of naphthalene). As it is in close contact with the catalyst, the released H_2 could be directly involved in hydrogenation/hydrogenolysis reactions just after its formation in the liquid phase. Therefore, it is interesting to evaluate the mass ratio between tetralin and naphthalene in order to evaluate the hydrogen release into the solution. For simplification, we assume that the total mass of tetralin and naphthalene kept constant at 70 g during the conversion. The mass ratio between them was determined by GC/FID, illustrated in Figure IV.23.

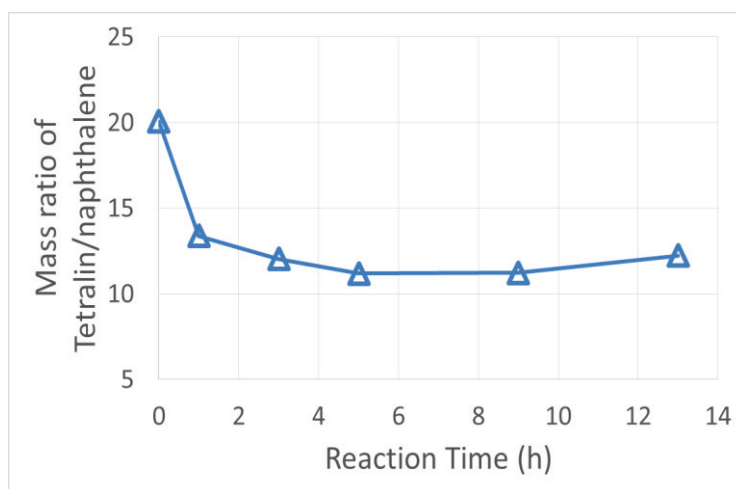


Figure IV.23: Tetralin/naphthalene mass ratio as a function of reaction time

It was found that tetralin was dehydrogenated to naphthalene in the first 1 h. It was thought that at the early stage of reaction, a high consumption of H_2 resulted in the low concentration of H_2 in the liquid, favoring the dehydrogenation reaction from tetralin to naphthalene. Between 3 and 13 h, the reaction involving tetralin and naphthalene seemed to reach a plateau observing the stability of mass ratio between them. Finally, about 7 wt% of introduced tetralin was converted to naphthalene. The conversion ratio corresponds to 0.08 moles of H_2 potentially available in the liquid. Compared to the total H_2 gas consumption at 13 h (1.30 moles), the H_2 provided by tetralin accounted only for 6%. That indicates, the main contributor for the hydrogenation and hydrogenolysis reactions was molecular H_2 gas.

IV.2.4.4 Conclusion of the transformations in the liquid phase

From the discussions above, some conclusions can be reached for main transformations in the liquid phase:

- ✓ Some short-chain oligomeric entities were formed by depolymerization of heavy lignin fragments, and solubilized in the liquid. Furthermore, these oligomeric entities proceeded to deoxygenating transformations.
- ✓ Due to the depolymerization reactions, basic phenolic units were continuously released from the oligomeric entities. Therefore, dimethoxyphenols, methoxyphenols and alkylphenols can be considered as primary products.
- ✓ The demethoxylation and demethylation of the methoxy-substituted phenols led to alkylphenols, further converted by HDO to aromatics and naphthenes.
- ✓ Fatty ester or acids are present in quite a large amount as heavy alkanes were observed up to 1.6 wt% of the initial lignin in the liquid phase. The formation of those alkanes being in relation to the presence of cutin or suberin-like moieties in the lignin fraction.
- ✓ The ferulic units must be present in high amount in the initial lignin as the 4-ethylphenol is one of the most abundant phenol.
- ✓ Tetralin was efficiently dehydrogenated to supply additional hydrogen atoms in the liquid for hydrogenation/hydrogenolysis reactions.

At 13 h of reaction, the water yield was around 18 wt% and the total monomer yield was around 17 wt%: alkylphenols (8.6 wt%), naphthenes (3.8 wt%), aromatics (2.2 wt%) and heavy alkanes (1.8 wt%). That means that a significant part (about 40 wt%) of lignin product was still in the form of oligomeric entities, but solubilized in the liquid. Undoubtedly, the fraction of oligomeric entities contains stronger C-C linkages which will be more challenging to cleave.

IV.3 Construction of reaction scheme

In this work, the catalytic hydroconversion of wheat straw soda lignin in tetralin solvent over CoMoS/Al₂O₃ catalyst lead to gases, oligomers, and monomers. The different fractions of products at different reaction times were deeply characterized by various analytic tools. Thanks to the comprehensive analysis, we are able to better understand the transformations occurring during catalytic lignin conversion. A representation of molecular pathways is shown in Figure IV.24.

During the early stage of reaction, the decarboxylation of carboxylic acidic functions and the dehydration of the aliphatic OH groups took place. The weak ether bonds were cleaved, creating short chains of lignin fragments, which could be THF-solubles or solubilized oligomers. Meanwhile, a certain amount of phenolic monomers (dimethoxyphenols, methoxyphenols and alkylphenols) was released due to the bond cleavage. In a second time, the lignin fragments were deoxygenated and became shorter. The catalytic stage occurred with the demethoxylation, demethylation and dehydroxylation of phenols to form progressively phenolic, aromatic and naphthenic monomers and oligomers in the liquid phase. As a result, CH₄ and H₂O were continuously formed at the same time. The intermediate product of catechols was formed and then dehydroxylated. At last, we found only alkylphenols, aromatics, naphthenes as well as deeply deoxygenated oligomers in the liquid phase.

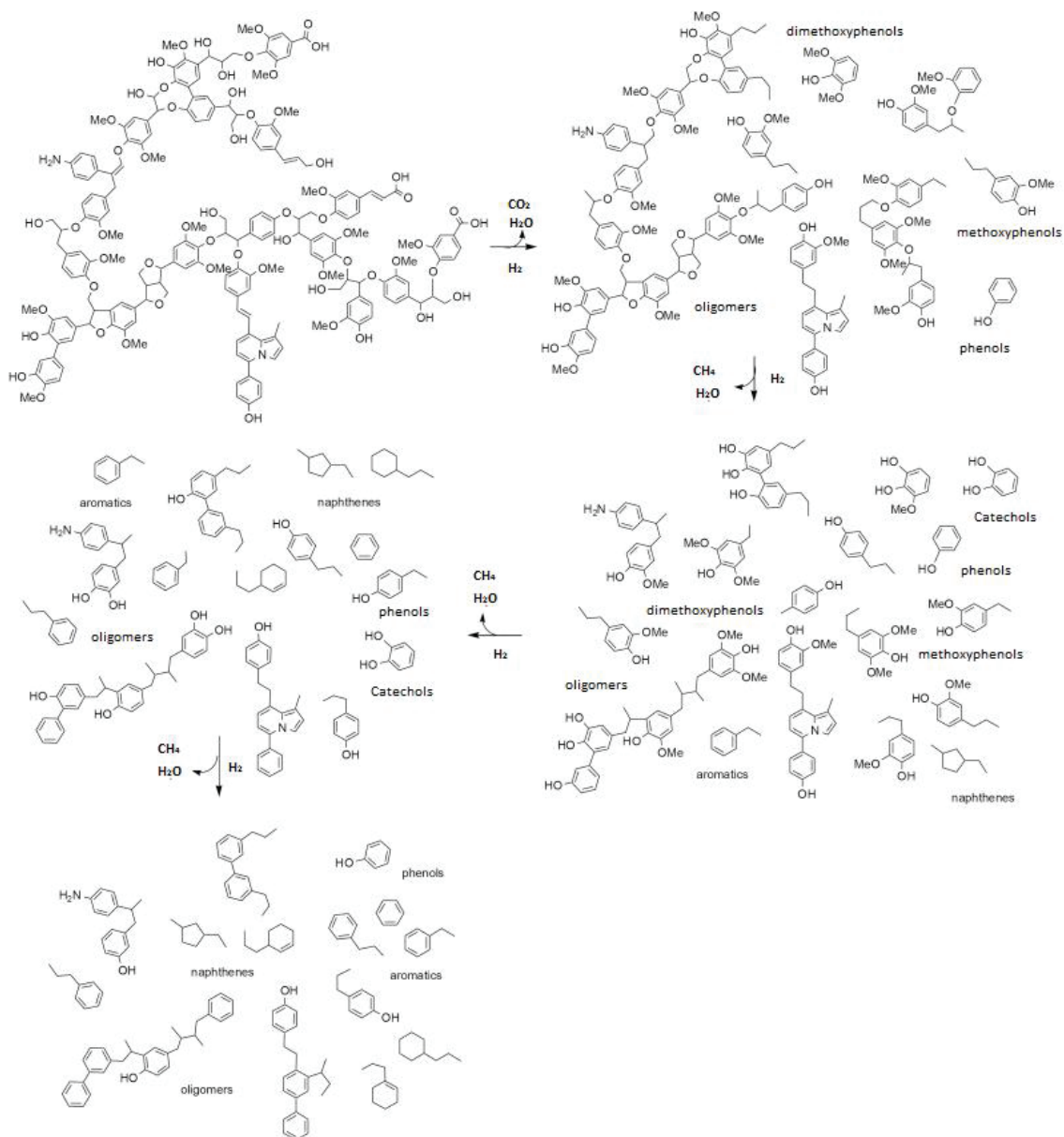


Figure IV.24: Progressive transformation scheme of lignin to oligomers and monomers under catalytic hydroconversion with $\text{CoMoS}/\text{Al}_2\text{O}_3$

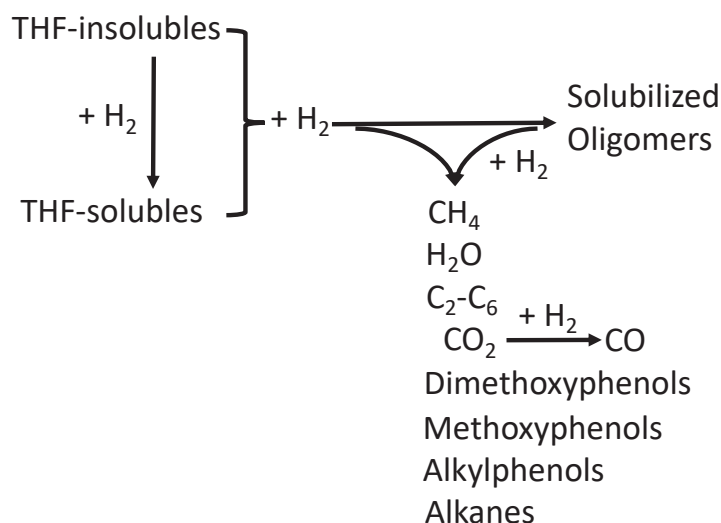
Besides the main pathways illustrated in Figure IV.24, there existed other minor pathways:

- ✓ The light alkanes ($\text{C}_2\text{-C}_6$) came from the C-C cleavage of alkyl chains in lignin.
- ✓ CO was produced from the reverse water-gas shift reaction of CO_2 .
- ✓ The heavy alkanes were produced from the impurities in the lignin.

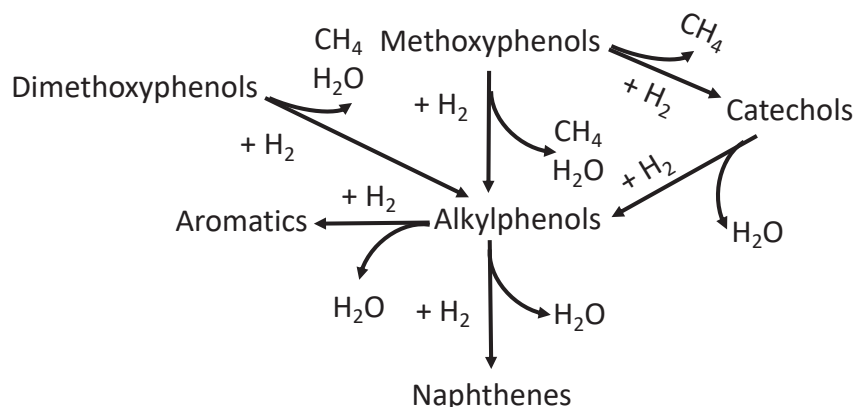
From the discussions above, the transformations of lignin hydroconversion may have two parallel catalytic pathways:

- The transformation of lignin fragments led to gaseous and liquid monomers.
- The deoxygenation process occurred to the liquid monomers.

A complete reaction scheme can be established on the basis of experimental observations, as shown in Scheme IV.14 and Scheme IV.15.



Scheme IV.14: General depolymerization of lignin



Scheme IV.15: Transformation of monomers in the liquid phase

The Scheme IV.14 represents the transformation of lignin fragments, leading to gaseous and liquid monomers:

- ✓ The oligomeric entities were cleaved into shorter oligomeric entities. The order in size of oligomer entities from large to small is THF-insolubles, THF-solubles, followed by the solubilized oligomers existing in the liquid phase.
- ✓ The primary phenolic compounds were continuously released from these oligomeric entities.
- ✓ The functional groups (-COOR, -OH, -OCH₃) on these oligomeric entities were reacted, releasing CO₂, CH₄ and H₂O.

The Scheme IV.15 shows the transformations of liquid monomers in the liquid phase:

- ✓ The demethoxylation and demethylation followed by dehydroxylation occurred to the methoxy-substituted phenolic compounds.
- ✓ The alkylphenols were reacted via HDO to form aromatics and naphthenes.
- ✓ CH₄ and H₂O were produced while converting the monomers.

IV.4 Evaluation of the role of catalyst

Two experiments (1 h and 5 h) have been carried out in thermal conditions without catalyst but in the presence of hydrogen and tetralin, in order to evaluate properly the role of catalyst. The distribution of products is presented in Figure IV.25 and compared to the catalytic experiments. Figure IV.6 gives the comparison of their gaseous product composition.

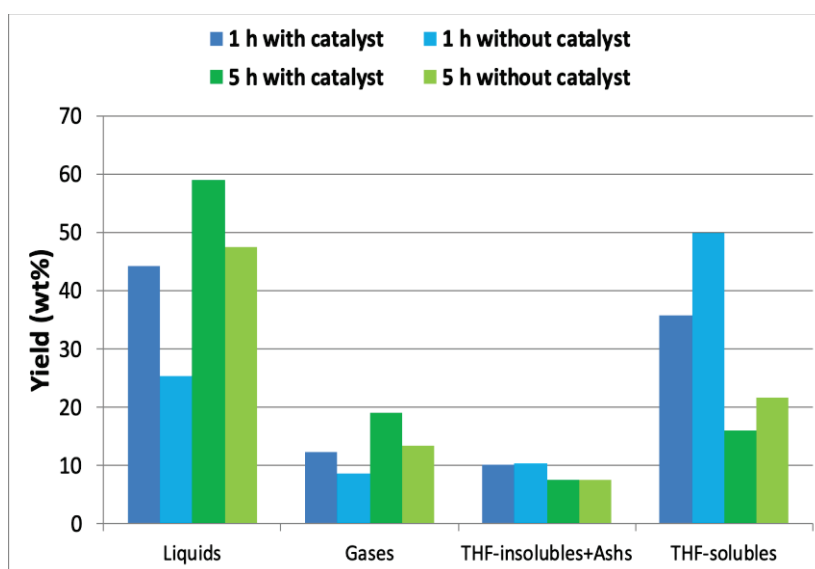


Figure IV.25: Distribution of lignin hydroconversion products with and without catalyst

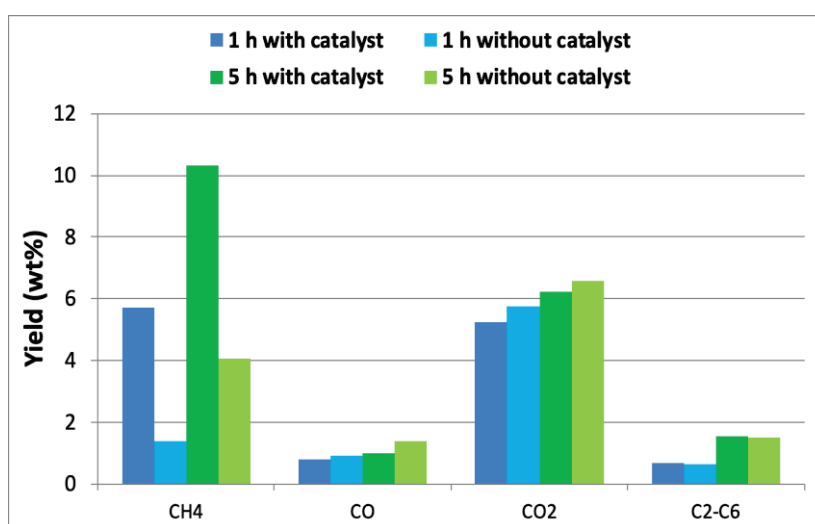


Figure IV.26: Gaseous production distributions with and without catalyst

Several observations were clearly seen:

- 1) The yield of THF-insolubles without catalyst was nearly equal to that with catalyst, indicating that the depolymerization of THF-insolubles was thermal and unaffected in the presence of catalyst.
- 2) The yields of THF-solubles, gases and liquids varied drastically as compared to the catalytic experiments at the same reaction time. So, it appears that the liquid and gas productions were favored in the presence of catalyst.
- 3) A simultaneous increase of CO and CO₂ for the experiments without catalyst was noticed as compared to the catalytic experiments. It can be explained methanation catalytic reaction from CO and CO₂ to CH₄ occurs in the presence of catalyst under our operating conditions contrarily to the experiments done without catalyst⁵.
- 4) A large enhancement in the production of CH₄ was observed in the presence of catalyst. CH₄ came mainly from the conversion of -OCH₃ groups. Thus, the catalyst had a quite active effect on the removal and conversion of -OCH₃ groups.

The GC×GC chromatogram obtained from the liquid (not shown) at 5 h indicated the presence of dimethoxyphenols and methoxyphenols as the main compounds and only some alkylphenols, aromatics and naphthenes. It suggests that the catalyst had a significant deoxygenating activity to the oxygenated monomers in the liquid phase.

IV.5 Comparison of performance with conventional batch system

For a conventional batch system, H₂ was consumed by reactions, leading to a progressive decrease in the H₂ concentration within the reactor. The main advantage of our ungraded semi-batch system is to supply continuously fresh H₂ in order to keep the H₂ concentration in the reactor at a high level. The performance of lignin conversion using the semi-batch system was then compared to that using the previous traditional batch system, with the same catalyst and under the same reaction conditions. The distribution of the different fractions under two systems is shown in Figure IV.27 (SB: semi-batch; B: batch).

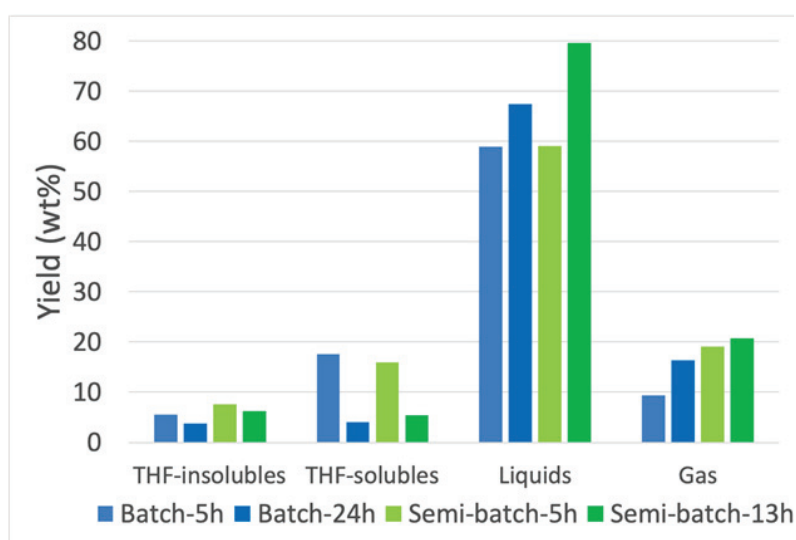


Figure IV.27: Performance comparison of lignin conversion between the semi-batch system and the conventional batch system

Under the same short reaction time of 5 h, the yields of THF-solubles and liquids for two systems were relatively close, while the gas yield for the semi-batch system was twice that of the batch system. As the reaction time increased, the yield of liquids obtained under the semi-batch system after 13 h was even higher than using the batch after 24 h. Moreover, the gas yield in the batch system after 24 h was lower than that using the semi-batch after 5 h. These observations suggest that, under the semi-batch system with a continuous supply of H₂, the release of gases and liquids was greatly accelerated. Figure IV.28 shows the comparison of H₂ consumption between these two systems. It can be seen that the H₂ consumption was much higher under the semi-batch system. It proves that by using the conventional batch system in the absence of additional supply, the H₂ concentration decreased to a low level in the reactor, which resulted in a relatively low conversion rate of lignin conversion. The semi-batch system with the supply of H₂ is demonstrated to be much more powerful than the conventional batch due to the avoidance of H₂ limitation.

Additionally, with the aid of the reflux condenser, we were able to follow the formation of water while the reaction proceeded, which is really impossible for the batch system.

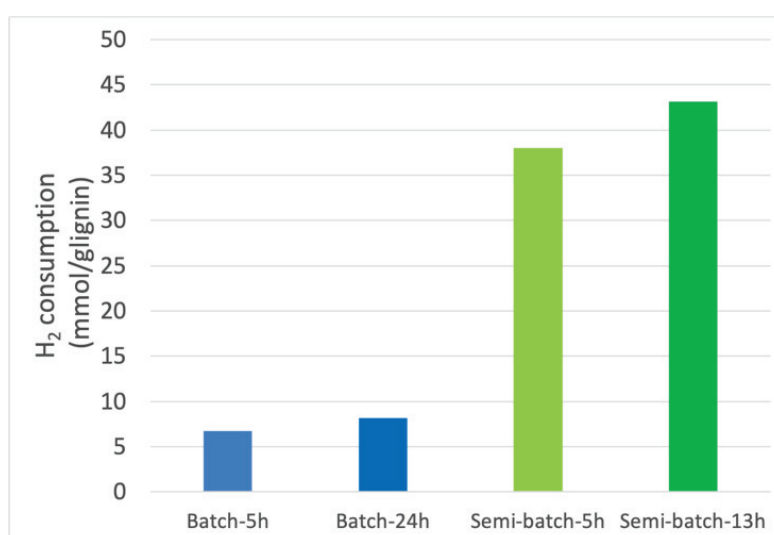


Figure IV.28: Comparison of H₂ consumption between the semi-batch system and the conventional batch system

IV.6 Characterization of the used catalysts

The CoMoS/Al₂O₃ catalysts used for 0 h, 1 h and 13 h catalytic tests were characterized and compared to the fresh sulfide catalyst, listed in Table IV.7 and illustrated in [Annex 7](#). The carbon content increased to 12 wt% after the heating slope and then remained stable. The sulfur content (corrected from C content), measured on the fresh sulfide catalyst at 7.5 wt%, decreased after the heating slope and then remained stable at approximately 6 wt%. It suggests that the changes occurred mostly during the heating step and then remained stable. The same observations are confirmed by for the textural analysis of the used catalysts. When reaching t_0 , the BET surface area was slightly lower compared to the fresh catalyst, as well as the average pore volume and porous size. However, the evolution of BET surface area, pore volume and porous size in function of reaction time showed that the main changes occurred after the first hour of the hydroconversion and then the catalyst seemed stable.

With regard to the catalytic activity, it was found that the deoxygenation process still occurred in the liquid phase at 13 h. This proves that, the partial coking did not prevent totally the activity of catalyst. It is quite interesting to note that compared to many works in lignin conversion in solvent, the quite low catalyst-to-lignin ratio used here (10 wt%) allowed to convert the lignin without being rapidly deactivated.

Table IV.7: C, S elemental analysis, BET surface area, pore diameter and pore volume for used catalyst and fresh catalyst

	Fresh catalyst	Used catalyst (0 h)	Used catalyst (1 h)	Used catalyst (13 h)
C (wt%)	0	12.1	11.9	13.1
S (wt%)	7.5	5.6	6.7	6.0
Bet surface area (m ² /g)	193	175	176	185
Total pore volume (cm ³ /g)	0.47	0.29	0.28	0.29
Average porous size (nm)	7.94	6.17	5.99	5.88

Table IV.8: XPS elemental analysis of the fresh and used CoMoS/Al₂O₃ catalysts

Atomic	O	Al	S	Mo	Co	S/(Co+Mo)	S/Mo
CoMoS/Al ₂ O ₃ Freshly sulfided	52	33	4.1	1.9	0.9	1.5	2.2
CoMoS/Al ₂ O ₃ Stored under air	67.9	25.3	3.9	2.1	0.8	1.3	1.8
0 h	67.8	25.9	3.4	2.0	0.9	1.2	1.7
1 h	64.2	29.3	3.2	2.1	1.0	1.0	1.5
3 h	65.7	28.1	3.2	1.9	1.1	1	1.7

The XPS elemental analyses (Table IV.8) of the catalysts after reaction showed also a decrease of the S content at the surface of the catalyst after reaching the reaction temperature but, then, a stable level of S at the surface of the catalyst between 0 h and 3 h. In addition, according the XPS decomposition (Table IV.9) the same amount of Mo^(IV) (MoS₂) was detected for the used catalysts after 0 h, 1 h and 3 h. Of course, this proportion of MoS₂ (63%) is lower than the freshly sulfided initial catalyst (83%) but the used catalysts were not re-sulfided after test but simply washed and kept under air; regarding the S2P analysis, sulfate were found, confirming partial oxidation at the surface. Thus, we can note that the main changes on the catalyst occurred during the heating period where lignin starts to be cleaved and transformed releasing mainly CO₂, water, methoxyphenolic monomers and oligomers. With our set-up system, gases are only briefly in contact with the catalyst as they are rapidly and continuously removed from the reacting mixture. The formation of water in the reactor during the heating period has been only evaluated by Karl-Fischer titration and the reflux system does not allow to remove formed water until reaction temperature was reached; this amount of water (evaluated at around 1 g)

could be in close contact with the catalyst before being transferred to the separator when the temperature of 350 °C was reached. We also know that THF-soluble lignin residue is one of the main product during this period, and, as seen by ³¹P NMR of this fraction, aliphatic OH were strongly impacted during this step which indicate that quite high quantity of water was formed in the liquid. Thus, the catalyst during the heating period could interact with water and phenolic oligomers/monomers. Nevertheless the used catalyst remained sulfided, with still a good S/Mo ratio for CoMoS phase. It still has a large surface area and an acceptable porosity. The pores are not totally blocked by the carbon deposit and active site (MoS₂) are still available. The catalyst is impacted but still have a strong effect on the selectivity of the process as phenolics compounds are gradually converted by hydrodeoxygenation to aromatic and naphthenic compounds as expected even if the process is slow.

Table IV.9: XPS decomposition of Mo3d and S2P species for fresh and used CoMoS/Al₂O₃ catalysts

BE eV (%)	Mo ^(IV)	Mo ^(V)	Mo ^(VI)	S ²⁻	S ₂ ²⁻	Sulfates
CoMoS/Al ₂ O ₃ Freshly sulfided	228.8 (80)	230.1 (12)	232.5 (8)	161.4 (84)	162.6 (16)	-
0 h	229.0 (63)	230.3 (15)	232.7 (22)	161.7 (56)	162.7 (20)	168.6 (24)
1 h	229.1 (61)	230.6 (17)	232.9 (22)	161.8 (53)	162.7 (23)	168.7 (24)
3 h	228.9 (64)	230.3 (15)	232.7 (21)	161.8 (62)	162.8 (13)	168.8 (25)

IV.7 Conclusion

Using the characterization methods described in **Chapter II**, we were able to follow the main reactions involved during the hydroconversion of lignin P1000 in tetralin and in the presence of CoMoS/Al₂O₃ catalyst in a semi-batch reactor. As a result, a pertinent reaction scheme was established to elucidate the progressive conversion of lignin. At the early stage of reaction, the oligomeric entities were decarboxylated and dehydroxylated with respect to the initial lignin. As the reaction progressed, we were able to show the decomposition and the deoxygenation of these oligomeric entities as well as the release of liquid monomers into the liquid phase. Initially, the liquid monomers mainly consisted of methoxy-substituted phenols and alkylphenols. Afterward, these methoxylated phenols were demethylated or demethoxylated to form catechols and alkylphenols. After a longer reaction time, the oxygenated compounds were dehydrated to form aromatics and naphthenes. The presence of heavy linear alkanes was not expected. As discussed, these long chains come from the hydrodeoxygenation and decarboxylation/decarbonylation reactions occurring to the fatty acids esters.

After 13 h of reaction, the main liquid compounds were alkylphenols (8.6 wt%), naphthenes (3.8 wt%), aromatics (2.2 wt%) and heavy alkanes (1.8 wt%). The gas yield was 20.7 wt% and water yield was around 18 wt%. Considering the low yield of aromatics at 13 h, it could suggest that CoMoS/Al₂O₃ may not the most efficient catalyst but seems to be quite stable under the operating conditions.

Concerning the oligomeric molecules, the THF-solubles and THF-insolubles yields were 5.3 wt% and 3.2 wt% respectively. However, a significant part (about 40 wt%) of lignin product was still in the form of oligomeric entities, but solubilized in the liquid. Without doubt, the fraction of oligomeric entities contains stronger C-C linkages which will be more challenging to cleave. So, the effort in the catalytic hydroconversion should be further focused on how to convert the oligomers still present in the liquid

phase. Finally, compared with the traditional batch system, the semi-batch system appears to be a very powerful reaction system for lignin hydroconversion.

Reference-IV

- [1] Bui, V.N., Laurenti, D., Afanasiev, P., Geantet, C., 2011. Hydrodeoxygenation of guaiacol with CoMo catalysts. Part I: Promoting effect of cobalt on HDO selectivity and activity. *Applied Catalysis B: Environmental* 101, 239–245.
- [2] Bredenberg, J., Huuska, M., Rätty, J., Korpio, M., 1982. Hydrogenolysis and hydrocracking of the carbon-oxygen bond: I. Hydrocracking of some simple aromatic O-compounds. *Journal of Catalysis* 77, 242–247.
- [3] Bredenberg, J., Huuska, M., Toropainen, P., 1989. Hydrogenolysis of differently substituted methoxyphenols. *Journal of catalysis* 120, 401–408.
- [4] Gevert, B.S., Otterstedt, J.E., Massoth, F.E., 1987. Kinetics of the HDO of methyl-substituted phenols. *Applied catalysis* 31, 119–131.
- [5] Joffres, B., 2013. Synthèse de bio-liquide de seconde génération par hydroliquéfaction catalytique de la lignine. PhD thesis, Université Claude Bernard Lyon 1.
- [6] Xu, feng, 2010. *Cereal Straw as a Resource for Sustainable Biomaterials and Biofuels*. Elsevier, 40.
- [7] Joffres, B., Nguyen, M.T., Laurenti, D., Lorentz, C., Souchon, V., Charon, N., Daudin, A., Quignard, A., Geantet, C., 2016. Lignin hydroconversion on MoS₂-based supported catalyst: Comprehensive analysis of products and reaction scheme. *Applied Catalysis B: Environmental* 184, 153–162.

Chapter V. Hydrodynamics, Mass transfer and Thermodynamics

V.1 Introduction

In the previous chapter, we presented the experimental results of catalytic lignin conversion. Based on the experimental observations, a reaction network usable for our kinetic model has been achieved. In order to obtain the accurate physico-chemical parameters by kinetic modeling, many chemical engineering aspects (hydrodynamics, mass transfer and thermodynamics) should be taken into consideration. Firstly, our experimental set-up was opened for the gas phase, the knowledge of gas mixing inside of experimental set-up should be necessary to treat accurately the outlet gases. Secondly, during the lignin catalytic hydroconversion, there could exist several phases in the reactor: gas, liquid and solid phases. For this type of multiphase reaction, it is necessary to deal with the interphase mass transfers, between gas and liquid or between liquid and solid, in order to know the gradient of concentration within different phases. In some experimental conditions, slow interface mass transfers could be the rate-limiting steps, which compete with kinetics and contribute to the overall reaction rates. Thirdly, a lot of kinetic models of lignin conversion were done on the basis of the cold liquid samples after reaction. However, under high temperature and pressure conditions, the effect of vaporization cannot be neglected especially for relatively light compounds such as aromatics, naphthenes and C₁ or C₂ phenols. So, the measured concentrations at “cold” conditions are possibly much higher than those at real “hot” conditions, leading to a potential underestimate of rate constants. Besides, the H₂ was mainly present in the vapor phase and only a fraction of H₂ was dissolved in the liquid phase. Knowing the dissolved H₂ concentration is also mandatory due to the participation of dissolved H₂ in various reactions. For these reasons, the study of vapor-liquid equilibrium appears necessary to illustrate the phase distribution under the reaction conditions.

In this chapter, a gas hydrodynamic model developed for our experimental set-up is presented firstly. The hydrodynamic characterization was realized by Residence Time Distribution (RTD) tests. Secondly, the gas-liquid (G/L) mass transfer characterization in our set-up is reported. A volume mass transfer coefficient between the G/L phases at operating conditions is determined on the basis of absorption/desorption phenomena of N₂ in tetralin. Finally, the choice of thermodynamic Vapor-Liquid Equilibrium (VLE) model used in our study is discussed. Moreover, the separation performance of the reflux condenser under operating conditions was simply modeled by a series of experiments using mixtures of model compounds.

V.2 Hydrodynamics and mass transfer

V.2.1 Theory of hydrodynamics

In practice, the concept of Residence-Time Distribution (RTD) has been used for many years to describe hydrodynamic behaviors and mixing characteristics in chemical reactors¹. In an ideal plug-flow reactor (PFR), all the molecules leaving the reactor have stayed inside it for exactly the same amount of residence time, since there is no dispersion within the reactor. In contrast, in an ideal continuous stirred-tank reactor (CSTR), all the molecules are thought to be mixed thoroughly and the feed introduced into it at any given time mixed completely with the molecules already existing in the reactor. For other reactors, the mixing occurring inside the reactor is not ideal, so the molecules in the feed

spend different time inside the reactor, and there is a distribution of residence time within the reactor. Studying the RTD of a reactor can directly reflect its hydrodynamic or overall mixing behavior, which is important to establish a reactor model with known kinetics.

The RTD is determined experimentally by tracer experiments: an inert chemical, molecule, or atom is injected into the feed stream entering the reactor at some time $t = 0$ and then its concentration is measured in the effluent during a sufficient time to recover all the injected compounds, as illustrated in Figure V.1. The compound is considered as a tracer if its concentration does not disturb the hydrodynamic behavior. Pulse and step inputs are two commonly used methods of injection. Here, we present the principles of pulse injection.

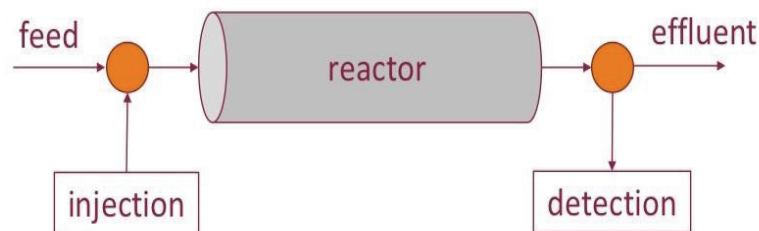


Figure V.1: Principle of RTD measurements

V.2.1.1 Pulse input

For a pulse input, an amount of concentrated tracer N_0 (N_0 is a mole number) is introduced into the feed stream entering the reactor in an extremely short time, such that it is quite close to the Dirac delta function. Figure V.2 shows an example of typical concentration-time curves at the inlet and outlet of a non-ideal plug-flow reactor.

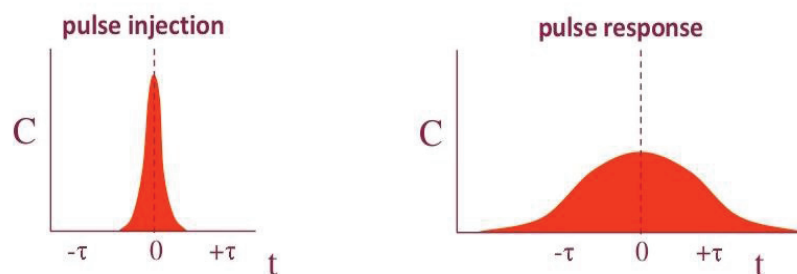


Figure V.2: Concentration-time curve at the inlet and outlet of the reactor for a pulse injection

For pulse injection, RTD function, $E(t)$, is defined as

$$E(t) = \frac{Q_v C(t)}{N_0} \quad (5.1)$$

where Q_v is the volumetric flowrate of effluent stream, $C(t)$ is the outlet tracer concentration. So that,

$$E(t)\Delta t = \frac{Q_v C(t)\Delta t}{N_0} \quad (5.2)$$

where Δt is an increment of time sufficiently small that $C(t)$ is constant over this time interval. Thus, the quantity $E(t)\Delta t$ represents the fraction of material that has spent time between t and $t + \Delta t$ inside the reactor. Normally, the initial injected amount of tracer N_0 is usually unknown or difficult to be quantified. Hence, in most cases, N_0 is obtained by summing up all the amounts of tracer at the outlet, from $t = 0$ to infinity as follows:

$$N_0 = \int_0^{\infty} Q_v C(t) dt \quad (5.3)$$

To do this, we must ensure that there is no leak in the set-up. Since the volumetric flowrate Q_v is constant, $E(t)$ can be transformed as the equation below which is mostly used to get the experimental RTD curve.

$$E(t) = \frac{C(t)}{\int_0^{\infty} C(t) dt} \quad (5.4)$$

Remarks: $\int_0^{\infty} E(t) dt$ is always equal to 1 since all the tracer must leave the reactor.

V.2.1.2 RTD of reactors

In the case of ideal reactors, the RTDs of CSTR and PFR are illustrated in Figure V.3. For an ideal PFR, the molecules entering the reactor leave such reactor at the same time. Therefore, the residence time displays as a pure delay in the RTD curve. For an ideal CSTR, the fluid inside the reactor and the outlet fluid have identical composition at all times, showing an exponential decrease in the RTD curve. In reality, not all the reactors are ideal which are perfectly mixed or behave like a PFR. In these situations, the deviation between non-ideal and ideal reactors can easily be reflected by RTD. In order to represent hydrodynamic behavior within the non-ideal reactors, a simple physical representation composed of ideal CSTRs are widely employed, so-called "Tanks-in-series model".

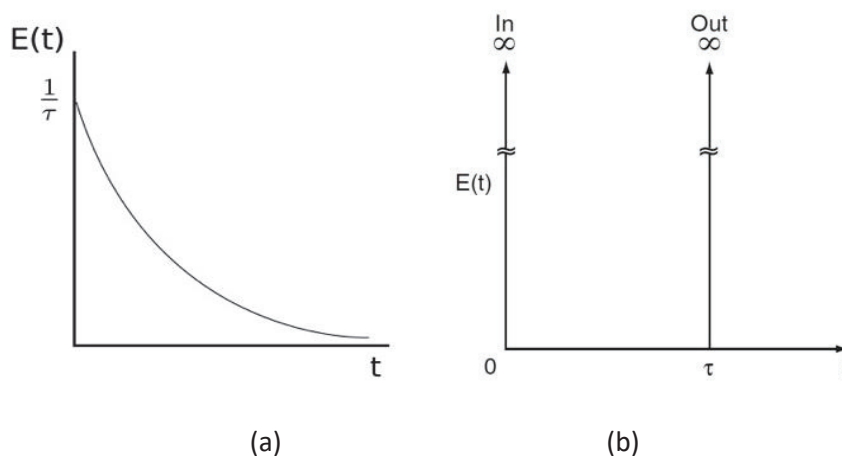


Figure V.3: $E(t)$ curves of ideal reactors: (a) CSTR; (b) PFR

For the Tank-in-series model, a non-ideal reactor is modeled as a series of n reactors which have an equal volume V_i , shown in Figure V.4. Each tank in the model behaves as an ideal CSTR, and the total volume of the series is nV_i , equal to the reactor volume V_R .

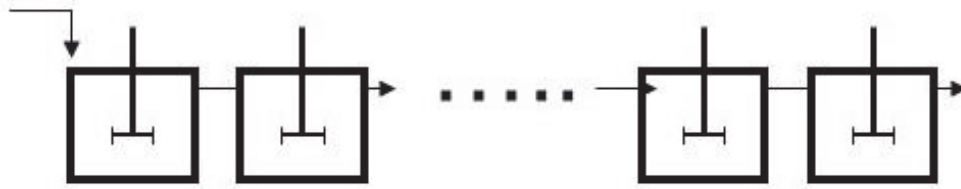


Figure V.4: Schematic representation of Tanks-in-series model

Figure V.5 illustrates RTD curves as a function of the number of CSTRs (n_{CSTR}) for a constant volume reactor. When $n_{CSTR} = 1$, $E(t)$ corresponds to a single perfectly mixed CSTR; when n_{CSTR} becomes larger, the RTD curves is narrowing and the peak of RTD curve is shifting to the right side; when n_{CSTR} is infinite, the behavior of the reactor approaches that of PFR. Thus, the optimal number of CSTRs using in the Tanks-in-series model can be determined by fitting the experimental RTD curve.

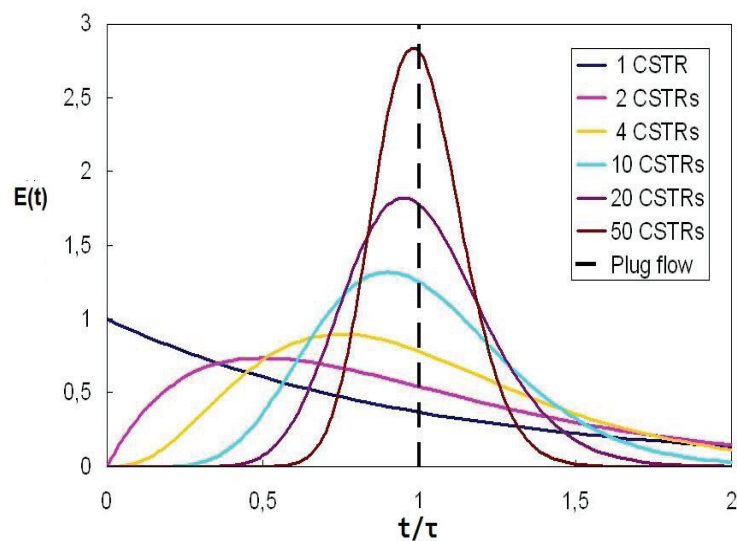


Figure V.5: $E(t)$ of Tank-in-series model in function of the number of CSTRs

V.2.1.3 Mean residence time

A characteristic time called the first moment of RTD is very useful in chemical engineering, to determine the effective volume of reactors or diagnose the troubles of existing reactors.

The first moment (t_m) can give the average residence time the effluent spent in the reactor:

$$t_m = \frac{\int_0^{\infty} tE(t)dt}{\int_0^{\infty} E(t)dt} = \int_0^{\infty} tE(t)dt \quad (5.5)$$

It was proved that in the absence of dispersion at the reactor entrance and outlet, and for constant volumetric flow Q_v , no matter what RTD for a particular reactor with a volume V_R , ideal or non-ideal, its space time τ is always equal to t_m .

$$\tau = \frac{V_R}{Q_v} \quad (5.6)$$

However in some cases, there is a stagnant or dead zone existing in the reactor that reduces the effective volume, so the calculated τ should be greater than t_m . In other cases where t_m is greater than τ , the reasons might be various, such as the flow bypassing, gas adsorption and gas absorption.

V.2.2 Theory of interphase mass transfer

The driving force for mass transfer is typically a difference in molar fractions of the transporting species molar fractions or a difference in concentrations when the total concentration is constant. Mass may transport from one phase to another, and the process is called interphase mass transfer. Figure V.6 show the concentration profile for a typical pseudo-component in a gas-liquid-solid (G/L/S) system, which is suitable for our study.

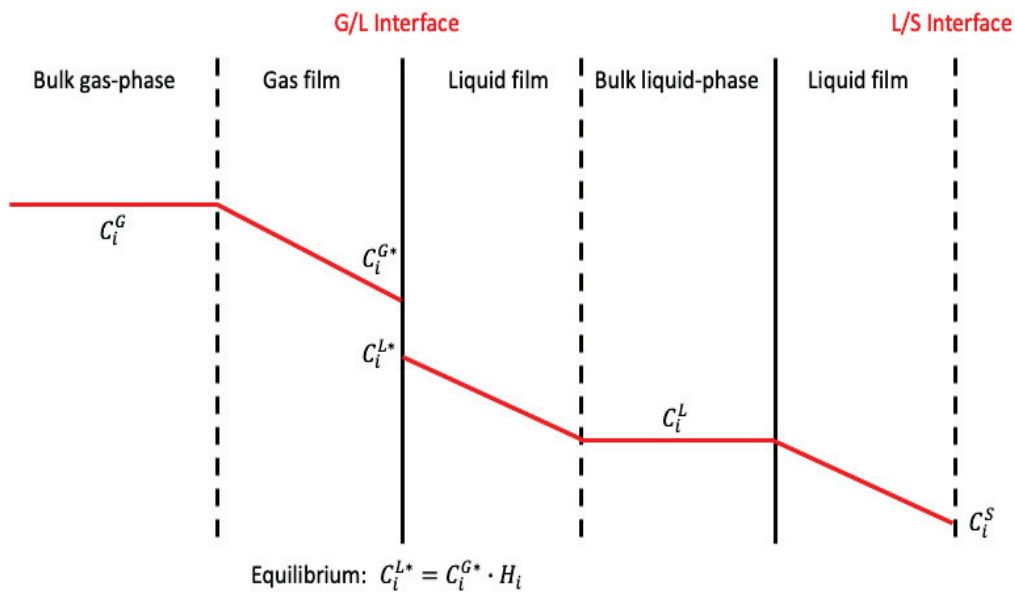


Figure V.6: Concentration profile for a typical pseudo-component in the model

V.2.2.1 G/L mass transfer

In our reactor, we had gas and liquid phases so that the G/L mass transfer should be studied. The simplest two-film model describing the mass transfer between the G/L phases was proposed by Whitman². The two-film model is expressed on the basis of these assumptions:

- 1) Near the interface, there exists a stagnant film for each side. In the film, the mass transport is governed essentially by molecular diffusion.
- 2) The equilibrium is attained at the interface.

Therefore, the flux transferred N_i ($\text{mol m}^{-2}\text{s}^{-1}$) in or out from one phase to another phase per unit of surface is given by:

$$N_i = k_G(C_i^G - C_i^{G*}) = k_L(C_i^{L*} - C_i^L) \quad (5.7)$$

where k_G and k_L are respectively the mass transfer coefficient for the gas phase and liquid phase (m s^{-1}), C_i^G and C_i^L are the concentration of species i at the bulk gas phase and liquid phase (mol m^{-3}), C_i^{G*} and C_i^{L*} are the interface concentrations (mol m^{-3}). At the interface, as the equilibrium is assumed, the relation between C_i^{G*} and C_i^{L*} is $C_i^{L*} = C_i^{G*} \cdot H_i$, where H_i is the Henry's coefficient. In practice, a volumetric G/L mass transfer coefficient ($k_L a$) was often used to characterize the G/L mass transfer flux $F_{i,exch}$:

$$F_{i,exch} = k_L a (C_i^{L*} - C_i^L) \quad (5.8)$$

The physical parameter $k_L a$ represents two independent characteristic values: liquid-side mass transfer coefficient (k_L) and interfacial area (a). Thus, various factors which can affect these two values may impact the value of $k_L a$, such as the stirring speed, the flowrate of gas feed, the configuration of reactor (type of impeller, geometry of the reactor), temperature, the fluid composition and properties. Many forms of correlation for the prediction of $k_L a$ have been proposed by numerous authors, based on experimental measurements of different reactors and different gas-liquid systems. Typically, the $k_L a$ was determined by physical dynamic method³. The principle is evaluating the temporal concentration in the liquid phase or in the exhaust gas flow during the absorption/desorption process. In our case, we studied the absorption/desorption process of N_2 to determine the $k_L a$.

V.2.2.2 L/S mass transfer

For a hererogenous reaction, the reactant was transferred from the bulk fluid to the external surface of the catalyst, so-called L/S mass transfer. The one-film model for L/S mass transfer is expressed on the basis of the assumption that there exists a stagnant film in the fluid side, near the interface of solid. In the film, the mass transport is governed essentially by molecular diffusion. The flux transferred N_i ($\text{mol m}^{-2}\text{s}^{-1}$) through the L/S interface is given by:

$$N_i = k_D(C_i^L - C_i^S) \quad (5.9)$$

where k_D is the mass transfer coefficient for the fluid phase (m s^{-1}), C_i^L and C_i^S are the concentration of species i at the bulk fluid phase and at the surface of solid phase (mol m^{-3}). The determination of $k_D a_s$ in a chemical reactor would be needful to characterize the L/S interface mass transfer $F_{i,exch}$.

$$F_{i,exch} = k_D a_s (C_i^L - C_i^S) \quad (5.10)$$

As for $k_L a$, the physical parameter $k_D a_s$ represents two independent characteristic values: liquid-side mass transfer coefficient (k_D) and specific area of catalyst (a_s). Various factors can affect k_D , such as the stirring rate, the configuration of reactor (type of impeller, geometry of the reactor), temperature, the fluid composition and properties. As for $k_L a$, its experimental assessment in our set-up would be interesting. However, the classical methods used in the literature (solid dissolution, fast chemical reaction, etc.) cannot be easily implemented at our experimental conditions (temperature, pressure,

etc.). Therefore, the k_D in our study is estimated by the correlation in the literature, which will be presented in **Chapter VI**.

V.2.3 Experimentation and methods to determine the hydrodynamic behavior and G/L mass transfer coefficient

N_2 is used as tracer for our RTD tests, as well as for the measurement of $k_L a$. In order to perform the N_2 injection, a N_2 tank at a high pressure of 100 bar was connected to H_2 pipeline close to the gas inlet of the reactor, shown in Figure V.7. The pulse injection was done by switching a three-way valve in an extremely short time. The shapes of each element are given in Table V.1, as well as their sizings.

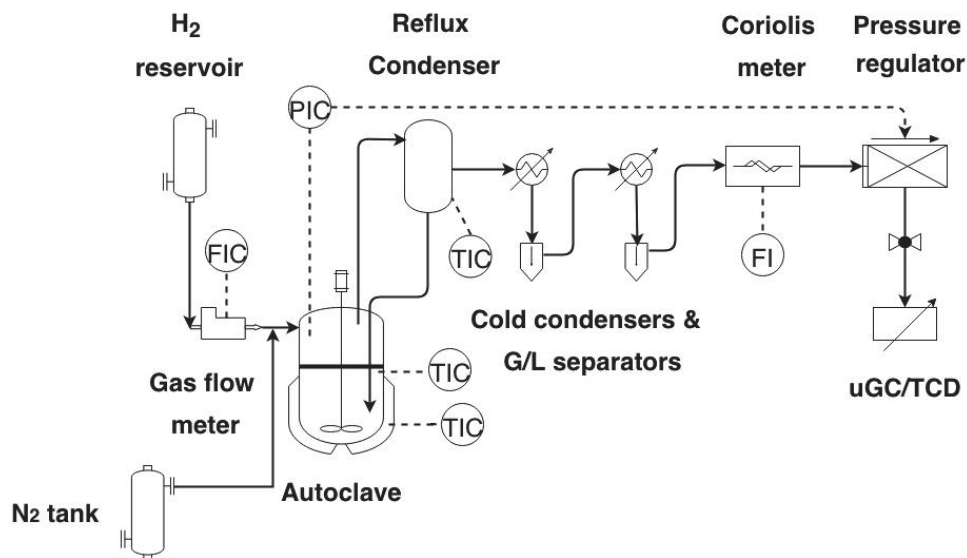


Figure V.7: Schematic diagram of the experimental set-up for RTD tests and $k_L a$ measurements

Table V.1: Shape and sizing of each element in the experimental set-up

Element	Shape	Sizing (mL)
Reactor	Cylindrical	300
Reflux condenser	Cylindrical	150
Cold trap 1	Tube-shaped	2.5
Separator 1	Cylindrical	17.6
Cold trap 2	Tube-shaped	2.5
Separator 2	Cylindrical	17.6
Connecting tubes	Tube-shaped	4.2

Table V.2: Operating conditions of our experiments

Test	1	2	3	4	5	6	7
Tetralin	0	0	100	100	100	100	100
Temperature of reactor (°C)	20	350	250	300	350	350	350
Temperature of reflux condenser (°C)	20	170	170	170	150	170	190
Other common conditions: $N = 800$ rpm; $P = 80$ bar; Temperatures of cold traps and separator: 15 and 4 °C							

The operating conditions for the performed experiments are given in Table V.2. For each test, three inlet H_2 flowrates (20, 40 and 60 NL h^{-1}) were performed. Test 1 and 2 were performed without the addition of tetralin in the reactor, in order to validate the effective volume of the experimental set-up and to investigate the physical representation of our set-up. For other tests with the aim of studying $k_L a$, 100 g of tetralin was introduced into the reactor, simulating the occupied volume by 30 g of lignin and 70 g of tetralin. The experimental procedure of all tests was as follows:

- 1) The reactor was previously filled with tetralin (if needed) and then closed and flushed 3 times with 10 bar of H_2 to remove the air.
- 2) The set-up was pressurized to 80 bar with a maximal flow of H_2 (200 NL h^{-1}).
- 3) As soon as the pressure reached 80 bar, the reactor and the reflux condenser were heating up to the desired temperature and the agitation ($N = 800$ rpm) was started. Meanwhile, the H_2 flow decreased to the desired value (20, 40 or 60 NL h^{-1}) and the pressure was kept constant at 80 bar during the whole period.
- 4) The steady-state conditions were attained, then a small quantity of N_2 was injected and mixed with the continuous H_2 feed flow. The moment of N_2 injection is defined as the starting point ($t = 0$).
- 5) At the outlet of set-up, the molar fraction of nitrogen (y_i) was analyzed online by μ GC-TCD until when no sign of N_2 was detected.

For each test, an evolution of y_i versus time was obtained. Considering the volumetric flowrate (Q_v) constant, the experiment RTD curve can be calculated by normalization as follows:

$$E(t) = \frac{C(t)}{\int_0^\infty C(t)dt} = \frac{y(t)}{\int_0^\infty y(t)dt} \quad (5.11)$$

V.2.4 Model and estimation method

V.2.4.1 Model description

As presented above, the hydrodynamics of an arbitrary reactor can be presented by a physical model composed of ideal reactors such as CSTR and PFR or a cascade of CSTRs.

The mass balance for tracer in a PFR reactor can be written as follows:

$$\frac{\partial C}{\partial t} + \frac{1}{\tau_{PFR}} \frac{\partial C}{\partial \zeta} = 0 \quad (5.12)$$

$$\tau_{PFR} = \frac{V_{PFR}}{Q_v} \quad (5.13)$$

where C is the concentration of tracer in the reactor, t is the time coordinate, ζ is the dimensionless axial coordinate, V_{PFR} is the volume of the PFR reactor and Q_v is the volumetric flowrate of fluid. In practice, the representation can be simply treated as a pure delay equal to its residence time (τ_{PFR}) in the RTD curve.

The mass balance for tracer in a CSTR i for a cascade of n CSTRs can be written as follows:

$$n_{CSTR} = \frac{V_R}{V_i} \quad (5.14)$$

$$\tau_i = \frac{V_i}{Q_v} \quad (5.15)$$

$$\frac{dC_i}{dt} = \frac{1}{\tau_i} (C_{i-1} - C_i) \quad (5.16)$$

where V_R is the volume of reactor, V_i is the volume of CSTR i , C_i is the concentration of tracer in the CSTR i and τ_i is the residence time of CSTR i .

Before establishing the model for our experimental set-up, several simplifying assumptions were made:

- 1) The temperature inside of each element is uniform at the set value.
- 2) Gases follow the ideal gas law.
- 3) The liquid volume of condensed tetralin in the reflux condenser and the separator are neglected.
- 4) The molar flowrate is constant within the set-up, equal to the inlet molar flowrate of H_2 .

The determined physical model of each element is illustrated in Figure V.8 and their corresponding mass balances of N_2 are given in Table V.3.

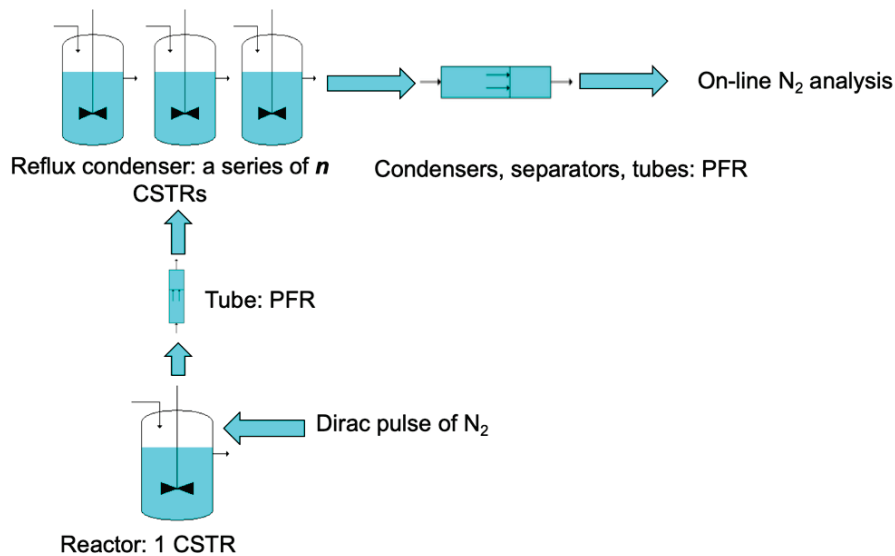


Figure V.8: Physical representation of the experimental set-up

Table V.3: Mass balances of N₂ in our experimental set-up

Element	Model	Equation
Reactor (Gas phase)	CSTR	$\frac{dC_R^G}{dt} = -k_L a (C_R^{L*} - C_R^L) \frac{V_R^L}{V_R^G} - \frac{1}{\tau_R^G} C_R^G$ (5.17)
Reactor (Liquid phase)	CSTR	$\frac{dC_R^L}{dt} = k_L a (C_R^{L*} - C_R^L)$ (5.18)
Reflux condenser	Tanks-in-series	$\frac{dC_{i,r}}{dt} = \frac{1}{\tau_{i,r}} (C_{i-1,r} - C_{i,r})$ (5.19)
Cold traps, separators and connecting tubes	PFR	$t_{delay} = \sum \tau_{i,PFR}$ (5.20)

The gas phase of the reactor was considered as a CSTR, and the mass balance of N₂ is given in Eq. (5.17), taking account into the N₂ transfer between phases, where C_R^G are the concentration of N₂ in the gas phase of the reactor, C_R^{L*} is the equilibrium concentration of N₂ at the liquid side of interface, V_R^L and V_R^G are respectively the volumes of liquid phase and gas phase in the reactor, and τ_R^G is the gas residence time. The mass transfer was expressed by a linear driving force as shown in Eq. (5.8).

The liquid phase was considered to be perfectly mixed and the only mass exchange in the liquid was mass transfer between phases, as shown in Eq. (5.18), where C_R^L is the concentration of N₂ in the liquid phase. For the tests performed without tetralin, the equation of the liquid phase and the terms of mass transfer in the Eq. (5.17) should be removed.

The reflux condenser was considered to contain only gases inside. It was represented using the Tanks-in-series model, as shown in Eq. (5.14), (5.15) and (5.19). Other elements in the experimental set-up were considered as ideal PFR, thus the delay induced by them is calculated by the addition of the residence time ($\tau_{i,PFR}$) of PFRs as given in Eq. (5.20).

Under high temperature and pressure conditions, the following parameters such as V_R^L and V_R^G were estimated using a two-phase flash calculation with the process simulator Prosim Plus. The entering effluent was 100 g of tetralin, H₂ and N₂. Using a Predictive Soave-Redlich-Kwong (PSRK) model, the simulation predicts the values of the liquid volume, the vaporization ratios of tetralin and the equilibrium constant of N₂ at the equilibrium state. These values at different temperatures are listed in Table V.4. The reactor volume is constant, so the gas volume is calculated by subtraction. Considering that there is no mass-transfer limitation on the gas side, so the equilibrium concentration of N₂ in the liquid phase (C_R^{L*}) was calculated as follows:

$$C_R^{L*} = C_R^G \frac{RT}{P} \frac{1}{K_{N_2}} C_{R,total}^L \quad (5.21)$$

where $C_{R,total}^L$ is the total concentration of all components in the liquid phase, that approximately equal to the concentration of tetralin in the liquid phase.

Table V.4: Simulation results under Prosim Plus

Stream: 100 g of tetralin + H ₂ + N ₂				
Pressure: 80 bar				
Thermodynamic model: PSRK				
Temperature (°C)	Vaporization ratio of tetralin (%)	V_R^L (mL)	V_R^G (mL)	K_{N_2}
250	1.6	129	171	13.0
300	3.3	137	163	10.1
350	6.6	146	154	7.2

V.2.4.2 Resolution of equation and parameter estimation

Figure V.9 shows the structure of our model. The objective of this model is to obtain the preferred n_{CSTR} to represent the hydrodynamics of the reflux condenser and the physical parameter $k_L a$. The numerical resolution of differential equations were performed in Matlab using the subroutine ode23s. The model input was the experimental $E(t)$ curve versus time, the model out was the simulated $E(t)$ curve by normalization of calculated $C(t)$ out of set-up. Parameter estimations were done using the subroutine lsqnonlin, whose objective function J is the minimization of the square difference between the experimental data and the simulated one, written as follows:

$$J = \sum_1^N [E(t)_{exp} - E(t)_{simu}]^2 \quad (5.22)$$

where N is the number of experimental data in one run.

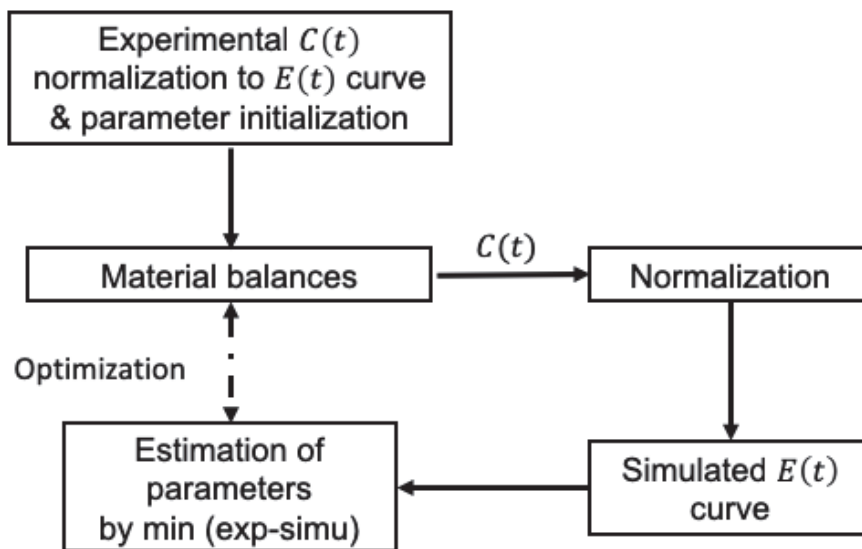


Figure V.9: Model structure and parameter estimation procedure for this study

The precision of the estimated parameters was calculated using the following assumptions. Firstly, errors associated to two successive measurements were independent and centered and follow a normal distribution. Moreover, the precision of estimated parameters was calculated as follows:

$$\hat{p} - s_{N-k}\sqrt{V\sigma^2} < p < \hat{p} + s_{N-k}\sqrt{V\sigma^2} \quad (5.23)$$

where \hat{p} is the estimate of the parameter p , V is the variation, σ is the standard deviation, s_{N-k} is the student variable (corresponding to 95 % probability confidence interval), N is the observation number and k is the parameter number. The variance V was calculated by the Jacobian matrix provided by the subroutine Isqnonlin.

V.2.5 Results and discussions

V.2.5.1 Hydrodynamic behavior

Firstly, the RTD tests (Test 1 and 2) without the addition of tetralin have been operated in order to verify the total volume of the experimental set-up and the physical model used in our study. Table V.5 and V.6 give the comparison between mean residence time (t_m) and calculated space time (τ), as well as the optimal number of CSTRs used to represent the reflux condenser. Figure V.10 and V.11 show the experiment RTD curves and simulated ones of Test 1 and 2 in function of gas flowrate.

Table V.5: Comparison between t_m and τ and optimal n_{CSTR} at different flowrates for Test 1 at ambient temperature

Flowrate (NL h ⁻¹)	t_m (min)	τ (min)	Relative difference between t_m and τ (%)	Optimal n_{CSTR}
20	109.2	115.9	5.8	2
40	56.7	58.0	2.2	4
60	38.7	38.6	0.3	5

Table V.6: Comparison between t_m and τ and optimal n_{CSTR} at different flowrates for Test 2 (Reactor at 350 °C, reflux at 170 °C)

Flowrate (NL h ⁻¹)	t_m (min)	τ (min)	Relative difference between t_m and τ (%)	Optimal n_{CSTR}
20	65.9	69.3	4.9	1
40	34.2	34.7	1.3	1
60	23.3	23.1	1.0	2

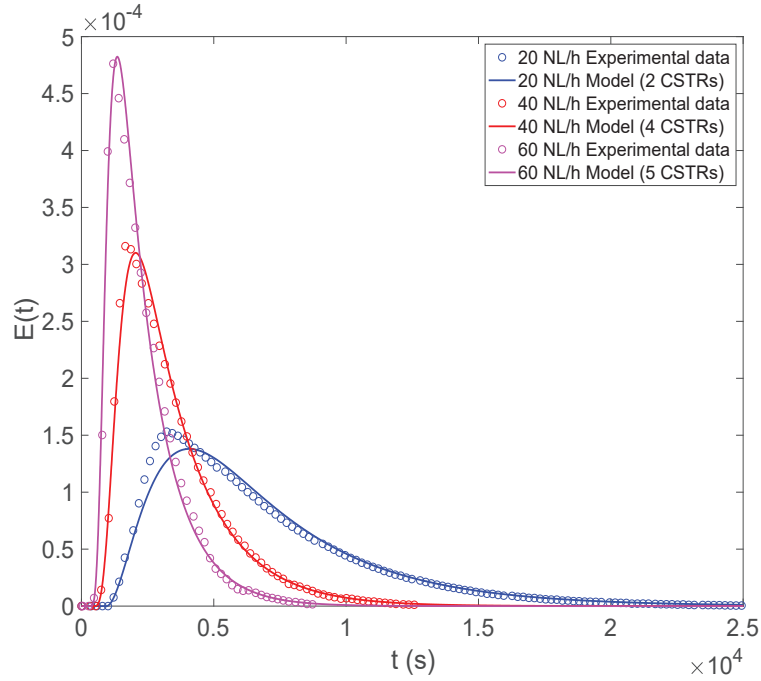


Figure V.10: Comparison between experimental (marker) and simulated (line) data after the optimization of n_{CSTR} at ambient temperature

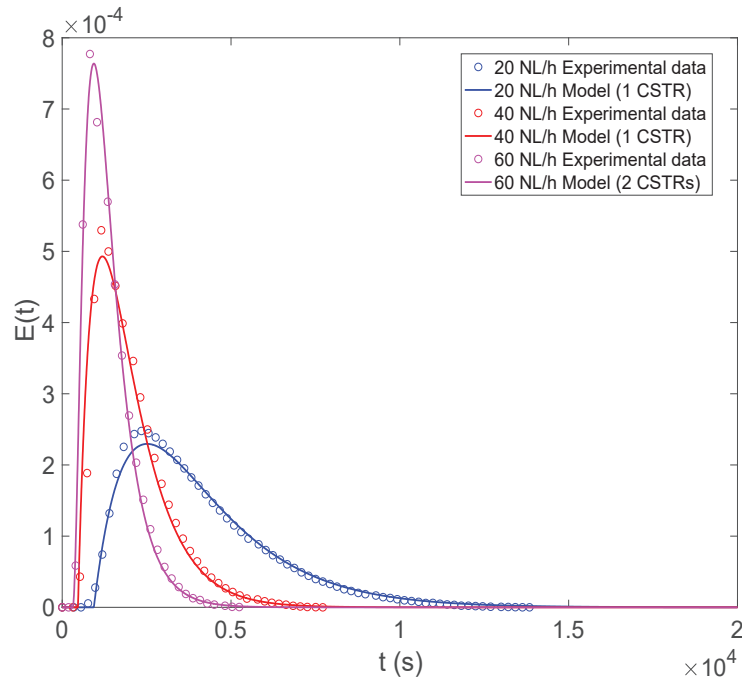


Figure V.11: Comparison between experimental (marker) and simulated (line) data after the optimization of n_{CSTR} in the case where the temperature of reactor is 350 °C and the temperature of reflux condenser is 170 °C

As seen in Table V.5 and V.6, the relative differences between t_m and τ were within an error margin of 6 %. Consequently, the sizing of each element listed in Table V.1 is reliable to be used. Concerning the delay induced by PFRs, it was found that experimental delays correspond well to the addition of

residence time of all PFRs, as shown in Figure V.10 and V.11. These results suggest that, regarding the effective volume of the set-up and the physical representation of PFRs, our model conforms to the experimental observations.

Besides, the gas flowrate and temperature were noticed to impact the physical representation of the reflux condenser. According to the simulated results, the optimal n_{CSTR} used to represent the reflux condenser at ambient temperature was 2, 4 and 5, respectively for the gas flowrate of 20, 40 and 60 NL h⁻¹. The increase of n_{CSTR} with increasing gas flowrate can be explained by the enhanced mass convection inside the reflux condenser, leading the mixing degree to deviate from that of ideal CSTR. The same observation was also valid under higher temperature conditions where the temperature of the reflux condenser was 170 °C, shown in Table V.6.

When it comes to the temperature, it was found that under the same gas flowrate, the mixing inside of the reflux condenser is getting close to the state of perfectly mix as temperature increases. For example, at the flowrate of 40 NL h⁻¹, optimal n_{CSTR} decreased from 4 to 1 while the temperature of reflux condenser increased from 20 to 170 °C. The observation was also valid for the cases under the gas flowrate of 20 and 60 NL h⁻¹. It is explained by that the axial dispersion in the reflux condenser is much enhanced with increasing the temperature.

To be concluded, the physical model illustrated in Figure V.8 can represent our model correctly, and the temperature and gas flowrate affect the mixing characteristic of the reflux condenser.

V.2.5.2 $k_L a$ estimation

For the tests performed with tetralin inside (Test 3-7 in Table V.2), the existing absorption/desorption process was proved by the comparisons between t_m and τ , as seen in the example given in Table V.7 where t_m greater than τ . Inside of the reactor, the injected N₂ was transferred from the gas phase to the liquid phase due to the concentration difference, leading to a storage of N₂ in the liquid phase, called “absorption”. As time increased, the N₂ reached the equilibrium state between gas and liquid at a certain moment. Afterward, a reverse transfer of N₂ from the liquid phase to the gas phase underwent, called “desorption”. The mass transfer of N₂ between phases can be expressed as Eq. (5.8) using the parameter of $k_L a$. The optimal values of $k_L a$ was also determined by fitting the $E(t)$ curves.

Table V.7: Comparison between t_m and τ at different flowrates for Test 6 (Reactor at 350 °C, reflux at 170 °C)

Flowrate (NL h ⁻¹)	t_m (min)	τ (min)	Relative difference between t_m and τ (%)
20	55.6	52.8	5.1
40	28.5	26.4	7.4
60	19.3	17.6	8.9

Hydrodynamic representation

As concluded above, temperature may affect the mixing characteristic of the reflux condenser. Under the same temperature of reactor at 350 °C, the temperature effect on the mixing characteristic of the

reflux condenser was evaluated within the range of 150-190 °C (Test 5-7 in Table V.2). Table V.8 shows mean residence time (t_m) in function of the temperature of reflux condenser. As expected, t_m decreased with increasing temperature or gas flowrate. However, at the same flowrate, the difference of experimental t_m is slight when the temperature of reflux condenser varies between 150 and 190 °C. Figure V.12 shows the experimental RTD curves in function of the temperature of reflux condenser. The well overlapped curves under the same flowrate indicate that, within the temperature range of 150-190 °C, the hydrodynamics inside of reflux condenser kept unchanged. So, the determined physical model in the previous part are still applicable: when the temperature of reflux condenser is between 150 and 190 °C, optimal n_{CSTR} for the gas flowrate between 20 and 40 NL h⁻¹ is 1 while for the gas flowrate of 60 NL h⁻¹ is 2.

Table V.8: Comparison between t_m and τ at different flowrates in function of the temperature of reflux condenser

Temperature of reflux condenser (°C)	150	170	190
Flowrate (NL h ⁻¹)	t_m (min)		
20	55.9	55.6	53.3
40	29.3	28.5	28.3
60	19.9	19.3	18.4

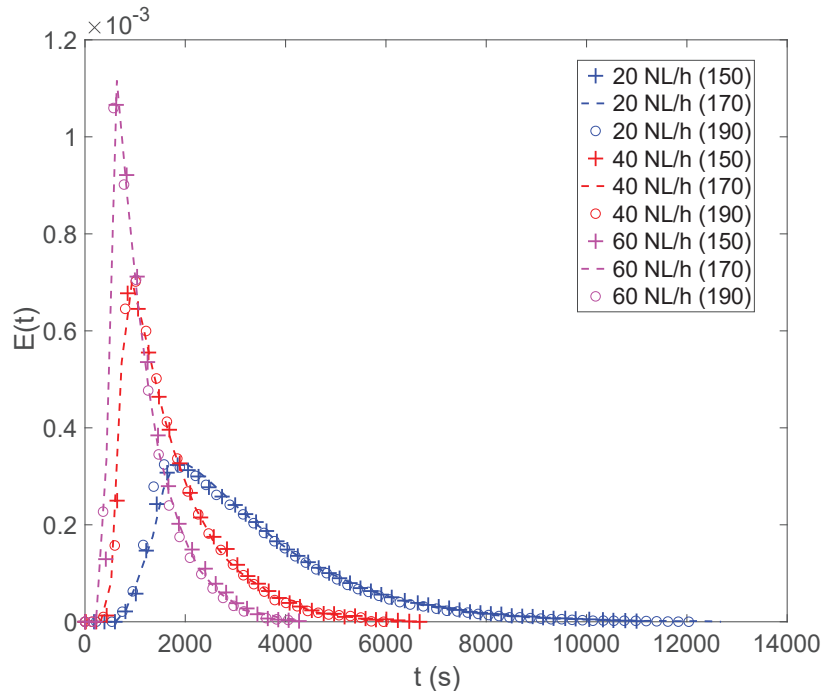


Figure V.12: Experimental RTD curves in function of the temperature of reflux condenser

$k_L a$ estimation

The $k_L a$ is a gas-liquid mass transfer characteristic inside of the reactor, which does not depend on the temperature of reflux condenser. For this reason, $k_L a$ should be identical for a given reactor temperature and a given flowrate, regardless of any temperature of reflux condenser between 150 and 190 °C. So, for each flowrate, a set of three RTD curves was used to estimate $k_L a$ when the temperature of reactor was 350 °C. Figure V.13 gives an example of experiment RTD curves and simulated ones at different flowrates for Test 6 ($T_{\text{Reactor}} = 350 \text{ °C}$, $T_{\text{Reflux}} = 170 \text{ °C}$). From the reasonably good fits between experimental points and simulated ones in Figure V.13, it suggests that our model related to $k_L a$ can describe the absorption/desorption of N_2 in the liquid phase correctly. Table V.9 gives the estimated values of $k_L a$ at 350 °C for each flowrate. The value of $k_L a$ increases with increasing gas flowrate. This reason for this increase might be various, mainly attributed to the increase of interfacial area (a) by higher gas flowrate.

Table V.9: Estimated value of $k_L a$ at different temperatures

Temperature of reactor (°C)	350	300	250
Flowrate (NL h ⁻¹)	$k_L a \text{ (s}^{-1}\text{)}$		
20	$1.5 \cdot 10^{-4} \pm 2.1 \cdot 10^{-5}$	$4.5 \cdot 10^{-4} \pm 1.1 \cdot 10^{-4}$	$6.9 \cdot 10^{-4} \pm 2.8 \cdot 10^{-4}$
40	$4.4 \cdot 10^{-4} \pm 1.2 \cdot 10^{-4}$	$9.8 \cdot 10^{-4} \pm 3.7 \cdot 10^{-4}$	$1.6 \cdot 10^{-3} \pm 5.1 \cdot 10^{-4}$
60	$1.5 \cdot 10^{-3} \pm 6.1 \cdot 10^{-4}$	$2.5 \cdot 10^{-3} \pm 1.5 \cdot 10^{-3}$	$3.4 \cdot 10^{-3} \pm 2.0 \cdot 10^{-3}$

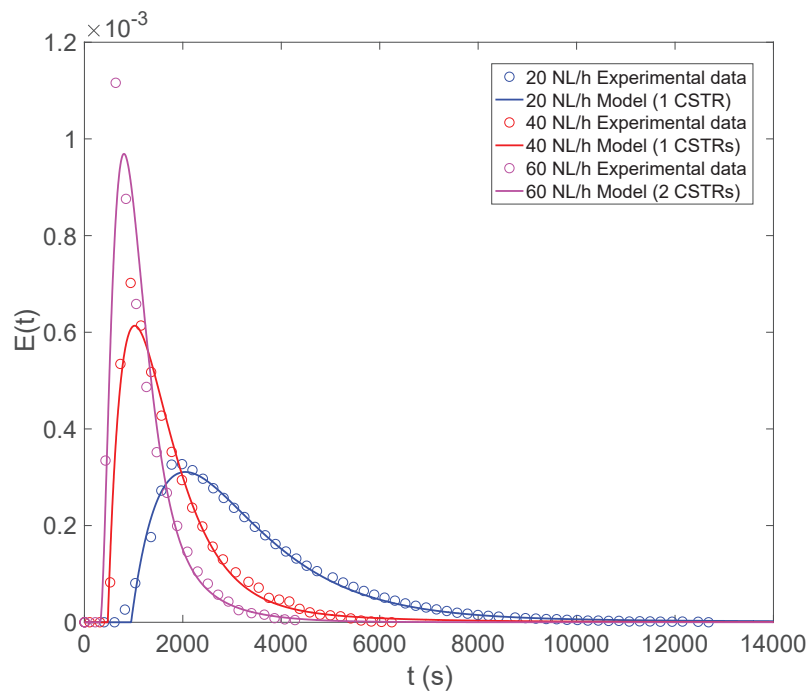


Figure V.13: Comparison between experimental (marker) and simulated (line) data of Test 6 (100 g of tetralin, $T_{\text{Reactor}} = 350 \text{ °C}$, $T_{\text{Reflux}} = 170 \text{ °C}$)

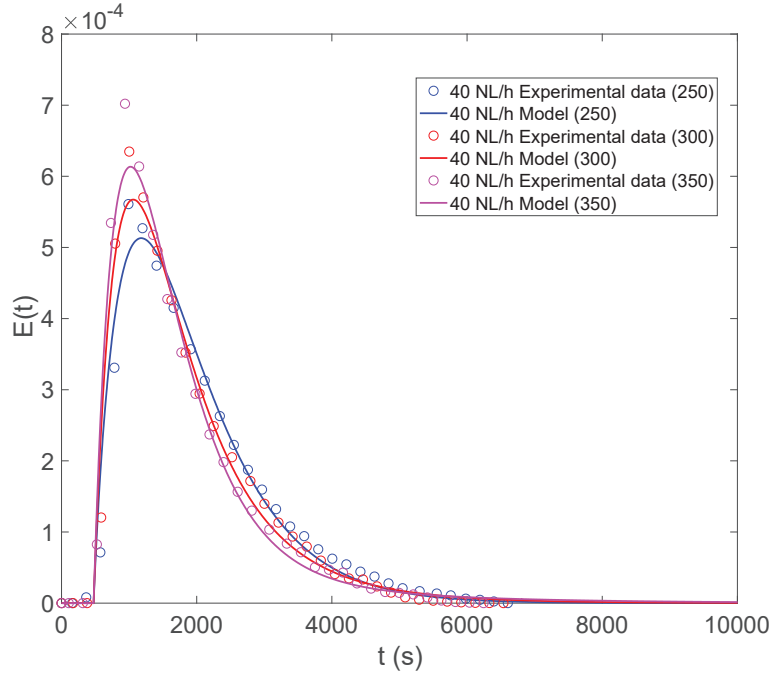


Figure V.14: Comparison between experimental (marker) and simulated (line) data at different temperatures of reactor under the flowrate of 40 NL/h

Moreover, the values of $k_L a$ at 250 and 300 °C were also investigated using experimental data from Test 3 and 4. Since the temperature of reflux was 170 °C, the physical model used to represent the reflux condenser kept unchanged. Figure V.14 gives an example of experiment RTD curves and simulated ones at different reactor temperatures under the flowrate of 40 NL h⁻¹. The model can fit the experiments well. The estimated values of $k_L a$ at different temperatures is given in Table V.9. The values of $k_L a$ decrease as temperature increases. However, it is difficult for us to make a precise conclusion about why it decreases because the temperature influences a lot of fluid properties, which may change $k_L a$ in both directions. In addition, it was found the absolute value of $k_L a$ for our stirred reactor was lower than those reported in the literature ($10^{-3} \sim 10^{-1}$). It can be explained by two reasons:

- The gas injection was not extended into the liquid phase, so that the reactor was not a gas-sparged gas-liquid system. As such, the performance of G/L mass transfer in our reactor was lower than those of gas-sparged ones.
- The transfer capacity of N₂ in liquid was lower than the traditional gases (H₂, O₂ and CO₂) used in the $k_L a$ measurements.

V.2.6 Conclusion of hydrodynamics and mass transfer

Thanks to performed RTD tests, we were able to describe the hydrodynamics of gas phase inside of the set-up. From the results, we are able to know that, under the operating conditions where lignin was converted in our previous tests ($T_{\text{Reactor}} = 350$ °C, $T_{\text{Reflux}} = 160$ °C), at the inlet H₂ flowrate of 40 NL h⁻¹, the gas phase of both the reactor and the reflux condenser can be considered as a perfectly mixed CSTR, and other element of the set-up can be represented by PFRs. Certainly, the develop gas flow model will be helpful for an accurate outlet gas prediction in the following kinetic model.

Moreover, the physical parameter $k_L a$ was also determined, which is useful to calculate the interphase mass transfer of species in the reactor.

V.3 Thermodynamics

V.3.1 VLE models

In chemical engineering, the vapor-liquid equilibrium (VLE) is to describe the distribution of a chemical species between the vapor phase and the liquid phase at a given pressure and temperature. For a multi-component system, the VLE is calculated using the notion of fugacity. The fugacity of component i in the liquid phase (f_i^L) is given by:

$$f_i^L = \phi_i^L x_i P_{tot} \quad (5.24)$$

where ϕ_i^L is the liquid fugacity coefficient of component i , x_i is the molar fraction of component i in the liquid phase and P_{tot} is the total pressure of system. With respect to the vapor phase, its fugacity (f_i^V) is given by:

$$f_i^V = \phi_i^V y_i P_{tot} \quad (5.25)$$

where ϕ_i^V is the vapor fugacity coefficient of component i and y_i is the molar fraction of component i in the vapor phase.

The phase equilibrium is achieved when the liquid and vapor fugacities of each component are equal in all phases: $f_i^L = f_i^V$, thus the equilibrium constant K_i of component i is calculated as follows:

$$K_i = \frac{y_i^*}{x_i^*} = \frac{\phi_i^{L*}}{\phi_i^{V*}} \quad (5.26)$$

where y_i^* and x_i^* are respectively the molar fraction of component i in the vapor phase and the liquid phase at the equilibrium state, ϕ_i^{L*} and ϕ_i^{V*} are respectively the liquid and the vapor fugacity coefficient at the equilibrium state.

Generally, the VLE model can be classed into three categories: (1) EOS model, (2) Heterogeneous model, (3) Combined model.

EOS model Equation of state (EOS) is a classical PVT relation to describe the state of the gas and liquid, known as a homogeneous model. Typical models are ideal gas law, Soave-Redlich-Kwong (SRK) and Peng-Robinson PR equations. They are not recommended for the VLE calculations since it cannot predict the non-ideal behavior of liquid phase accurately.

Heterogeneous model Heterogeneous model is a thermodynamic model alternatively employed for the mixtures, with EOS model applied for the vapor phase and the liquid phase represented by an activity coefficient model.

$$f_i^L = \gamma_i x_i f_i^{0L} \quad (5.27)$$

$$K_i = \frac{\gamma_i f_i^{0L}}{\phi_i^V P_{tot}} \quad (5.28)$$

where γ_i is the activity coefficient of component i in the liquid phase, and f_i^{0L} is the liquid fugacity of pure component i at the temperature and pressure.

Compared to the EOS model, heterogeneous model can better represent mixtures containing non-ideal liquid. Typical models are NRTL, UNIQUAC, Wilson and UNIFAC. However, the disadvantages of the heterogeneous model are its poor performance for the conditions containing supercritical gases, and that its accuracy requires a lot of binary interaction parameters by experiments.

Combined model

The combined model means a prediction method which combines EOS (mostly cubic) with the activity coefficient models based on group contributions, such as UNIFAC. The activity coefficient is used to calculate the EOS parameters by the G^E -based mixing rules. The model widely used includes PSRK, MHV1, MHV2, PPR78 and VTPR. The combined model is proved to cover the traditional limitations of EOS model, and usable for mixtures of polar compounds even in the supercritical state.

Choice of thermodynamic model

Under the operating conditions of lignin hydroconversion, the reaction system contains several polar compounds such as phenols and water, and components that would be in supercritical state (H_2 , CH_4 , etc.). That means that the VLE model used for our model should be usable for polar compounds and supercritical state. Unfortunately, little information is available on the VLE of such complex systems.

Turpeinen *et al.* performed the isothermal VLE for the mixture of methyl heptanoate and m-xylene at 398.15 and 408.15 K⁴. The experimental results were correlated with various thermodynamic models. The results showed that PSRK model was the best model under the conditions. The same types of combined models such as SRK with a MHV1 mixing rule, SRK with a MHV2 mixing rule were also proposed in other studies⁵⁻⁶. It appears that using a model employing EOS in combination with an activity coefficient model is preferred. However, there are several thermodynamic models which vary in the mixing rules and the UNIFAC group contribution table: MHV1, MHV2, PSRK and VTPR. Those models have different mixing rules and UNIFAC group tables. The PSRK model is preferred over other models because the matrix of the binary parameters between the groups defined in the UNIFAC table is wider and more abundant. Moreover, classical thermodynamic models do not allow a satisfactory representation of VLE in mixtures with water. A specific calculation of water equilibrium is proposed by Prosim Plus⁷, using the following equation:

$$K_{water} = \frac{P_{water}^0}{x_{sol}P_{tot}} \quad (5.29)$$

where P_{water}^0 is the vapor pressure at the temperature of system and x_{sol} is the parameter depending on the temperature and the nature of hydrocarbons. It was reported that it can give a satisfactory result of the phase equilibrium in water-hydrocarbons mixtures.

On the basis of the considerations presented above, we selected PSRK model with a special calculation for water as the VLE model. The detailed description of PSRK model is reported in [Annex 8](#). The chosen model consists of a specific calculation of water equilibrium constant and in a standard calculation of the equilibrium constants for other components.

The chosen model was used to predict the VLE equilibrium of several binary or ternary mixtures under the software of Prosim Plus: (1) tetralin and H_2 ⁸, (2) tetralin and H_2O ⁹, (3) tetralin and m-cresol¹⁰, (4) m-cresol, H_2O and H_2 ¹¹, (5) tetralin, m-xylene and H_2 ¹². The comparisons between simulated results and experimental data are illustrated in [Annex 9](#). The simulated results predicted by our model appeared to give reasonable accuracy and so, this model was used.

V.3.2 Modeling the condensation effect of hot reflux condenser

As mentioned in **Chapter II**, the function of the reflux condenser in our experimental set-up is condensing the vaporized solvent as well as removing some relatively light products such as water and aromatics from the reaction medium. Hence, the set temperature of the reflux condenser should be lower than that of the reactor, but much higher than ambient temperature. With respect to our previous lignin conversion tests, the temperature of the reflux condenser was fixed at 160 °C. Under the operating conditions, the vapor flux at 350 °C entered into the reflux condenser at 160 °C, condensation phenomena occurred due to the decrease of temperature. For the lignin conversion, the experimental results presented in **Chapter IV** showed, water and some relatively light compounds such as aromatics, naphthenes and phenols were successfully removed and cumulated in the separator versus time. The complete condensation effect to the relatively heavy products such as dimethoxyphenols and long-chain alkanes in the reflux was also seen according to their absences in the separator. Moreover, less than 10 g of tetralin was found in the separator after 13 h of reaction, proving a fairly good recycling efficiency thanks to the reflux condenser.

By the simulation with the PSRK model under Prosim Plus, tetralin and most products were supposed to be totally condensed in the reflux condenser if the equilibrium state was attained at 160 °C. Therefore, we cannot treat the reflux condenser as an ideal flash distillation. Here, we met a problem of how to describe the condensation effects with regard to different products from the lignin hydroconversion under the operating conditions. In order to solve this problem, a set of experiments using mixtures of lignin-derived model compounds was performed in order to follow the product distribution in the separator and the reactor versus time. During the process, these molecules were vaporized in the reactor, then flowed through the reflux condenser where the condensation phenomena occurred. By modeling the process, a simplifying representation of condensation effect in the reflux condenser was achieved, which will be detailed in the following part.

V.3.2.1 Experimentation and results

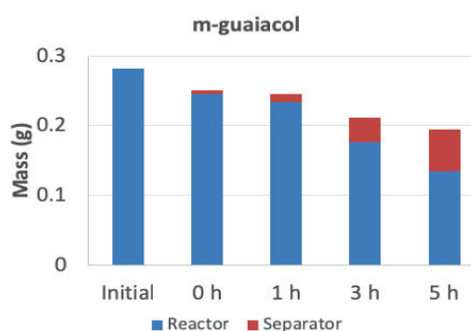
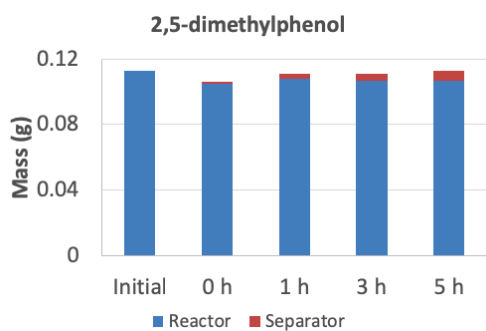
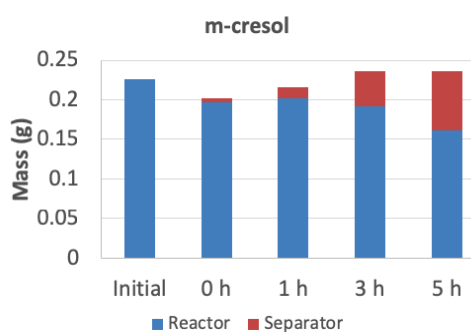
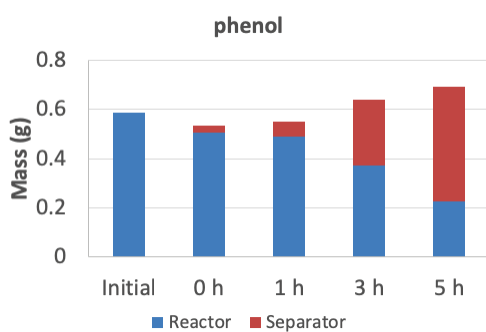
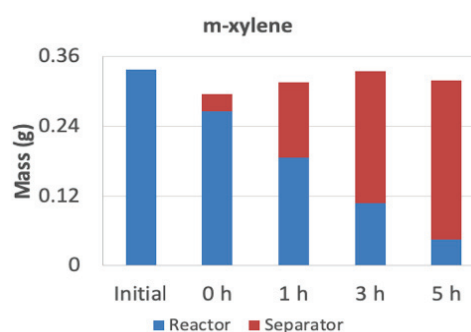
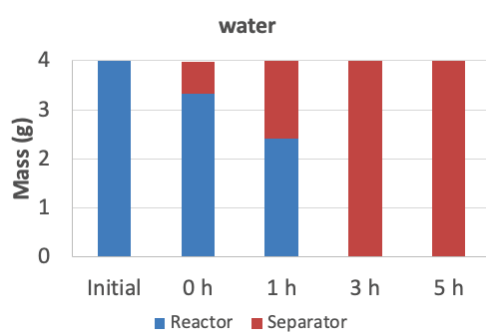
The mixture of model compounds using in the experiments is given in Table V.10. For each test, the mixed solution was introduced into the reactor without the addition of catalyst. The experimental procedures were exactly the same as that of lignin conversion tests, which presented in **Chapter II**. The operation conditions were as follows:

- * $T_{\text{Reactor}} = 350 \text{ °C}$
- * $T_{\text{Reflux}} = 160 \text{ °C}$
- * $P = 80 \text{ bar}$
- * $N = 800 \text{ rpm}$
- * $Q_{\text{H}_2} = 40 \text{ NL h}^{-1}$

Four different residence times (t_0 , 1 h, 3 h and 5 h) were performed. The mass balance for all the tests can be reached at least 98 wt%. That shows that negligible amount of compounds was stripped by the gas and escaped from the G/L separator. Similarly, two liquid mixtures (reactor and separator) were obtained after each test. The identification and quantification of organic compounds were done by GC×GC technique. Figure V.15 shows the product distributions in the reactor and the separator versus residence time.

Table V.10: The mixture of model compounds used in our experiments

Compounds	Mass (g)	Molar mass (g mol ⁻¹)	Boiling point at 1 atm (°C)
water	4	18	100
m-xylene	0.34	106	139
phenol	0.59	94	182
m-cresol	0.23	108	203
2,5-dimethylphenol	0.11	122	212
m-guaiacol	0.28	124	205
tetralin	78	132	207
2,6-dimethoxyphenol	0.18	154	261
hexadecane	0.32	226	287



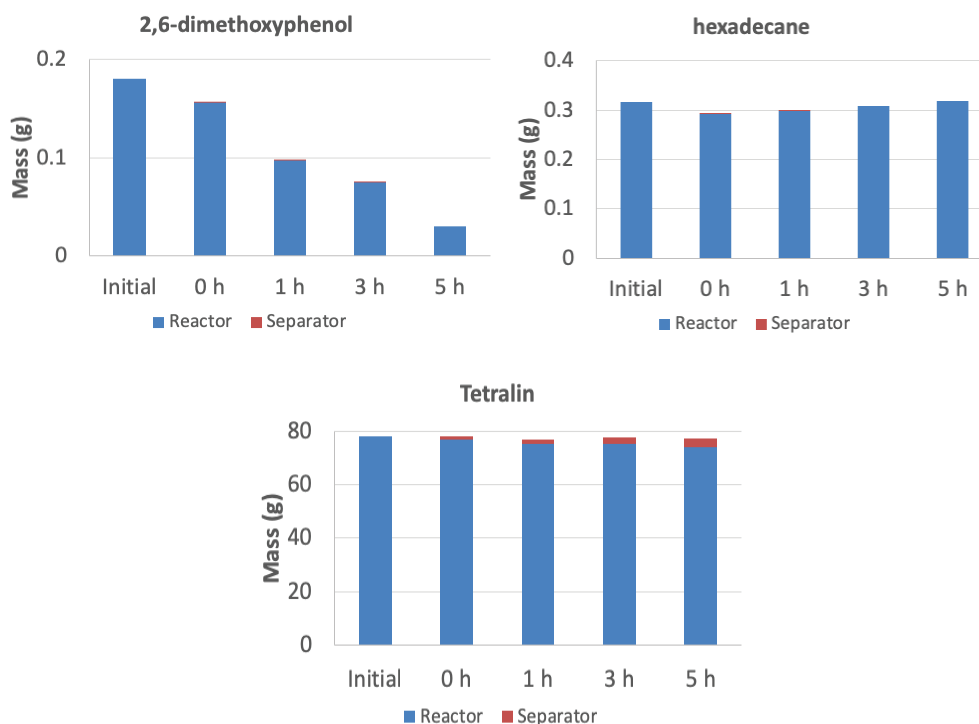
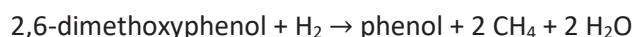
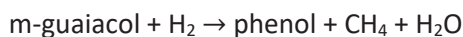


Figure V.15: Product distributions in the reactor and the separator versus time

According to the production distribution evolution, these model compounds can be easily classified in three categories:

- 1) water, m-xylene and phenol: These compounds were trapped quickly in the separator versus time, meaning that the condensation effect in the reflux condenser was relatively poor.
- 2) m-cresol, 2,5-dimethylphenol, m-guaiacol and tetralin: these compounds were cumulated slowly in the separator, showing a relatively good condensation effect but that a portion of them still could pass through the reflux condenser.
- 3) 2,6-dimethoxyphenol and hexadecane: these compounds were not found in the separator, suggesting a complete condensation of them in the reflux condenser.

Incidentally, we noticed the decrease of total mass for m-guaiacol and 2,6-dimethoxyphenol, and the mass increase of phenol as well as the formation of CH₄. These methoxylated phenols were supposed to convert into phenol due to pure thermal decomposition, with the formation of CH₄ and H₂O. By the way, no catechol and pyrogallol were found. Thus, the reaction schemes were as follows:



V.3.2.2 Model description

For the model development, it requires the following experimental data as model inputs:

- 1) The measured mass of each model compound in the reactor for each residence time (9×4 = 36 experimental points).

- 2) The measured mass of each model compound in the separator for each residence time ($9 \times 4 = 36$ experimental points).
- 3) The dynamic outlet gas flowrate of each gas component (H_2 and CH_4) for the longest experiment of 5 h ($94 \times 2 = 188$ experimental points).

Heating reactor stage

During the heating period, as the temperature of reactor increased, the volatile products started to evaporate. So, the mass exchange of species between phases and the condensation of compounds may occur. Considering the complexity, a simplified heating stage representation was developed:

- 1) During the heating period, no model compounds were removed from the reactor and only H_2 was filled in the reflux condenser.
- 2) At t_0 point, H_2 reached the vapor-liquid equilibrium state in the reactor at $350\text{ }^\circ\text{C}$.
- 3) Experimentally at t_0 , a portion of liquids was recovered in the separator. They were assumed to be in the form of vapor existing in the reactor. Due to the fast depressurization following the heating period at t_0 , they were evacuated from the reactor to the separator.

Here, it must be pointed out that, the aim of the heating stage representation is not to describe any physical phenomena within the set-up, but to have a coherent approximation of the initial gas and liquid phase compositions for each element in the set-up at t_0 point, that is the starting point of our model.

Stationary period

Before establishing the model, these simplifying assumptions were made:

- 1) Liquid-gas mass transfer is represented by a linear driving force ($k_L a \cdot \Delta C$).
- 2) The molar volume (V_{mol}^G) of gas phase in each unit is equal to that of H_2 (V_{mol,H_2}^G) at the corresponding conditions, and the liquid phase follows the law of ideal mixing.
- 3) The thermal decomposition only occurs in the liquid phase.
- 4) The volumes occupied by liquid in the reflux condenser and the separator are neglected.

The schematic representation of our general model is shown in Figure V.16, and the corresponding material balances of our model are given in Table V.11. In the following paragraphs, the reaction system was discussed in detail as the order of:

- 1) Reactor (Liquid phase)
- 2) Reactor (Gas phase)
- 3) Reflux condenser (Gas and Liquid phases)
- 4) Separator (Liquid phase)
- 5) Gas outlet (Gas phase)

Table V.11: Material balances for the semi-batch pilot

Element	Equation
Reactor (Liquid phase)	$\frac{dn_{i,R}^L}{dt} = V_R^L R_i + V_R^L k_L a_i (C_{i,R}^{L*} - C_{i,R}^L) + F_{i,r}^L \quad (5.30)$
	$V_R^L = \sum_{i=1}^n (V_{mol,i}^L \cdot n_{i,R}^L) \quad (5.31)$
Reactor (Gas phase)	$\frac{dn_{i,R}^G}{dt} = F_{i,in}^G - V_R^L k_L a_i (C_{i,R}^{L*} - C_{i,R}^L) - F_{i,out}^G \quad (5.32)$
	$\frac{dV_R^G}{dt} = -\frac{dV_R^L}{dt} \quad (5.33)$
	$F_{out}^G = F_{in}^G - \frac{1}{V_{mol}^G} \frac{dV_R^G}{dt} - \sum_{i=1}^n V_R^L k_L a_i (C_{i,R}^{L*} - C_{i,R}^L) \quad (5.34)$
Reflux condenser	$F_{i,r}^L = F_{i,out}^G \cdot \alpha_i \quad (5.35)$
	$\sum_{i=1}^n F_{i,out}^G (1 - \alpha_i) = F_{pass}^G \quad (5.36)$
	$\frac{dn_{i,r}^G}{dt} = F_{i,out}^G (1 - \alpha_i) - \frac{n_{i,r}^G}{n_r^G} F_{pass}^G \quad (5.37)$
Separator (Liquid phase)	$\frac{dn_{i,s}^L}{dt} = F_{i,pass}^G \quad (5.38)$
Gas outlet (Gas phase)	$F_{i,pass}^G _t = F_{i,\mu GC}^G _{t+delay} \quad (5.39)$
	$delay = \frac{n_{PFRS}}{F_{pass}^G} \quad (5.40)$

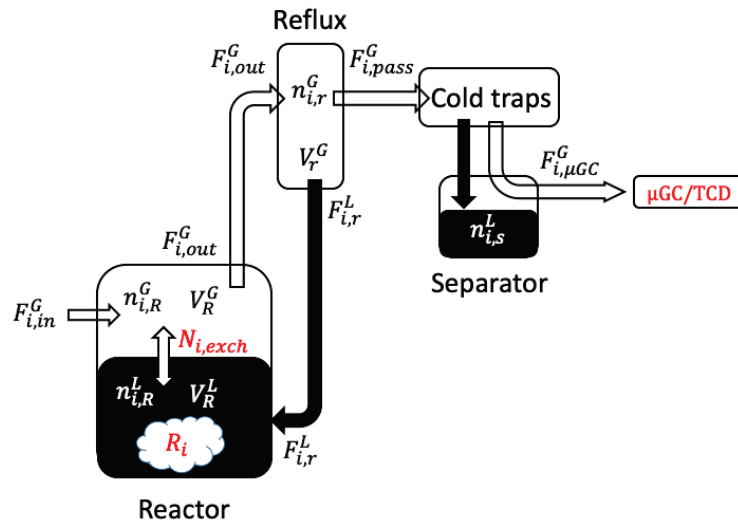


Figure V.16: Schematic representation of our general model (black: liquid, white: gas)

Reactor (Liquid phase)

The material balance for liquid phase in the reactor is given by Eq. (5.30), where $n_{i,R}^L$ is the number of moles (mol) of component i , V_R^L is the volume (m^3) of liquid phase, R_i is the overall reaction rate ($\text{mol s}^{-1} \text{m}^{-3}$) of component i , $C_{i,R}^{L*}$ is the equilibrium concentration (mol m^{-3}) of component i in the liquid phase, $F_{i,r}^L$ is the recycling liquid flowrate (mol s^{-1}) of component i from the reflux condenser to the reactor. The total liquid volume V_R^L is given by Eq. (5.31), calculated through the addition of molar volume ($V_{mol,i}^L$) of each component at reaction conditions.

The thermal decomposition of m-guaiacol and 2,6-dimethoxyphenol were considered as first-order reactions, so

$$R_i = \sum v_i^j r_i \quad (5.41)$$

$$r_i = k_j C_R^L \quad (5.42)$$

where v_i^j is the stoichiometric coefficient of component i and k_j is the rate constant of reaction j . The components involved in reactions were m-guaiacol, 2,6-dimethoxyphenol, phenol, CH_4 , H_2O and H_2 .

The equilibrium concentration ($C_{i,R}^{L*}$) of component i at the interface was calculated using partition coefficients (K_i) determined by Prosim Plus. For the liquid phase composition ($n_{i,R}^L$) and the gas phase composition ($n_{i,R}^G$) at any given moment, the phase compositions ($n_{i,R}^{L*}$ and $n_{i,R}^{G*}$) at the equilibrium state can be achieved by an iterative flash calculation. The objective Rachford-Rice equation for iteration is as follows¹³:

$$\sum \frac{\frac{n_{i,R}^G + n_{i,R}^L}{\sum n_{i,R}^L + \sum n_{i,R}^G} (K_i - 1)}{1 + (K_i - 1) \frac{n_{i,R}^{L*}}{\sum n_{i,R}^L + \sum n_{i,R}^G}} = 1 \quad (5.43)$$

Thus, the equilibrium concentration is given by:

$$C_{i,R}^{L*} = \frac{n_{i,R}^{L*}}{V_R^{L*}} \quad (5.44)$$

where $n_{i,R}^{L*}$ is the liquid number of moles at the equilibrium state and V_R^{L*} is the volume of liquid phase at the equilibrium state.

Reactor (Gas phase)

The material balance for the gas phase in the reactor is given by Eq. (5.32), where $F_{i,in}^G$ is the inlet gas molar flowrate (mol s^{-1}) of component i , $F_{i,out}^G$ is the outlet gas molar flowrate (mol s^{-1}) of component i . The variation of gas phase volume V_R^G was associated to the volume change of liquid phase, since total reactor volume is constant as presented in Eq. (5.33). The total outlet gas flow (F_{out}^G) is given by Eq. (5.34) and was calculated taking account: the inlet H_2 flow, the total mass transferred between phases and the volume change of the gas phase.

Reflux condenser (Gas and Liquid phases)

In the reflux condenser, the fluid transition happened from vapor state into liquid state due to the temperature decrease from 350 to 160 °C. For us, it was impossible to get any information about the fluid composition inside. Hence, we cannot know precisely the condensation efficiency of our reflux

system. Here, we used a simplified approach to describe the condensation effect due to the reflux condenser. For the inlet gas flow ($F_{i,out}^G$) of component i at any given time, a condensation ratio of α_i was defined. By the approach, a liquid flow ($F_{i,r}^L$) representing the condensed part and a gas flow representing the non-condensed part were created. As we assumed no liquid cumulating in the reflux, the instant recycling liquid flow was given by Eq. (5.35). According to the experimental results presented above, the condensation ratios (α_i) of relatively light compounds such as water and m-xylene were defined as 0, indicating that the reflux condenser had no condensation effect to them and they were not recycled to the reactor at all. Logically, for those relatively heavy compounds such as 2,6-dimethoxyphenols and hexadecane, α_i was defined as 1, suggesting a complete condensation in the reflux condenser. For those intermediate compounds (phenol, m-cresol, 2,5-dimethylphenol, m-guaiacol and tetralin), the condensation ratios (α_i) were determined by parameter estimations.

Since the volume of reflux and the gas molar volume were constant, the total gas flow out of reflux condenser (F_{pass}^G) is given by Eq. (5.36). As presented in the hydrodynamic part, the reflux condenser can be modeled as perfectly mixing at 40 NL h⁻¹. Consequently, the gas composition out of reflux condenser is exactly the same as that inside of it, as given in Eq. (5.37), where $n_{i,r}^G$ is the number of moles of component i and n_r^G is the total number of moles in the reflux condenser.

Separator (Liquid phase)

After passing the cold traps at 15 °C, the condensable compounds were cumulated in the separator versus time. The material balance in the separator is given by Eq. (5.38), where $n_{i,s}^L$ is the number of moles of component i cumulated in the separator and $F_{i,pass}^G$ is the molar gas flowrate of condensable component i out of reflux condenser.

Gas outlet (Gas phase)

With the respect to the non-condensable gases, the delay between the reflux condenser and the μ GC is necessary to consider. At constant gas molar flowrate conditions, the delay can be calculated by the addition of residence time of all PFRs. However, this approach did not work in our case because the gas flow changed due to the gas formation, especially for the case of lignin conversion. Here, the delay induced by PFRs at a given time was calculated by Eq. (5.40), where n_{PFRs} is the number of moles contained in all the elements considered as PFRs.

Cooling and depressurization period

After the set residence time, the reactor was cooled to 160 °C while the reflux condenser maintained at 160 °C. During this process, some components in the gas phase of the reactor may be transferred to the liquid phase because of the temperature decrease. Here, we also estimated the condensation phenomena using the previously α_i describing the fluid transition from 350 to 160 °C. The number of moles of component i ($n_{i,c}$) transferred to the liquid phase was calculated as follows:

$$n_{i,c} = \alpha_i \cdot n_{i,R}^G \quad (5.45)$$

When the cooling was done, a fast depressurization started and all the gases inside of the set-up (gases in the reflux and the reflux condenser included) were evacuated. Certainly, condensable components among the gases flowed through the cold traps and trapped in the separator. Thus, for a given time, the real liquid composition ($n_{i,s}^{L,output}$) in the separator as model output was as follows:

$$n_{i,s}^{L,output} = n_{i,s}^L + n_{i,r}^G + (1 - \alpha_i) \cdot n_{i,R}^G \quad (5.46)$$

Similarly, the real liquid composition ($n_{i,R}^{L,output}$) in the reactor as model output was as follows:

$$n_{i,R}^{L,output} = n_{i,R}^L + \alpha_i \cdot n_{i,R}^G \quad (5.47)$$

V.3.2.3 Properties of compounds and model parameters

In the case of the gas phase, the molar volume was simply assimilated to the molar volume of H₂ since the majority of gas in the set-up was H₂. Table V.12 gives the gas molar volume of H₂ at different temperatures under 80 bar of pressure using the SRK equation. Using the API 6A2.22 method for hydrocarbons with the Rackett Equation for other compounds, the liquid molar volumes of pure compounds at the reaction conditions were calculated are presented in Table V.13.

Table V.12: Gas molar volume of H₂ at different temperatures under the pressure of 80 bar

Temperature (°C)	350	160	15	4
V_{mol}^G (m ³ kmol ⁻¹)	0.665	0.467	0.320	0.303

Table V.13: Liquid molar volume and equilibrium constant of model compounds at 350 °C

Compound	$V_{mol,i}^L$ (m ³ kmol ⁻¹)	K_i (-)
H ₂	0.064	8.60
CH ₄	0.099	3.93
H ₂ O	0.032	2.51
m-xylene	0.199	0.50
phenol	0.134	0.47
m-cresol	0.144	0.32
2,5-dimethylphenol	0.179	0.32
m-guaiacol	0.183	0.42
tetralin	0.190	0.23
2,6-dimethoxyphenol (*)	0.226	0.17
hexadecane	0.384	0.08

- * 2,6-dimethoxyphenol does not exist in the databases of Prosim, so its liquid molar volume and equilibrium constant were estimated by extrapolation method of other phenolic compounds, using the liquid molar volume versus the molar mass and equilibrium constant versus boiling point at 1 atm respectively.

The equilibrium constants were estimated by a two-phase flash calculations using Prosim Plus. Figure V.17 shows the process flow diagram used. The effluents entering in the flash were the experimental liquid composition in the cooled reactor and the hydrogen. By using the set of experimental data at different residence times as the process input, the intermediate equilibrium constant of each component was obtained, as given in Table V.13.

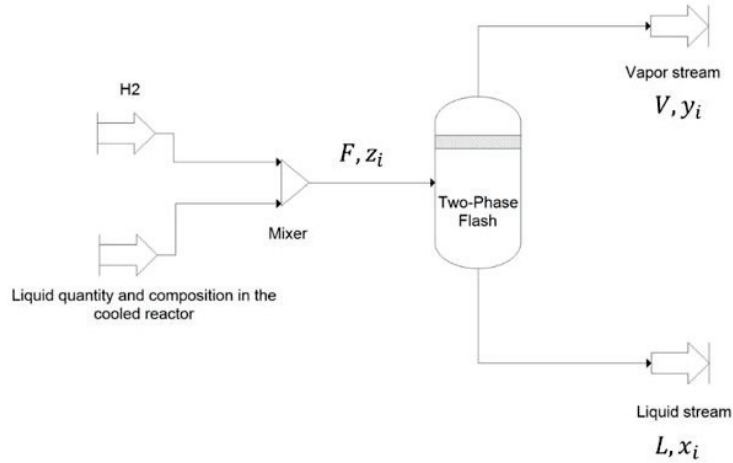


Figure V.17: Process flow diagram used for the flash calculation under Prosim Plus

We assumed that the estimated $k_L a$ between the G/L phases in the previous work was still usable in this model, although the liquid total volume and composition was already different from 100 g of tetralin in the reactor. The $k_L a$ for different compounds¹⁴ are calculated according to the Eq. (5.48), and the diffusivity ratios in tetralin were obtained from the Reddy-Doraiswamy Equation¹⁵. The diffusivity ratios used were given in Table V.14.

$$\frac{k_L a_i}{k_L a_{N_2}} = \frac{D_i}{D_{N_2}} \quad (5.48)$$

Table V.14: Estimated diffusivity ratios in tetralin by Reddy-Doraiswamy Equation

Compounds	H ₂	H ₂ O	CH ₄	Other compounds
$\frac{D_i}{D_{N_2}}$	1.3	1.2	1	0.7

V.3.2.4 Model structure and parameter estimation

A schematic representation of the structure and the parameter estimation procedure of our model is presented in Figure V.18. It was written in Matlab and the principal subroutines involved were ode15i and Isqnonlin.

The model was developed to simulate our system behavior functioning from the point t_0 to the depressurization. Firstly, the initial phase compositions in each element of set-up was estimated. Once the initial conditions were established, the differential and algebraic equations representing the material balances were solved in combination with the interface concentrations provided by VLE calculation. The hydrodynamic behavior of the gas phase was taken into account as well as the effect of cooling and depressurization stage. The model outputs were the simulated gas outlet flows versus time and the liquid compositions in the reactor and the separator at four residence times (t_0 , 1 h, 3 h and 5 h).

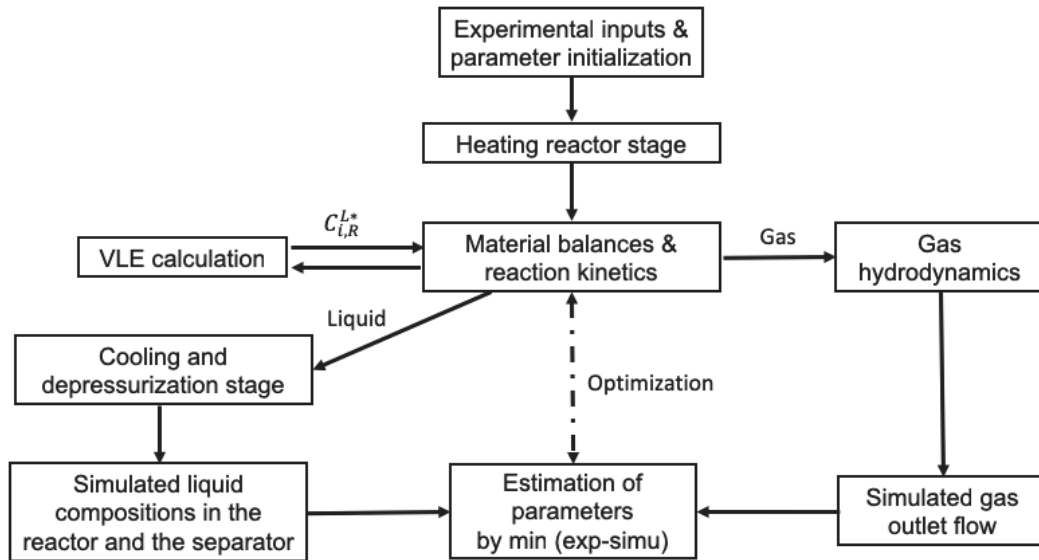


Figure V.18: Model structure and parameter estimation procedure

The 7 estimation parameters in the model were as follows:

- 1) Condensation ratios (α_i) of fives compounds: phenol, m-cresol, 2,5-dimethylphenol, m-guaiacol and tetralin.
- 2) Rate constants (k_i) of two reactions: the thermal decomposition of 2,6-dimethoxyphenol and m-guaiacol.

The model fitting and parameter estimation was carried out by minimizing the difference of weighted least squares between the experimental ($S_{i,exp}$) and simulated results ($S_{i,simu}$), as given in Eq. (5.49), where w_i is the weight factor. The reason for using weight factors was the varying orders of magnitude in the difference of least squares. The level of 95 % confidence intervals was also addressed.

$$J = \sum_1^N w_i (S_{i,exp} - S_{i,simu})^2 \quad (5.49)$$

V.3.3 Results and discussions

The values of the estimated parameters and their confidence limits are given in Table V.15. The results seem to be consistent with the experimental observations. As would be expected, the estimated condensation ratios were related to the molecular size of compound. For the light compound like phenol, the condensation ratio was around 0.20. For the heavier compounds such as 2,5-dimethylphenols, the condensation ratio was high as 0.93. Furthermore, the rate constant of thermal decomposition of 2,6-dimethoxyphenols was higher than that of m-guaiacol.

Table V.15: Parameter estimation results

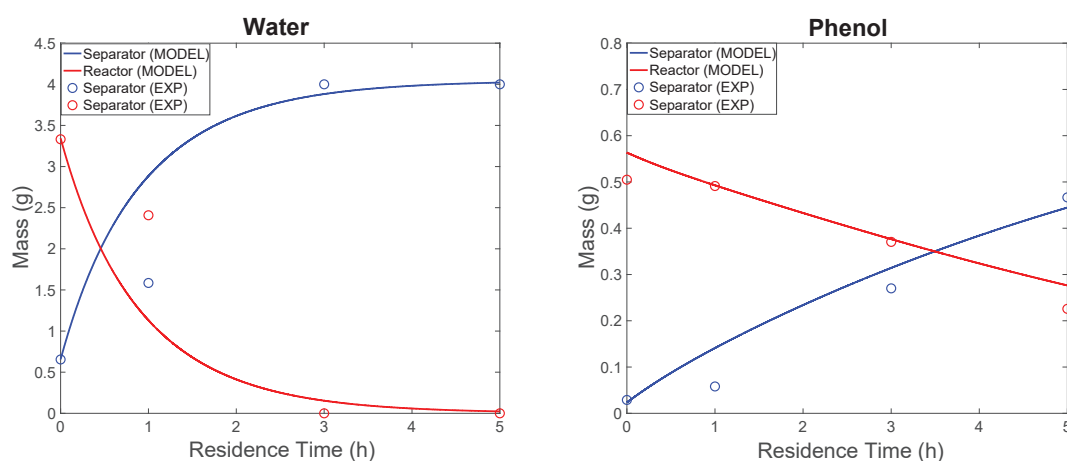
Parameter	Representation	Value
Condensation ratio (-)		
α_1	phenol	0.18 ± 0.06
α_2	m-cresol	0.62 ± 0.13
α_3	2,5-dimethylphenol	0.93 ± 0.05
α_4	m-guaiacol	0.67 ± 0.20
α_5	tetralin	0.94
Rate constant of thermal reactions (s^{-1})		
k_1	m-guaiacol	$1.4 \cdot 10^{-5} \pm 7.6 \cdot 10^{-6}$
k_2	2,6-dimethoxyphenol	$1.2 \cdot 10^{-4} \pm 1.5 \cdot 10^{-5}$

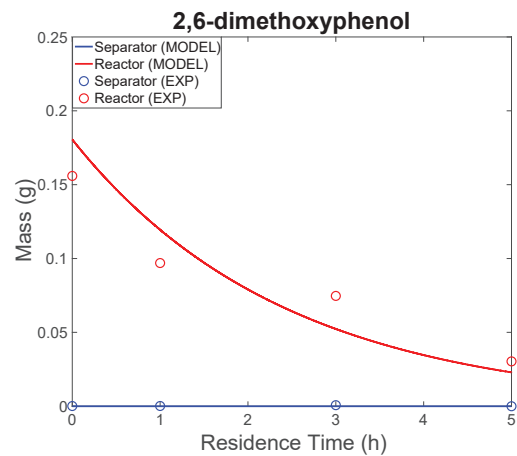
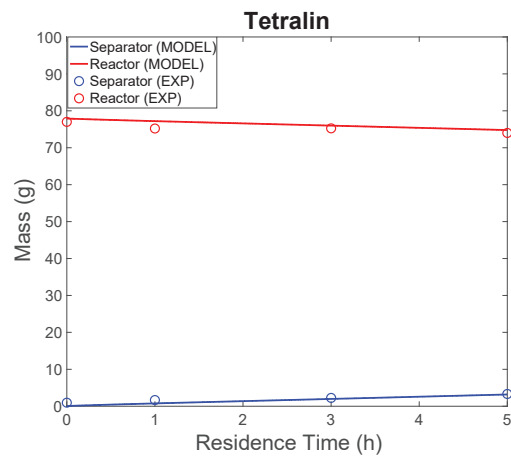
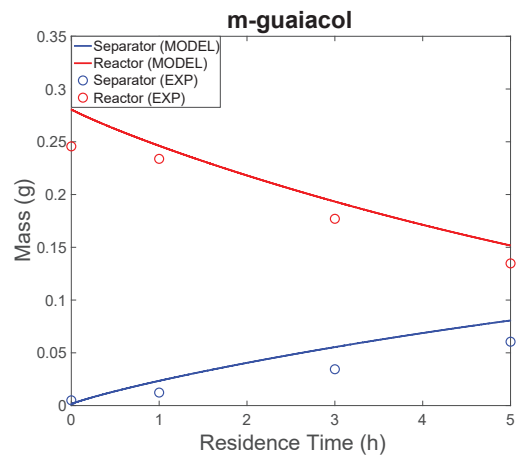
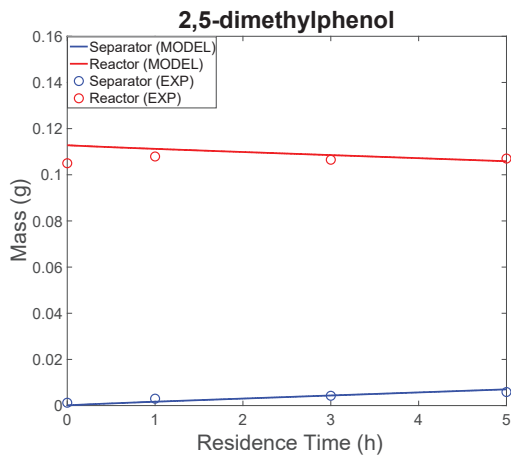
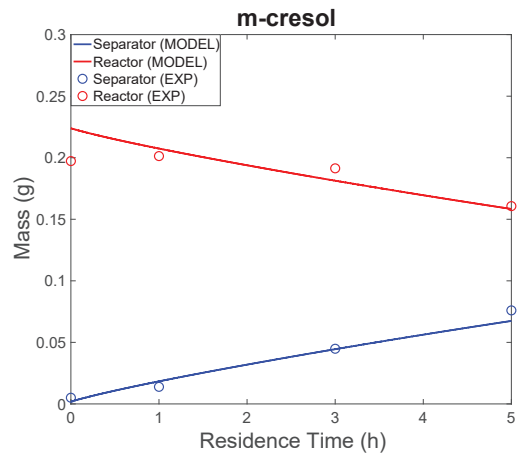
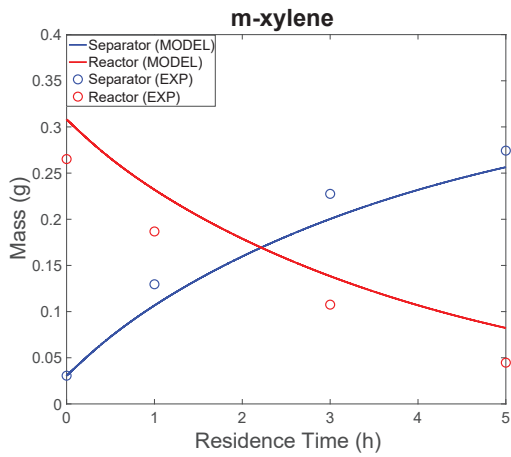
- * The condensation ratio of tetralin was observed to be stable, thus its value was fixed at 0.94 during the estimation process.

Figure V.19 compares the model results to the experimental data at different residence times. The simulated ones follow the experimental data well. Thus, by introducing the parameters of condensation ratio, the separation phenomena occurred in the reflux condenser were properly represented. For water, at the low residence time of 1 h, there was a relatively big error between the experimental data and the model result. This may be caused by the calculation of cooling period. In the model, we assumed that water in the vapor phase of reactor was not condensed during the cooling period using the ice batch. Probably, a portion of water was transferred in the liquid phase of reactor in reality, leading to a less quantity in the separator. Overall, the removal of water from the reaction medium was really fast, since almost all the water was found in the separator at 3 h.

For other compounds such as phenol, m-xylene, m-cresol, 2,5-dimethylphenol, m-guaiacol and tetralin, they were removed from the reactor as time progressed. Their removal rates were lower than that of water, which can be explained by their supposed lower vaporization ratios at the operating condition as well as the reflux effect realized by the reflux condenser.

For the relatively heavy compounds, the model can predict their complete condensation inside of the reflux condenser. Thus, they cannot flow through the reflux condenser as the experimental data shows.





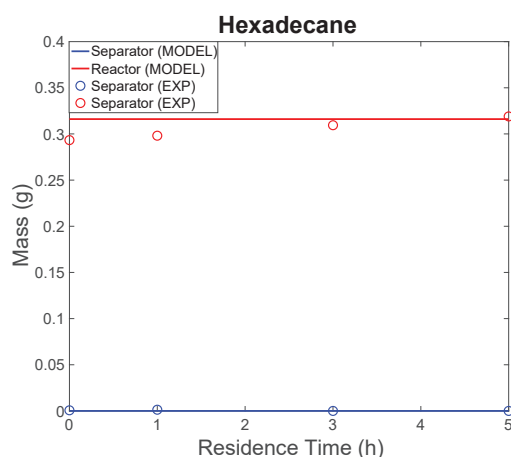


Figure V.19: Comparison between experimental data and model outputs at different residence times

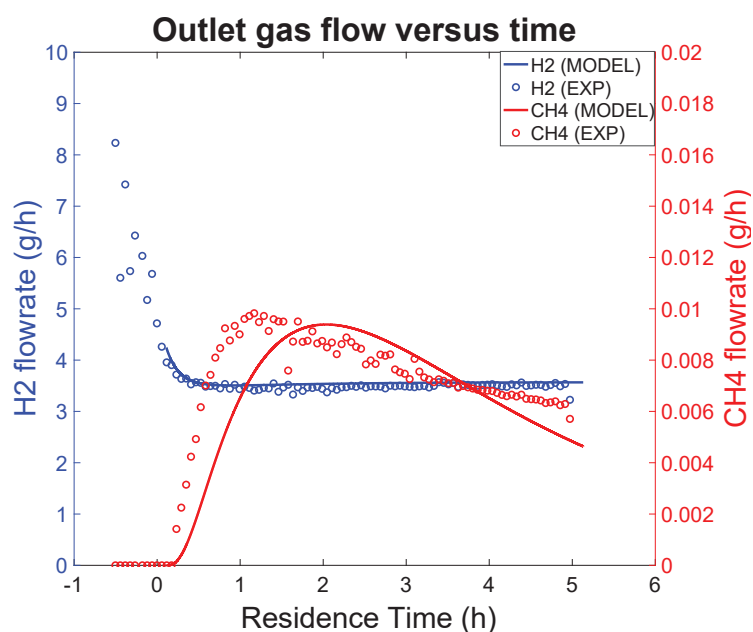


Figure V.20: Comparison between the calculated outlet gas flow and experimental data

Simultaneously, the rate constants of thermal decomposition reactions occurred to m-guaiacol were achieved by fitting the outlet gas flowrate. Figure V.20 shows that the outlet gas flow calculated by the model are in a good agreement with the experimental points. The decreasing part of the experimental data before t_0 corresponds to the heating period when the pressure was maintained at 80 bar. From the estimated rate constants, it suggests that the decomposition of 2,6-dimethoxyphenol was much faster than that of m-guaiacol. Table V.16 gives the results of different kinetic studies of thermal decomposition of methoxyphenols in the literature. These estimated orders of rate constant by our work seem to be in a reasonable agreement with other studies.

The characteristic time ($\tau_{reaction}$) is often used to describe how fast the reaction is, calculated by:

$$\tau_{reaction} = \frac{1}{kC^{n-1}} \quad (5.50)$$

where n is the reaction order. The calculated $\tau_{reaction}$ were 2-2.7 h and 13-43 h, respectively for the thermal decomposition of 2,6-dimethoxyphenol and m-guaiacol. The values indicate that, the thermal decomposition of methoxylated phenols are relatively slow in the absence of catalyst.

Table V.16: Kinetic studies of thermal decomposition of methoxyphenols in the literature

Source	Reactant	Temperature (°C)	k_i (s ⁻¹)
This work	guaiacol 2,6-dimethoxyphenol	350	$1.4 \cdot 10^{-5} \pm 7.6 \cdot 10^{-6}$ $1.2 \cdot 10^{-4} \pm 1.5 \cdot 10^{-5}$
[16]	Lignin (methoxyphenols)	220-380	$4.4 \cdot 10^{-5} \sim 2.9 \cdot 10^{-4}$
[17]	Lignin (methoxyphenols)	360	$1.4 \cdot 10^{-4}$
[18]	guaiacol	210-290	$5 \cdot 10^{-6} \sim 1.7 \cdot 10^{-5}$
[19]	Lignin (methoxyphenols)	400	$6.3 \cdot 10^{-4}$
[20]	guaiacol	325	$2.8 \cdot 10^{-5}$

V.3.4 Conclusion of thermodynamics

Concerning the thermodynamic model, we compared the different existing models on the basis of the properties of our reaction mixtures. As a result, the PSRK model in combination with a specific calculation of water seems to be preferred, and its applicability was also validated by the comparisons between the model out and the experimental data for several binary or ternary mixtures. Moreover, we used a simple approach to describe the condensation effects with regard to lignin-derived compounds. The simple approach was also validated by experiments using mixtures of lignin-derived compounds. The results show that the condensation effect was directly related to their molecule sizes.

V.4 Conclusion

In this chapter, we investigated the gas hydrodynamics, mass transfer characterization and VLE of our experimental set-up. The hydrodynamics were determined by RTD measurements and represented by an adapted physical model using a combination of ideal reactors. Concerning the mass transfer characterization, the volumetric mass transfer coefficient was estimated at the operating conditions, in order to describe the mass transfer between phases. The combination between the hydrodynamics and the interphase mass transfer as well as the preferred PSRK VLE model, we were already able to establish a complete reactor model to simulate the chemical and physical phenomena involved with some model compounds and a few of reaction pathways. For the following kinetic modeling of catalytic lignin hydroconversion, the established reactor model is still suitable, but the number increase of compounds and reaction pathways involved in the reaction medium would be a challenge.

Reference-V

- [1] Danckwerts, P.V., 1953. Continuous flow systems: distribution of residence times. *Chemical Engineering Science* 2, 1–13.
- [2] Whitman, W.G., 1962. The two film theory of gas absorption. *International Journal of Heat and Mass Transfer* 5, 429–433.
- [3] Benyahia, F., Jones, L., 1997. Scale Effects on Hydrodynamic and Mass Transfer Characteristics of External Loop Airlift Reactors. *Journal of Chemical Technology & Biotechnology* 69, 301–308.
- [4] Turpeinen, E.-M., Sapei, E., Uusi-Kyyny, P., Keskinen, K.I., Krause, O.A.I., 2011. Finding a suitable thermodynamic model and phase equilibria for hydrodeoxygenation reactions of methyl heptanoate. *Fuel* 90, 3315–3322.
- [5] Zhong, C., Peters, C. J., De Swan Arons, J., 2002. Thermodynamic modeling of biomass conversion processes. *Fluid Phase Equilibria*, 508-815.
- [6] Lu, Y., Guo, L., Zhang, X., Yan, Q., 2007. Thermodynamic modeling and analysis of biomass gasification for hydrogen production in supercritical water. *Chemical Engineering Journal* 131, 233–244.
- [7] http://www.prosim.net/bibliotheque/File/Exemples-Applications-PSP/En/PSPS_E03_EN-Three_Stage_Letdown.pdf
- [8] Simnick, J.J., Lawson, C.C., Lin, H.M., Chao, K.C., 1977. Vapor-liquid equilibrium of hydrogen/tetralin system at elevated temperatures and pressures. *AIChE Journal* 23, 469–476.
- [9] Christensen, S.P., Paulaitis, M.E., 1992. Phase equilibria for tetralin-water and 1-methylnaphthalene-water mixtures at elevated temperatures and pressures. *Fluid phase equilibria* 71, 63–83.
- [10] Niesen, V.G., Yesavage, V.F., 1988. Vapor-liquid equilibria for m-cresol/tetralin and tetralin/quinoline at temperatures between 523 and 598 K. *Journal of Chemical and Engineering Data* 33, 253–258.
- [11] Dinh, C.M., Kim, H., Lin, H., Chao, K., 1985. Vapor-liquid equilibrium in water+ m-cresol+ hydrogen mixtures at high temperatures and pressures. *Journal of chemical and engineering data* 30, 326–327.
- [12] Oliphant, J.L., Lin, H.-M., Chao, K.-C., 1979. Gas-liquid equilibrium in hydrogen+ tetralin+ diphenylmethane and hydrogen+ tetralin+ m-xylene. *Fluid Phase Equilibria* 3, 35–46.
- [13] Leibovici, C.F., Neoschil, J., 1995. A solution of Rachford-Rice equations for multiphase systems. *Fluid Phase Equilibria* 112, 217–221.
- [14] Lemoine, R., 1998. Hydrodynamics, mass transfer and modeling of the toluene oxidation process. Ph.D. thesis, University of Pittsburgh.
- [15] Reddy, K.A., Doraiswamy, L.K., 1967. Estimating Liquid Diffusivity. *Industrial & Engineering Chemistry Fundamentals* 6, 77–79.

- [16] Forchheim, D., Hornung, U., Kruse, A., Sutter, T., 2014. Kinetic Modelling of Hydrothermal Lignin Depolymerisation. *Waste and Biomass Valorization* 5, 985–994.
- [17] Gasson, J.R., Forchheim, D., Sutter, T., Hornung, U., Kruse, A., Barth, T., 2012. Modeling the Lignin Degradation Kinetics in an Ethanol/Formic Acid Solvolysis Approach. Part 1. Kinetic Model Development. *Industrial & Engineering Chemistry Research* 51, 10595–10606.
- [18] Wahyudiono, Sasaki, M., Goto, M., 2011. Thermal decomposition of guaiacol in sub- and supercritical water and its kinetic analysis. *Journal of Material Cycles and Waste Management* 13, 68–79.
- [19] Jegers, H.E., Klein, M.T., 1985. Primary and secondary lignin pyrolysis reaction pathways. *Industrial & Engineering Chemistry Process Design and Development* 24, 173–183.
- [20] Vuori, A., 1986. Pyrolysis studies of some simple coal related aromatic methyl ethers. *Fuel* 65, 1575–1583.

Chapter VI. Kinetic Modeling of Catalytic Lignin Hydroconversion

VI.1 Introduction

To proceed with the development of a kinetic model for catalytic lignin hydroconversion, the following key elements have been presented in the previous chapters. The characterization of lignin feedstock was presented in **Chapter III**, the reaction network representing the transformations occurring during the conversion was proposed on the basis of experimental observations in **Chapter IV** and hydrodynamic and thermodynamic characteristics of our set-up were studied in **Chapter V**. In addition, the established reactor model in **Chapter V** was able to simulate the dynamic variations of some model compounds involved with a few of reaction pathways.

In this chapter, a tentative kinetic model is realized to simulate the catalytic lignin hydroconversion in our set-batch reactor. Firstly, a kinetic model description of catalytic lignin hydroconversion is presented with its reaction network, reaction equations and corresponding rate equations, as well as the fixed parameters in the model such as molar mass and thermodynamic properties of each lump. Secondly, the suitable reactor model for catalytic lignin hydroconversion is presented. Thirdly, the resulting kinetic model is reported followed by a discussion of the results of estimated rate constants and stoichiometric coefficients.

VI.2 Model description

On the basis of the experimental results presented in **Chapter IV**, reaction products from lignin hydroconversion were able to be regrouped into several lumps according to their states or functional groups and each of these lumps was considered to be a single chemical species:

- Oligomeric entities: THF-insolubles, THF-solubles and solubilized oligomers;
- Liquid lumps: dimethoxyphenols, methoxyphenols, alkanes, alkylphenols, catechols, aromatics, naphthenes and H₂O;
- Gas lumps: CH₄, H₂O, C₂-C₆, CO₂ and CO.

A lumped reaction network representing the transformations of lignin hydroconversion was already illustrated in Scheme IV.14 and IV.15. As a result, a lumped kinetic approach was chosen to simulate the lignin hydroconversion process. The main advantage of using the lumped model in our study is the reduction in the number of compounds and reaction pathways. Meanwhile, a mechanistic representation to describe the reactions at the macro-level can be ensured.

VI.2.1 Interphase mass transfer in the reactor

The reactor had three phases inside: a gas phase, a liquid phase and a solid phase.

- Gas phase: It contained gases and vaporized liquid lumps.
- Liquid phase: It contained tetralin, liquid lumps, dissolved gases and solubilized oligomers. In addition, the lignin residues (THF-solubles and THF-insolubles) were also present in the liquid phase, which were unknown to their states. To our knowledge, the normal melting point of

lignin is around 200-300 °C, so we assumed that they were melted and dispersed in the liquid phase under our operating conditions.

- Solid phase: Ashes and catalyst extrudates were present as the solid phase in the reactor with a stirring rate of 800 rpm. A good catalyst suspension in tetralin was observed with a cold model study. However, it was difficult to verify experimentally the suspension state of catalyst under the operating conditions. Using the Zwietering's correlation¹, it was proved that the catalysts were also well suspended in the liquid phase under the operating conditions.

It can be realistic that the reactants and products underwent interphase mass transfer between any two of these phases. In most cases, we assumed that there was no contact between the gas and solid phases. Thus, only G/L and L/S mass transfers were considered in our study.

The interphase mass transfer between the G/L phases with only tetralin has been investigated in **Chapter V**. However, in the real catalytic lignin hydroconversion, the G/L mass transfer becomes more complex. On one hand, the formed liquids may change the liquid compositions and properties, which may have an effect on the interphase mass transfer. On the other hand, the melted lignin residues, which were dispersed in the liquid phase, were gradually self-decomposed and consumed H₂ for the stabilization of the radicals formed. As such, H₂ may react with the melted lignin residues directly at the interface between the gas bubbles and the melted lignin dispersed in the liquid phase. Here, we assumed that the G/L mass transfer was not influenced by the change in liquid compositions and properties. However, the $k_L a$ of H₂ should be taken into account exceptionally, which will be detailed in [§ VI.2.3](#).

In a heterogeneous catalyzed reaction, the L/S mass transfer of reactants firstly takes place from the bulk liquid to the external surface of catalyst. The characterization of the L/S mass transfer was not implemented in our work, but we evaluated the external resistance fraction expressed as $f_{ex} = (C_i^L - C_i^S)/C_i^L$, which is a simple comparison between the concentration in the bulk liquid and that at the surface of catalyst. If $f_{ex} < 0.05$, we can assume that the L/S mass transfer is rapid so that C_i^L is almost equal to C_i^S . The f_{ex} for our study will be evaluated for the mass transfer limitation at the end of this chapter, in [§ VI.3.3](#).

VI.2.2 Chemical kinetics

Noting that the heating slope led to the inevitable conversion of lignin, the starting point of our kinetic model was t_0 point, when there already existed a distribution of reaction products. Firstly, a list of assumptions pertaining to the chemical kinetics was made:

- 1) The reactor was isothermal.
- 2) The liquid and vapor phases were perfectly mixing.
- 3) The solid catalysts were dispersed in the liquid phase.
- 4) Adsorption/desorption process was not considered and there was no internal and external diffusion limitation in the catalyst particles so that the reaction kinetic expression can be written with respect to liquid-phase concentrations.
- 5) The reaction of decarboxylation to CO₂ and reverse water-gas shift reaction from CO₂ to CO were thought to be achieved instantaneously at t_0 point.
- 6) The conversion of tetralin to naphthalene was not taken into account. By Figure IV.23, we can estimate the amount of released H₂ by tetralin from t_0 to 13 h. The mass of naphthalene was about 3.3 g at t_0 and 5.0 g at 13 h. The mass variation corresponds to 0.03 moles of H₂ provided

by the conversion from tetralin. Compared to the total consumption of H₂ at 13 h (1.30 moles), the fraction was negligible.

Reaction network

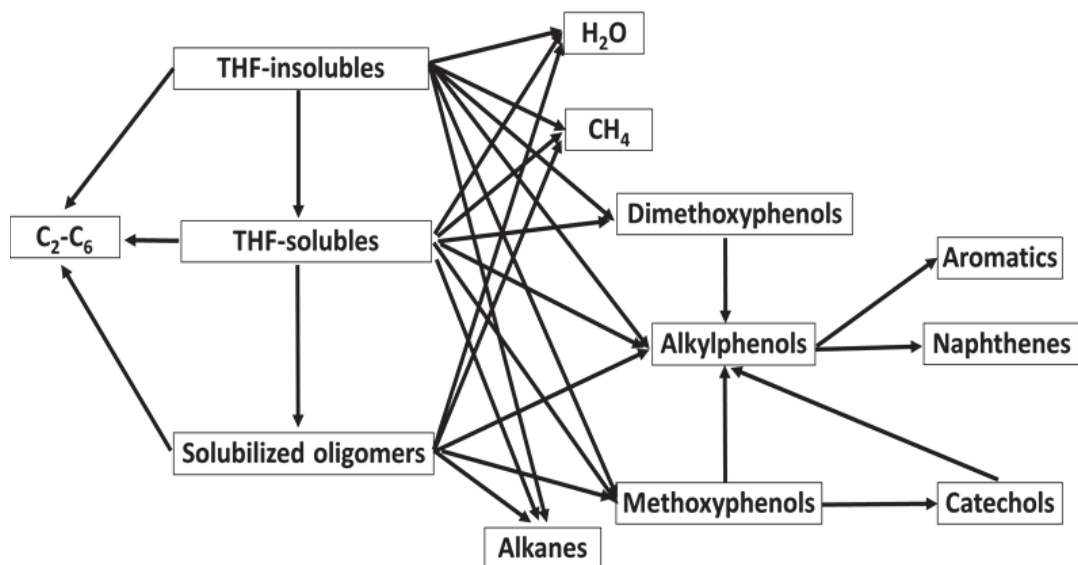


Figure VI.1: Reaction network for catalytic lignin hydroconversion

According to Scheme IV.14 and IV.15, the reaction network for catalytic lignin hydroconversion can be constructed as shown in Figure VI.1. During the simulation process, it appears that some simplifications could be done for the reaction network in order to limit the number of estimated kinetic parameters. The reasons for these simplifications in the reaction network are as follows:

- 1) Sensibility of stoichiometric coefficients: THF-insolubles was supposed to be depolymerized into various lighter fragments: THF-solubles, solubilized oligomers, liquid monomers and gaseous products. Due to the significant difference in molar mass (in § VI.2.3) between THF-insolubles (M_w : 16000 g mol⁻¹) and other fragments (M_w : 16~500 g mol⁻¹), the model is not sensitive enough to be used for the determination of stoichiometric coefficients for small molecules. Therefore, we considered THF-solubles as the only product from the depolymerization of THF-insolubles.
- 2) Competition kinetics: Regarding dimethoxyphenols and methoxyphenols, they may be released directly from oligomeric entities such as THF-insolubles, THF-solubles and even solubilized oligomers. However, both of them showed the highest yields at t_0 point and then their yields decreased versus time. That indicates, the rates of their disappearances were always faster than the rate of their appearances at any given time after t_0 . In the situation, the appearance rates for dimethoxyphenols and methoxyphenols are uncertain and cannot be predicted by the model, so that they were not introduced as products from oligomeric entities.
- 3) Experimental observations: We noticed that the production rates of CH₄ and H₂O were quite slow after 5 h whereas the yield of solubilized oligomers increased versus reaction time. It can be suggested that the conversion from solubilized oligomers into CH₄ and H₂O was not worth mentioning. Otherwise, we would observe a faster production of CH₄ and H₂O with increasing

solubilized oligomers. Thus, the alkylphenols were considered as the only product from solubilized oligomers.

So, the simplified reaction network used for the kinetic model is illustrated in Figure VI.2.

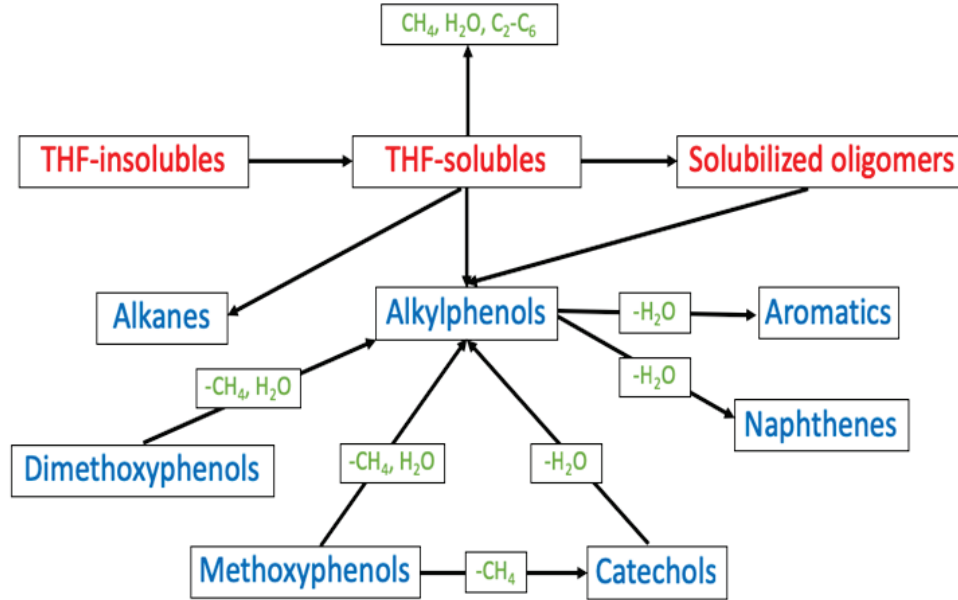
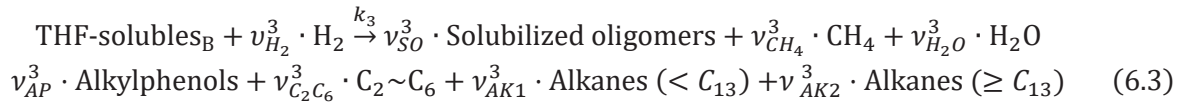
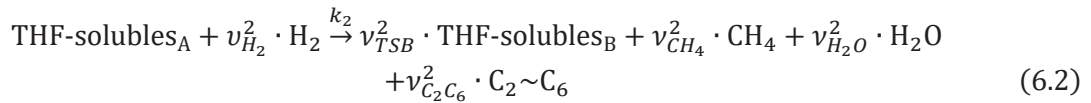


Figure VI.2: Simplified reaction network used for the kinetic model

Reaction equations

According to the simplified reaction network in Figure VI.2, the reaction equations in the kinetic model are listed with three additional remarks:





where k_j is the rate constant of reaction j and v_i^j is the stoichiometric coefficient of lump i in the reaction j .

Three remarks on these reaction equations are as follows:

- 1) H_2 was not placed in reactions (6.1) and (6.4), respectively for reasons of low parameter sensibility (significant difference in molar mass) and experimental observations (low H_2 consumption in the presence of concentrated solubilized oligomers after 5 h). In fact, they consumed H_2 during the reaction. As a result, our model will overestimate the consumption of H_2 by THF-solubles to compensate that consumed by other oligomeric entities.
- 2) A first-order reaction was attempted to simulate the formation of CH_4 , H_2O and C_2-C_6 from THF-solubles with failure. It was found that their formations involved a two-step mechanism: the first step consisted of a fairly fast reaction at the early stage of reaction, followed by the second step at a relatively slow rate. In order to solve the large variation of kinetics as a function of reaction time, we divided the lump of THF-solubles into two fractions in the model: THF-solubles_A and THF-solubles_B, as presented in reactions (6.2) and (6.3). The evolutions of these two fractions in the model are given in Figure VI.3. We assumed that only THF-solubles_A was present in the reactor at t_0 . The conversion of THF-solubles_A was carried out in a rather short time, along with a rapid formation of CH_4 , H_2O and C_2-C_6 . As time progressed, the formed THF-solubles_B was depolymerized into lighter fractions at a relatively slow rate, accompanying slower formations of CH_4 , H_2O and C_2-C_6 than those from THF-solubles_A. As such, the problem of the variation in kinetics as a function of reaction time was solved in the model.

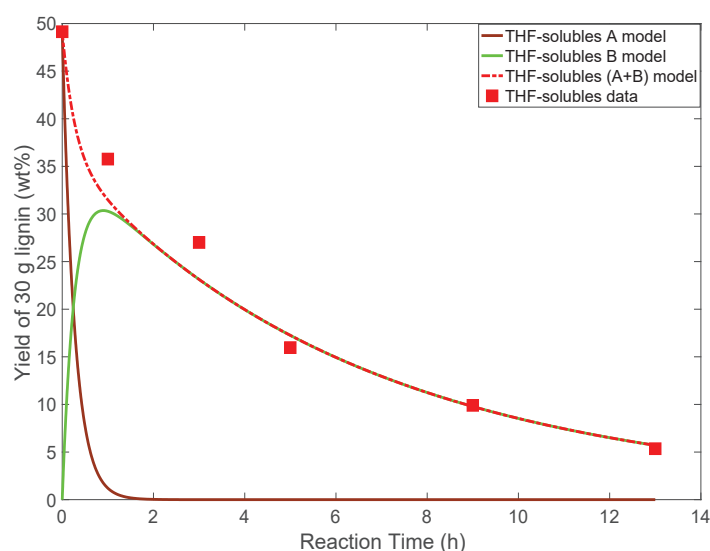


Figure VI.3: Evolution of THF-solubles_A and THF-solubles_B in the model

- 3) The lump of alkanes was divided into two parts: alkanes ($<C_{13}$) and alkanes ($\geq C_{13}$) for thermodynamic concerns, since the properties (V_{mol}^L and K_i) of alkanes vary considerably depending on the carbon number. These two properties influence the calculation of liquid volume, the vaporization ratios, and the condensation effect in the reflux condenser as well as the gathering place (reactor or separator).

Reaction type

Under our operating conditions, information on the lignin solubility in tetralin was unknown and the access of oligomeric entities to the catalyst pore depends largely on the steric properties. It has been reported that the degradation of lignin by C-O and C-C cleavage, which is not really impacted by the presence of catalyst, proving that the initial depolymerization of lignin is mostly thermal². In contrast, the composition of liquid phase varies drastically in the presence of catalyst, indicating a catalytic effect to liquid fragments. It can be therefore assumed that the depolymerization of lignin is initially thermal and then becomes catalytic when its solubilized fragments can interface with the catalyst.

In our case, reactions (6.1), (6.2) and (6.3) with respect to large lignin fragments were thought to be independent of the H_2 concentration. However, H_2 was consumed to stabilize the formed radicals and to participate in the hydrogenation/hydrogenolysis reactions on the large lignin fragments. For other reactions of solubilized fragments from (6.4) to (6.10), they were thought to be catalyzed at the surface of catalyst.

Reaction order and rate equations

For reactions from (6.1) to (6.3), assuming a first-order with respect to the reactant:

$$r_j = k_j C_R^L \quad (j = 1\sim 3) \quad (6.11)$$

where r_j is the reaction rate for reaction j per unit volume of liquid and C_R^L is the concentration of reactant in the liquid phase.

For reactions (6.4) to (6.10), assuming a first-order with respect to each lump and hydrogen:

$$r_j = k_j C_R^L C_{H_2,R}^L \quad (j = 4\sim 10) \quad (6.12)$$

where $C_{H_2,R}^L$ is the concentration of dissolved H_2 in the liquid phase.

Therefore, the overall reaction rate (R_i) for each lump can be expressed as:

$$R_i = \sum_{j=1}^{10} v_i^j r_j \quad (6.13)$$

where v_i^j is the stoichiometric coefficient of lump i in the reaction j .

Estimation parameters

The estimated parameters in the model are the following:

- 10 rate constants: $k_1, k_2, k_3, k_4, k_5, k_6, k_7, k_8, k_9$ and k_{10}
- 11 stoichiometric coefficients: $v_{H_2}^2, v_{CH_4}^2, v_{C_2C_6}^2, v_{H_2}^3, v_{H_2O}^3, v_{CH_4}^3, v_{H_2O}^3, v_{AP}^3, v_{C_2C_6}^3, v_{AK1}^3$ and v_{AK2}^3

Stoichiometric coefficients

The stoichiometric coefficients such as v_{TSB}^1 , v_{AP}^4 , $v_{H_2}^5$, $v_{H_2}^6$, $v_{H_2}^7$, $v_{H_2}^8$, $v_{H_2}^9$ and $v_{H_2}^{10}$ were calculated directly by mass conservation constraints. Their values are presented in Table VI.1. The stoichiometric coefficients of v_{TSB}^2 and v_{SO}^3 were also calculated respecting the mass conservation for reaction equation during the parameter estimation process.

Table VI.1: Stoichiometric coefficients determined by mass conservation

v_{TSB}^1	v_{AP}^4	$v_{H_2}^5$	$v_{H_2}^6$	$v_{H_2}^7$	$v_{H_2}^8$	$v_{H_2}^9$	$v_{H_2}^{10}$
14.6	4.3	8.0	5.0	2.5	2.5	1.0	1.5

VI.2.3 Fixed parameters in the model

Molar mass

First of all, it was necessary to determine the molar mass of each lump in order to calculate the molar concentrations.

Oligomeric entities

Three types of oligomeric entities were co-existing in the reaction medium from large to small: THF-insolubles, THF-solubles followed by solubilized oligomers. For THF-solubles and solubilized oligomers, their temporal variations in molar mass have been reported in **Chapter IV**. The temporal variation of the molar mass of THF-insolubles was not determined experimentally. The variations of molar mass for them at different conversion ratios were neglected in order to keep the stoichiometric coefficients constant. Thus, we took the initial average M_w value for THF-insolubles and intermediate average M_w values for THF-solubles and solubilized oligomers in the model. Their corresponding M_w values are respectively 16000, 1100 and 500 g mol⁻¹.

Gas

During the reaction, the C₂ to C₆ light alkanes were formed. We regrouped them as one lump "C₂~C₆" and its average M_w was fixed 50 g mol⁻¹ by averaging from the cumulative productions of C₂~C₆ at 13 h.

Liquid lumps

In our case, the variation of the molar mass for each lump at different reaction times was also neglected. Table VI.2 gives the average M_w of the liquid fractions in the reactor and the separator after 13 h of reaction. As expected, the differences in M_w between in the reactor and the separator were slightly elevated for alkylphenols, alkanes (<C₁₃) and methoxyphenols, since their contained compounds were in a wide range of carbon numbers and boiling points. By the separation of reflux condenser, the relatively light ones were trapped in the separator and the heavier ones remained in the reactor, which resulted in a higher average M_w in the reactor. For the sake of simplification, M_w used for all the lumps in the model was calculated by the weighted average of two liquid fractions, as shown in Table VI.2.

Table VI.2: Average molar mass of liquid lumps after 13 h of reaction

Lump	Average M_w in the reactor (g mol^{-1})	Average M_w in the separator (g mol^{-1})	M_w used in the model (g mol^{-1})
Aromatics	102.6	100.1	101
Naphthenes	102.2	101.6	102
Alkylphenols	122.0	102.6	117
Alkanes ($<C_{13}$)	144.3	124.7	127
Catechols	139.8	-	140
Methoxyphenols	148.7	129.6	146
Dimethoxyphenols	168.7	-	169
Alkanes ($\geq C_{13}$)	270.2	-	270

Thermodynamic properties

In the case of the gas phase, the molar volume was simply assimilated to the molar volume of H_2 since the majority of gas in the set-up was H_2 . The gas molar volumes of H_2 at different temperatures under 80 bar were already reported in Table V.12.

Using the API 6A2.22 method for pure hydrocarbons and the Rackett-Mixture Equation for other compounds, the liquid molar volumes of pure substances were obtained under the software of Prosim Plus. However, each lump contains various substances with a wide range of liquid molar volumes, making it difficult to calculate the liquid molar volume for each lump accurately. In our case, the liquid molar volume of each lump was estimated by interpolation or extrapolation method from the liquid molar volumes of pure substances, using the approximate linear relationship between liquid molar volume and molar mass. Example of an estimation of liquid molar volume for aromatics is presented in Figure VI.4. The estimated liquid molar volumes of each lump (compound) at 350 °C in our model are given in Table VI.3.

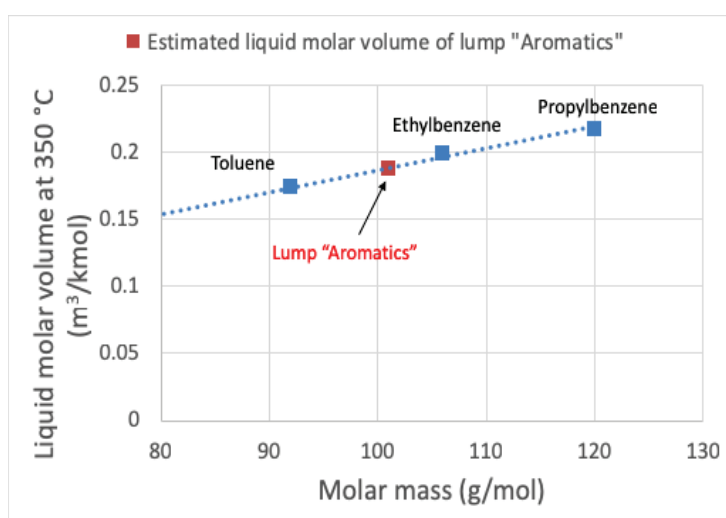


Figure VI.4: Estimation of the liquid molar volume of lump "aromatics" by interpolation method

Table VI.3: Liquid molar volume and equilibrium constant at 350 °C

Lump (compound)	V_{mol}^L ($m^3 \text{ kmol}^{-1}$)	K_i (-)
H ₂	0.064	4.57
CH ₄	0.099	3.22
CO	0.095	3.00
CO ₂	0.093	1.50
C ₂ -C ₆	0.129	1.75
H ₂ O	0.032	2.51
Aromatics	0.187	0.52
Naphthenes	0.208	0.61
Alkylphenols	0.174	0.30
Tetralin	0.190	0.23
Alkanes (<C ₁₃)	0.269	0.48
Catechols	0.209	0.21
Methoxyphenols	0.203	0.23
Dimethoxyphenols	0.241	0.06
Alkanes(≥C ₁₃)	0.441	0.05

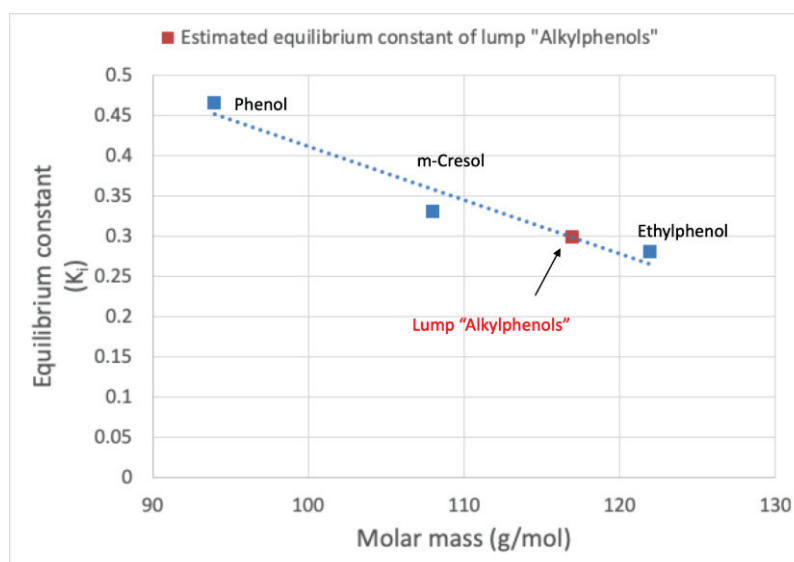


Figure VI.5: Estimation of the equilibrium constant of lump "alkylphenols" by interpolation method

Using the PSRK thermodynamic model, the simulation of two-phase flash calculation in Prosim Plus allows us to calculate the equilibrium constant of every component in a mixture. The effluent entering into the flash contains gaseous products (H₂, CO, CO₂, etc.), tetralin and representative compounds for each lump (C₁-C₃ benzene, C₁-C₃ phenol, etc.). The molar composition of the effluent was close to the actual composition of these lumps under the reaction conditions. The values of equilibrium constant

for each lump were also estimated by the interpolation or extrapolation methods from those of pure compounds in the lump. An example of the estimation of equilibrium constant for alkylphenols is given in Figure VI.5. The estimated equilibrium constants of each lump (compound) at 350 °C in our model are given in Table VI.3.

***k_La* value**

The $k_L a$ values for all the compounds were firstly calculated using their diffusivity coefficients in tetralin relative to that of N₂, as shown in Table V.14. With this calculated $k_L a$ for H₂, it was found that the amount of H₂ transferred from the gas phase into the liquid phase was far from sufficient to provide the necessary moles of H₂ for the reactions in the liquid phase, and thus the negative moles of H₂ was observed between 0-1 h when there was a high H₂ consumption. The guesses can be as follows:

- Overestimation of H₂ consumption in the liquid phase: As previously mentioned, there may have a direct contact between the gas bubbles and the melted lignin residue phase. As such, the consumption of dissolved H₂ in the liquid phase was overestimated in this model because a fraction of consumed H₂ came from the gas bubbles in the liquid phase instead of the dissolved H₂. This overestimation can probably lead to the negative moles of H₂ in the liquid phase when H₂ consumption was high.
- Underestimation of H₂ mass transfer between the G/L phases: As is known, the interphase mass transfer was calculated using two parameters: $k_L a$ and the concentration gradient between the phases ($\Delta C = C_i^{L*} - C_i^L$). For the latter, it depends greatly on the VLE model. So, the underestimation of H₂ mass transfer may be attributed to two reasons: (1) The $k_L a$ for H₂ was underestimated using the correlation; (2) The VLE model was not suitable for H₂, leading to an underestimation of C_i^{L*} . Anyway, this underestimation of H₂ mass transfer can also lead to the negative moles of H₂ in the liquid phase when H₂ consumption was high.

However, it was difficult to find the exact reasons in our operating conditions. Evidently, this $k_L a$ for H₂ was not suitable for our model. It was necessary to increase the $k_L a$ for H₂ in order to have a sufficient amount of H₂ in the liquid phase. So in the model, the $k_L a$ for H₂ was increased by three times.

VI.2.4 Material balances

Heating reactor stage

During the heating slope, there was a distribution of liquid and gaseous products in the reactor whereas no liquid products were found in the separator. Given the complexity of modeling the real process with temperature-varying reactions, a simplified heating stage representation was developed to have a coherent approximation of the initial gas and liquid compositions for each element in the set-up at t_0 point, which is the starting point of our model. Taken the liquid and gaseous products produced in account, the representation is as follows:

- 1) No liquid compounds were in the vapor state existing in the reactor. Thus, the liquid compounds recovered experimentally at t_0 were completely in the liquid state inside the reactor.
- 2) The gas composition in the reflux (H₂, CH₄, C₂-C₆, CO₂ and CO) was calculated from the outlet gas composition and the gas composition in the reactor was calculated by matching the cumulative gas production at t_0 . Moreover, it was thought that the CO₂ and CO reactions were instantaneous so that their cumulative gas productions used corresponds to the values of 13 h instead. In addition, all the gases reached the state of vapor-liquid equilibrium in the reactor.

Stationary period

The established reactor model and the assumptions presented in § V.3.2.2 are still suitable for kinetic modeling of catalytic lignin hydroconversion. Here, we just present the condensation ratios (α_i) used to describe the condensation effect of our reflux system. The values of α_i used for the kinetic modeling of lignin hydroconversion are given in Table VI.4. The α_i of the relatively light gases, water and lumps (aromatics, naphthenes and alkanes (<C₁₃)) were defined as 0 and the relatively heavy lumps (catechols, dimethoxyphenols and alkanes (≥C₁₃)) were defined as 1. The values of α_i of other lumps such as alkylphenols and methoxyphenols were interpolated using the relationship between α_i and molar mass. An example of the estimation of α_i for lump alkylphenols is given in Figure VI.6.

Table VI.4: Condensation ratios for each lump in the model

Lump	non-condensable gases	H ₂ O	Aromatics	Naphthenes	Alkanes (<C ₁₃)	Alkylphenols
Value	0	0	0	0	0	0.8
Lump	Tetralin	Catechols	Methoxyphenols	Dimethoxyphenols	Alkanes (≥C ₁₃)	
Value	0.94	1	0.9	1	1	

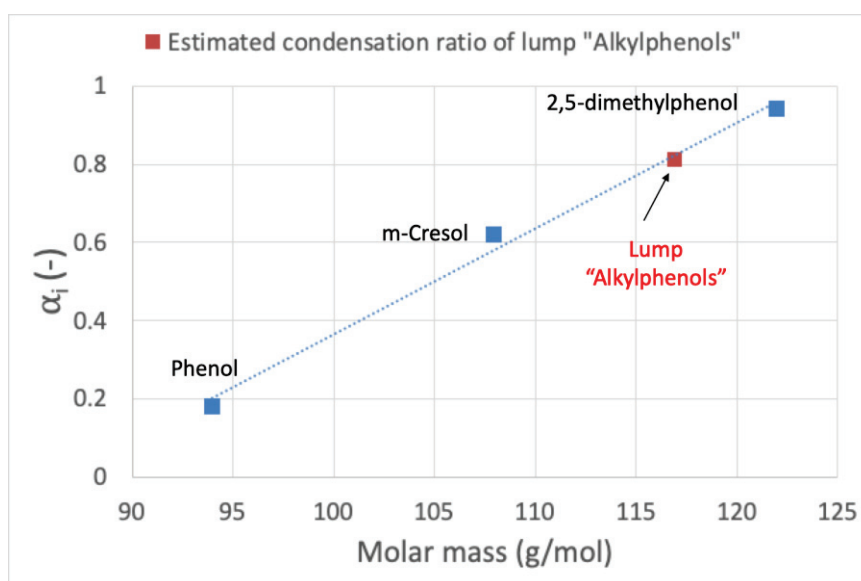


Figure VI.6: Estimation of α_i for lump "alkylphenols" by interpolation method

Cooling and depressurization periods

The assumptions and calculations for the cooling and depressurization periods in § V.3.2.2 are still suitable for this part.

VI.2.5 Model structure and parameter estimation

The schematic representation of the structure and the parameter estimation procedure of our model is the same as that presented in Figure V.18. For the parameter estimation, it requires the following experimental data as model inputs:

- The mass of the THF-insolubles, THF-solubles, solubilized oligomers and liquid lumps in the reactor for each reaction time ($13 \times 6 = 78$ experimental points).
- The mass of the liquid lumps in the separator for each reaction time ($10 \times 6 = 60$ experimental points).
- The dynamic outlet gas mass flowrate of each gas component (H_2 , CO_2 , CO , CH_4 and $\text{C}_2\text{-C}_6$) for the longest experiment of 13 h ($5 \times 224 = 1120$ experimental points).

The model outputs were the simulated compositions in the reactor and the separator at six reaction times (t_0 , 1 h, 3 h, 5 h, 9 h and 13 h) and the simulated gas outlet flows versus reaction time. The model fitting and parameter estimation were carried out using weighted least-squares method, which are given in Eq. (5.49). The level of 95 % confidence interval was addressed.

VI.3 Results and discussions

VI.3.1 Model results

Comparisons between the experimental data and model results are presented from Figure VI.7 to Figure VI.13. First of all, Figure VI.7 shows the results for the oligomeric entities. It can be observed that the yield evolutions for THF-insolubles, THF-solubles and solubilized oligomers are fairly well predicted by the model. The experimental data of solubilized oligomers was calculated by subtraction of measuring mass, leading to a wide margin of experimental error. As the reaction progressed, the THF-insolubles and THF-solubles were converted to lighter fragments so that their yield decreased. Solubilized oligomers, one of the lighter fragments, show a progressive increase with respect to reaction time.

Figure VI.8, VI.9 and VI.10 respectively compare the experimental and simulated outlet gas flow for CH_4 and CO_2 , CO and $\text{C}_2\text{-C}_6$ and H_2 . These figures show that the outlet gas flows calculated by the model are in good agreement with the experimental data.

The CO_2 and CO productions were detected at the outlet of experimental set-up before t_0 and their maximum flowrates were very close to t_0 , which proves rapid reactions below $350\text{ }^\circ\text{C}$. With regard to CH_4 , its maximum flowrate was at around 1 h and it was barely detectable at the outlet of experimental set-up after 8 h. For $\text{C}_2\text{-C}_6$, its maximum flowrate was at the same position as CH_4 , but continuous production was observed throughout the reaction.

Regarding the outlet H_2 flow, a significant decrease was observed between 0 and 1 h. This is due to the high consumption of H_2 in the reactor and the high concentrations of other gas components in the outlet flow at the beginning of the reaction. The high consumption of H_2 can be attributed to the relatively fast reactions of decarboxylation, dehydration, demethylation and demethoxylation. Subsequently, the other gas components decreased while the H_2 flow increased slowly. After 5 h, very low H_2 consumption was observed due to the shortage of reactive functional groups such as $-\text{OCH}_3$ in the lignin residues.

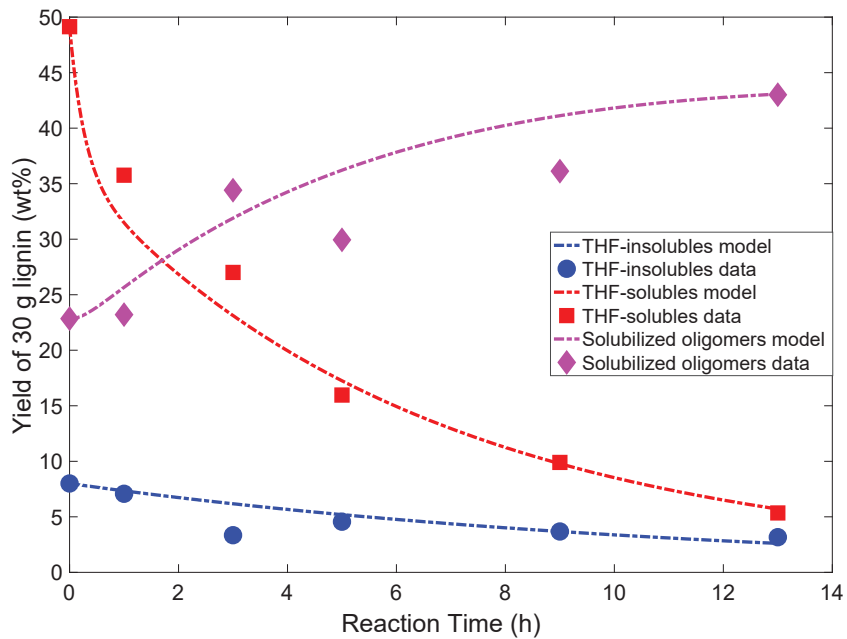


Figure VI.7: Comparison between experimental data and model results for the yield of THF-insolubles, THF-solubles and solubilized oligomers versus reaction time

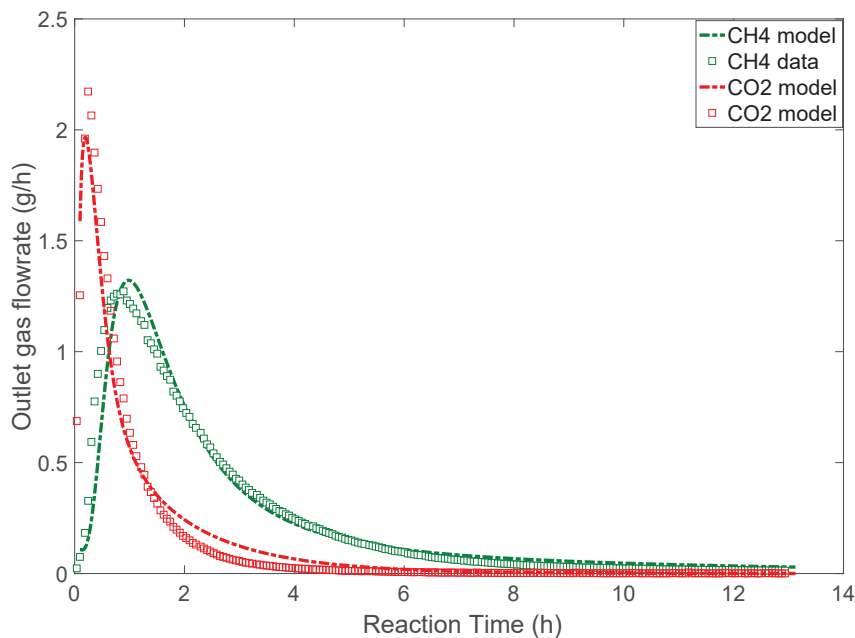


Figure VI.8: Comparison between experimental data and model results for outlet flowrate of CO_2 and CH_4 versus reaction time

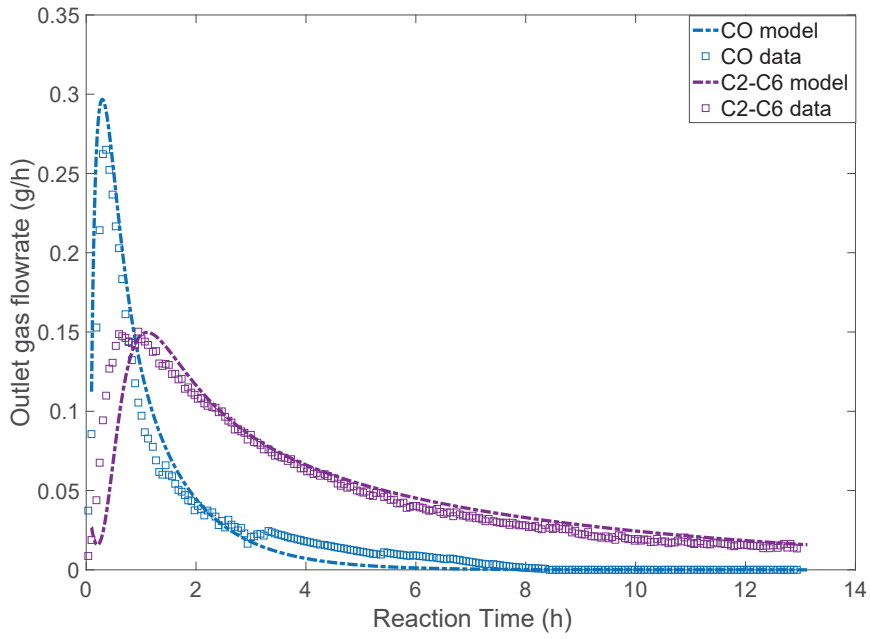


Figure VI.9: Comparison between experimental data and model results for outlet flowrate of CO and C₂-C₆ versus reaction time

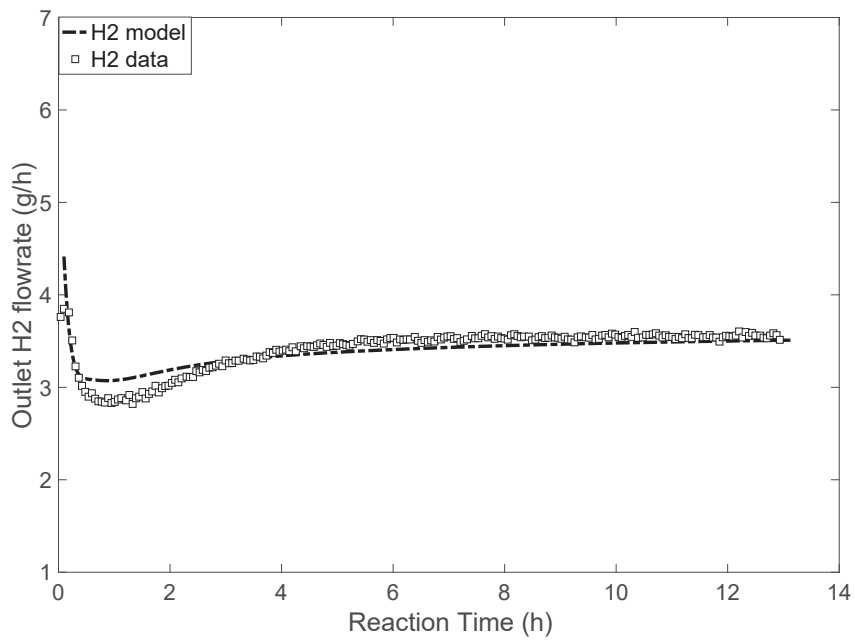


Figure VI.10: Comparison between experimental data and model results for outlet H₂ flowrate versus reaction time

Figure VI.11 compares the experimental and model results for water production. The simulated values follow the experimental data. It was observed that water formation was rapid at the beginning of the reaction and water existed both in the reactor and in the separator. After 5 h, the water production was quite slow and mainly removed from the reactor to the separator.

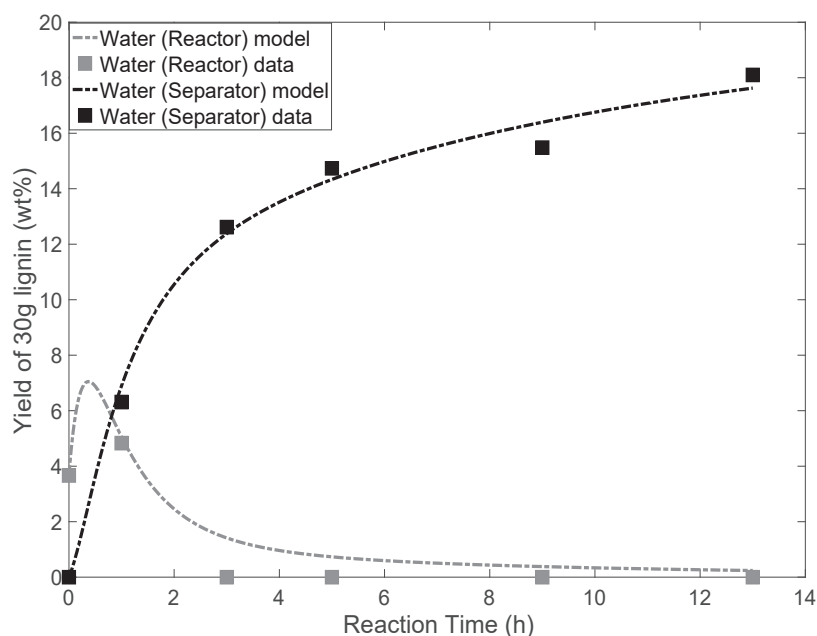


Figure VI.11: Comparison between experimental data and model results for water production versus reaction time

Figure VI.12 and VI.13 give the comparisons between the experimental and simulated liquid compositions in the reactor and the separator, respectively. The model seems to be able to predict well the conversions occurring in the reactor and the liquid accumulations in the separator. Within the reactor, dimethoxyphenols and methoxyphenols disappeared as a function of reaction time due to deoxygenation reactions. The alkylphenols show an increase before 5 h due to a high production rate, and then tend to decrease after 5 h due to a slow production rate as well as the transfer from the reactor to the separator. We also observe the increase of the yields of deoxygenated compounds such as naphthenes and aromatics, which confirms the deoxygenation of phenolic OH groups. As expected, the majority of them were found in the separator.

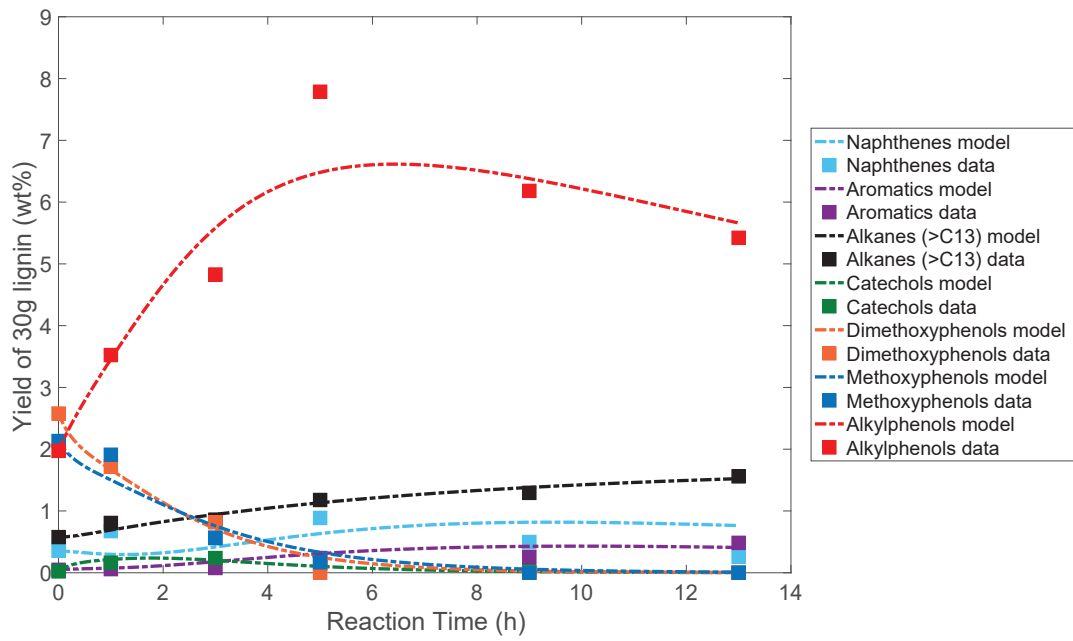


Figure VI.12: Comparison between experimental data and model results for the liquid composition in the reactor versus reaction time

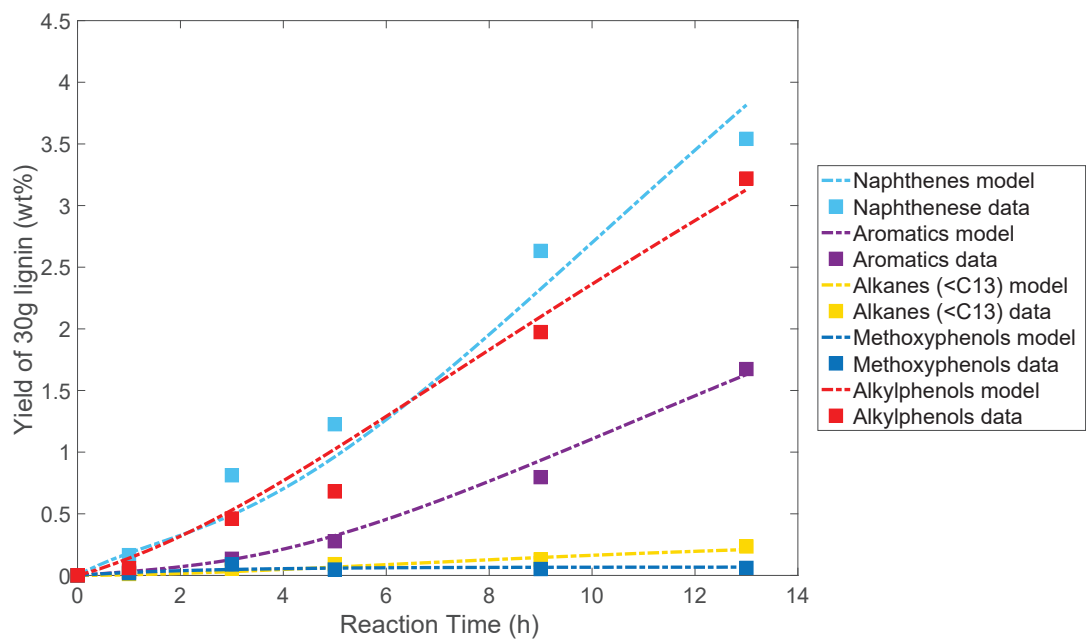


Figure VI.13: Comparison between experimental data and model results for the liquid composition in the separator versus reaction time

VI.3.2 Kinetic parameters

Table VI.5 gives the values of the estimated parameters and their confidence limits. With a 95 % confidence interval, the uncertainty of all the parameters was less than 33 %. The first three rate constants correspond to first-order reactions and the others correspond to second-order reactions, thus they have different units.

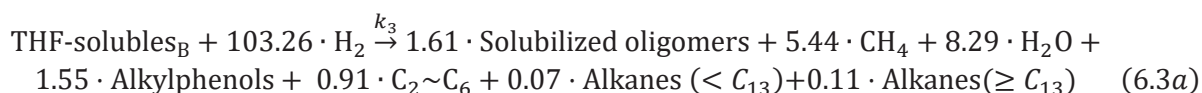
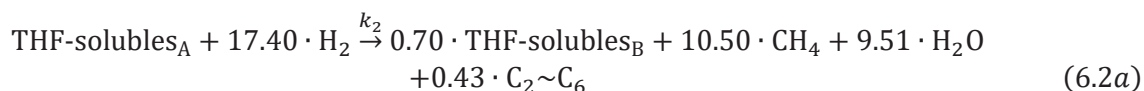
Table VI.5: Parameter estimation results of our kinetic model

Rate constant	Value	Stoichiometric coefficients	Value
k_1	$(2.40 \pm 0.10) \cdot 10^{-5} \text{ (s}^{-1}\text{)}$	$\nu_{H_2}^2$	17.40 ± 3.25
k_2	$(1.03 \pm 0.18) \cdot 10^{-3} \text{ (s}^{-1}\text{)}$	$\nu_{CH_4}^2$	10.50 ± 0.65
k_3	$(4.75 \pm 0.58) \cdot 10^{-5} \text{ (s}^{-1}\text{)}$	$\nu_{C_2C_6}^2$	0.43 ± 0.07
k_4	$(3.42 \pm 0.90) \cdot 10^{-9} \text{ (mol m}^{-3} \text{ s}^{-1}\text{)}$	$\nu_{H_2O}^2$	9.51 ± 1.01
k_5	$(1.76 \pm 0.30) \cdot 10^{-7} \text{ (mol m}^{-3} \text{ s}^{-1}\text{)}$	$\nu_{H_2}^3$	103.26 ± 16.88
k_6	$(6.25 \pm 0.02) \cdot 10^{-8} \text{ (mol m}^{-3} \text{ s}^{-1}\text{)}$	$\nu_{CH_4}^3$	5.44 ± 1.84
k_7	$(7.54 \pm 0.16) \cdot 10^{-8} \text{ (mol m}^{-3} \text{ s}^{-1}\text{)}$	$\nu_{H_2O}^3$	8.29 ± 1.89
k_8	$(3.60 \pm 0.75) \cdot 10^{-7} \text{ (mol m}^{-3} \text{ s}^{-1}\text{)}$	ν_{AP}^3	1.55 ± 0.34
k_9	$(1.04 \pm 0.11) \cdot 10^{-8} \text{ (mol m}^{-3} \text{ s}^{-1}\text{)}$	$\nu_{C_2C_6}^3$	0.91 ± 0.30
k_{10}	$(2.19 \pm 0.12) \cdot 10^{-8} \text{ (mol m}^{-3} \text{ s}^{-1}\text{)}$	ν_{AK1}^3	0.07 ± 0.01
		ν_{AK2}^3	0.11 ± 0.02

Reaction rate

Depolymerization of oligomeric entities

With the determined stoichiometric coefficients, the reaction equations concerning oligomeric entities are as follows:



We considered that the reactions of equations (6.1a), (6.3a) and (6.4a) correspond to the depolymerization of oligomeric entities. In order to compare their rate constants using the same unit, the apparent rate constant for the depolymerization of solubilized oligomers, reaction (6.4a), was calculated as follows:

$$k'_4 = k_4 \overline{C_{H_2,R}^L} \quad (6.15)$$

where $\overline{C_{H_2,R}^L}$ is the time-average concentration of H₂ in the liquid phase. Comparison of the rate constants for depolymerizing the oligomeric entities are listed in Table VI.6.

Table VI.6: Rate constants of the depolymerization of different oligomeric entities

Decomposition	Rate constant	Value (s ⁻¹)
THF-insolubles	k_1	$(2.40 \pm 0.10) \cdot 10^{-5}$
THF-solubles	k_3	$(4.75 \pm 0.58) \cdot 10^{-5}$
Solubilized oligomers	k_4'	$(2.80 \pm 0.74) \cdot 10^{-6}$

We observe that the depolymerization rates for THF-insolubles and THF-solubles are of the same order of magnitude. The depolymerization rate of THF-solubles is found to be twice as high as that of THF-insolubles, probably because of a potential catalytic effect on some small-sized THF-solubles, which accelerated the depolymerization. Furthermore, the depolymerization rate of solubilized oligomers was more than ten times lower than those of THF-insolubles and THF-solubles. This can be attributed to the fact that the size of solubilized oligomers was much reduced and it could only contain stronger C-C linkages which are more difficult to cleave, although the solubilized oligomers were supposed to be catalyzed on the surface of catalyst. The kinetic model clearly proves that the relatively stable solubilized oligomers hinder the production of more liquid monomers.

Conversion of liquid lumps

With the determined stoichiometric coefficients, the reaction equations with respect to liquid lumps are as follows:



The results of estimated rate constants for these reactions are reported in Table VI.5. The methoxy-substituted phenols (dimethoxyphenols and methoxyphenols) tend to have a rapid decomposition rate by the cleavage of the methyl C-O bonds to form catechols and alkylphenols. These three values (k_5 , k_6 and k_7) were underestimated in our model because the formation of methoxy-substituted phenols from oligomeric entities was not taken into account.

Methoxyphenols was shown to undergo two parallel routes: demethoxylation to alkylphenols (6.6a) and demethylation to catechols (6.7a). There is very little difference between the values of k_6 and k_7 , which indicates that the reaction rates of two parallel pathways are almost equal. The high rate constant of k_8 suggests that intermediate catechols were dehydroxylated easily to alkylphenols. However, sequentially, the removal OH of alkylphenols into aromatics or naphthenes is more difficult,

proven by the lowest rate constants of k_9 and k_{10} . It is suggesting that the HDO of alkylphenols is the rate-limiting step during the post-conversion of liquid monomers.

Analysis of reaction contributions to products

With the rate constants and stoichiometric coefficients for each reaction, we are able to calculate the contribution (Δn_i^j) of each reaction j to product formation and H_2 consumption as follows:

$$\Delta n_i^j = \int_{t=t_0}^{t=13\text{ h}} \nu_i^j r_j V_R^L dt \quad (6.16)$$

Here, we evaluate the formation of CH_4 and H_2O as well as the consumption of H_2 .

CH_4

Noting that CH_4 originates either from the hydrogenation of the cleaved $-OCH_3$ groups or the demethylation of $-OCH_3$ groups, its source may be the oligomeric entities or the methoxy-substituted phenols in the liquid phase. Table VI.7 gives the calculated distribution of CH_4 formation according to its source using the model.

Before t_0 , $-OCH_3$ groups were little affected under $350\text{ }^\circ\text{C}$. After reaching $350\text{ }^\circ\text{C}$, a large enhancement in the production of CH_4 was measured, especially during the first two hours when the majority was already produced (see Figure VI.9). By comparing the CH_4 yields, it was observed that the production of CH_4 from oligomeric entities was much higher than that of methoxy-substituted phenols. It can be suggested that $-OCH_3$ groups were reacted mostly by demethylation or demethoxylation reactions directly on the oligomeric entities, instead of being depolymerized into methoxy-substituted monomers followed by demethylation or demethoxylation. That is to say, the linkages of $-OCH_3$ in the lignin was easily cleaved.

Table VI.7: Calculated distribution of CH_4 formation according to its source from the model

Reaction	Duration of reaction (h)	CH_4 yield on 30 g lignin (wt%)
Before t_0	~ 0.6	0.18
(6.2a + 6.3a) THF-solubles $\rightarrow CH_4$	13	10.21
(6.5a) Dimethoxyphenols $\rightarrow CH_4$	~ 5	0.49
(6.6a + 6.7a) Methoxyphenols $\rightarrow CH_4$	~ 5	0.23

H_2O

As known, H_2O originates from OH groups (1 mole of OH produces 1 mole of H_2O) or $-OCH_3$ groups (1 mole of $-OCH_3$ leads to an equal molar production of H_2O and CH_4 or 1 mole of CH_4 and 1 mole of phenolic OH). Table VI.8 gives the calculated distribution of H_2O formation according to its source using the model.

Before t_0 , the yield of H_2O was about 3.7 wt% on lignin intake. This fraction corresponds to the aliphatic OH groups, which were dehydroxylated easily at the relatively low temperature. During the first two hours at $350\text{ }^\circ\text{C}$, H_2O was also produced largely as CH_4 (see Figure VI.13). The approximate equality of $\nu_{CH_4}^2$ and $\nu_{H_2O}^2$ in the reaction (6.2a) suggests that the demethoxylation reaction was the main reaction

occurring at this stage. The same result was also observed in the work of Joffres³, proposing that demethoxylation reaction is much favored in the presence of catalyst. As expected, the HDO reaction of phenolic OH groups into H₂O was quite slow. During 13 h, only about 1.10 wt% on lignin intake of water was produced from the alkylphenols. This production from phenolic OHs was quite lower compared to those produced from aliphatic OH and -OCH₃ groups, consistent with the fact that the HDO of alkylphenols is the rate-limiting step during the lignin hydroconversion.

Table VI.8: Calculated distribution of H₂O formation according to its source calculated from the model

Reaction	Duration of reaction (h)	H ₂ O yield on 30 g lignin (wt%)
Before t_0	0.6	3.67
(6.2a + 6.3a) THF-solubles → H ₂ O	13	12.30
(6.5a) Dimethoxyphenols → H ₂ O	~ 5	0.55
(6.6a) Methoxyphenols → H ₂ O	~ 5	0.11
(6.8a) Catechols → H ₂ O	~ 9	0.14
(6.9a + 6.10a) Alkylphenols → H ₂ O	13	1.10

Overall, the major oxygenated groups originally present in the lignin are the aliphatic OH groups, ether linkages, phenolic OH group, -OCH₃ groups and carboxylic groups. The ethers linkages, aliphatic OH groups and carboxylic groups were cleaved at the relatively low temperature and -OCH₃ exhibited a relatively high reactive activity at 350 °C, but the removal of phenolic OHs was quite slow. Therefore, regarding the oligomers and liquid monomers at 13 h, the resistant phenolic OH groups was the only remaining oxygenated groups, which is in accordance with the following experimental observations:

- Only *p*-hydrophenolic and catechol units still presented in the THF-solubles by ³¹P NMR
- Alkylphenols as the only oxygenated monomers in the liquid phase according to GC×GC analysis.

H₂

Hydrogen can not only react with the formed radicals in the carbon framework, but also participates in the hydrogenation and hydrogenolysis reactions. Table VI.9 gives the calculated distribution of H₂ consumption according to its source using the model. Compared with the value of total H₂ consumption obtained experimentally at 13 h (~1300 mmol), the model seems to overestimate the consumption of H₂. The error caused by the model may be attributed to two aspects: (1) overestimation of initial H₂ quantity in the set-up at t_0 point; (2) overestimation of H₂ consumption between 4 h and 13 h.

Before t_0 , about 0.4 mole of H₂ was consumed to serve for various reactions: stabilization of free radicals, cleavage of ether bonds, dehydroxylation of aliphatic OH groups, decarboxylation of carboxylic acid groups and saturation of aliphatic double bonds. After reaching 350 °C, these weakest linkages all disappeared while H₂ continued to stabilize the formed radicals and began to react with -OCH₃ groups and phenolic OH groups. From the distribution of H₂ consumption, it can be observed that the majority of H₂ was consumed by the oligomeric entities and that the fraction consumed by liquid monomers was quite low.

Table VI.9: Calculated distribution of H₂ consumption according to its source calculated from the model

Reaction	Duration of reaction (h)	H ₂ consumption (mmol)
Before t_0	0.6	400
(6.2a + 6.3a) THF-solubles	13	1200
(6.5a) Dimethoxyphenols	~ 5	37
(6.6a + 6.7a) Methoxyphenols	~ 5	16
(6.8a) Catechols	~ 9	6
(6.9a + 6.10a) Alkylphenols	13	25

VI.3.3 Validation of the absence of mass transfer limitation

In a heterogeneous catalyzed reaction system, mass transfer of reactants firstly takes place from the bulk fluid to the external surface of catalyst (called “external diffusion”). Then the reactants diffuse from the external surface into the pore surface within the catalyst (called “internal diffusion”), where the reactions take place. If the diffusion from the bulk fluid to the external surface of catalyst is slow, the external mass transfer becomes limited and there is an important concentration difference between the bulk fluid and the catalyst external surface. In case of slow internal diffusion competing with reactions, the concentration profile would vary across the pore, leading to an important concentration difference between the external surface and the pore surface. Thus, it is necessary to identify the mass transfer limitation and evaluate the gradient of concentration from the bulk phase to the pore surface.

With respect to the depolymerization of THF-solubles, it may be partially catalyzed on the surface of catalyst. However, this fraction of THF-solubles being catalyzed was unknown in our operating conditions, making the evaluation of mass transfer impossible. So here, we only evaluate mass transfer limitations for the reactions occurring with the liquid monomers.

External mass transfer

The external resistance fraction f_{ex} , which is a simple comparison between the apparent reaction rates and the maximal interphase mass transfer between the bulk fluid and the solid. If f_{ex} was lower than 0.05, we considered that there is no external mass transfer.

$$f_{ex} = \frac{\bar{r}_i L}{k_D C_i^L} \quad (6.17)$$

$$L = \frac{V_P}{A_P} = 3 \cdot 10^{-4} \text{ (m)} \quad (6.18)$$

where L is the characteristic length of catalyst particle, V_P is the external volume of catalyst particle and A_P is the external surface area of catalyst particle.

$$k_D = \frac{Sh \cdot D_m}{d_P} \approx 10^{-3} \text{ (m s}^{-1}\text{)} \quad (6.19)$$

where d_p is the equivalent particle size, Sh is the Sherwood number estimated using the correlation for agitated systems in the literature⁴ and D_m is the molecular diffusion coefficient. The viscosity and density of fluid was approximate to those of tetralin.

$$\bar{r}_i = \frac{\sum_{j=5}^{j=10} v_i^j k_j C_i^L C_{H_2}^L V^L}{V^S} \quad (6.20)$$

where \bar{r}_i is the apparent reaction rate of component i per unit volume of catalyst, V^L and V^S are respectively the liquid volume and the catalyst volume. The f_{ex} for all the components were less than 0.01, so we can neglect the influence of external mass transfer in our case.

Internal mass transfer

The internal resistance is evaluated by Weisz Criterion:

$$\phi'_s = \frac{\bar{r}L^2}{D_e C_i^S} \quad (6.21)$$

where D_e is the effective diffusion coefficient and C_i^S is the concentration of component i on the external surface which is nearly equal to C_i^L in the absence of external mass transfer limitation. The ϕ'_s for all the components were less than 0.05. If ϕ'_s is lower than 0.1, the internal resistance is negligible. Therefore, the influence of internal mass transfer can be also neglected.

VI.4 Conclusion

The chapter provides a kinetic model for catalytic lignin hydroconversion over sulfided CoMo/Al₂O₃ based on experiments carried out in our semi-batch pilot. The model was built on a lumped reaction network, combined with the hydrodynamic, mass transfer and thermodynamic characteristics. It maintains the positive aspects of lumped models, such as relative simplicity and a direct relationship with measured data, whilst incorporating more reaction pathways than other kinetic modeling works. The results of model fit relatively well with the experimental data, elucidating the depolymerization of lignin oligomeric entities as well as the transformations occurring in the liquid phase.

The resulting kinetic model allows an in-depth understanding of lignin conversion mechanisms. By comparison of the estimated kinetic parameters, the model clearly shows the bottlenecks of lignin depolymerization. It reveals that the formed solubilized oligomers were relatively stable at the operating conditions, hindering the release of more liquid monomers. With respect to the transformations of liquid monomers, it has been proven that the HDO reaction of phenolic OH groups is the rate-limiting step. Furthermore, we found that the oligomeric entities are the main contributor to the formation of CH₄ and H₂O, and the main consumer of H₂.

As a result, the effort on the lignin conversion should be focused more on the deeper conversion of the soluble oligomeric fraction present in the liquid phase in order to maximize the monomers yield, as well as on how to accelerate the HDO reactions to obtain more deoxygenated compounds.

Reference-VI

[1] Zwietering, T.N., 1958. Suspending of solid particles in liquid by agitators. Chemical Engineering Science 8, 244–253.

[2] Joffres, B., Lorentz, C., Vidalie, M., Laurenti, D., Quoineaud, A.-A., Charon, N., Daudin, A., Quignard, A., Geantet, C., 2014. Catalytic hydroconversion of a wheat straw soda lignin: Characterization of the products and the lignin residue. *Applied Catalysis B : Environmental* 145, 167–176.

[3] Joffres, B., 2013. Synthèse de bio-liquide de seconde génération par hydroliquéfaction catalytique de la lignine. PhD thesis, Université Claude Bernard Lyon 1.

[4] Armenant, P.M., Kirwan, J.K, 1989. Mass transfer to microparticles in agitated systems. *Chemical Engineering Science* 44, 2781-2796.

Conclusion and Perspectives

Conclusion

With the depletion of fossil fuels as a source for fuels, chemicals, and energy, the fraction of energy and chemicals supplied by renewable resources such as biomass can be expected to increase in the near future. Among these resources, lignin holds considerable potential as a renewable resource for the production of fuels and platform chemicals thanks to its unique aromatic structure. Currently, only 5 wt% of lignin that are available from the pulp and paper industry are used commercially for the production of lignin-based materials, while the remainder (95 wt%) is simply burned as a low-value fuel. However, being the only renewable aromatic-based resource, a wide variety of bulk and fine aromatic chemicals can potentially be derived from lignin by depolymerization.

In the literature, different thermochemical pathways have been proposed to convert lignin into the valuable chemicals. It appears that lignin hydroconversion under H_2 pressure using a hydrotreating catalyst in the presence of a H-donor solvent could be a most promising way to get high yields of liquid products. The combination of thermal degradation and stabilization of free radicals by molecular hydrogen and H-donor solvent can avoid severe condensation reactions so as to increase the liquid yield. With the participation of well-chosen catalysts, it has been reported that the depolymerization of lignin and the hydrogenolysis/hydrogenation reaction occurred, resulting in a high yield of deoxygenated monomers.

Experimental study

In this study, a wheat straw soda lignin (P1000) was taken as the starting materials to perform hydroconversion under H_2 pressure at 350 °C and in the presence of tetralin with a sulfided CoMo catalyst on Al_2O_3 in a semi-batch reactor. Firstly, the initial lignin was deeply characterized with advanced spectroscopic and chromatographic techniques in order to get the initial organic functions in lignin and the size of lignin. Secondly, lignin hydroconversion experiments were performed from t_0 (time at which the temperature was reached) to 13 h. After each reaction time, four product fractions were recovered: a THF-non-extractible solid lignin residue (THF-insolubles), a THF-extractible solid lignin residue (THF-solubles), gases (CO_2 , CO, CH_4 , C_2-C_6) and liquids (H_2O , monomers and some solubilized oligomers). The quantified and detailed analyses for each fraction were performed with appropriate analytical techniques. The formed gas was analyzed by μGC -TCD and quantified by Coriolis meter. Regarding the lignin residues, they were characterized by NMR techniques to follow the evolution of characteristic functions, and characterized by GPC to follow the evolution of the size of lignin residues. For the liquids, the monomers were identified by GC \times GC-MS and quantified by GC \times GC-FID. By analyzing the evolution of these fractions versus reaction time, we were able to follow the reactions occurring during the conversion.

At the early stage of reaction, the weak ether bonds in lignin were cleaved, creating lignin residues with shorter chains, which is then transferred to THF-soluble or solubilized oligomers. The lignin and lignin residues were decarboxylated and dehydroxylated, accompanied by the formation of CO_2 and water. In addition, a certain amount of phenolic monomers (mostly methoxy-substituted) was released into the liquid phase. In a second step, the lignin residues became shorter and were deoxygenated due to the reactions of demethoxylation, demethylation and dehydroxylation of phenolic OH. As a result, CH_4 and H_2O were largely formed during the period. Meanwhile, a deep deoxygenation was also observed for liquids. After the longest reaction time (13 h), we found only alkylphenols, aromatics,

naphthenes and heavy linear alkanes as well as deeply deoxygenated soluble oligomers in the liquid phase. The presence of heavy linear alkanes coming from the hydrogenation of the impurities of fatty acids esters was confirmed. Based on all the experimental observations, a reaction scheme usable for the following kinetic model has been proposed.

The characterization of used catalyst showed that the main changes of catalyst occurred at the early stage of reaction and then the catalysts properties remained stable. The sulfided CoMoS/Al₂O₃ used allowed to convert the lignin fragment by hydrodeoxygenation as previously observed with guaiacol HDO study without strong deactivation. Finally, it has been shown that, compared to the traditional batch system, the H₂-fed semi-batch reactor can accelerate the lignin conversion due to less H₂ limitation.

Kinetic model

On the basis of the experimental results, it was found that reaction products from lignin hydroconversion were able to regrouped into lumps according to their states and functional groups. Hence, a lumped kinetic approach was chosen to simulate the process of lignin hydroconversion in our semi-batch reactor.

To proceed our kinetic model, these key steps have been realized step-by-step:

- The lignin feedstock description and the reaction network were obtained in the experimental part.
- The characteristic of set-up in which the reactions take place was studied under the operating condition, including the gas hydrodynamics and the G/L mass transfer.
- Based on our reaction mixtures, a suitable thermodynamic VLE model (PSRK model) was chosen to illustrate the phase distribution under the operating conditions.

Then, the material balances for our semi-batch pilot were established with the combinations of hydrodynamics, mass transfer, VLE and reaction rate equations. A set of differential and algebraic equations were constructed, which can describe the dynamic variations of compounds in each element of our semi-batch reactor. By the parameter estimation method, the resulting kinetic model can fit relatively well with experimental data. The kinetic model can elucidate the depolymerization of lignin as well as the transformations occurring in the liquid phase. The kinetic parameters obtained such as rate constants and stoichiometric coefficients for each reaction step involved in the lignin hydroconversion can help us better understand of lignin conversion mechanisms.

By comparison of the estimated kinetic parameters, the kinetic model clearly shows the bottlenecks of lignin hydroconversion. On one hand, it reveals that the formed solubilized oligomers were relatively stable under the operating conditions, hindering the release of more liquid monomers. On the other hand, with respect to the transformations of liquid monomers, it has been proven that the HDO reaction of phenolic OH groups is the rate-limiting step.

After 13 h, two experimental observations were noticed in accordance with the kinetic model:

- A significant part (about 40 wt%) of solubilized oligomers were found in the liquid phase, which appeared to be quite resistant under the operating conditions.
- Both for lignin residues and liquids, phenolic OHs were the only remaining oxygenated groups.

Consequently, the experimental observation and the kinetic model both reveal that, if we aim to obtain more deoxygenated monomers, the effort on the lignin conversion should be focused on the following two points:

- Maximize the monomers yield by a deeper conversion of the soluble oligomeric fraction present in the liquid phase
- Obtain more deoxygenated monomers by finding a better catalyst to accelerate HDO reactions

Perspectives

With the objective of higher yield of BTX, the current methodology of the experimental study in combination of kinetic modeling in this thesis can be easily used by varying the operating conditions:

- ✓ Lignin feedstock: Different lignins with various chemical composition.
- ✓ Temperature: As we know, an increase in temperature can increase reaction rates. However, the condensation of free radicals can occur severely under higher temperature. So, it will be quite interesting to study the effect of temperature on reaction rates in order to find an optimal temperature to get higher BTX yield.
- ✓ Pressure: The increase in pressure can increase the dissolved H_2 in the liquid phase, may leading to higher HDO reaction rates.
- ✓ Inlet H_2 flowrate: An optimization of inlet H_2 flowrate can be performed not only for the conversion performance, but also for an economy purpose.
- ✓ Catalysts: Considering the low rate of HDO reactions over $CoMoS/Al_2O_3$, this may suggest that more catalyst screening can be performed to find the most efficient catalyst for HDO reactions in those conditions.

For the future work of kinetic modeling, the following points might be involved:

- ✓ It might be interesting to investigate the temperature influence on the kinetic parameters, and to integrate the Arrhenius's Law in the chemical kinetics in order to obtain a generalized kinetic model over a wide temperature range.
- ✓ With the development of knowledge on lignin itself and lignin residues, it might be interesting to incorporate all the structural information in a further kinetic model.

Annex

Annex 1 ^1H spectra of THF-solubles at different reaction times

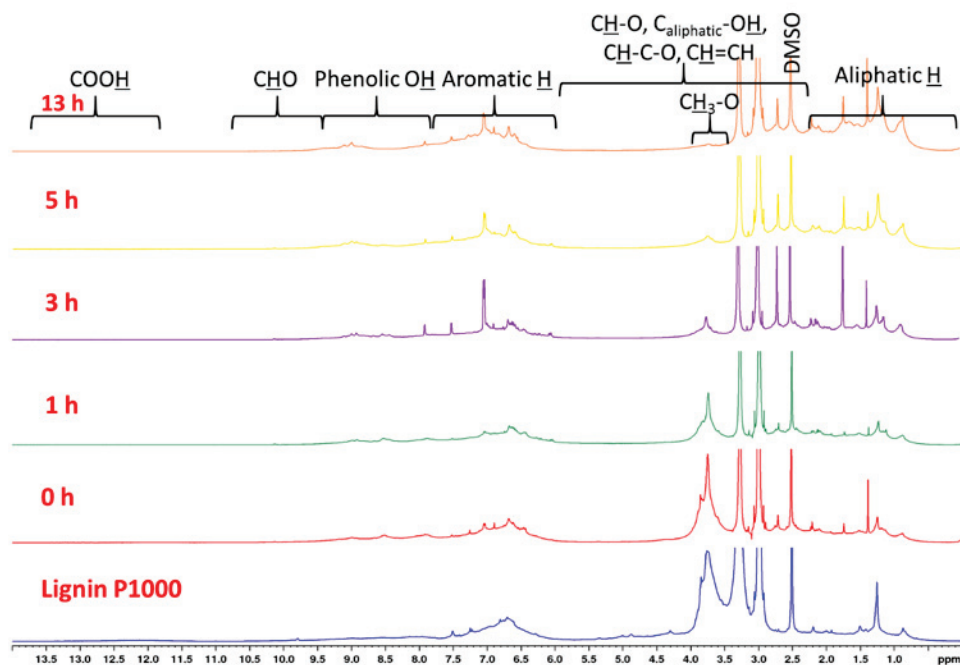


Figure A.1: ^1H spectra of THF-solubles in function of reaction time

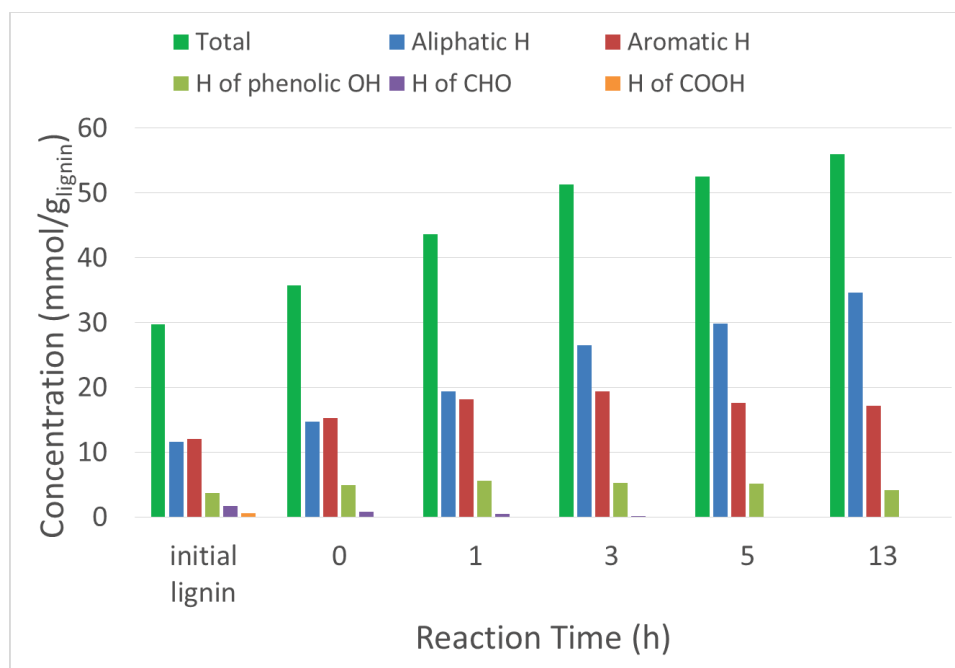


Figure A.2: Quantification by ^1H NMR of THF-solubles as a function of reaction time

Annex 2 ^{13}C spectra of THF-solubles at different reaction times

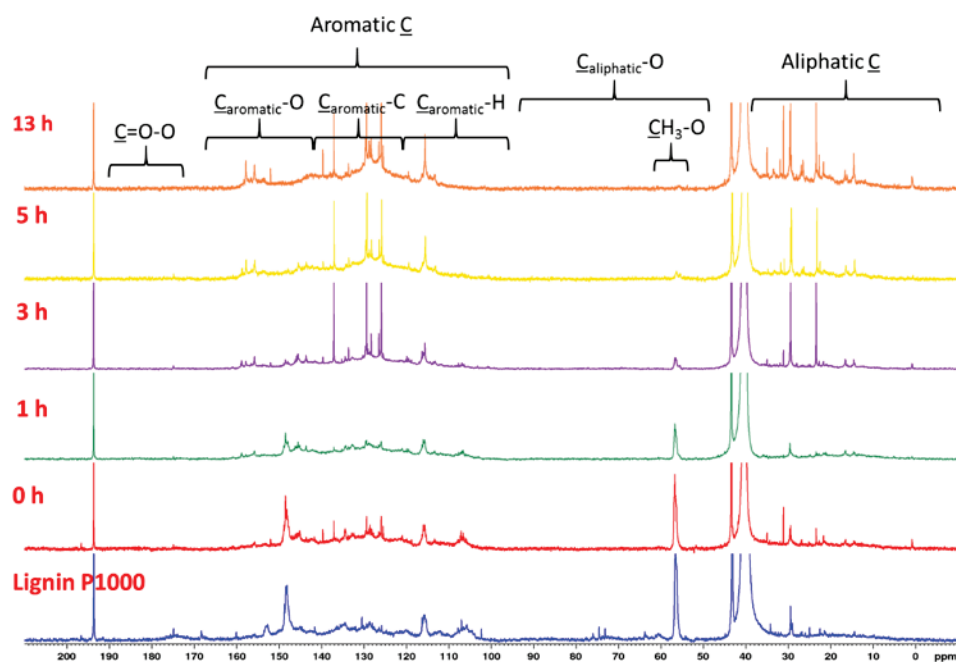


Figure A.3: ^{13}C spectra of THF-solubles in function of reaction time

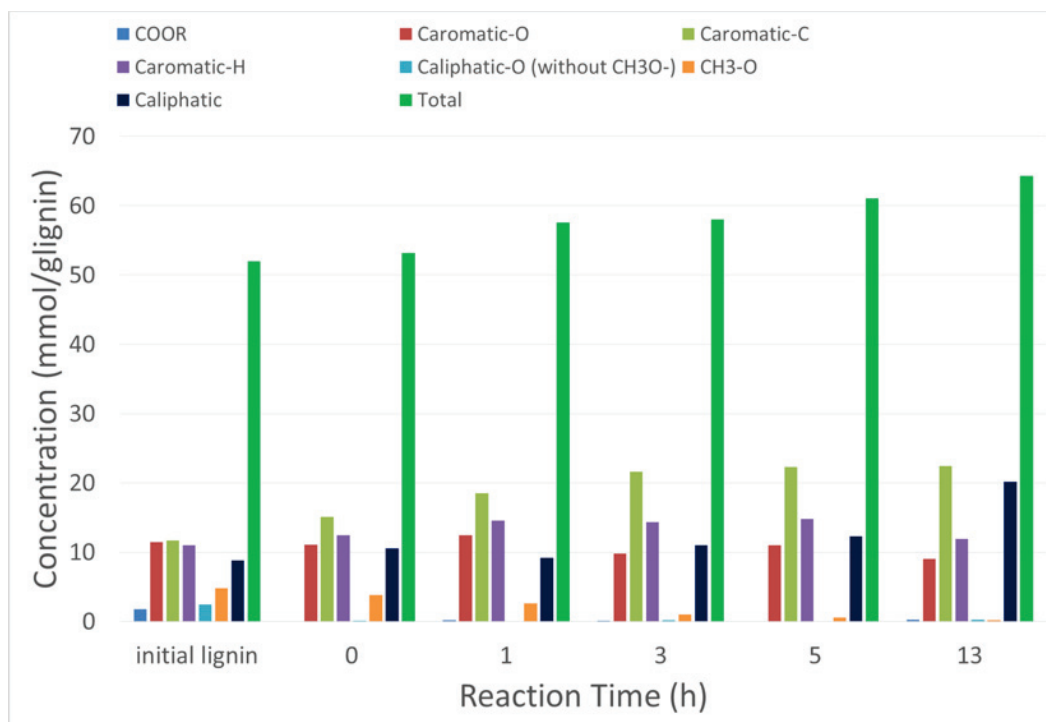


Figure A.4: Quantification by ^{13}C NMR of THF-solubles as a function of reaction time

Annex 3 ^{31}P spectra of THF-solubles at different reaction times

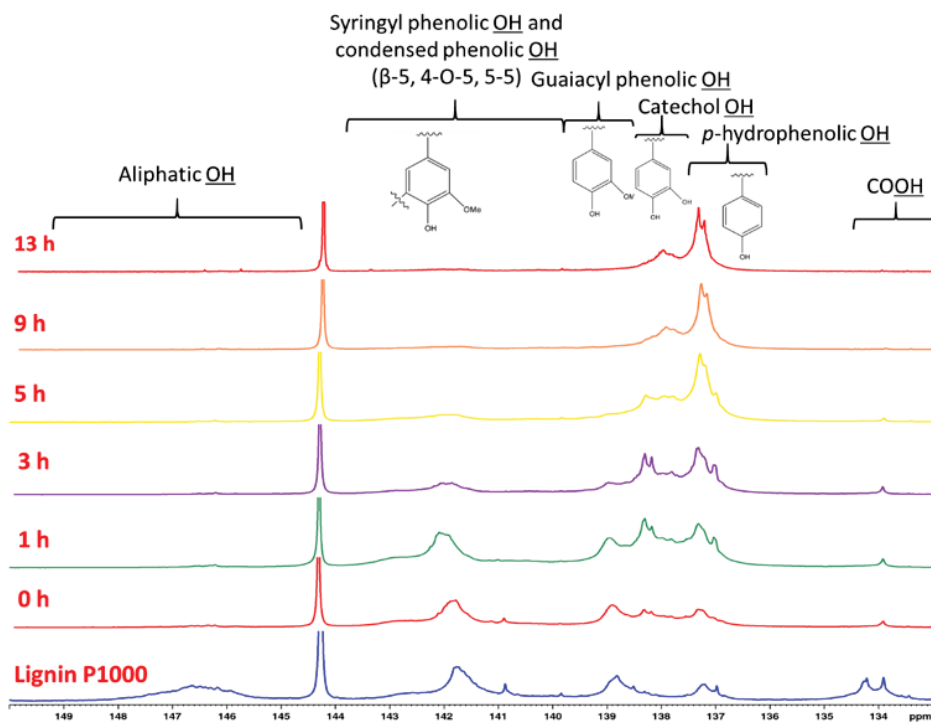


Figure A.5: ^{31}P spectra of THF-solubles in function of reaction time

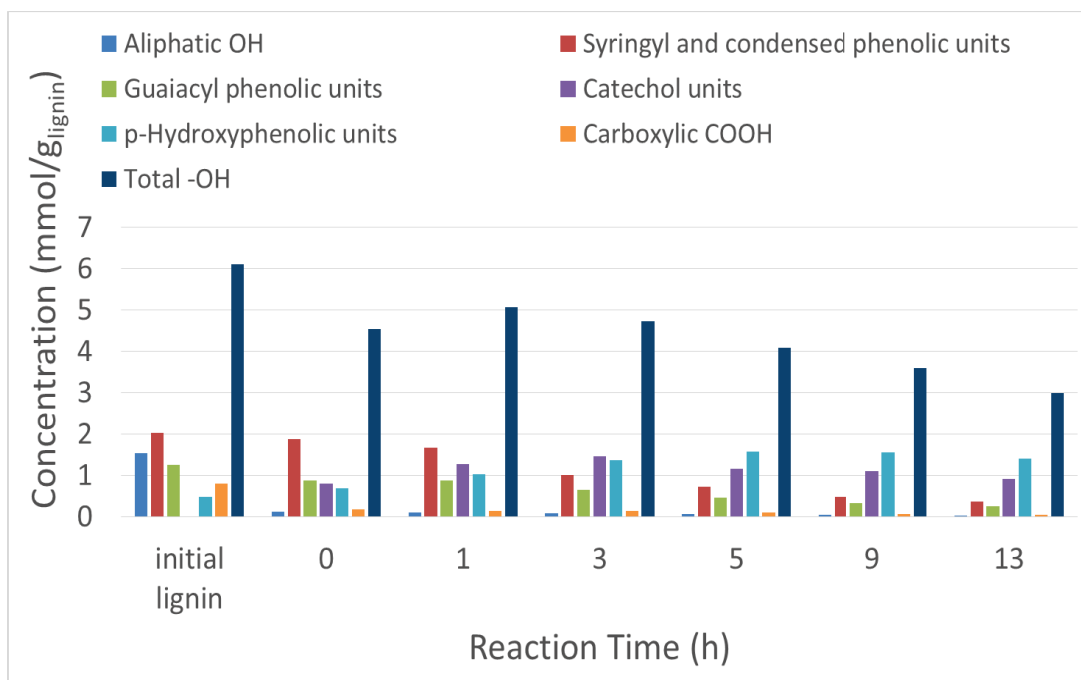


Figure A.6: Quantification by ^{31}P NMR of THF-solubles as a function of reaction time

Annex 4 Comparisons between THF-solubles and precipitated lignin-type residue

Table A.1: Elemental composition of THF-solubles and precipitated lignin-type residue in function of reaction time

	THF-soluble lignin				Precipitated lignin			
Reaction time (h)	3	5	9	13	3	5	9	13
C	78.6	80.9	82.5	81.8	77.8	80.5	82.1	83.6
H	6.7	7.0	7.4	7.5	6.9	7.2	7.0	7.3
O	14.4	11.4	10.1	9.5	14.3	11.8	11.1	9.2
N	1.1	1.3	1.3	1.3	1.0	1.2	1.3	1.4
S	0.1	0.1	0.1	0.1	0.2	0.1	0.11	0.0
Total	100.9	100.8	101.3	100.2	100.2	100.8	101.6	101.6
Atomic ratio								
H/C	1.02	1.04	1.07	1.10	1.07	0.08	0.03	1.05
O/C	0.14	0.11	0.09	0.09	0.14	0.11	0.10	0.08

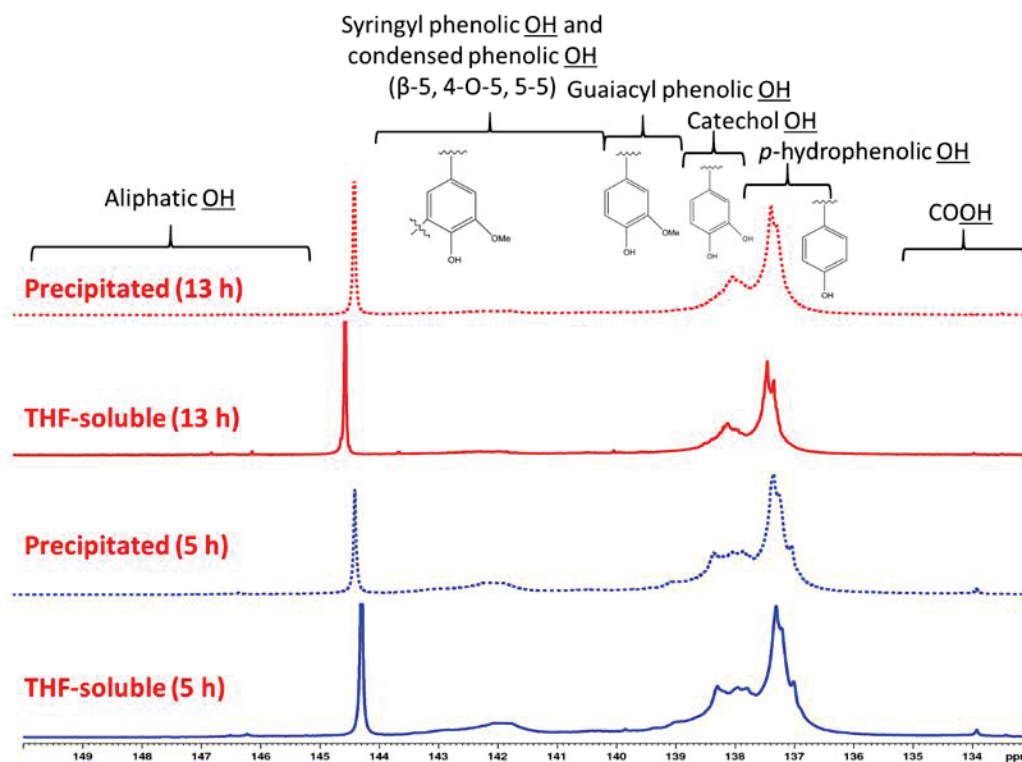


Figure A.7: ^{31}P spectra of THF-solubles and precipitated lignin-type residue at 5 h and 13 h

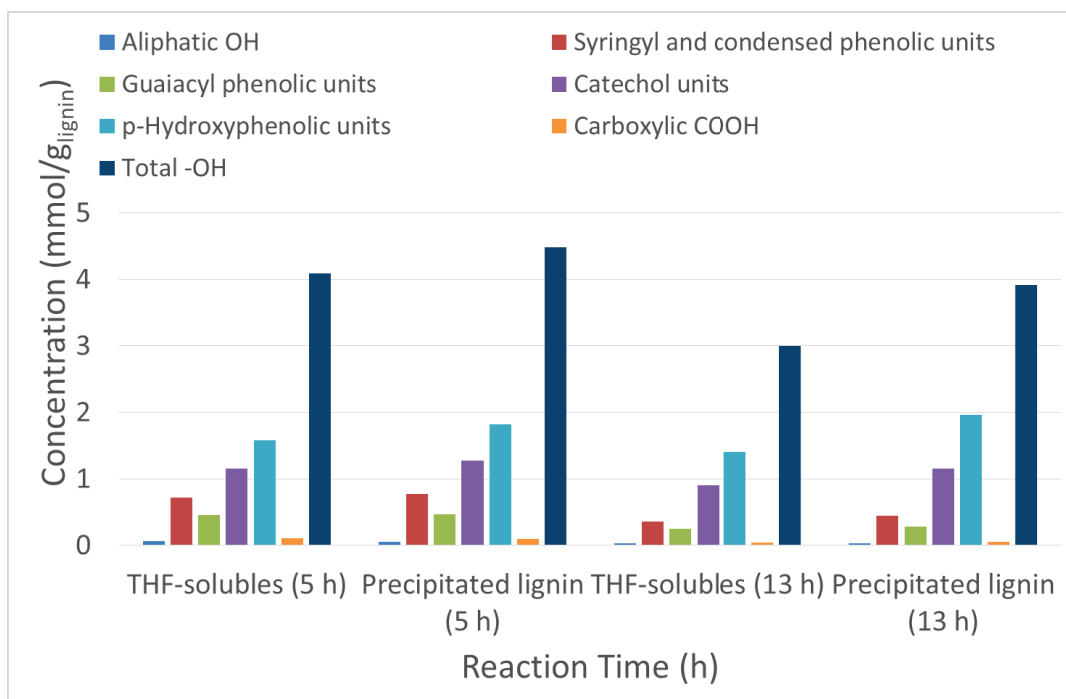


Figure A.8: Quantification by ^{31}P NMR of THF-soluble and precipitated lignin after the reaction of 5 h and 13 h

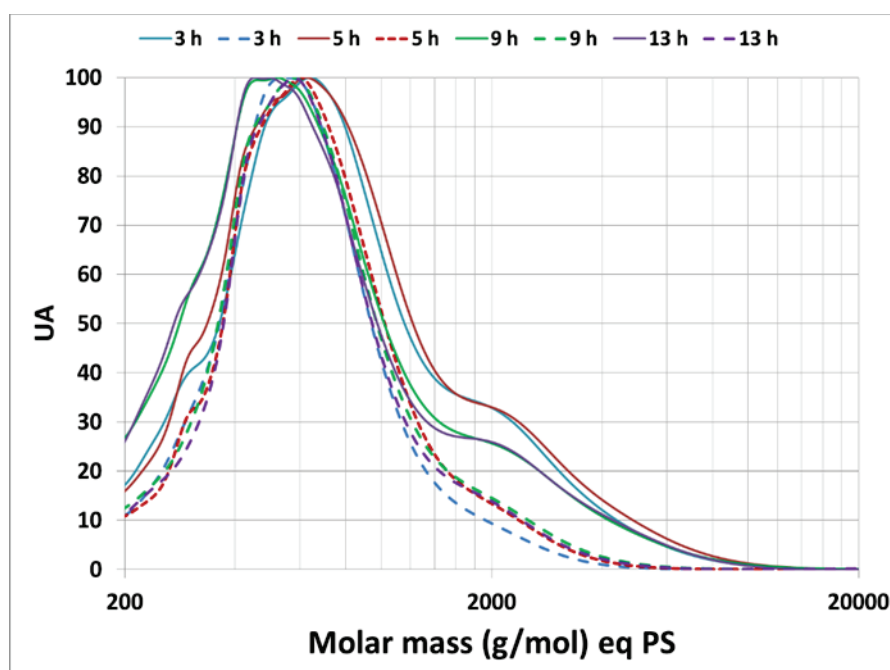


Figure A.9: GPC curves of THF-soluble and precipitated lignin as a function of reaction time (solid line: THF-solubles; dash line: precipitated lignin)

Annex 5 Quantitative data of different alkyl substituents in each family of products
(Reactor)

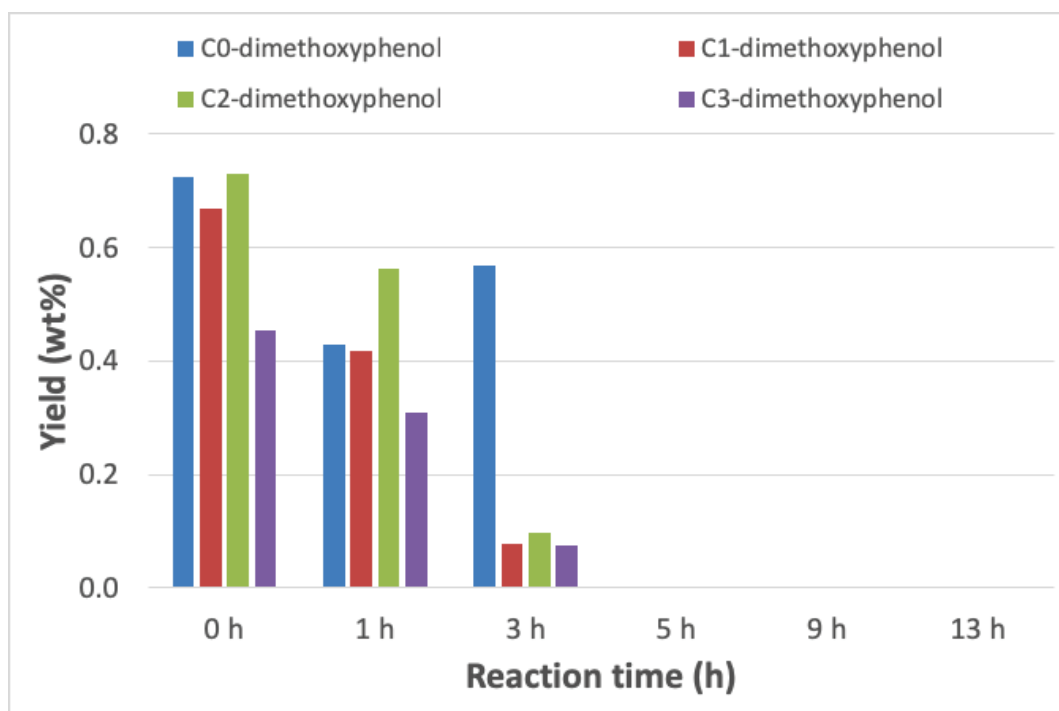


Figure A.10: Yield of different dimethoxyphenols in the reactor as a function of reaction time

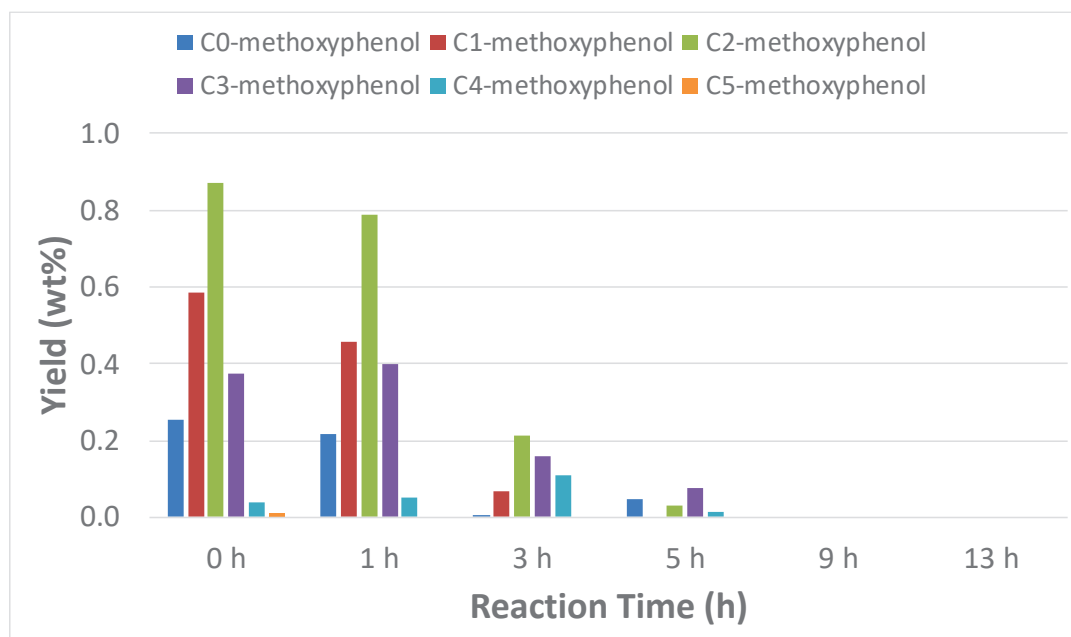


Figure A.11: Yield of different methoxyphenols in the reactor as a function of reaction time

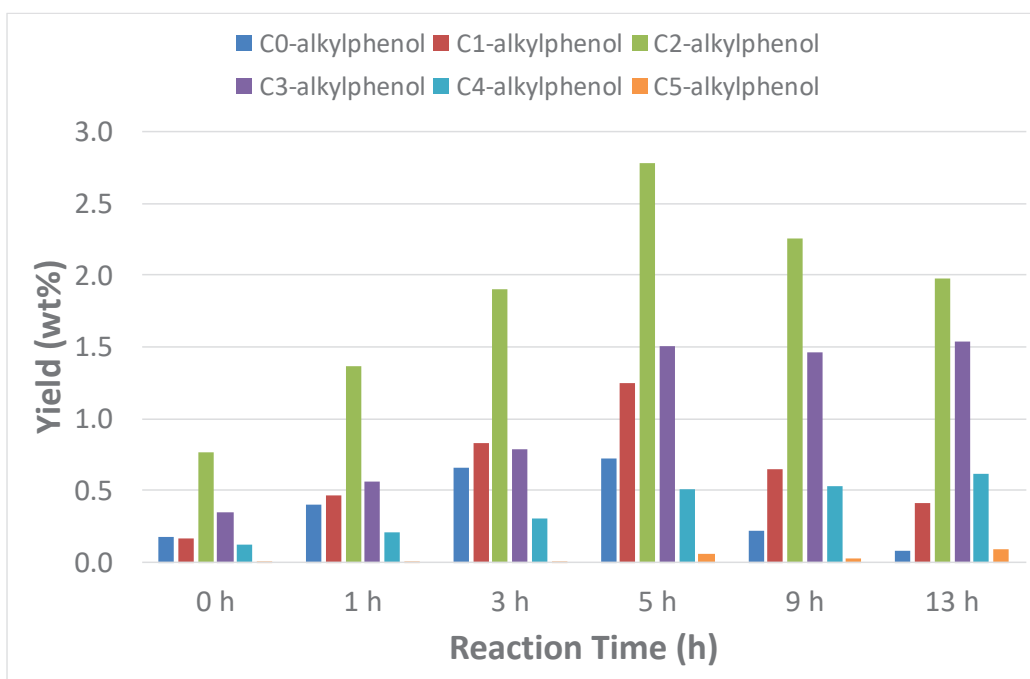


Figure A.12: Yield of different alkylphenols in the reactor as a function of reaction time

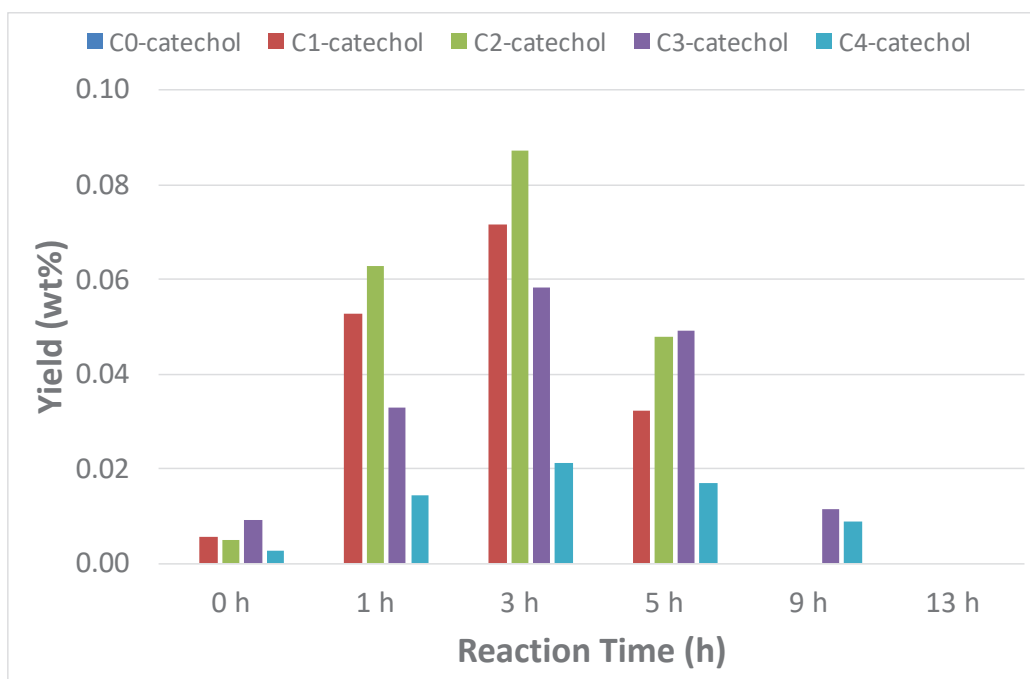


Figure A.13: Yield of different catechols in the reactor as a function of reaction time

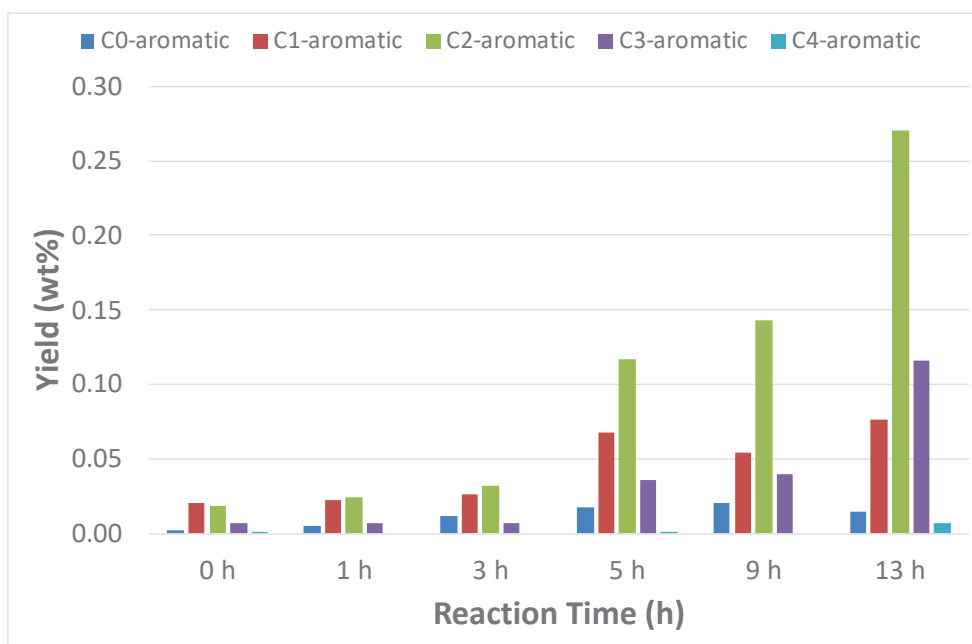


Figure A.14: Yield of different aromatics in the reactor as a function of reaction time

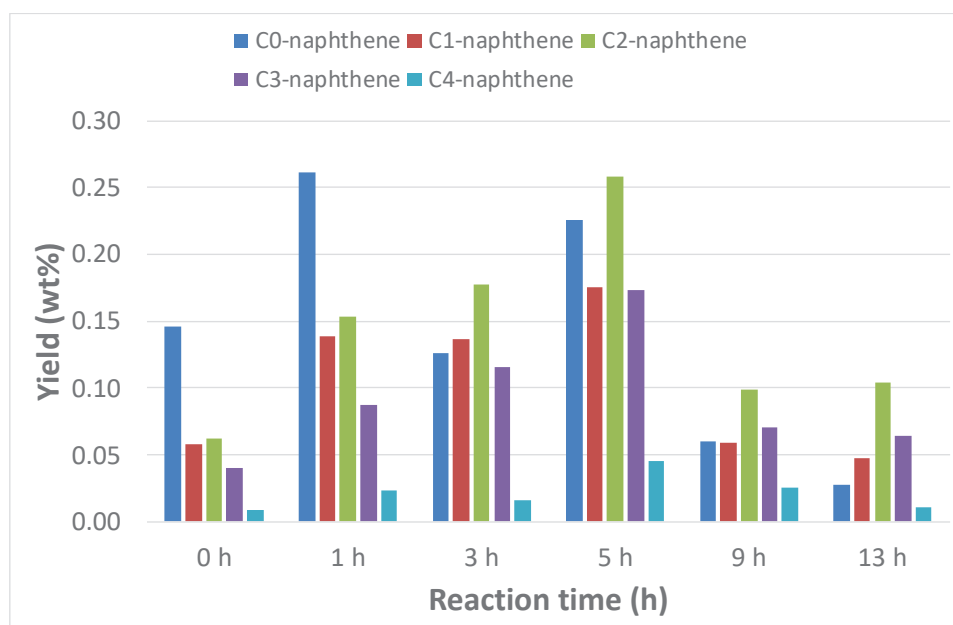


Figure A.15: Yield of different naphthenes in the reactor as a function of reaction time

Annex 6 Quantitative data of different alkyl substituents in each family of products
(Separator)

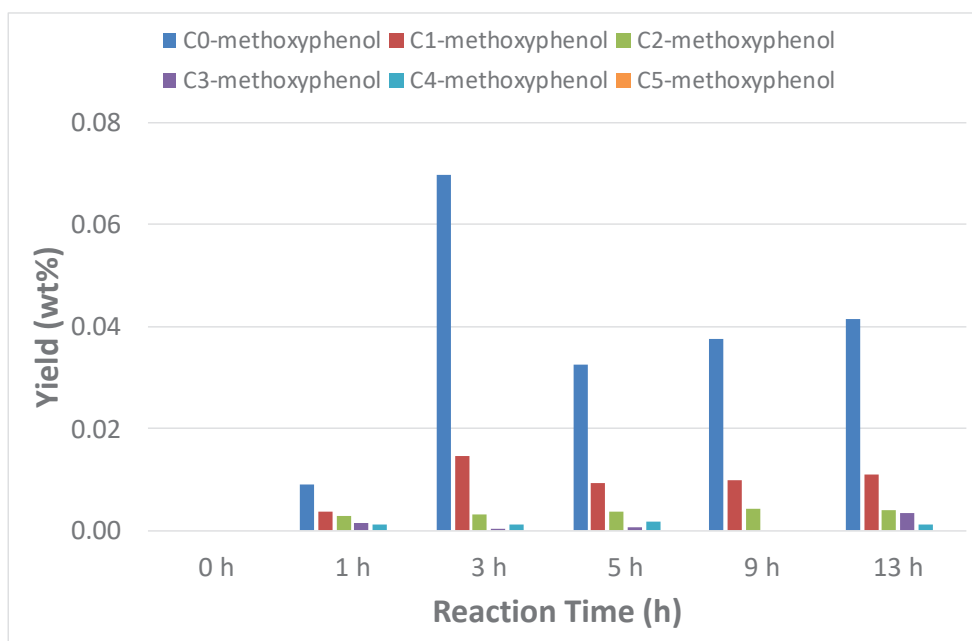


Figure A.16: Yield of different methoxyphenols in the separator as a function of reaction time

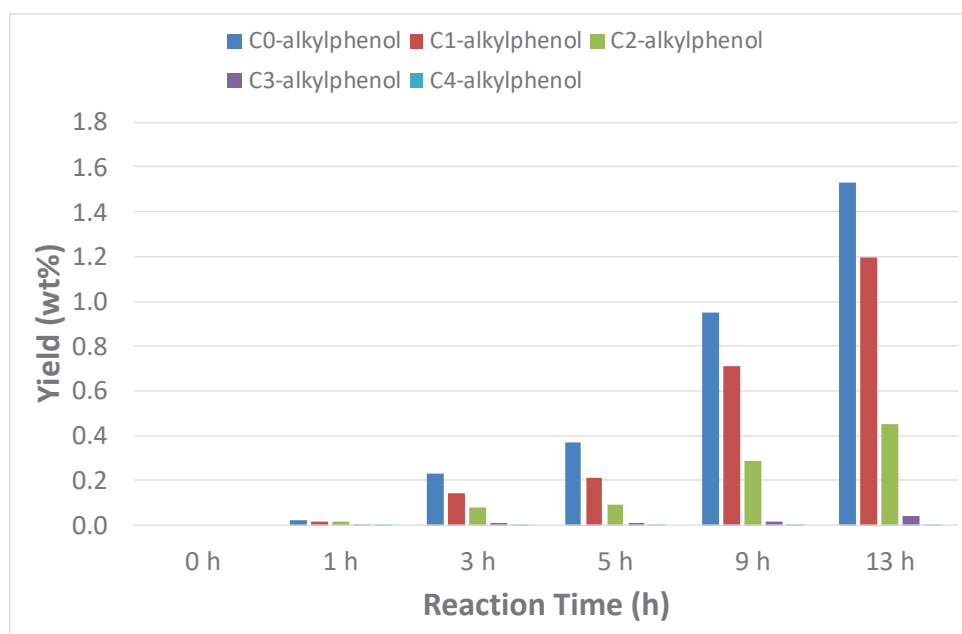


Figure A.17: Yield of different alkylphenols in the separator as a function of reaction time

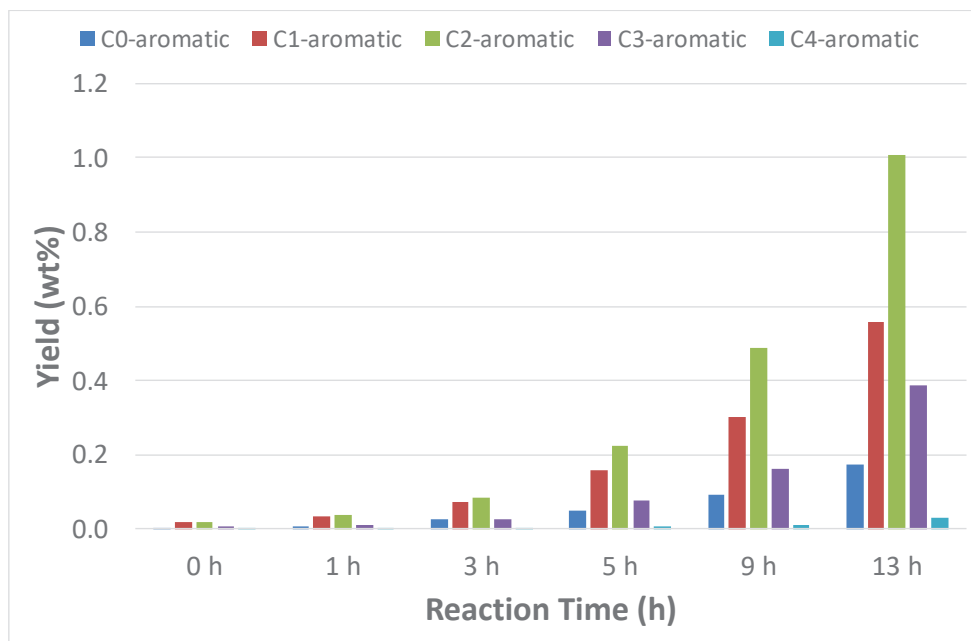


Figure A.18: Yield of different aromatics in the separator as a function of reaction time

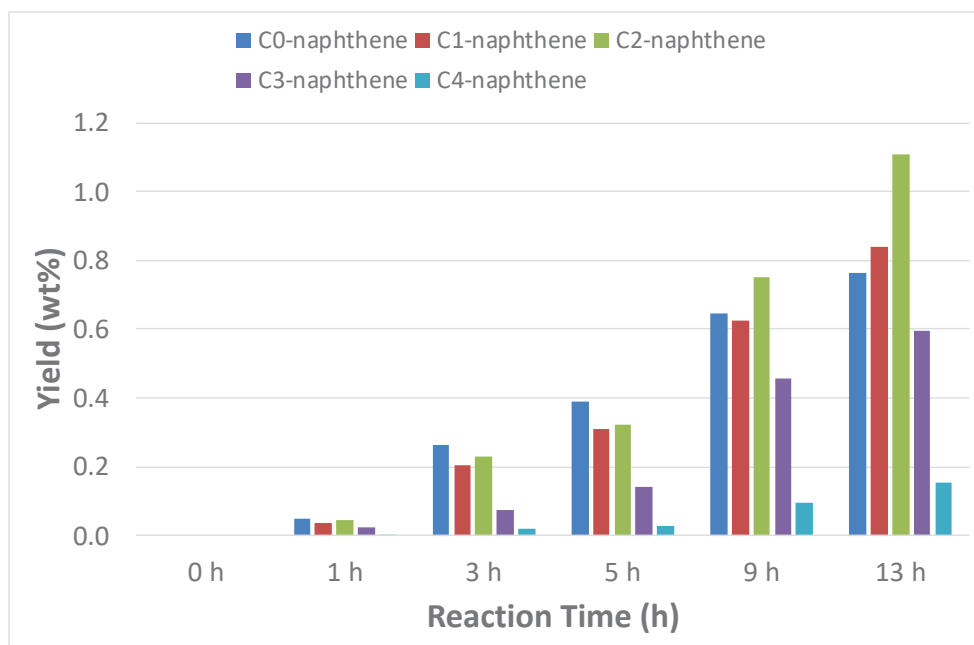


Figure A.19: Yield of different naphthenes in the separator as a function of reaction time

Annex 7 Characterization of the used catalysts

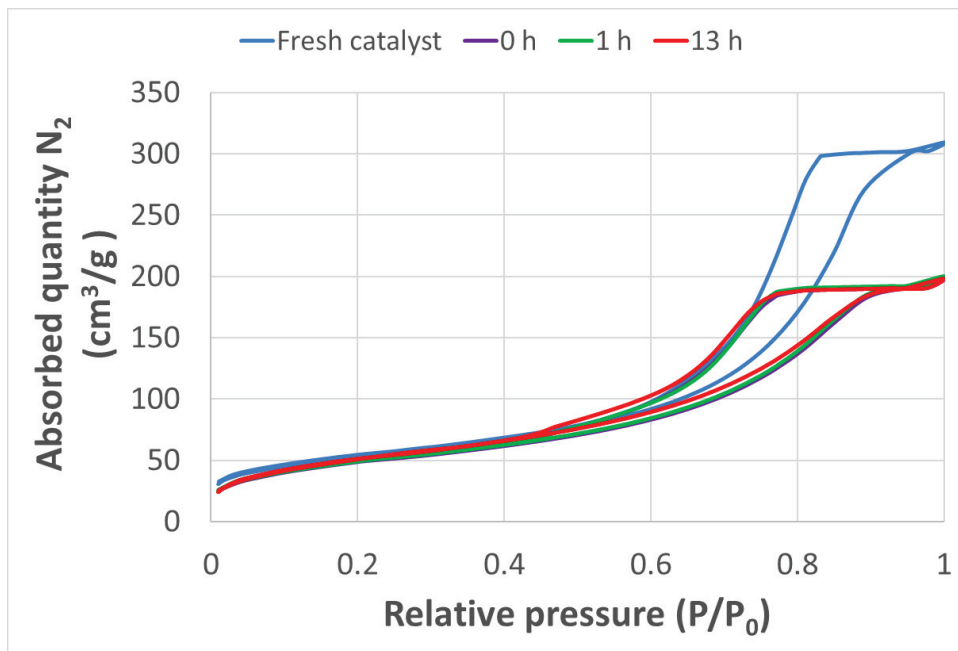


Figure A.20: Evolution of N_2 -adsorption isotherm curves of the CoMoS catalyst at different reaction times

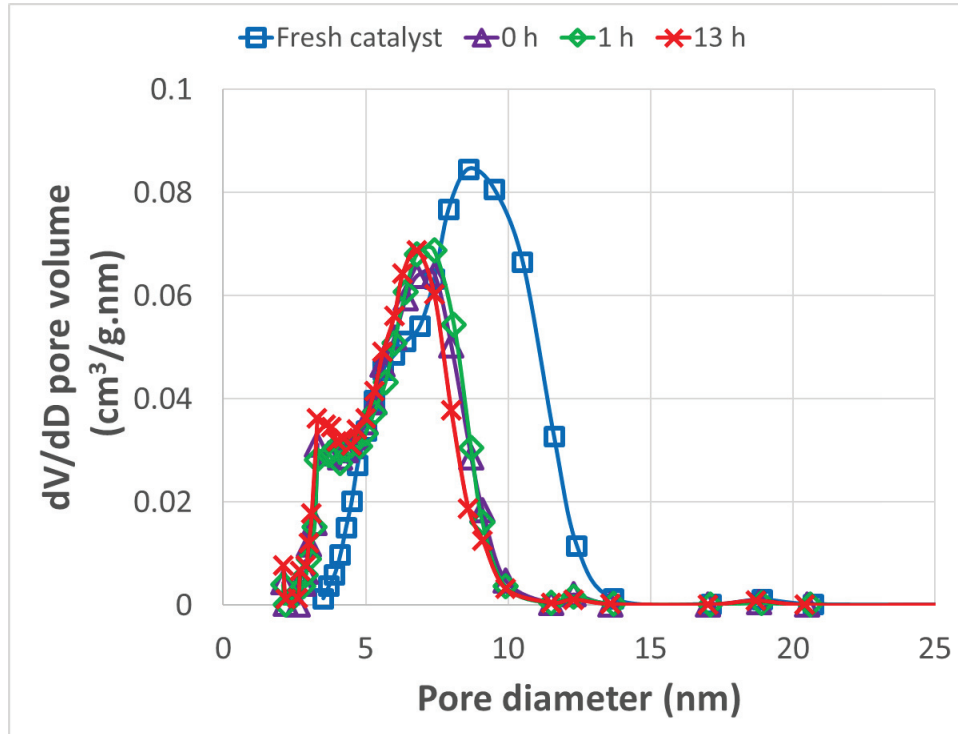


Figure A.21: Evolution of BJH Desorption dV/dD pore volume of the CoMoS catalyst at different reaction times

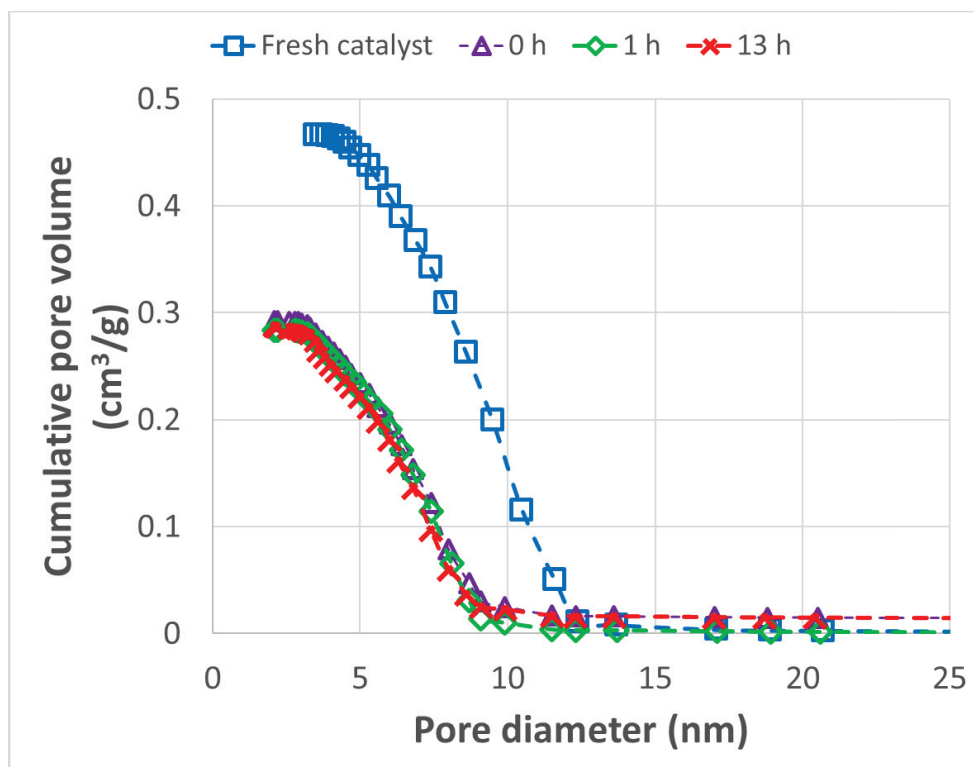


Figure A.22: Evolution of BJH Desorption cumulative pore volume of the CoMoS catalyst at different reaction times

Annex 8 Detailed description of PSRK model

The PSRK model is based on a combination of SRK equation with a mixing rule whose parameters are determined by the UNIFAC method.

Equation of SRK with the function of Mathias-Copeman:

$$P = \frac{RT}{V_m - b} - \frac{a\alpha(T)}{V_m(V_m + b)}$$
$$a = \frac{0.42747R^2T_c^2}{P_c}$$
$$b = \frac{0.08664RT_c}{P_c}$$
$$\alpha(T) = [1 + c_1(1 - \sqrt{T_r}) + c_2(1 - \sqrt{T_r}) + c_3(1 - \sqrt{T_r})]^2$$
$$T_r = \frac{T}{T_c}$$

where P is the pressure, T is the temperature, V_m is the molar volume, T_c and P_c are the temperature and pressure at the critical point, c_1 , c_2 and c_3 are the parameters of Mathias-Copeman function.

The PSRK mixing rules calculates the parameter a and b of the equation of state by:

$$a = \sum_i x_i a_i + \frac{1}{q_1} \left[\frac{G_0^E}{RT} + \sum_i x_i \ln \frac{b}{b_i} \right]$$
$$b = \sum_i x_i b_i$$

where a_i and b_i are those of the pure substances, x_i is the molar fraction, G_0^E is the excess Gibbs energy which is calculated by the predictive activity coefficient model based on group contribution UNIFA model.

The PSRK group matrix is shown in Figure A.23.

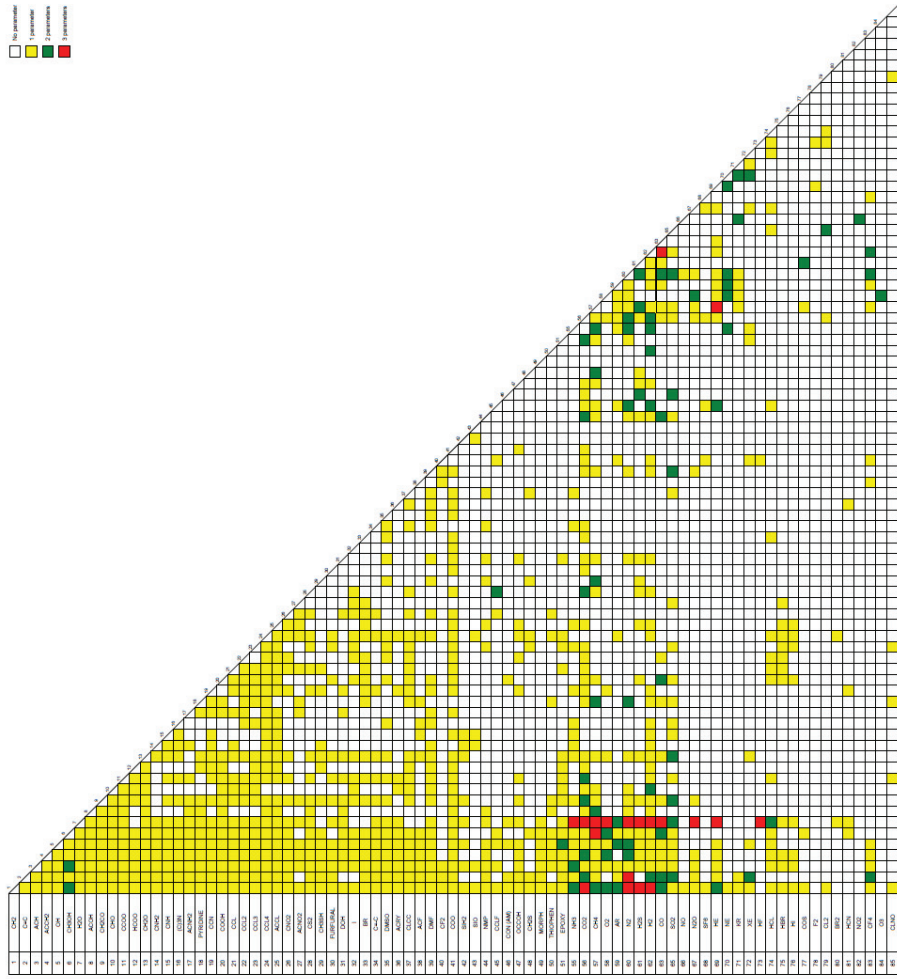


Figure A.23: PSRK group matrix in Prosim plus

Annex 9 Comparison of different thermodynamic models for multi-component mixtures

Tetralin + H₂ binary system

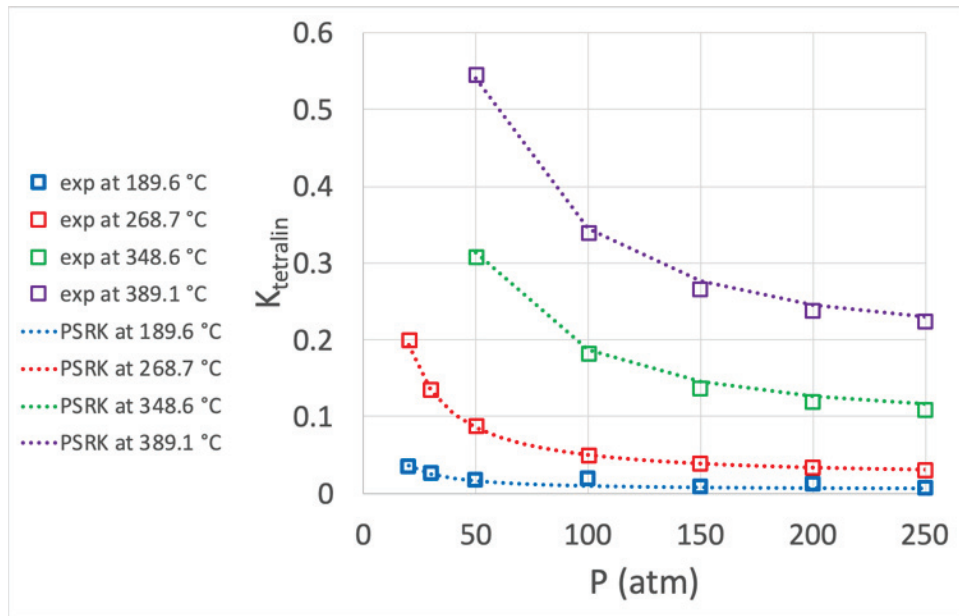


Figure A.24: Comparison of $K_{tetralin}$ between the experimental data and the simulated one

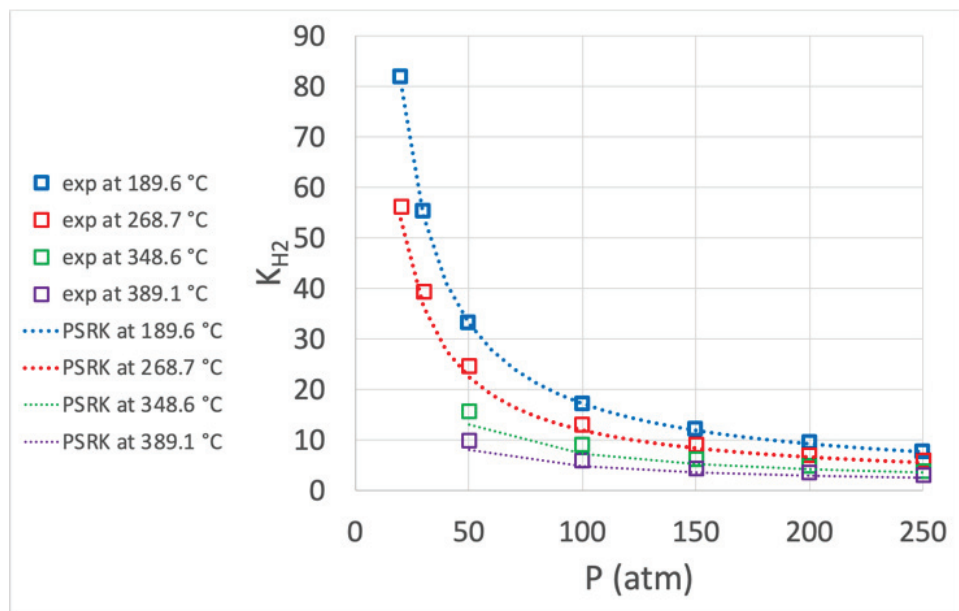


Figure A.25: Comparison of K_{H_2} between the experimental data and the simulated one

Tetralin + H₂O binary system

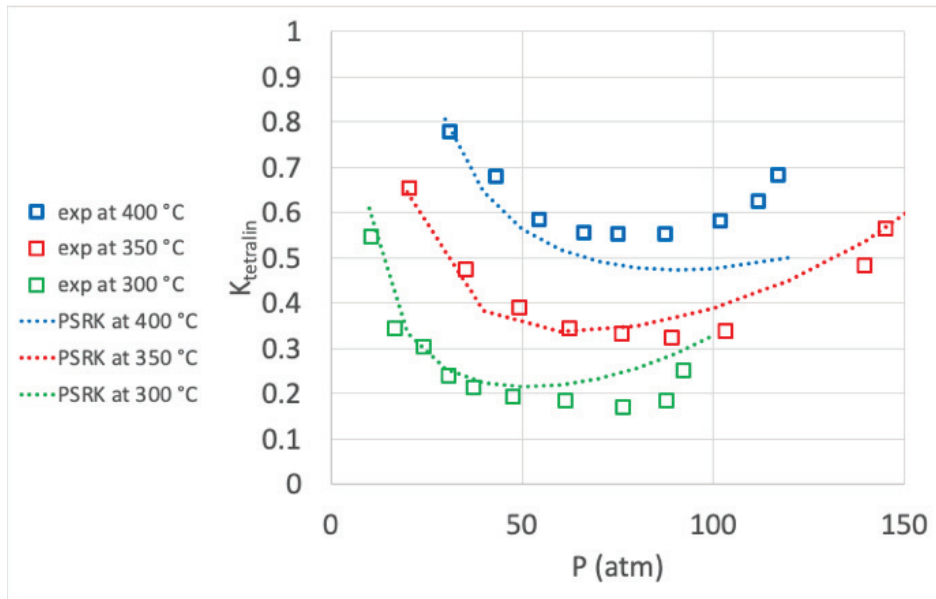


Figure A.26: Comparison of K_{tetralin} between the experimental data and the simulated one

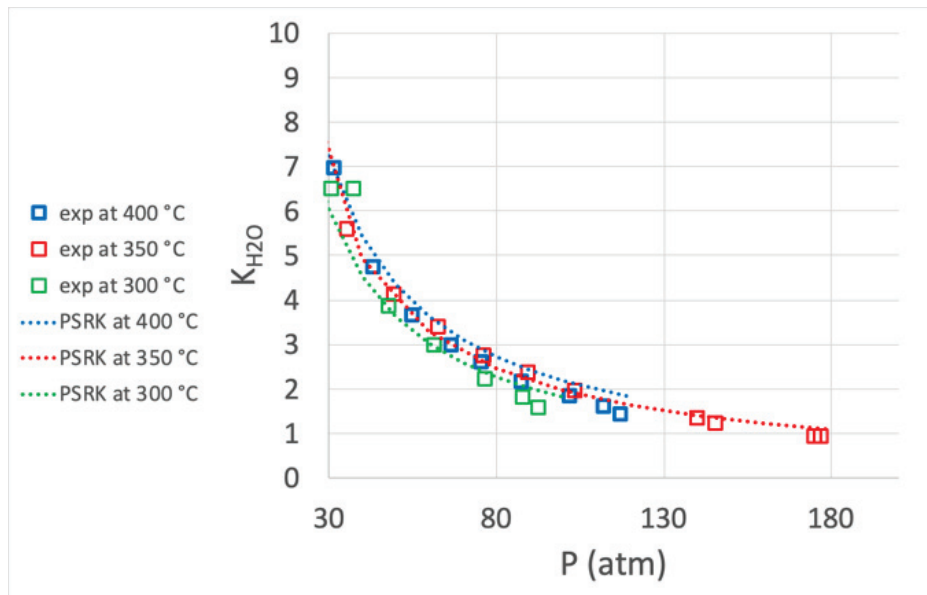


Figure A.27: Comparison of $K_{\text{H}_2\text{O}}$ between the experimental data and the simulated one

Tetralin + m-cresol binary system

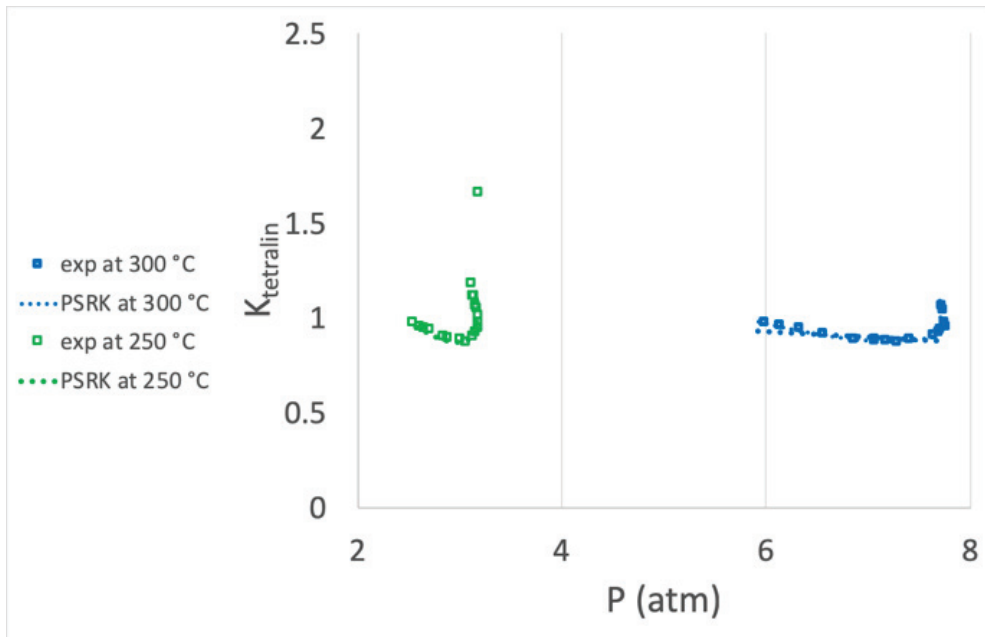


Figure A.28: Comparison of $K_{tetralin}$ between the experimental data and the simulated one

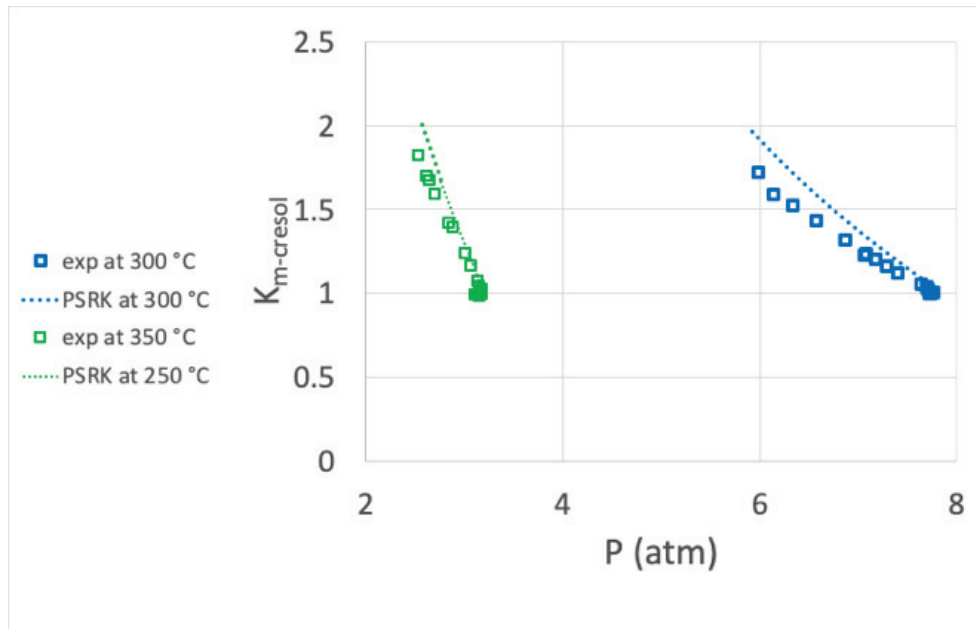
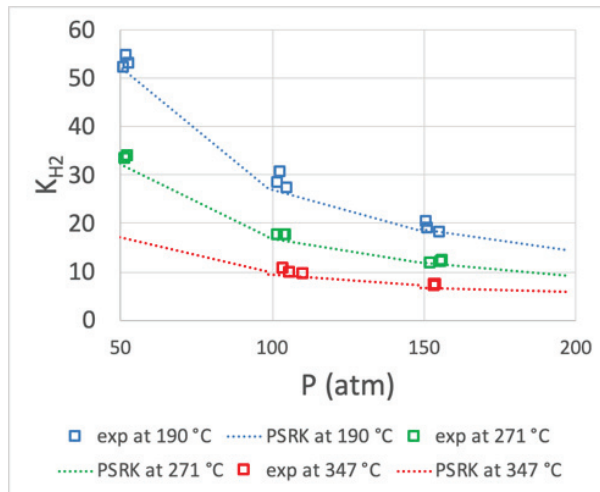
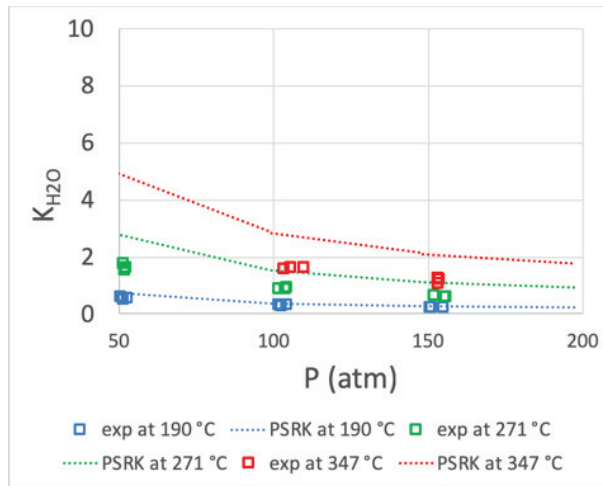


Figure A.29: Comparison of $K_{m-cresol}$ between the experimental data and the simulated one

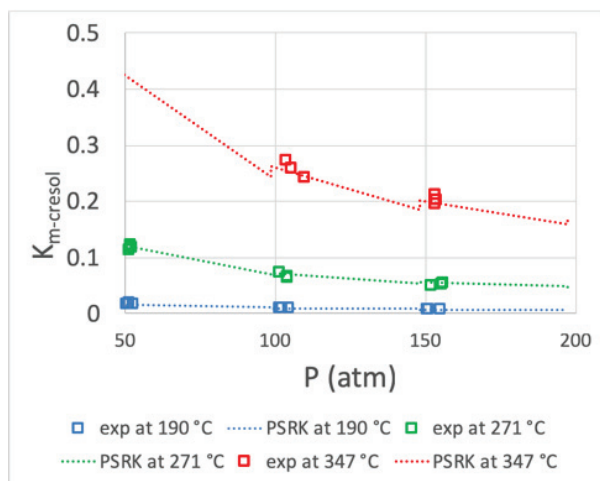
H₂, H₂O and m-cresol ternary system



(a)



(b)

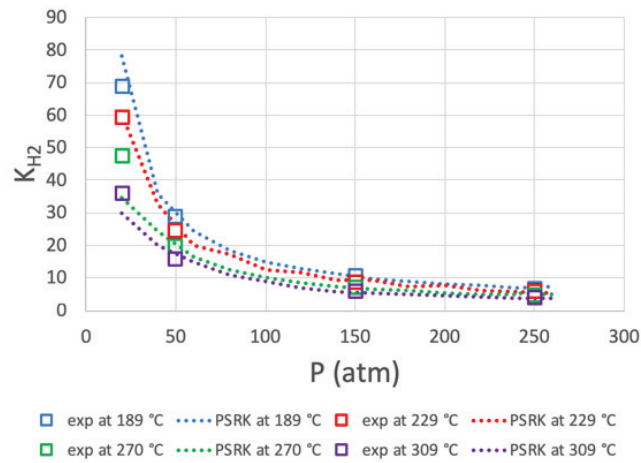


(c)

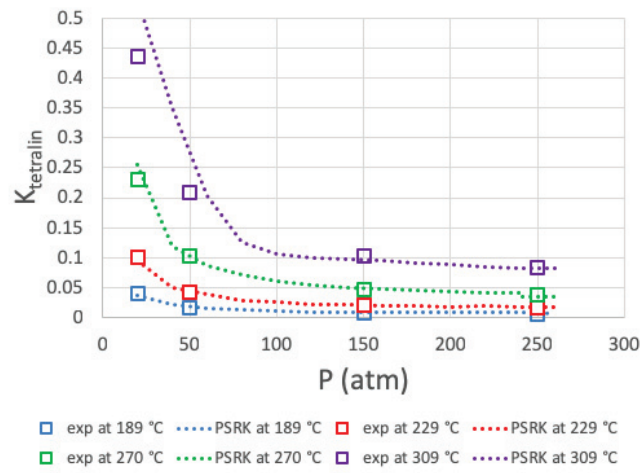
Figure A.30: Comparison between the experimental data and the simulated one (a) K_{H_2} ; (b) K_{H_2O}

(c) $K_{m-cresol}$

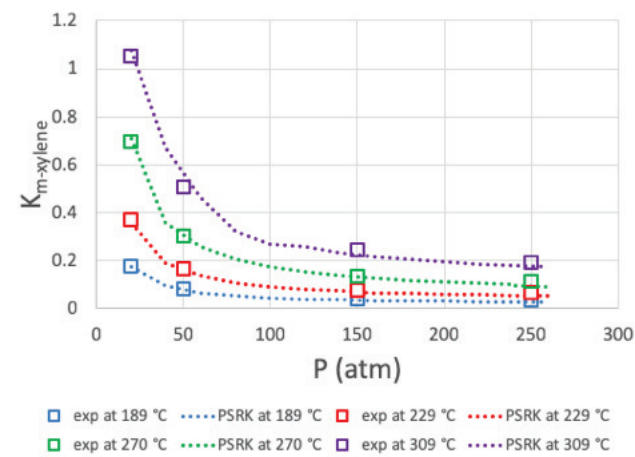
H₂, tetralin and m-xylene ternary system



(a)



(b)



(c)

Figure A.31: Comparison between the experimental data and the simulated one

(a) K_{H_2} ; (b) K_{H_2O} (c) $K_{m-xylene}$

Scientific Productions

Publications

1. Kinetic modeling of lignin catalytic hydroconversion in a semi-batch reactor
Authors: **Junjie Pu**, Dorothée Laurenti, Christophe Geantet, Mélaz Tayakout-Fayolle, Isabelle Pitault;
Chemical Engineering Journal (submitted 30/10/2018).
2. Lignin catalytic hydroconversion in a semi-continuous reactor: an experimental study
Authors: **Junjie Pu**, Than Son Nguyen, Emmanuel Leclerc, Chantal Lorentz, Dorothée Laurenti, Isabelle Pitault, Mélaz Tayakout-Fayolle, Christophe Geantet;
Applied Catalysis B: Environmental (submitted 4/12/2018).

Communications

1. Catalytic hydroconversion of lignin towards aromatics
Authors: **J. PU**, T.S. NGUYEN, C. JALLUT, M. TAYAKOUT, C. GEANTET, I. PITAULT, D. LAURENTI;
French-Chinese conference on Green Chemistry (FC2GChem), Lyon, France, 9-13/5/2016.
2. Catalytic hydroconversion of lignin towards aromatic compounds in a semi-batch reactor
Authors: **J. PU**, M. TAYAKOUT, I. PITAULT, D. LAURENTI;
10th International Symposium on Catalysis in Multiphase Reactors (CAMURE-10), Qingdao, China, 7-10/7/2017.
3. Lignin catalytic hydroconversion: an experimental and modeling study
Authors: J. PU, T. NGUYEN, **D. LAURENTI**, I. PITAULT, M. TAYAKOUT, C. GEANTET;
Europacat, Florence, Italy, 27-31/8/2017.
4. Lignin catalytic hydroconversion: an experimental and modeling study
Authors : **J. PU**, D. LAURENTI, C. LORENTZ, I. PITAULT, M. TAYAKOUT, C. GEANTET;
4th International Congress on Catalysis for Biorefineries (Catbior 2017), Lyon, France, 11-15/12/2017.
5. An experimental and modeling study of lignin catalytic hydroconversion
Authors : **J. PU**, I. PITAULT, M. TAYAKOUT-FAYOLLE, C. GEANTET, D. LAURENTI;
ISCRE 25, Florence, Italy, 20-23/5/2018.
6. Hydroconversion catalytique de la lignine: étude expérimentale et modélisation
Authors: J. PU, **D. LAURENTI**, M. TAYAKOUT-FAYOLLE, I. PITAULT, C. GEANTET;
GECat2018, Trégunc, France, 22-25/05/2018.
7. Experimental and Kinetic Modeling Study on the Catalytic Hydroconversion of Lignin
Authors: J. PU, **D. LAURENTI**, C. GEANTET, I. PITAULT, M. TAYAKOUT;
Gordon Conference-Towards viable solutions for lignin valorization, Easton, USA, 5-10/8/2018.
8. Lignin catalytic hydroconversion: a semi-continuous experimental study
Authors: J. PU, D. LAURENTI, I. PITAULT, **M. TAYAKOUT**, C. GEANTET;
8th Tokyo Conference on Advanced Catalytic Science and Technology (TOCAT8), Yokohama, Japan, 5-10/8/2018.
9. Lignin catalytic hydroconversion: a combined experimental and modeling study
Authors: J. PU, **D. LAURENTI**, M. TAYAKOUT-FAYOLLE, I. PITAULT, C. GEANTET;
GDRI Biomasse, St Petersburg, Russia, 4-6/09/2018.

